UNIVERSITY OF MINES AND TECHNOLOGY, TARKWA

FACULTY OF ENGINEERING

DEPARTMENT OF ELECTRICAL AND ELECTRONIC ENGINEERING

A THESIS REPORT ENTITLED

GRINDING MEDIA CHARGE PREDICTION OF WET BALL MILLS FOR OPTIMAL POWER DRAW USING ARTIFICIAL NEURAL NETWORKS

BY

ABAARE JACOB ATEWIN

SUBMITTED IN FULFILMENT OF THE REQUIREMENT FOR THE AWARD OF THE DEGREE OF MASTER OF PHILOSOPHY IN ELECTRICAL AND ELECTRONIC ENGINEERING

THESIS SUPERVISOR

……

MR ERWIN NORMANYO

TARKWA, GHANA

AUGUST 2020

DECLARATION

I declare that this thesis is my own work. It is being submitted for examination and approval for the Degree of Master of Philosophy in Electrical and Electronic Engineering in the University of Mines and Technology, Tarkwa. It has not been submitted for any degree, examination or approval in any other University.

.....

(Signature of Candidate)

…….. day of December, 2020.

ABSTRACT

Undercharging of grinding media leads to grinding inefficiencies. However, overcharging on the other hand increases the overall mill weight thereby increasing the torque of the mill motor accordingly. Counterbalancing the increase in load torque by mill motor is achieved by drawing more current to produce enough power capable of overcoming the load. More power used means increase in cost. Studies reported in the literature have established that both undercharging and overcharging are undesirable since they contribute negatively to the overall economics of the grinding process. In this research, a non-linear ANN-based predictive model of optimal grinding media charge of the ball mill with consideration of minimum power draw was developed. Operational data of the ball mill involving nine variables were collected over a period of time from a gold mine in the Western Region of Ghana and employed in developing four predictive models. Further, the best performing model was optimised using Grey Wolf Optimisation (GWO) algorithm and Optimal Charging Practices (OCPs) datasets for the purpose of predicting 60 mm grinding media balls. Finally, investigations on how sensitive power draw and grinding media charge were to changes in selected input variables namely, throughput, ore hardness and grinding media wear rate were conducted. Both single and multiple variables analyses were performed in an attempt to find out the possibility of grinding with minimal power draw and minimal grinding media charge while maximising throughput. The analysed scenarios and cases revealed that, it is desirable to grind at 80.0% passing 106 μm and that minimisation of 60 mm grinding media charge is achievable at the expense of the mill power draw.

DEDICATION

This work is specially dedicated to the Almighty God for His infinite love towards my family.

ACKNOWLEDGEMENTS

My greatest thanks go to the Almighty God for granting me sufficient strength and divine health throughout my research.

I would also like to express my deepest gratitude to my supervisor, Mr Erwin Normanyo whose immeasurable efforts convincingly conveyed a spirit of adventure in regard to this research work and scholarship. Without his guidance and persistent help, this research decision would not have been possible.

A special gratitude goes to Dr Solomon Nunoo for providing me with computational resources to help me carry out my model simulations. I am so thankful for his kind gesture.

The immense help and expert advice of Dr. Clement Owusu and Mr. Emmanuel Abotar of the Minerals Engineering Department are worth acknowledging. I appreciate their time and inputs in helping shape this research piece.

To all the graduate students of the 2018 – 2019 year group that space would not permit me to write all your names, I appreciate your inputs. Special mention goes to Kobina Abakah – Paintsil, Akorli David, Richmond Kwesi Amoah, Shiphrah Ohene Adu, Norbert Kyereboah Mensah, John Afetsi Addo and Emmanuel Kweku Mensah for their unparalleled support.

Finally, I would like to appreciate lecturers of the Electrical and Electronic Engineering Department whose lecture pieces have served as a foundational material for this endeavour.

TABLE OF CONTENTS

LIST OF FIGURES

LIST OF TABLES

LIST OF ABBREVIATIONS

Abbreviation	Meaning
AI	Artificial Intelligence
ANFIS	Adaptive Neuro – Fuzzy Inference System
ANN	Artificial Neural Networks
BR	Bayesian Regularisation
BWI	Bond Work Index
DEM	Discrete Element Modelling
ES	Expert Systems
FBNN	Feedback Back-propagation Neural Network
FEM	Finite Element Method
FL	Fuzzy Logic
GA	Genetic Algorithms
GGS	Gates – Gaudin – Schuhmann
GMWR	Grinding Media Wear Rate
GRNN	General Regression Neural Network
GUI	Graphical User Interface
GWO	Grey Wolf Optimisation
HPGR	High Pressure Grinding Rolls
JADE	Java Agent Development Environment
LASSO	Least Absolute Shrinkage and Selection Operator
MEEMD	Modified Ensemble Empirical Mode Decomposition
MIW	Mill Infeed Water
ML	Machine Learning
MLPF	Mill Load Parameter Forecasting
MPC	Model Predictive Control
MSE	Mean Square Error
NCP	Non-optimal Charging Practices
NN	Neural Networks
OPC	Optimal Charging Practices
PBM	Population Balance Models
PD	Power Draw
PFEM	Particle Finite Element Method
PNN	Probabilistic Neural Network

PSD	Particle Size Distribution
RBFNN	Radial Basis Function Neural Network
RF	Random Forest
RNN	Recurrent Neural Networks
SAG	Semi – Autogenous Mill
SEN	Selective Ensemble
TGM	Total Grinding Media
TPH	Tonnes per Hour Milled
TTM	Total Tonnes Milled
USEIA	United States Energy Information Administration
VSD	Variable Speed Drive

LIST OF SYMBOLS

A decreasing function of comminution energy absorbed per unit mass	$f(d_r)$
Acceleration due to gravity	g
Ball-ore ratio	R
Ball load of statistical model	BL
Ball mill shoulder's angular position	θ_s
Ball mill speed	N_r
Ball mill toe's angular position	θ_T
Ball mill's inner surface radius	r_i
Ball mill's internal radius	r_m
Ball size of statistical model	BS
Bias	b_0
Breakage function	b_{ij}
Breakage function for the matrix model	B_m
Center of the function	μ_c
Center of the radial function	μ_r
Constant related to the material type	K
Constant which depends on the mill type	K_t
Constant which relates to wear law	Δ
Cost of energy per unit time	$E_c t^{-1}$
Critical speed	N_c
Cross-term for maximum power	χ_p
Density of slurry	ρ_p
Density of the ball mill charge	ρ_c
Density of the liquid	ρ_w
Density of the solid	ρ_s
Desired value of the jth output neuron	T_j
Diameter inside the shell liners	D_t
Diameter of ball make-up	b_t
Effect of mill load on power consumption	Z_x
Effect of rheology on power consumption	Z_r
Energy-normalised breakage rate parameter	S_i^E

Power input to the mill in (kW)	P
Energy consumed	E
Energy input in kilowatt hours per metric ton	W
Error Contributed by the jth output neuron	E_j
Euclidean distance	D_G
Factor for diameter inside the shell liners	A
Factor for mill speed expressed as a percentage of mill critical speed	C
Factor for mill type and charge volume	B
Feed passing sizes in micrometers (80%)	F_{80}
Final predicted value	$\hat{Y}_G$
Fixed cost per unit time	$F_c t^{-1}$
Fraction of power reduction per fractional	α_p
Fractional filling of voids with slurry	U
Grinding time in (s)	t
Infinitesimal specific energy required to reduce a particle with size x	dE_c
Input pattern	X_R
Input to the hidden layer	H_j
Input variable	x
Inputs from the input layers	x_{ij}
Largest ball size in the mill	d_{max}
Length of the mill (m)	L
Length of grinding chamber (m)	L_c
Load volume as a fraction of the mill volume	J_L
Mass fraction of balls in the load which are smaller than d	P(d)
Mass fraction of material in the i-*th* class in (kg)	w_i
Mass fraction of the feed in size class *i*	f_i
Mass holdup in the mill	M_{sl}
Mass of particles broken in (kg)	SF
Mass of the feed material in the mill in (tons)	W_e
Maximum mill motor power	P_{max}
Maximum value of the data point	X_{max}
Mill diameter	D
Mill electric power consumption	PWR
Mill speed	SPD

Mill throughput per unit time	σ
Minimum value of the data point	X_{min}
Mixing coefficient	D_i
Net electric power drawn by the ball mill	P_{Net}
Normalised data point	X_N
Original data point	X
Output value of the jth output neuron	Y_j
Percentage of critical speed of the mill	C_s
Percentage of particles below 38-micron	S_{38}
Percentage of particles below 75-micron	S_{75}
Positive nonlinear symmetric radial function	G
Power change for solids fraction	δ_{P_x}
Power change parameter for volume	δ_{P_v}
Predicted value of the ith data	$\hat{\hat{y}}_i$
Product passing sizes in micrometers (80%)	P_{80}
Profit per unit time of the mill	Pt^{-1}
Radius of the radial function	σ_r
Real value of the ith data	y_i
Representative size	d_r
Selection function	S_i
Slurry density	ρ_{sl}
Slurry toe angle for grate discharge mills	θ_{OT}
Ball mill filling	j_t
Smallest ball size in the mill which is still retained	d_{max}
Smoothing factor	σ_s
Space coordinate in the axial direction	l
Specific energy input to the mill	$\bar{E}$
Specific gravity of the feed ore	sg
Total error in the feedforward loop	E_T
Transformed hidden layer by the activation function	Y_j
Unit cost of desired product	PSE_c
Unit cost of infeed ore	MFO_c
Velocity of convective transport of particles in the axial direction (ms^{-1})	u_i

Void volume fraction	ε_v
Volume of the mill	V_m
Von Rittinger's energy consumed in size reduction	E_R
Von Rittinger's measure of feed particle size	F_R
Von Rittinger's measure of product particle size	P_R
Wear rate parameter	K
Weight fraction of solids in the mixture	w_s
Weight indicating the effect of that input variable	w_j
Work index in kilowatt hours per metric ton	W_i
Work index of the feed	WI

INTERNATIONAL SYSTEM OF UNITS (SI UNITS)

Quantity	**Unit**	**Symbol**
Electric current	ampere	A
Electric potential	volt	V
Electric resistance	ohm	Ω
Frequency	hertz	Hz
Temperature	degree Celsius	˚C
Time	second	s

CHAPTER 1

GENERAL INTRODUCTION

1.1 Background to the Research

Electrical energy is a valuable commodity that improves the quality of life in every facet of human endeavour. Though not entirely exploited during its invention, it later became a critical determinant for most developing economies during the advent of the industrial revolution. The rise in demand for electrical energy in the wake of the industrial era was mainly justified by the transition of most manufacturing companies from hand production methods to more advanced methods such as the development of machine tools and the rise of the factory system. Electrical energy has not only been at the forefront of industrial transformations but has also played revolutionary roles in the success stories of other sectors such as domestic, transportation and commercial ventures which form part of the intensive energy demand sectors.

More recently, studies by Metayer *et al.* (2015) established that, there has been a total energy demand growth of about 70% over the last two decades and future projections expect energy demand to grow by an additional 40% in the year 2040. The studies also revealed that demand in the industrial sector alone is growing at a rate of 0.7% annually, by far the highest among the three other sectors aforementioned. Affirming these studies, reports by United States Energy Information Administration (USEIA) further supported that the industrial sector uses more delivered energy than any other end user sector, consuming about 54% of the world's total delivered energy. A disaggregated view of this composition sees comminution alone accounting for about 60% of mine electric power load and more than 35% of the operation's greenhouse gas emissions (Jeswiet and Szekeres, 2016).

Comminution, which is one of the most important stages during mineral processing, plays a very crucial role in progressively reducing the size of ore bearing rocks to desirable sizes for further processing. The works of Napier-Munn (2015), Taylor *et al.* (2020) and Wills and Finch (2016) unanimously agreed that comminution is a very energy intensive process and consumes about 30% - 70% of the total energy used in mineral processing plants. Grinding is considered as the last stage in the comminution chain and is accomplished by abrasion and impact of the ore with moving media such as rods or balls inside the mill. According to Abbey *et al.* (2015), grinding is the most energy intensive process and ranks ahead of blasting and crushing in terms of energy consumption in the comminution circuit. Yu (2017) also stated that

it is remarkable and worth noting that energy consumption of grinding far exceeds the energy consumption of other processes, reaching 40% of all the energy used by equipment across the mining industry.

Globally, grinding is estimated to consume about 2% of the energy produced in the world. However, Mor *et al.* (2019) in his studies revealed that existing methods of milling are very inefficient and use only 5% of the input energy for real size reduction while the rest is consumed by the machine itself. The accounted inefficiencies during the grinding process included a greater percentage of the input energy dissipated as heat in ore bearing rocks due to uncontrolled velocity (Esteves *et al*., 2015). All these inefficiencies contribute significantly to a greater percentage of electrical energy wasted in mineral processing which is no longer consistent with modern sustainability recommendations.

Optimisation of the usage of electrical energy is crucial in achieving improved energy efficiency in the minerals processing industry which invariably has the tendency to make significant contribution to solving local, national and global energy problems. More importantly, the need for the reduction of energy consumption associated with the ball mill comminution process is ever greater in recent times due to its direct interrelation with the cost of production. Griffin *et al*. (2016) revealed that 85% of minerals processing industries waste capital or more money in meeting energy cost. Recent significant increment in electricity tariffs has hard-pressed the minerals processing industry to find solutions to optimally use electrical energy so as to pay lower bills and increase profit margins.

1.2 Problem Definition

The wet ball mill is a very common form of grinding equipment in the industrial production process. Widely used in ceramics, chemicals, cement, glass, refractories and other industries, it is a critical equipment which helps with the grinding process in the comminution chain (Nath, 2017). Grinding media is always used in conjunction with the wet ball mill to achieve grinding. Kinetic energy in the rotating grinding media is transferred to the ore to cause breakage during mill operation. The grinding media used depends to a larger extent on the particle size desired, infeed ore size and energy considerations. Efficient grinding is achieved by the type and size of grinding media used. Attaining the required product particle size according to production standards is dependent on the proper charging of grinding media.

Both undercharging and overcharging are undesirable practices in the minerals processing plant (Rupare *et al*., 2013). Undercharging of grinding media leads to grinding inefficiencies while

overcharging on the other hand, increases the overall mill weight and increases electromagnetic torque required to drive the mill motor. Increased torque means more power is used in overcoming the mill load. More power used per time means increase in energy cost. In most continuous milling plants, there is the need to replenish grinding media while the mill is in operation. Foucher *et al*. (2014) established that charging of grinding media in most mineral processing plants is done manually at the experience of the mill operator. This condition leaves operators in the swing of trading in-between attaining the required product particle size for downstream processing and paying exorbitant electricity bills for the cost of electric power (Machalek *et al*., 2020; Nath, 2017). The work further revealed that mill overcharging in most cases is the resultant effect of manual replenishing of grinding media.

According to Rupare *et al*. (2013), overcharging does not only lead to increased power consumption but increases both wear rate of steel balls and down times. Significant reduction in the cost associated with grinding over the years has been achieved by improving the design of crushers and mills (Bian *et al.*, 2017). However, there has not been any major breakthrough in improving the energy efficiency of the comminution process. Today, the utilisation of both conventional and non-conventional energy resources is under critical review. This research seeks to address the problem of predicting optimal grinding media charging of the ball mill to achieve the required product particle size and reduce the cost of energy demanded by the ore size reduction.

1.3 Purpose of the Research

This research aims at predicting optimal grinding media charge of the ball mill in order to minimise the power drawn without compromising on the required product particle size.

1.4 Objectives of the Research

The main objective of this research work is to predict optimal grinding media charge to minimise the electrical energy wasted by ball mills due to inefficient charging practices.

The specific objectives of this research are to:

i. Develop ANN-based models of the ball mill comminution process from experimental data;
ii. Investigate the scenarios of undercharging and overcharging using the developed model;

iii. Optimise the electric power drawn by the ball mill and the quantity of grinding media charged; and

iv. Perform sensitivity analysis on the effect of input variables on both the power draw and grinding media charge requirement for a desirable product particle size.

1.5 Expected Outcomes

The following outcomes are expected after the implementation of findings of this research work:

i. An accurate model developed for the purpose of optimal charging of grinding media;

ii. Reduction in electrical energy wasted as a result of overcharging of the ball mill; and

iii. Appropriate quantity of steel balls required for size reduction of ore in the ball mill.

1.6 Research Questions and Hypothesis

This research was guided by the following questions.

i. Is it possible to develop accurate models for the purpose of optimally charging ball mill with grinding media?

ii. Is it possible to reduce the amount of power drawn during ore size reduction in tumbling wet ball mills at the required product particle size?

Therefore, the research hypothesis is stated as: An ANN-based model can optimally make decisions on the amount of grinding media charge to reduce the power drawn by tumbling wet ball mills during grinding at the required product particle size.

1.7 Scope of the Research

This research work is dedicated to predicting grinding media charge for optimal power draw of wet ball mills in a closed loop comminution circuit for ore size reduction using Artificial Neural Networks (ANN).

1.8 Research Methods Used

The following methods were employed to attain the set objectives:

i. Literature review on existing solutions to the problem and their limitations;

ii. Field visits, data collection, validation and analysis;

iii. Development of optimal models using ANN techniques;

iv. Investigation of the accuracy of the developed models against standard performance metrics;

v. Use of Artificial Neural Networks – Grey Wolf Optimisation (ANN – GWO) algorithm to optimally predict the charging of grinding media and power draw;

vi. Computer simulations using scripts in MATLAB software version 2019b environment; and

vii. Sensitivity analyses to validate robustness of predictions.

1.9 Facilities Used for the Research

The following facilities were deployed in this research:

i. Library, Laboratory, Computer and Internet facilities at UMaT;

ii. Laptop Computer with MATLAB/Simulink software; and

iii. Ball mill circuit facility of a mineral processing plant in the Prestea – Huni Valley district.

1.10 Significance of the Research

The significance of this research is stated as follows:

i. The successful implementation of research outcome will go a long way to cut down on total electric power wasted during comminution due to overcharging of ball mills with grinding media and eventually, raise profit margins of mill operations; and

ii. Establish a more appropriate grinding media requirement for ore size reduction in tumbling overflow wet ball mills.

1.11 Limitations of the Research

Since ball mills are an integral part of the production flow in a typical mineral processing setting, shutting it down for the purpose of this investigation would cost companies under consideration millions of dollars. Hence, this work resorted to the use of data driven models and computer simulations. However, influential factors and data that affect mill power draw and optimal operation are used for the purpose of model development and analyses.

1.12 Definition of Terms and Key Concepts

Ball mill: A type of equipment used to grind and blend materials for use in mineral processing plants and other industrial setting.

Comminution: It is the reduction of solid materials from one average particle size to a smaller average particle size, by blasting, crushing, grinding, cutting, vibrating, or other processes.

Critical speed: the speed at which the mill charge centrifuges.

Grindability: It is a measure of an ore's resistance to grinding.

Grinding media in ball mills: It refers to loaded steel balls used for grinding in the ball mill.

Load level: It is the level of the free surface of the load with respect to the mill axis when the mill is stopped.

Media: This may be steel balls in a ball mill, or large lumps of ore in an autogenous mill or a mixture of lumps of ore and balls in a semi – autogenous mill, as well as the slurry that makes up the operating charge.

Mill charge residence time: It is the time taken between the entry of the feed into the mill and its discharge from the mill.

Mill load: It refers to the mill content which consists of a mixture of grinding media and pulp or slurry.

Ore: A type of rock that contains sufficient minerals with important elements including metals that can be economically extracted from the rock.

Prediction of process variables: It is the technique of determining the output of a particular process variable in previously unseen data using a developed model.

Slurry: It is a mixture of fine solids and water produced in the ball mill.

Throughput: It is the rate of production of products.

1.13 Organisation of the Thesis

This thesis consists of six chapters. Chapter 1 covers the general introduction which comprises background to the research, problem definition, purpose of the research, objectives of the research, expected outcomes, research methods used, facilities used for the research, significance of the research, limitations of the research and organisation of the thesis.

Chapter 2 is devoted to the literature review, which consists of an intensive review of theories and concepts, review of related works on prediction of mill process variables, and statement of research gap in the literature that the research seeks to address.

Chapter 3 deals with the methodology used in the development of the predictive models. It expounds on data acquisition, pre-processing, data analysis, representation and interpretation. It examines the performance of the various predictive models developed based on standard performance metrics. It finally looked at the investigation of overcharging and undercharging using the best of the developed models.

Chapter 4 focuses on the development of an optimised grinding media consumption prediction model using a bionic optimisation algorithm for enhanced performance. The grinding media prediction model is developed from optimal charging practices identified from the test dataset in the previous chapter.

Chapter 5 performs sensitivity analysis of investigated scenarios and their effect on mill power draw and grinding media consumed while desirably keeping product particle size constant.

Chapter 6 gives the conclusions and recommendations, research contributions and future work.

CHAPTER 2

LITERATURE REVIEW

2.1 Introduction

Electric power is a key player in any industrial setting. It serves as an engine on which a lot of processes thrive. Industrialisation over the past few decades has seen a significant rise in electric power demand. With the present trajectory of load growth, there is the need to conserve electric power at every level within the industrial setup to help meet demand as well as cut down on extra expenses.

Ball mill grinding media charging control is vital in ensuring that electric power is efficiently used and conserved. It has a significant effect on the power drawn and the particle size required for downstream processing. It is therefore needful to optimally charge grinding media to meet the two seemingly competing parameters, namely power drawn and output product particle size. One critical parameter that is very essential during downstream processing is the final particle size. The fragmentation of the ore bearing rocks to the required particle size is dictated largely by the number of balls inside the ball mill at a time per the loaded mill feed (Esteves, 2015; Siwella, 2017).

Currently in most mining companies within the Prestea-Huni valley district, grinding media charging of ball mills is done manually or semi-automated without consideration of other influential factors. The ideal condition is for the model to help in optimally charging grinding media to result in minimum power draw by the mill as well as meeting the required product particle size. However, this is rarely achieved. In most cases, the process is done based on the experience of mill operators. The efficient charging of ball mill grinding media will help in the reduction of electric power consumed (Rupare *et al*., 2013).

This chapter therefore gives an elaboration of some theories and concepts of the ball mill and mill grinding efficiency. Some related works are equally reviewed to serve as a foundation for this research.

2.2 Ball Mills

The ball mill is a machine that is deployed to reduce the size of mineral bearing ore, chemical, ceramic raw materials and paint into fragments that can be used for downstream processing. It basically consists of a hollow cylinder containing balls mounted on a metallic frame which gives it the flexibility to rotate about its longitudinal axis. The grinding media is made up of

either balls or rods. The balls which could be made of different diameters occupy 30% to 50% of the mill volume and their size depends on the feed and mill size (Calistus, 2016). Grinding in ball mills is achieved by impact and attrition (Piras *et al*., 2019).

2.2.1 Constructional Features of Ball Mills

There are different types of ball mills usually differentiated by the discharge system (Yu, 2017). Grate discharge, conical, air swept, tube, screen discharge and batch mills are some examples of the types of ball mills available. The empirical construction of all ball mills is fundamentally the same irrespective of their peculiar use. However, variations can be seen in the design based on the size of the mill, the feeders that are used to load the starting material and the system employed for discharging the output product.

2.2.2 Principle of Operation of Wet Ball Mills

Fig. 2.1 (Aguila-Camacho *et al.*, 2017) shows a closed loop wet ball mill comminution circuit which comprises the mill with load, sump, sump pump and the hydrocyclone.

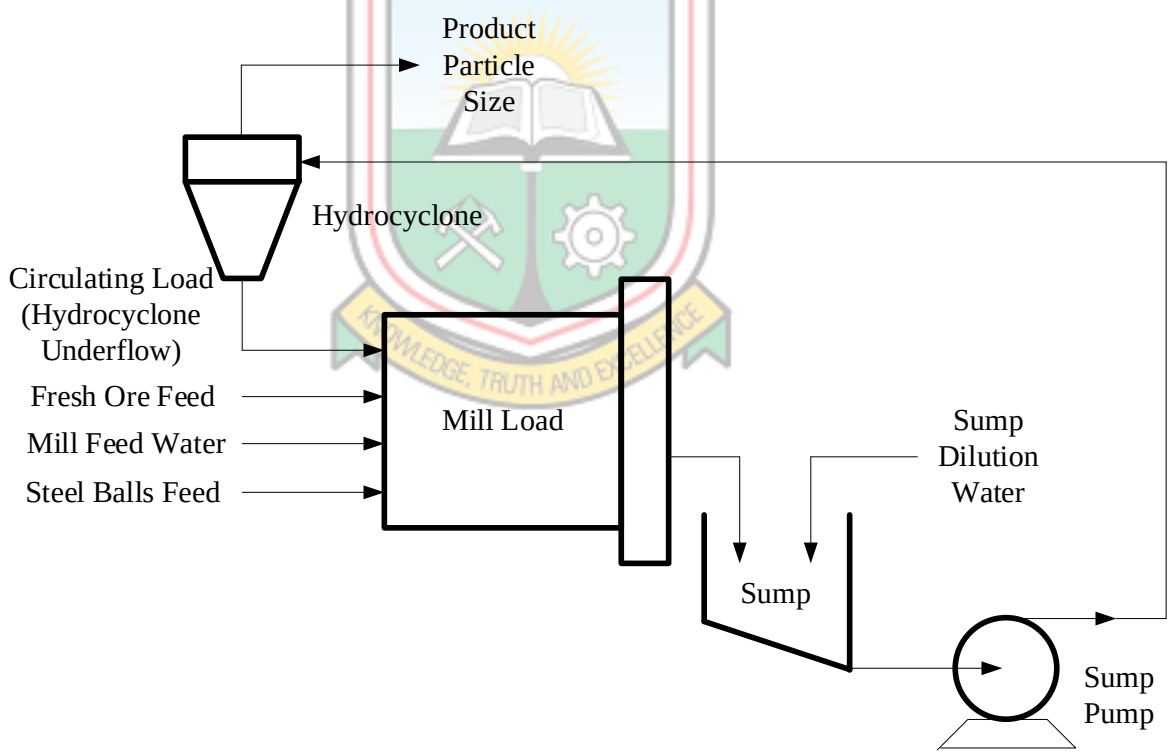

Fig. 2.1 A Closed Loop Wet Ball Mill Comminution Circuit

The operating principle of the wet ball mill consists essentially of milling and separation. In a continuous operating ball mill, the mill receives four streams as inputs: mill feed ore, mill infeed water to assist with material transport, steel balls to assist with ore breakage, and underflow from the hydrocyclone. The fraction of the mill filled with charge is known as the

mill load. The ground ore in the mill mixes with water to form slurry. The slurry is discharged from the mill into the sump through an end-discharge grate. The end-discharge grate limits the solids particle size of the discharged slurry. The slurry in the sump is diluted with water and pumped to the hydrocyclone for classification. The total volume of slurry in the sump is known as the sump volume. The pump is usually fitted with a variable speed motor to manipulate the hydrocyclone feed flow rate. The hydrocyclone feed density can be adjusted by the sump dilution water as long as the sump does not overflow or run dry.

The hydrocyclone is responsible for the separation of the in-specification and out-of-specification ore discharged from the sump. The lighter, smaller in-specification particles in the slurry pass to the overflow of the hydrocyclone, while the relatively heavier, larger and out-of-specification particles pass to the underflow. The hydrocyclone underflow is passed to the mill for further grinding while the overflow flows to a downstream process for beneficiation.

The volumetric flow rate of solids in the overflow is the throughput of the circuit and it is equal to the volumetric infeed rate of ore at steady-state operation of the circuit (Le Roux *et al.*, 2016). The quality of the circuit product is indicated by the fraction of particles in the overflow smaller than specification size of the material fed through the central hole into the drum and moves there along, being exposed by grinding media. The material grinding occurs during impact of falling balls and abrasion of the particles between the balls. Then, discharge of ground material is performed through the central hole in the discharge cap or through the grid (mills with center unloading the milled product and mills with unloading the milled product through the grid).

2.3 Comminution

Comminution is the process whereby ore size is progressively reduced until the mineral of interest is liberated from the matrix of gangue within the rock and can be separated through physical or other means (Resabal, 2017). Crushing and grinding are two major processes that are of utmost importance within the comminution chain after blasting. Crushing is accomplished by compression of the ore against rigid surfaces, or by impact against surfaces in a constrained motion path. According to Wang (2012), crushing is usually done in dry conditions. Grinding on the other hand is accomplished by abrasion and impact of the ore by the free motion of discrete media such as rods, balls or pebbles. Size reduction however is fundamentally an energy intensive operation, consuming about 3% to 4% of the total electrical energy consumed worldwide (Abbey *et al.*, 2015; Napier-Munn, 2015; Petrakis *et al*., 2017a). Also, comminution is estimated to consume the largest part of the energy used in mining

operations, from 30% to 70% according to Diaz *et al*. (2018) and Taylor *et al*. (2020). To a greater extent, in the comminution process, it takes energy to fracture a particle and progressively reduce it to the size required for downstream processing.

At every point in time a particle requires different amounts of energy depending on the distribution of flaw sizes, rate of stress application and the orientation of particle in the size field. Greater amounts of energy transmitted to particles lead to finer average size of the product population. This is usually rarely achieved due to inefficient methods of milling according to Hlabangana *et al*. (2018) and Singh *et al*. (2013). The relationship between comminution energy absorbed per unit mass and the representative size is defined by a differential equation according to King (2012) as presented in Equation (2.1).

$$f(d_r) = \frac{dE}{dd_r} \tag{2.1}$$

where, $f(d_r)$ = a decreasing function of d_r reflecting the fact that more energy per unit mass is required as the particles get smaller

dE = is the increment in energy to effect an incremental decrease in representative size (d_r)

d_r = representative size

2.3.1 Theories of Comminution

Over the last century, there has been progressive research pertaining to the development of theoretical comminution models. According to Petrakis *et al*. (2017a), the main and well known theories that first described the relationship between specific energy requirements and size reduction in comminution are those of Von Rittinger propounded in 1867, Kick in 1885 and Bond in 1952. Von Rittinger's theory tried to explain the relationship between the input power and the change in surface area from feed to product size material. Von Rittinger's theory states that the energy consumed in size reduction is proportional to the area of new surface produced. Mathematically, Rittinger's theory is represented by Equation (2.2) (Wills and Finch, 2016).

$$E = K\left(\frac{1}{P} - \frac{1}{F}\right) \tag{2.2}$$

where, E_R = Von Rittinger's energy consumed in size reduction

K = constant related to the material type

F = measure of feed particle size (diameter in μm)

P = measure of product particle size (diameter in μm)

Works by Kick considered that energy requirement depends only on the reduction ratio, and not on the original size of the particles. Equation (2.3) (Wills and Finch, 2016) depicts energy required as a proportion to the reduction in volume of the particle as stated by Kick.

$$E = K\left(\ln\frac{F}{P}\right) \tag{2.3}$$

Bond's theory, often referred to as the "third theory" saw the addition of new crack tip length as an extension to the works done by Rittinger and Kick. Input energy is proportional to the new crack tip length produced in particle breakage. The theory of Bond is commonly expressed as the governing Equation (2.4) (Wills and Finch, 2016).

$$W = 10 \times W_i\left(\frac{1}{\sqrt{P_{80}}} - \frac{1}{\sqrt{F_{80}}}\right) \tag{2.4}$$

where, W = energy input (work) in kilowatt hours per metric ton

W_i = work index in kilowatt hours per metric ton

F_{80} = 80% feed passing sizes in micrometers

P_{80} = 80% product passing sizes in micrometers

Leveraging on works done earlier, Walker and Shaw in 1937 proposed the differential equation consisting of the theories of Rittinger, Kick and Bond as partial cases and states, that the energy required to make a small change in the size of an object is proportional to the size change and inversely proportional to the object size raised to the power *n* as depicted in Equation (2.5) (Petrakis *et al*., 2017a). This equation is known as the general energy-based comminution equation in differential form.

$$dE_c = -K \cdot x^{-n} dx \tag{2.5}$$

where, dE_c = the infinitesimal specific energy required to reduce by dx the size of a particle with size x (kWhr/t)

K = constant related to the material type

n = constant indicating the order of the process

In the integral form, Equation (2.5) is transformed into Equation (2.6).

$$E = -K\int_{F}^{P} x^{-n}\,dx \tag{2.6}$$

Bond's model remains the most widely used model, at least for conventional comminution equipment (Wills and Finch, 2016). With the advent of separator technology, earlier comminution theories fell short as they did not incorporate the concept of Particle Size Distribution (PSD). Models such as Gates-Gaudin-Schuhmann (GGS) evolved to address some of the limitations that were associated with improvements in grinding efficiency due to the use of separator technology.

2.3.2 Mathematical Comminution Models

The basic idea of modelling comminution processes (crushing and grinding) is to obtain mathematical relations between the feed and the size of the product. The basic approach is to recognise the fact that comminution processes accept ore and impart physical energy, either single impact or multiple impacts till disintegration occurs. Disintegration only occurs to produce a distribution of smaller sizes if the total breaking energy imparted is greater than the bonding energy between individual particles.

In the development of comminution models, a material balance of components and an energy balance of the comminution system are first established. The material balance and the energy balance of the operation are given by Equation (2.7) and Equation (2.8), respectively.

$$\left[\text{Feed in} + \text{Breakage}\right] = \left[\text{Total Product out}\right] \tag{2.7}$$

$$\begin{bmatrix}\text{Energy input}\\ \text{for breakage}\end{bmatrix} = \begin{bmatrix}\text{Energy transmitted for}\\ \text{particle breakage}\end{bmatrix} + \begin{bmatrix}\text{Energy transformed as}\\ \text{heat and sound energy}\end{bmatrix} \tag{2.8}$$

Usually, energy transformed as heat and sound energy are neglected due to their insignificant contributions. Also, a fundamental assumption in the approach is that the residence time of particles in the mill is the same as if the entire charge is mixed thoroughly and is uniform. Three comminution models are commonly accepted in the literature: Kinetic, energy and matrix models (Monov *et al*., 2012). However, other ball mill operational models such as Banerjee, statistical and ANN are also considered.

Kinetic model

The kinetic model of the grinding process is based on the population balance or mass-size balance equations. This involves tracking and manipulating whole or partial particle size distributions along the comminution chain. This model allows the simulation of grinding

circuits without generalising that all particle sizes have the same normal shape but allows for specifications by giving room for additional model configuration to fit the simulation scenario perfectly. Assuming that the mill is a perfectly mixed model, a kinetic model of second order is given in the form of Equation (2.9) (Monov *et al*., 2012).

$$\frac{dw_i(l,t)}{dt} = -S_i w_i(l,t) + \sum_{j=1}^{i-1} S_j b_{ij} w_j(l,t) + D_i \frac{d^2 w_i(l,t)}{dl^2} - u_i \frac{dw_i(l,t)}{dl} \tag{2.9}$$

where, $\frac{dw_i(l,t)}{dt}$ = variation of the mass of fraction of the material in size class *i* within a particular time interval in (kg)

t = grinding time in (s)

l = space coordinate in the axial direction

w_i (l, t) = mass fraction of material in the *i*-th size class in (kg)

b_{ij} = breakage function

S_i = selection function

D_i = mixing coefficient

u_i = velocity of convective transport of particles in the axial direction (ms^{-1})

The first and second terms in the right hand side represent the mass of disappearing and appearing particles in this class, respectively. The third term describes the axial dispersion and the last term represents the convective transport of particles in the axial direction with velocity, u_i. The kinetic model in Equation (2.9) (Monov *et al*., 2012). is subject to the following boundary conditions:

$$w_i(l,0) = f_i(l) \tag{2.10}$$

$$w_i(l,t) = u_i w_i(l,t) - D_i \frac{d\,w_i(l,t)}{dl} \text{ for } l = 0 \tag{2.11}$$

$$\frac{dw_i(l,t)}{dt} = 0 \quad \text{for } l = L \tag{2.12}$$

where, $f_i(l)$ = mass fraction of the feed in size class *i*

L = length of the mill in (m)

Considering an operation where the charge is assumed to be thoroughly mixed and uniform in both radial and axial directions, Equation (2.9) can be represented as Equation (2.13) (Monov *et al*., 2012).

$$\frac{dw_i(t)}{dt} = -S_i w_i(t) + \sum_{j=1}^{i-1} S_j b_{ij} w_j(t) \tag{2.13}$$

Energy model

Energy-based models are very similar to kinetic models used in describing the grinding process. However, the energy-based model differs from the kinetic model in that, the energy-based equation used in describing the grinding kinetics is expressed in terms of the specific energy as an independent variable instead of the grinding time. Equation (2.14) gives the energy-balance equation modelling of the grinding process.

$$\frac{dw_i\left(\overline{E}\right)}{d\overline{E}} = -S_i^E w_i\left(\overline{E}\right) + \sum_{j=1}^{i-1} S_j^E b_{ij} w_j\left(\overline{E}\right) \tag{2.14}$$

where, $\overline{E}$ = specific energy input to the mill in (kWh/t)

S_i^E = energy-normalised breakage rate parameter defined as in equation (2.15)

$$S_i^E = \frac{S_i}{P_E/W} \tag{2.15}$$

where, P_E = power input to the mill in (kW)

W= mass of the feed material in the mill in (tonnes)

Matrix model

The matrix model developed by Lynch, expresses the relationship between selection function S_i and feed analysis representing the feed and product size distributions as N size ranges. The model assumes that S_i is the proportion of particles within a sieve fraction, i, that would break preferentially. Considering the masses of the material in each size fraction as F_1, F_2…..F_n and the proportion of particles that have the probability of breaking in the corresponding size interval as S_1, S_2…..S_n. The matrix model can be written as in Equation (2.16) and Equation (2.17) (Gupta and Yan, 2016).

$$\begin{array}{cccc} \text{Size} & \text{Feed} & \text{Selection function} & \text{Mass of particle broken} \\ \begin{bmatrix} 1 \\ 2 \\ \vdots \\ N \end{bmatrix} & \begin{bmatrix} F_1 \\ F_2 \\ \vdots \\ F_N \end{bmatrix} \bullet & \begin{bmatrix} S_1 & 0 & \dots & 0 \\ 0 & S_2 & \dots & 0 \\ \vdots & \vdots & \ddots & \vdots \\ 0 & 0 & \dots & S_N \end{bmatrix} = & \begin{bmatrix} F_1S_1 \\ F_2S_2 \\ \vdots \\ F_NS_N \end{bmatrix} \end{array} \tag{2.16}$$

From the matrix above, the entire breakage operation being a sum of broken and unbroken particles can now be expressed by the general Equation (2.17).

$$P = B \cdot S \cdot F + (I - S) \cdot F \tag{2.17}$$

P = particle size distribution

where, $(I - S) \cdot F$ = mass of particles unbroken in (kg)

$S \cdot F$ = mass of particles broken in (kg)

B = breakage function

Banerjee model

Mathematical model developed by Banerjee is given in Equation (2.18) and Equation (2.19). Experimental data used in the development of the model were based on ball diameter (D_b), ball–ore ratio (R) and grinding time (t). The model was developed for the purpose of optimising ball mill load, ball size, ball to ore ratio, grinding time, pulp density and ball mill rpm. Ball mill rpm and pulp density were ignored during the model development due to their negligible contribution on product particle size distribution.

$$S_{75} = 19.30 - 0.31 D_b + 12.60 R + 0.47 t \tag{2.18}$$

$$S_{38} = 4.39 - 16 D_b + 9.52 R + 0.31 t \tag{2.19}$$

where, S_{75} = percentage of particles below 75 micron

S_{38} = percentage of particles below 38 micron

D_b = ball diameter

R = ball-ore ratio

t = grinding time

Statistical model

Statistical models are derived from statistical modelling. The statistical model given in

Equation (2.20) and Equation (2.21) (Singh *et al*., 2013) is an extension of the Banerjee model, giving room for more number of inputs to ensure better reliability of the model.

$$S_{75} = 23.3 - 0.11BS_{4.0} - 0.89BS_{25} - 0.98BS_{18} + 0.43BL + 3.98R + 0.43t \qquad (2.20)$$

$$S_{38} = -0.39 - 0.017BS_{40} + 0.002BS_{25} + 0.015BS_{18} + 0.35BL + 2.71R + 0.31t \qquad (2.21)$$

where, BS = ball size

BL = ball load

R = ball to ore ratio

Artificial neural networks model

An ANN model learns and develops the relationship between input parameters and particle size distribution using operational data sets collected over a period of time. Input data such as ball size, ore type and grinding time and output targets such as the particle size distribution obtained were used to train the model to be able to predict future particle size distribution based on input parameters that the mill will be configured with. Fig. 2.2 (Singh *et al.*, 2013) shows the ANN model of the ball mill.

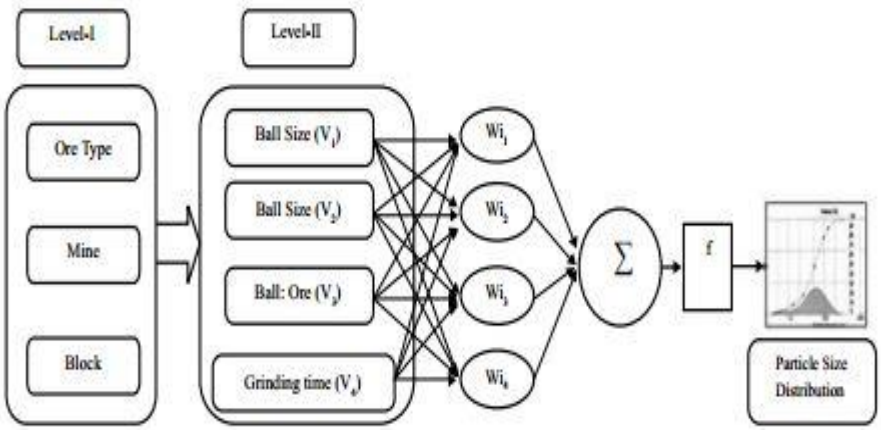

Fig. 2.2 Artificial Neural Network Model of a Ball Mill

2.3.3 Grinding Efficiency of Tumbling Wet Ball Mills

The grinding action in wet ball mills is induced by relative motion between free motion of unconnected media such as rods, balls or pebbles. This motion can be characterised as collision with breakage induced primarily by impact or as rolling with breakage induced primarily by crushing and attrition (King, 2012). In autogenous grinding machines, fracture of the media particles also occurs by both impact (self-breakage) and attrition.

The relative motion of the media is determined by the tumbling action which in turn is quite strongly influenced by the liners and lifters that are fixed inside the shell of the mill. The liners protect the outer shell of the mill from wear and are renewable while lifters prevent slipping between the medium and slurry charge in the mill and the mill shell. Slippage consumes energy wastefully but more importantly, reduces the ability of the mill shell to transmit energy to the tumbling charge (Taylor *et al*., 2020). This energy is required to cause grinding of the material in the mill. The geometry (liners, lifters and mill diameter) and the energy applied is indicative of the movement of the grinding media inside the mill (Francioli, 2015).

The rotary motion of the ball mill exerts a partial centrifugal force that keeps the charge close to the internal mill shell. At sufficient height right above the stable point (the bottom of the mill), the centrifugal force is not sufficient enough to keep the ball and ore attached to the shell leading to a sudden fall to the bottom. By this action, the balls impinge on the ore leading to particle size reduction. Fig. 2.3 (Lv *et al*., 2018) shows the load behaviour in a dynamic wet ball mill.

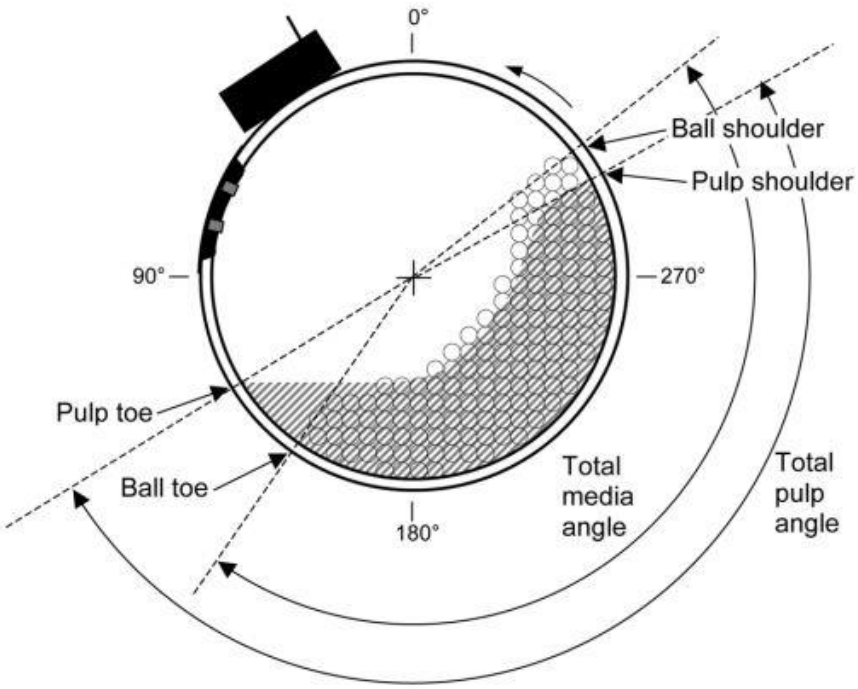

Fig. 2.3 Load Behaviour of a Dynamic Wet Ball Mill

Size reduction is the most inefficient and energy consuming operation in any beneficiation process (Abbey *et al.*, 2015; Hlabangana *et al.*, 2018; Petrakis *et al*., 2017b). Research into maximising grinding efficiency, reducing energy consumption and subsequently reduction in operational cost is a major leeway to fill the gap. Grinding efficiency is however affected by a

number of factors such as feed particle size and composition, mill loading, mill speed, slurry properties and grinding media size distribution.

Feed particle size and composition

A change in feed size influences particle-particle and particle-grinding media interactions (Hlabangana *et al.,* 2018). The shape and structure of the crushed ore affects the product particle size in a ball mill grinding circuit (Abazarpoor and Halali, 2017; Ghassa *et al.,* 2016). In order to ensure higher grinding efficiency of the grinding circuit, control of mill feed particle size distribution can be achieved by optimising crushers and using screening circuits to ensure that output particle size from the crusher falls within the infeed particle size specification. Also, feed particle size greatly influences optimum grinding media size selection. In fine grinding, steel ball size is very important in providing accurate crushing force to grind the ore and improve fine grinding efficiency (Xiao *et al.,* 2014). Use of oversized steel balls reduces grinding time considerably but produces fine product particles which are undesired.

On the other hand, smaller balls lead to finer grinds but have the demerit of energy loss. Energy loss can be reduced by limiting the production of ultrafine particles which can be achieved by increasing grinding media size (Vijayakumar, 2016). Grinding efficiency can be improved in the case of ore size variability by employing different sizes of grinding balls. According to Hlabangana *et al*. (2018), this process has an added advantage in that different particle sizes can be effectively milled because each media size can effectively break a particular particle size during the size reduction process ensuring that the product fineness is optimised. However, rapid variation of the feed size will affect the final product size considerably as it poses the challenge of a corresponding buffer with an equivalent grinding media size.

Mill loading

One key to efficient milling is a properly charged mill, since the performance of ball mills is very sensitive to the volumetric mill filling. Volumetric fill, to a greater extent influences grinding media wear rates, throughput, power draw, and product grind size. The charge (grinding media, infeed ore and infeed water) is specified as a percentage of the overall mill volume. Optimum grinding rates are obtained with about 30% to 50% charge filling with grinding media alone (Calistus, 2016; Usman, 2015), This gives a cascading surface equal to the diameter of the mill, representing the maximum surface length. Too much media or too little of it will decrease the length of this cascading zone and increase milling time. According to Helmi *et al*. (2016) and Rashidi *et al*. (2017) increasing grinding media increases the grinding performance until the saturation point where an increase in grinding media does not

correspondingly increase product fineness. Further increase in grinding media above this saturation point which can be anywhere between the 30% - 50% leads to overcharging.

Overcharging is characterised by inefficient grinding and increased grinding media wear due to rigorous collision between the overcrowded grinding media inside the mill. Mill electric power consumption increases due to increased mill load by the expression given in Equation (2.22) (Li *et al*., 2017).

$$\mathrm{PWR} = \mathrm{P_{max}}\{1 - \delta_{\mathrm{P_v}} \cdot \mathrm{Z_x^2} - 2 \cdot \chi_{\mathrm{P}} \cdot \delta_{\mathrm{P_v}} \cdot \delta_{\mathrm{P_s}} \cdot \mathrm{Z_x} \cdot \mathrm{Z_r} - \delta_{\mathrm{P_s}} \cdot \mathrm{Z_r^2}\} \cdot (\mathrm{SPD})^{\alpha_{\mathrm{P}}} \qquad (2.22)$$

where, PWR = mill electric power consumption (kWh)

$\mathrm{P_{max}}$ = maximum mill motor power (kW)

$\delta_{\mathrm{P_v}}$ = power change parameter for volume

$\mathrm{Z_x}$ = effect of mill load on power consumption

χ_{p} = cross – term for maximum power

$\delta_{\mathrm{P_s}}$ = power change for solids fraction

$\mathrm{Z_r}$ = effect of rheology on power consumption

(SPD) = mill speed

α_{p} = fraction of power reduction per fractional reduction from maximum mill speed

Moreover, a mill with undercharged grinding media is characterised by an overcharged infeed material. Too much material interferes with efficient grinding by creating a shock-absorbing cushion between the media, thus compounding the inefficiency with a combination of the reduced cascading zone in addition to the cushioning effect of the overcharged material.

Speed of ball mill

The speed at which the ball mill rotates is responsible for maintaining the slope of the cascading media pile, known as the “angle of break”. This angle can be between 40 to 65 degrees as measured from the horizontal. Shallow angles do not allow grinding media to cascade much from one end to the other. Steeper angles on the other hand cause inefficiencies in the cascading action since grinding media break free and fall from top to bottom without striking anything. The speed of rotation of the mill also determines the basic operating modes of the mill (Bian *et al*., 2017; Monov *et al*., 2012). Slow rotation leads to the mill operating in a cascading regime. In this regime, grinding is achieved by attrition, which produces finer product particle size but compromises on mill liner wear.

Faster rotation causes the grinding media to cataract. This causes impact grinding, leading to coarser product particle size but with reduced liner wear and lower mill torque as a result of grinding media being transformed into turning moments supporting the rotation of the mill. Very fast speeds cause the grinding media to centrifuge away from the pile and not cascade or cataract at all, reducing mill active load. The speed at which this begins to occur is known as the critical speed (Francioli, 2015; Tripathy *et al*., 2017). Operation of the mill in any of the three regimes can be achieved by operating at a speed which is a percentage of the critical speed. Mathematically, critical speed is represented in Equation (2.23) (Tripathy *et al*., 2017).

$$N_c = \frac{42.3}{\sqrt{D}} \tag{2.23}$$

where, N_c = critical speed in (rpm)

D = the mill diameter in (m)

According to works by Sinnott *et al.* (2017) and Wills and Finch (2016), operating the ball mill at a speed range of 70% to 80% of the critical speed causes the mill to operate in the cascading regime relative to the mill volumetric fill. Increasing the speed above 80% of the critical speed leads to the grinding media assuming a dominant cataracting regime and above 100% of the critical speed or slightly below the critical speed at higher volumetric fills causes a transition of the mill to start to centrifuge. According to Hoseinian *et al*. (2017), mill speed has the most direct effect on mill power draw since there is a linear relationship between the two as expressed in Equation (2.22). Increase in mill speed leads to a corresponding increase in electric power draw of the mill because of an increase in the electromagnetic torque required to rotate the mill at that speed.

Moreover, studies by Bazin and Lavoie (2016), further established the fact that, increasing speed does not only lead to an increase in power draw but changes the operating regime from cascading to cataracting which has significant effect on the grinding efficiency. Results showed that increasing the mill speed improves the rate of breakage of the coarse size intervals due to additional energy drawn from the acceleration of the mill. Inefficiencies however arise since most of the energy is lost in heating the slurry and in the vaporisation of water (Makokha and Letting, 2019). To ensure that maximum throughput is obtained at low cost (low energy consumption and reduced wear of grinding media and liners), the choice of mill operating speed can be regulated using a variable speed drive while optimising volumetric charge of the mill in the best proportion of infeed ore, infeed water, circulating load and the infeed grinding media charged.

Slurry properties

Mineral slurry is a proportionate mixture of fine ore particles and water. The water which is added as a proportion to the mill ore feed rate acts as carrier fluid, distributing the ore particles within the mill load and subsequently transporting it out of the mill. Slurry density and slurry viscosity are two crucial properties that significantly influence the efficient flow of slurry within the mill and greatly affects grinding efficiency (Vos, 2017). Viscosity of a fluid can generally be defined as a measure of the fluid's resistance to flow. Optimum value of slurry viscosity is always needful to achieve maximum breakage rate. Excessively high viscosity forms thick slurries which act as a cushion reducing the stressing force necessary for breakage action. Too dilute slurries on the other hand increases metal-to-metal contact, giving rise to increased steel ball consumption due to wear and reduced efficiency.

Slurry density is closely related to slurry viscosity. For a mixture of media and slurry, the density is estimated as percentage by weight of solids in the mixture. A change in the slurry density affects the internal charge action, that is the movement pattern of the balls and the flowing ability of slurry within the ball charge during the tumbling process. Slurry density can be estimated using Equation (2.24) (Vos, 2017).

$$\rho_{sl} = \frac{1}{\left(\frac{w_s}{\rho_{solids}} + \frac{(1-w_s)}{\rho_{water}}\right)} \tag{2.24}$$

where, ρ_{sl} = slurry density (kg/m^3)

ρ_{solids} = density of the solid (kg/m^3)

ρ_{water} = density of the liquid (kg/m^3)

w_s = weight fraction of solids in the mixture (%)

Flow and mixing behaviour of slurry within the mill determines the slurry residence time in the mill and consequently breakage rate, holdup volume and mill power draw which have a large influence on the milling efficiency. The holdup volume influences the effectiveness of material transport to the breakage zones and the rate of breakage. Slurry density is related to its mass hold-up in the mill according to Equation (2.25) (Vos, 2017).

$$M_{sl} = \rho_{sl} U \varepsilon_v J_L V_m \tag{2.25}$$

where, M_{sl} = mass hold-up in the mill (tonne)

U = fractional filling of voids with slurry (%)

ε_v = void volume fraction (m^3)

J_L = load volume as a fraction of the mill volume (%)

V_m = volume of the mill (m^3)

Decreasing solid content optimally decreases mass hold-up rate and increases movability of particles which causes effective interaction between ore and grinding media (Vos, 2017). Sorgenfrei (2016) revealed that too high mill solid concentration can lead to blockade in the mill which in a continuous plant is undesirable due to downtime economic losses. Studies by Flach *et al*. (2016) showed that to ensure higher efficiency at reduced grinding media wear rate, ball mills should operate between 65% and 80% solids by weight, depending on the ore. Works by Costea *et al*. (2017) and Aguila – Camacho *et al*. (2017) focused on the design of controllers to ensure proportionate ratio of infeed ore and water to obtain optimal slurry density.

Besides key mill control parameters, predicting the optimal slurry residence time and mass hold-up which correspond to efficient grinding warrants undivided attention. Results of Makokha *et al*. (2014) while using a salt tracer to investigate the mean residence time of an industrial ball mill, indicated that residence time is greatly influenced by slurry concentration and ball loading. Earlier works by Vos (2017), which focused on the development of a model to better predict residence time distribution at various operating conditions of the mill, revealed that the mean residence time of slurry in a mill is affected greatly by slurry concentration than ball loading. Other findings included the inverse relationship between the mean residence time and the feed flow rate.

Grinding media size distribution

Grinding media size distribution is very imperative in achieving higher efficiencies in grinding circuits. Works by Kabezya and Motjotji (2015) showed that there are significant variations in mill performance when different ball size diameters are used as well as different proportions of ball size diameters. According to Deniz (2016) and Shahbazi *et al*. (2020), the selection of optimal grinding media can considerably enhance mill performance and reduce operating cost. From empirical studies reported in literature, optimal grinding media loading is estimated to be within the range of 30% to 50% of the total mill charge. However, the right proportion of grinding media sizes plays an integral role in the determination of mill power draw and grinding media wear rate. Some influential factors that should be taken into consideration when selecting grinding media sizes include ore hardness which is always considered as a disturbance and feed particle sizes.

The use of larger ball sizes has benefited from the advantage of providing larger impact forces for breaking larger ores faster, reducing ore grinding time and increasing product throughput but compromises on product particle size, leading to higher circulating loads. Smaller balls on the other hand, suffer from the drawbacks of either not able to break larger ore sizes or take a considerably long time to grind ore into micron fine particles required for downstream processing due to low impact forces exerted by them (Francioli, 2015). Grinding with smaller balls has the tendency to attain desired product particle size which is an advantage but uses more kilowatt hours in the process which is expensive. To ensure efficient grinding in ball mills characterised by higher throughput, lower mill power draw and finer or optimal product particle size, Simba and Moys (2014) and Hlabangana *et al*. (2018) suggested the use of a mixture of different ball sizes to meet the requirements of the different feed material sizes to be ground. According to Tripathy *et al*. (2017), the top make–up size of balls during mono-sized ball selection can be computed using the relation expressed in Equation (2.26):

$$b = \left[\left(\sqrt{\frac{F_{80}}{K}}\, 3\sqrt{\frac{sgWI}{(\%C_s)\sqrt{9.2ID}}}\right)\right] \times 25.4 \qquad (2.26)$$

where, b = diameter of ball make-up in (mm)

F_{80} = the feed size in (μm) (80% passing)

K = a constant which depends on the mill type

sg = the specific gravity of the feed ore

WI = the work index of the feed in (kWhr/t)

% C = the percentage critical speed of the mill in (%)

D = the diameter inside the shell liners in (m)

Works by Tripathy *et al.* (2017) considered the selection of only mono sized balls which has the limitation of not being able to handle varying particle size distributions and this consequently affects grinding efficiency. Other researchers highly appreciated the role of ball charge and wear rate on ball size distribution and the complexity involved with controlling the ball size distribution parameter. Based on valuable insights provided by the works of Chimwani *et al*. (2015), Hassanzadeh (2018b) and Hlabangana *et al*. (2018) from their investigations they concluded that a binary mixture of make-up ball sizes among other factors such as feed size, the product particle size, the mill diameter and the breakage parameters, perform better than a mixture of three ball sizes. The Austin and Klimpel model given by Equation (2.27) was then adopted to investigate the best make-up ball charge distribution at any given time and mill

efficiency. Equation (2.27) is used to represent make-up balls consisting of two balls d_1 and d_2 of mass fraction m_1 and m_2, respectively.

$$P(d) = \begin{cases} \dfrac{d^{4-\Delta} - d_{min}^{4-\Delta}}{Kd_{max}^{4-\Delta} + (1-K)d_2^{4-\Delta} - d_{min}^{4-\Delta}} & ; \ d_{min} \le d < d_2 \\ \dfrac{Kd^{4-\Delta} + (1-K)d_2^{4-\Delta} - d_{min}^{4-\Delta}}{Kd_{max}^{4-\Delta} + (1-K)d_2^{4-\Delta} - d_{min}^{4-\Delta}} & ; \ d_2 < d \le d_1 = d_{max} \end{cases} \tag{2.27}$$

where, P(d) = mass fraction of balls in the load which are smaller than d

K = wear rate parameter

d_{max} = largest ball size in the mill in (mm)

d_{min} = smallest ball size in the mill which is still retained in (mm)

Δ = constant which relates to wear law and determines the steady state of P (d)

To calculate the ball size distribution at any given time, an initial estimate of the wear parameter is made possible by employing the formulae expressed by Equation (2.28) (Chimwani *et al.*, 2015).

$$K = \left[1 + \frac{m_2}{m_1} \left(\frac{d_1}{d_2} \right)^3 \right]^{-1} \tag{2.28}$$

Employing binary ball size distribution, Panjipour and Barani (2018) investigated the effect of ball size distribution on power draw, charge motion and breakage mechanism. Results showed that at a constant mill filling, the power draw was changed with changing the ball size distribution and for all mill fillings, the minimum power draw occurred when the fraction of small balls was between 30% – 40%. The effect of ball size distribution increased with increasing mill filling and for the mill filling of 35%, the ball size distribution had the maximum effect on the power drawn.

2.3.4 Grinding Mill Optimisation: Profit Function

The grinding circuit like any other process has to be operated to maximise profit. According to Zuo *et al.* (2015), the mineral industry is facing increasing challenges in improving comminution energy efficiency and reducing operational cost. Effective optimisation of the mill is needful to improve the product quality, market competition and cut down energy consumption (Niu *et al.*, 2017). The function of the grinding mill is to reduce the infeed ore particle size using grinding media such that the valuable mineral constituent is exposed and

can be recovered in the subsequent flotation operation. For a grinding mill, the profit function can be expressed as given by Equation (2.29) (Ghanei, 2020).

$$Pt^{-1} = \left\{\sigma\left[PSE_c - MFO_c\right] - E_c t^{-1} - F_c t^{-1}\right\} \tag{2.29}$$

where, Pt^{-1} = profit per unit time of the mill (USD)

σ = mill throughput per unit time (USD)

PSE_c = unit cost of desired product (USD)

MFO_c = unit cost of infeed ore (USD)

$E_c t^{-1}$ = cost of energy per unit time (USD)

$F_c t^{-1}$ = fixed cost per unit time (USD)

In order to maximise the profit function, efforts should be geared towards increasing throughput, reducing energy cost and fixed costs associated with the grinding process.

Increased throughput

Low qualified rate of product particle size causes unacceptable economic loss in any comminution process. Increased throughput is usually desired in any mine economic operation for the purposes of profit maximisation. However, increased throughput is largely dependent on grinding efficiency of the mill, sump water addition rate and separation efficiency of the hydrocyclone. Optimum grinding conditions inside the mill are prerequisites to obtain higher throughputs. Besides the higher power consumed during overgrinding which is considered as an inefficiency, production of slimes reduces significantly the total product throughput and consequently the efficiency of recovery in the floatation process. Also, slime production increases drastically the cost of sedimentation in the final tailings discharge from the mill. Undergrinding on the other hand also leads to lower throughputs since ground ore does not qualify to overflow during the separation process in the hydrocyclone. This leads to higher circulating loads which in most cases exceed the 250% optimum acceptable circulating load range according to studies by Yang *et al*. (2017).

Optimisation of parameters such as, ball size distribution, proportionate addition of infeed ore and water to control slurry density and viscosity and residence time distribution is a major leeway to achieve grinding efficiency and consequently yield higher throughputs. Moreover, cyclone inefficiencies may be another reason that account for reduced throughputs. Inappropriate selection of equipment can lead to size classification failure. Works by Botha *et al*. (2015) investigated hydrocyclone modifications to increase product throughput by

employing a non-linear model predictive controller in the switching of the hydrocyclones. Results revealed that higher throughput could be achieved by switching of the hydrocyclones and treating the discrete switching of hydrocyclones as a manipulated variable. Throughput can be increased by regulating hydrocyclone's slurry infeed density. This is possible by optimising sump water addition rate. Effective sump control is critical to stable operation without which, an off specification particle size product and poor flotation performance result thereby reducing product throughput.

Nunan and Delboni Junior (2017) on the other hand studied different mill operating scenarios to ascertain whether installation of new equipment or the optimisation of existing ones could lead to an increase in mill throughput. The studied scenarios were: (1) adding a third ball mill in series with existing two ball mills, (2) adding a third ball mill in parallel with existing mills, (3) adding a vertical mill in series with existing mills and (4) adding High Pressure Grinding Rolls (HPGR) to existing mills. Simulations were carried out on design considerations of the respective circuits, assessing how easy it will be to interface the newly considered scenarios with existing equipment and installations, and finally comparing the energy consumption requirements of the proposed expansion alternatives. Apart from the HPGR alternative, all simulations of the three other scenarios resulted in the required product particle size (P_{80}) without compromising on the capacity. Among the three selected scenarios that showed promising results, the Vertimill alternative showed the smallest energy consumption.

Energy consumption

Energy consumption reduction strategies in the mining industry are on the rise lately, gaining widespread attention due to energy cost increments. According to Abbey *et al*. (2015), energy requirement as well as cost per tonne of ore comminuted increases from blasting (0.43 kWh/t) through crushing (3.24 kWh/t) to grinding (10.0 kWh/t). It can be deduced from the foregoing discussion that, given the large power consumption figures involving grinding in ball mills, a small increase in efficiency in the grinding processes may have a large impact on the operating cost of the plant. This stands to yield a palpable reflection in the profit function in Equation (2.29), as well as on the conservation and optimisation of energy resources (Melero *et al*., 2014).

Energy consumption in a mill relates to net mill power drawn and grinding time through the relationship expressed in Equation (2.30):

$$E = P \cdot t \tag{2.30}$$

where, E = energy consumed (kWh)

P_{Net} = net mill power drawn (kW)

t = grinding time (s)

Minimisation of energy consumption lies in the ability to optimally control mill charge volume which has a direct bearing on power draw and grinding time. Cost of energy per unit time increases as a result of excessive power draw due to running overloaded mills, prolonged grinding time and sometimes, running mills above the optimal speed relative to the critical speed. Works by Esteves *et al.* (2015), Sorgenfrei (2016) and Wang *et al*. (2020) revealed that 40% of charging of grinding media resulted in optimal grinding in ball mills and deviation from this value resulted in increased electric power draw to handle the high load torque exerted on the mill motor. Rupare *et al.* (2013) however, noted from the expression in Equation (2.31) that poor charging practices of grinding media during replenishing was a major cause of running overloaded mills since grinding media constituted a greater percentage of mill load and consequently led to an increment in power draw in ball mills.

$$P = A \times B \times C \times L \tag{2.31}$$

where, P_{Net} = power drawn in a ball mill (kW)

A = factor for diameter inside the shell liners

B = factor for mill type and charge volume (% loading)

C = factor for mill speed expressed as a percentage of mill critical speed

L_c = length of grinding chamber measured between head liners at the junction of the shell and head liners (m)

Soleymani *et al.* (2015) further added that apart from mill ball filling which has a direct influence on power draw, mill speed, slurry volume and solid concentration of mills are contributing factors to power increment as well. The relationship between power draw and these variables are shown in Morrel's net power model of the ball mill and expressed by Equation (2.32) according to King (2012).

$$P_{Net} = \frac{\pi g L N_r r_m}{3(r_m - z r_i)}\left[2r_m^3 - 3z r_m^2 r_i + r_i^3(3z-2)\right] + \left[\begin{array}{l}\rho_c(\sin\theta_s - \sin\theta_T) \\ +\rho_p(\sin\theta_T - \sin\theta_{OT})\end{array}\right] + L\rho_c\left[\frac{N_r r_m \pi}{(r_m - z r_i)}\right]^3\left[(r_m - z r_i)^4 - r_i^4(z-1)^4\right] \tag{2.32}$$

where, P_{Net} = net electric power drawn by the ball mill in kWhr

ρ_c = density of the ball mill charge in (tonnes/m^3)

ρ_p = density of slurry in (tonnes/m^3)

N_r = ball mill speed in (rpm)

L = length of ball mill in (m)

g = acceleration due to gravity (m/s^2)

r_m = ball mill's internal radius in (m)

r_i = ball mill's inner surface radius (m)

θ_S = ball mill shoulder's angular position in (rad)

θ_T = ball mill toe's angular position in (rad)

θ_{OT} = slurry toe angle for grate discharge mills in (rad)

j_t = the ball mill filling (%)

$z = (1 - j_t)^{0.4532}$

Also, reduction in energy consumption can be achieved by reducing the time used in grinding one tonne of ore. Optimisation of this can be met by using a mixture of grinding balls. Larger balls for faster grinds and smaller balls for finer grinds.

Grinding media wear rate

In a continuous mill, grinding balls are replenished to compensate for ball wear inside the mill to ensure efficient grinding (Chimwani *et al.*, 2015). According to observation by Foucher *et al.* (2014), the process of replenishing which is usually done manually at the experience of the mill operator leads to overcharging in most cases. Overcharging is not only undesirable in the energy variable of the profit function in Equation (2.29) but also has adverse effects on the operating cost due to faster wear rate of grinding media.

Sorgenfrei (2016) observed that under normal conditions of the grinding process, the expected wear on the grinding media should be caused by the interaction of the media, water and ore, but due to overcharging, there is increased and rigorous collision between the grinding media resulting in breakage and increased wear. Jankovic *et al.* (2016) on the other hand attributed faster wear rates to ore type. Softer ores accounting for 10 – 15 μm/hr wear and abrasive gold, copper and molybdenum all contributing to 20 μm/hr wear, respectively.

As of 2006, 0.23 billion kg of steel in the United States of America and over 0.45 billion kg in the world were estimated to be consumed each year in wet grinding (Rupare *et al.*, 2013). These

alarming figures are not only inconsistent with sustainable development concepts of responsible consumption but also has a direct impact on the operational cost.

Media milling expenses account for about 37% of the total 50% operational cost associated with the grinding circuit. Hassanzadeh (2015) in his industrial optimisation study on a primary grinding circuit performance at Sarcheshmeh concentrator plant, stated that an average of 750 g/t of steel balls are consumed in the grinding circuit using 80 mm forged steel balls per tonne of ore milled. Results from his study noted that this amounted to more than USD 100,000.00 lost per month for a single mill reflecting about 80% of the total grinding cost.

Ensuing from the enumerated research, a significant reduction in production costs can be achieved if media milling properties (i.e., top ball size, ball size distribution and charge volume) in operating wet ball mills are appropriately optimised (Hassanzadeh, 2017b). Optimisation lies in properly replenishing grinding media to prevent overloading and consequently higher wear rates. This calls for accurate grinding media charge prediction. Also, ore type should be considered when selecting grinding media (ball size diameter) to ensure that they can appropriately handle the intrinsic characteristics of the ore without wearing at a faster rate.

2.4 Prediction of Process Variables

According to Bunker and Thabtah (2019), prediction refers to the output of an algorithm after it has been trained on a historical dataset and applied to new data when forecasting the likelihood of a particular outcome. The algorithm will generate probable values for an unknown variable for each record in the new data, allowing the model builder to identify what that value will most likely be.

The advantages of prediction include the following (Ghasemi *et al*., 2016; Kim *et al*., 2016; Wang and Srinivasan, 2016):

i. Compared with engineering methods, AI-based prediction methods require less detailed physical information of the plant. There is no need for model developer to have high level knowledge of the physical parameters of plant, which in return saves both time and cost for conducting the prediction;
ii. The process of data acquisition and data loading is relatively convenient, which means the prediction model can be easily established; and
iii. AI-based prediction methods provide promising prediction accuracy once the model is well trained.

The demerits of prediction are (Ghasemi *et al*., 2016; Kim *et al*., 2016; Wang and Srinivasan, 2016):

i. There is no explicit relation between the physical plant parameters and model inputs, which makes it impossible to extrapolate energy performance of plant once the design and/or operation of the plant has changed;
ii. The AI-based method is hard to be applied in plant design phase as it requires historical plant performance data to train the prediction model;
iii. AI-based prediction method requires extensive training data for model establishment and maintenance of prediction quality; and
iv. The AI-based prediction model needs to be re-trained once changes are made to the plant envelope, system or operation.

2.4.1 Prediction of Wet Ball Milling Process Variables

Process variables are generally categorised into three broad groups, namely, manipulative variables, state variables and controlled variables. Although there are several input and output process parameters that characterise the ball mill, a few are used for the purpose of modelling, simulations and performance evaluation. The three most often controlled variables in the grinding mill circuit include the product particle size, the slurry level in the sump and the hydrocyclone feed density (Collins, 2016; Hassanzadeh, 2018b). State variables on the other hand include mill load, mill power draw, mill speed, slurry density and viscosity, residence time and wear rate of grinding media and liners (Le Roux *et al*., 2020). Difficulty in the measuring of state variables due to the rigorous internal action of wet ball mills always results in the use of indirect methods to estimate them. Input or manipulative variables such as ore feed rate, infeed water rate, circulating load and balls feed rate are usually considered.

Disturbances that affect the whole grinding circuit and consequently its overall efficiency include change in feed rate and size of ore, change in hardness of ore (grindability), change in sump and infeed water addition which usually result in change in slurry properties (Ebadnejad, 2016; Khodadadi and Ghadiri, 2019). The various parameters grouped under the broad categories are subject to change based on the variables of interest or evaluation. State variables such as mill speed can be considered as manipulative-based when mill is fitted with a Variable Speed Drive (VSD).

So far, a number of predictions on mill operating variables have been researched and duly reported in the literature in recent times. These include the prediction of Residence Time Distribution (Breitung-Faes, 2016; Hassanzadeh, 2017a; Hassanzadeh, 2018a; Shi, 2016),

slurry pool level (Morrell, 2016; Mulenga, 2017a), solids concentration of slurry (Faria *et al*., 2019; Iwata and Mori, 2020), grinding media wear (Abdelhaffez, 2018; Azizi *et al*., 2016; Peng *et al*., 2017). Works on the prediction of mill load and product particle size are summarised in Table 2.1 and Table 2.2, respectively.

Table 2.1 Prediction of Mill Load

SN	Author and Year	Title of Paper	Contribution	Limitation
1.	Mulenga and Bwalya (2019).	Determination of the Formal Powder Filling of a Wet Ball Mill in Open Circuit Configuration.	Predicted powder filling of open circuit overflow mill using three estimation models.	Only one steel ball size was used. Closed circuit was not used.
2.	Pedrayes *et al*. (2018).	Frequency Domain Characterisation of Torque in Tumbling Ball Mills using DEM Modelling: Application of Filling Level Monitoring.	A methodology to predict mill filling level using DEM based load torque spectral analysis under dry grinding conditions.	Wet ball mill was not considered.
3.	Cai *et al*. (2020).	Load State Identification Method for Wet Ball Mills based on the MEEMD Singular Value Entropy and PNN Classification	Use of MEEMD singular value entropy magnitude of cylinder vibration signals and PNN classification to predict the wet ball mill load.	Optimisation of the algorithms was not considered.
4.	Tang *et al*. (2018).	Mechanism Characteristic Analysis and Soft Measuring Method Review for Ball Mill Load based on Mechanical Vibration and Acoustic Signals in the Grinding Process.	Proposed an industrial application of soft techniques in predicting ball mill load.	Power draw was not considered.
5.	Tang *et al*. (2017).	Modelling Mill Load Parameter based on Least Absolute Shrinkage and Selection Operator (LASSO) using Multi-scale High Dimensional Frequency Spectra Data.	Proposed a Mill Load Parameter Forecasting (MLPF) method based on LASSO and Selective Ensemble (SEN) algorithm.	Power draw was not considered.

1. DEM – Discrete Element Modeling
2. MEEMD – Modified Ensemble Empirical Mode Decomposition
3. PNN – Probabilistic Neural Network

Table 2.2 Prediction of Product Particle Size Distribution

SN	Author and Year	Title of Paper	Contribution	Limitation
1.	Tavares (2017).	A Review of Advanced Ball Mill Modelling.	Reviewed literature on the application of models based on distributed collision energy information to predict size reduction in tumbling ball mills.	Power draw was not considered.
2.	Lee *et al*. (2019).	Analysis of Grinding Kinetics in a Laboratory Ball Mill using Population-Balance-Model and Discrete-Element-Method.	Predicted the particle size distribution of ball mills using PBM and DEM methods.	Optimisation of the methods were not considered.
3.	Petrakis and Komnitsas (2017).	Improved Modelling of the Grinding Process through the Combined use of Matrix and Population Balance Models.	Used matrix and population models with MATLAB codes to predict size distribution of grinding products of quartz, marble quartzite and metasandstone.	Power draw was not considered.
4.	Gharehgheshiagh *et al*. (2017).	Investigation of Laboratory Conditions Effect on Prediction Accuracy of Size Distribution of Industrial Ball Mill Discharge by using a Perfect Mixing Model. A Case Study: Ozdogu Copper-molybdenum Plant.	Use of matrix and energy models to predict the particle size distribution of industrial ball mill discharges.	Power draw was not considered.
5.	Chimwani and Hildebrandt (2019).	Modelling of an Open Mill with Scalped Feed for the Maximum Production of a Desired Particle Size Range.	Development of a mathematical grinding simulation model to obtain highest production by optimal combination of ball filling mill speed and energy consumption.	Closed circuit ball mill and minimal grinding media charge were not given consideration.
6.	Fragnière *et al*. (2018).	Predicting Effects of Operating Condition Variations on Breakage Rates in Stirred Media Mills.	Successful experimentation of the breakage rates in wet operated stirred mills.	Wet ball mill circuit and power draw were not considered.

Table 2.2 Cont'd

7.	Rocha *et al*. (2018).	Predicting the Particle Size Distribution from a Laboratory Vertical Stirred Mill.	Designed a model to predict the response of particle size distribution in vertical stirred ball mill.	Wet ball mill circuit and power draw were not considered.
8.	Davey (2017).	Prediction of the Performance of Regrind/Floatation Circuit using Laboratory Tests and Quantitative Mineralogical Information.	Investigated three regrind circuits and predicted the product particle size distribution and mineralogy from process audits.	Power draw was not considered.
9.	Wentao *et al*. (2019).	Research on Prediction Model of Ore Grinding Particle Size Distribution.	Predicted the particle sizes of cassiterite polymetallic sulfide ore and lead-zinc ore based on the drop weight test, batch grinding test of media motion in ball mill and population balance model.	Power draw was not considered.
10.	Rosales-Marin *et al*. (2019).	Study of Lifter Wear and Breakage Rates for Different Lifter Geometries in Tumbling Mill: Experimental and Simulation Analysis using Population Balance Model.	Prediction of product particle size distribution of tumbling ball mill for different lifters and critical speeds.	Power draw was not considered.

PBM – Population Balance Model

Further prediction of mill operating variables is looked at in Section 2.4.2 in terms of mill power draw and grinding media consumption.

2.4.2 Review of Related Works on Grinding Media Charge and Mill Power Draw Predictions

This section reviews recent researches on the mill with regard to prediction of mill power draw and grinding media consumption. Morrell (2016) reported on the structure of a slurry pool level-based power draw predictive model developed by Citic SMCC Process Technology Pty Ltd for tumbling autogenous, semi-autogenous and ball mills. Model was tested using a large operational data. Validation of model was based on comparison of measured and predicted power draws. The overall power draw was obtained as an addition of power draws of slurry and grinding media phases and so served as the contribution of the paper. The slurry phase

volume was dependent on discharge system design, volume occupied by the grinding media and slurry flow rate. In this very work, neural networks known for accurate predictions were not utilised. Also, grinding media consumed were not predicted alongside prediction of the power drawn. Overcharging of grinding media results in ball-to-ball collisions giving rise to higher power draw and resultant less use of it to cause actual size reduction in the tumbling ball mill.

Cleary and Owen (2018) developed models to predict power draw of a generic 8.4 m diameter semi-autogenous mill using charge slope, mill operating parameters (fill level, lifter height and mill speed) and 3D Discrete Element Modelling (DEM) simulations. Parametric models were used for validation. Once again, prediction of grinding media consumption as well as the ball mill were not considered.

In the prediction of power draw of semi-autogenous mill using hybrid Genetic ANN (GANN), Hoseinian *et al*. (2018) avoided long experiments by considering seven operating parameters namely feed moisture, mass flowrate, mill load cell mass, mill solid percentage, inlet and outlet water to the mill and work index. Sensitivity analysis on the parameters was conducted. Authors however failed to predict grinding media consumption alongside the prediction of power draw. Also, grinding media wear rate was not considered and this research was not conducted for the ball mill.

In a review paper on the effects of grinding media geometries on tumbling mill performance factors, Shahbazi *et al*. (2020) made clear the fact that shoulder and toe positions in a tumbling mill are dependent on the type of media and surface area used and, cylpebs draw less power compared to the relatively more used spherical steel balls. According to the authors, the grinding energy and steel media consumption constitute 40% of milling costs. This underlines the fact that the two factors should be predicted together for effective analysis.

Larsson *et al*. (2020) considered among others power draw of wet comminution in stirred media mills. Their approach involved modelling of slurry using Particle Finite Element Method (PFEM), modelling of grinding media using the DEM and modelling of mill structure by way of Finite Element Method (FEM). Power draw was calculated after prediction of slurry motion and grinding media. Indirectly, power draw was predicted together with direct prediction of grinding media consumption. These however, were not accomplished for the tumbling wet ball mill lest to make use of data on operational variables. Furthermore, direct prediction of the power draw could serve as a better option compared to its indirect determination.

Avalos *et al*. (2020) predicted semi-autogenous mill energy consumption or power draw making use of real-time operating data on feed tonnage, bearing pressure and spindle speed in machine learning and deep learning environments where six methods were studied and Recurrent Neural Networks (RNN) was strongly recommended. This study in the first place was not conducted for the tumbling wet ball mill. Secondly, influencing factors such as ore hardness and grinding media wear rate were not considered.

A Random Forest (RF) power draw predictive model was accomplished for an iron ore processing, constant speed, industrial overflow discharge ball mill plant by Tohry *et al*. (2020) to overcome setbacks of empirical stepwise regression-based models. The ten parameters used in variable importance measurement determination using RF in developing the model were power draw, feed rate, ball charge, F_{80}, work index, P_{80}, water weight, slurry weight, volumetric flow rate of slurry to the mill and ball consumption. They declared grinding media consumption and work index as most important factors. A coefficient of determination value of 0.98 was achieved. It is important to predict two variables simultaneously, namely power draw and grinding media consumption. This could enable exploitation of the possibility of grinding at minimum values of the two input variables.

With regard to prediction of grinding media consumption, Petrakis *et al*. (2017b) investigated population balance modelling based simulation of the grinding of quartz and then identified optimal mill operating parameters for use in prediction of the optimal ball filling volume of mill. Authors however did not predict mill power draw alongside the prediction of filling volume. Also, in the determinations, ball size and other operating variables such as ore hardness and grinding media wear rate were not considered.

Diaz *et al*. (2018) experimentally predicted grinding media consumption of three Chilean copper sulphide ores using empirical and predictive models that considered ore grindability, operational variables (pulp pH and grinding time) and ore mineralogy. The advanced mineral characterisation techniques used to estimate the grinding media consumption included reflectance spectroscopy, X-ray diffraction and portable X-ray fluorescence. They concluded that the pH of pulp and ore grindability greatly influence grinding media consumption. In this paper however, authors could not give equal attention to the simultaneous prediction of mill power draw.

The grinding media consumption and work index are considered as very important variables that influence grinding media consumption (Tohry *et al*., 2020) and mill power draw. Additionally, throughput or ore feed rate merit equal attention. Much of the time, practices at

the milling plant give rise to increasing the throughput for the sake of profitability. From the related works, few publications considered all of these three highly influential variables. More importantly, hardly any publication predicted the mill grinding media consumption and power draw to establish further clarity with regard to the prediction.

2.5 Summary and Research Gap

This chapter gave an elaboration on some comminution theories and concepts of the wet ball mill and mill grinding efficiency. Works relating to the prediction of wet ball mill process variables were extensively reviewed. A major development from the reviewed literature established that steel media and grinding energy contributed greatly to the overall economics of the grinding process. Yet, little work has been done with regards to establishing the optimal combination of these variables. Therefore, the prediction of the right amounts of the aforementioned influential parameters presented cost savings opportunities. Prediction of optimal grinding media charge for a possible minimal power draw using historical plant data and investigation of the effect of changes in plant throughput, ore hardness and grinding media wear rate on power draw and grinding media demand constitute a glaring research gap that merits further research.

The focus of this research work is to develop a non-linear ANN-based predictive model of optimal grinding media charge of the wet ball mill with consideration of a possible minimum power draw.

CHAPTER 3

PREDICTIVE MODELS OF THE MILL POWER DRAW AND PRODUCT PARTICLE SIZE

3.1 Introduction

This chapter focuses on the development of ANN-based models to determine appropriate charging of grinding media with regard to mill power draw and product particle size. The chapter expounds on the wet ball mill grinding circuit, data collection and interpretation, models development and the prediction of power draw and the product particle size. Three major ANN predictive models and Adaptive Neuro – Fuzzy Inference System (ANFIS) are employed in MATLAB/Simulink software version 2019b environment for the prediction.

3.2 The Wet Ball Mill Grinding Circuit

Fig. 3.1 shows the ball mill grinding circuit under consideration.

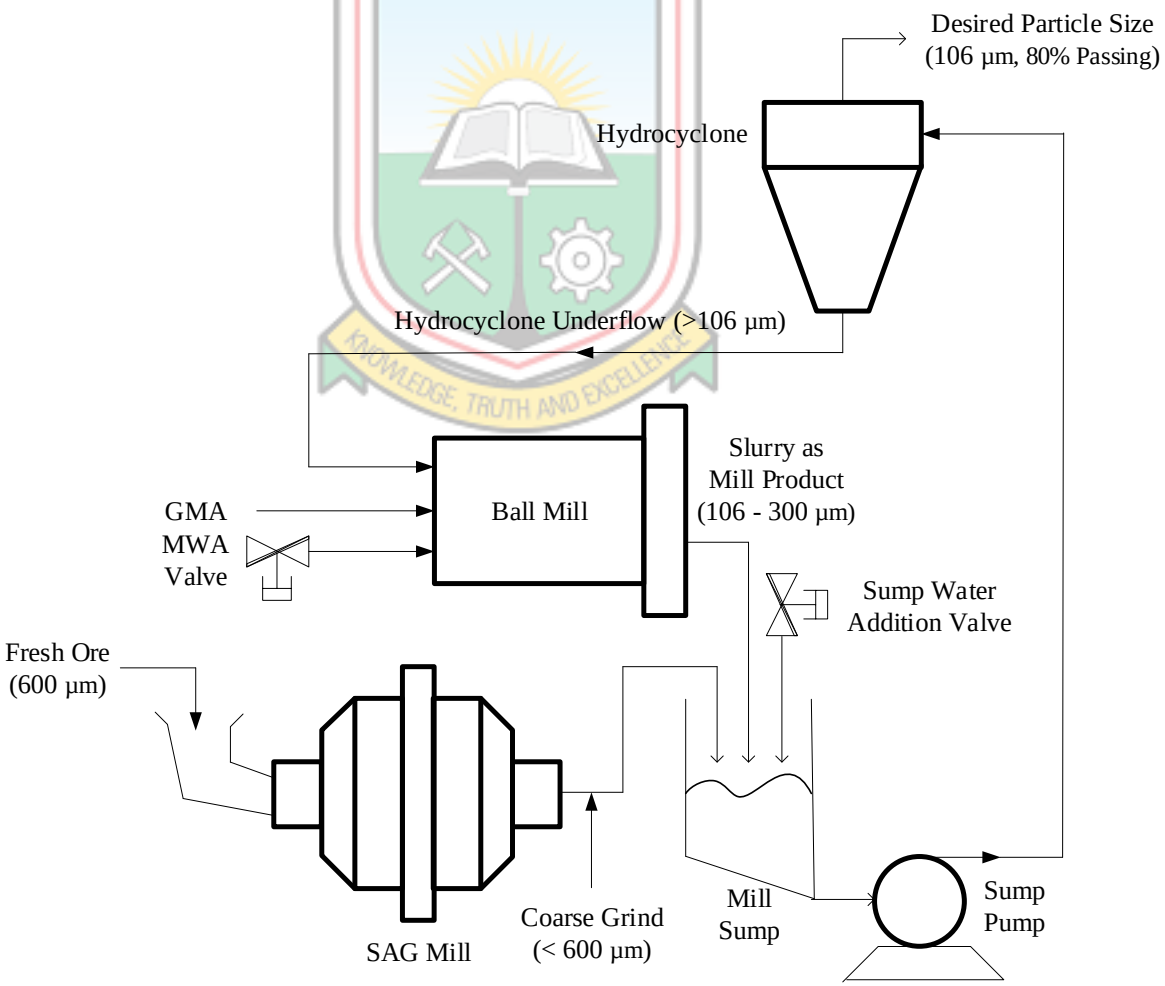

Fig. 3.1 The Wet Ball Mill Grinding Circuit

For better recovery rates, a product particle size of 106 μm is always expected at the overflow for downstream processing. The process is also qualified as a reverse process, since the ball mill receives its infeed from the underflow of the hydrocyclone. The hydrocyclone in the circuit initially receives its feed from the SAG mill through the mill sump. After the classification process, coarse ores greater than 106 μm to 600 μm are fed to the ball mill. In a single stage circuit, the underflow from the hydrocyclone to the ball mill is known as circulating load. The infeed from the hydrocyclone to the ball mill is by gravity action and regulated by the rate of classification of the hydrocyclone. The faster the hydrocyclone classifies its infeed, the more ore is fed into the ball mill. The 5.8 MW rated ball mill motor drives the 6.1 m by 9.0 m grate discharge ball mill through a gear coupling arrangement. The motor drives the ball mill at 75% of the critical speed which is 13.1 rpm to prevent centrifuging and enable grinding to take place. The mill sump receives ground ore from the ball mill discharge and with the help of the sump pump, the ground ore is pumped to the hydrocyclone for classification.

The grinding media charge process of the considered circuit is not automated. Mill operators with the help of a crane help replenish the ball mill with Hi – chrome steel balls. The chart presented in Fig. 3.2 (Gupta and Yan, 2016) is used by mill operators to determine the proportion of grinding media size distributions to use to ensure effective grinding at the start of the mill.

Ball diameter Inches		5.0	4.5	4.0	3.5	3.0	**2.5**	2.0	1.5	1.25	1.0	0.5	0.25
	mm	127.0	114.3	101.6	88.9	76.2	**63.5**	50.8	38.1	31.8	25.4	12.7	6.4
5.0	127.0	17.0											
4.5	114.3	25.0	16.0										
4.0	101.6	20.0	30.0	20.0									
3.5	88.9	15.0	21.5	32.0	22.0								
3.0	76.2	10.0	14.0	21.0	35.0	26.0							
2.5	**63.5**	**6.4**	**9.1**	**12.5**	**19.0**	**36.0**	**32.0**						
2.0	**50.8**	**3.8**	**5.4**	**8.6**	**14.6**	**22.0**	**39.0**	**38.0**					
1.5	38.1	2.8	2.4	3.4	5.3	9.2	**16.5**	35.0	28.0				
1.25	31.8		1.6	1.2	2.0	3.2	**6.1**	13.0	36.0	30.0			
1.0	25.4			1.3	1.0	1.7	**2.9**	6.4	16.0	32.0	22.0		
0.5	12.7				1.1	1.9	**1.4**	3.1	8.0	14.5	52.0	24.0	
0.25	6.4						**2.1**	4.5	12.0	23.5	26.0	76.0	100.0

Fig. 3.2 Ball Charge Distribution during Mill Start-Up

A mixture of grinding balls of different sizes is needed to ensure that after the bigger balls with the larger impact have reduced ore bearing rocks to smaller sizes, the smaller balls will continue the size reduction. Also, the smaller balls are usually employed to fill the cavities or spaces in-between the larger diameter balls.

In reading Fig. 3.2, the column and the row labelled “mm” is the approximate possible ball size. The approximate highest ball size is usually identified and traced to the “inches” column, the value on the “inches” column is then traced downward to know the percentage composition by weight of the various ball sizes that should be used for the start of the mill.

The highest ball size used at the plant is 60 mm. Based on the approximate ball size traced, from the highlighted numbers on Fig. 3.2, it means the charge distribution during the start should be in the following proportions, 32% of 60 mm balls, 39% of 50 mm balls, 16.5% of 38 mm balls, 6.1% of 30 mm balls, 2.9% of 25 mm balls, 1.4% of 12 mm balls and 2.1% of 6 mm balls.

However, it is the bigger ball size that is always charged with the assumption that, as they wear, they do so into the sizes of the specified smaller balls. All things being equal, replenishing is supposed to be composed of only the bigger balls since the balls that wear are to fill in for the other smaller balls. Mill operators have to determine the right distribution of ball sizes to replenish at some points in time so as to prevent excessive power draw due to overcharging. At the same time, proper grinding need to be ensured to attain the required product particle size. However, replenishing is done at a constant rate of 8 tonnes a day (6 tonnes of 60 mm balls and 2 tonnes of 50 mm balls). The constant nature of the charging practice has the tendency to increase the overall mill content above the 35% filling since the estimated rate of wear is not constant. The current research work seeks to develop a data-based model establishing the relationship between the input and output variables using the collected data and investigating how parameter variations influence charging of the grinding media for desirable electric power draw and the product particle size.

3.3 Data Collection and Interpretation

Data on important parameters that affect the performance of the mill were gathered for a period of 18 months for the purpose of this research. Information on key design parameters was obtained from manufacturers’ manuals of the systems used in the mine for validity and reliability purposes. Operational data on crucial parameters that affect the performance of the mill were also obtained from the metallurgical department of the mine.

The data collected on operational parameters were basically structured since they were highly organised. In all, 520 data points were collected over the period considered. The data points captured were the average values of the recordings measured within the three shifts run in a day. The operational parameters taken into consideration included the ones that had the tendency to alter the two competing needs, namely, the power draw and the product particle size percentage passing. Power draw was measured with a Wattmeter while product particle size percentage passing was determined by output samples that were taken at regular intervals to the mineral laboratory for testing. The various input parameters that were considered included, Total Tonnes Milled (TTM), Tonnes per Hour Milled (TPH), Mill Infeed Water (MIW), 60 mm Balls (GM_{60}), 50 mm Balls (GM_{50}), Total Grinding Media (TGM), Grinding Media Wear Rate (GMWR) and Bond Work Index (BWI).

Power draw and product particle size passing through a benchmark criterion were used to locate optimal points within the dataset to determine the state of the charge. Windows of data trends were captured and analysed.

3.3.1 Manufacturer's Design Data

The ball mill parameters, mill motor and grinding media specifications are provided in Table 1, Table 2 and Table 3, respectively.

Table 3.1 Ball Mill Parameters

SN	Parameter	Value
1.	Effective Length of Mill	9.0 m
2.	Effective Diameter of Mill	6.1 m
3.	Speed of Mill	13.1 rpm
4.	Mill Load (Volumetric Fill)	35%
5.	Mill Solid Concentration	75% solids and 78% solids
6.	Fresh Ore Hardness	16.5 kWh/t
7.	Hydrocyclone Overflow	40% solids and 45% solids
8.	Hydrocyclone Underflow	80% solids and 85% solids
9.	Feed Ore Size	80% passing 600 μm
10.	Product Particle Size	80% passing 106 μm

(Source: Datasheet)

Table 3.2 Mill Motor Specifications

SN	Parameter	Value
1.	Motor Rated Power (kW)	5800
2.	Power Factor	0.89
3.	Operating Power Range (kW)	4000 – 4500

(Source: Datasheet)

Table 3.3 Grinding Media Parameters

SN	Parameter	60 mm Balls	50 mm Balls
1.	Grinding Media Type	Hi – chrome Steel Balls	Hi – chrome Steel Balls
2.	Charge Rate	Daily	Daily
3.	Average Quantity of Grinding Media Charged (kg)	6 000	2 000
4.	Average Wear Rate (kg/t)	0.7	0.7
5.	Mass of Steel Balls per Tonne Milled (kg/t)	1	1

(Source: Datasheet)

3.3.2 Operational Data

The operational data presented in the form of plots in Fig. 3.3, Fig. 3.4, Fig. 3.5 and Fig. 3.6 are snapshots of the months of October 2017 and February 2018 are trends selected from the entire dataset presented at Appendix A. The selection was done in a way to capture the most dominant operational trends that existed in the dataset for the purpose of analysis.

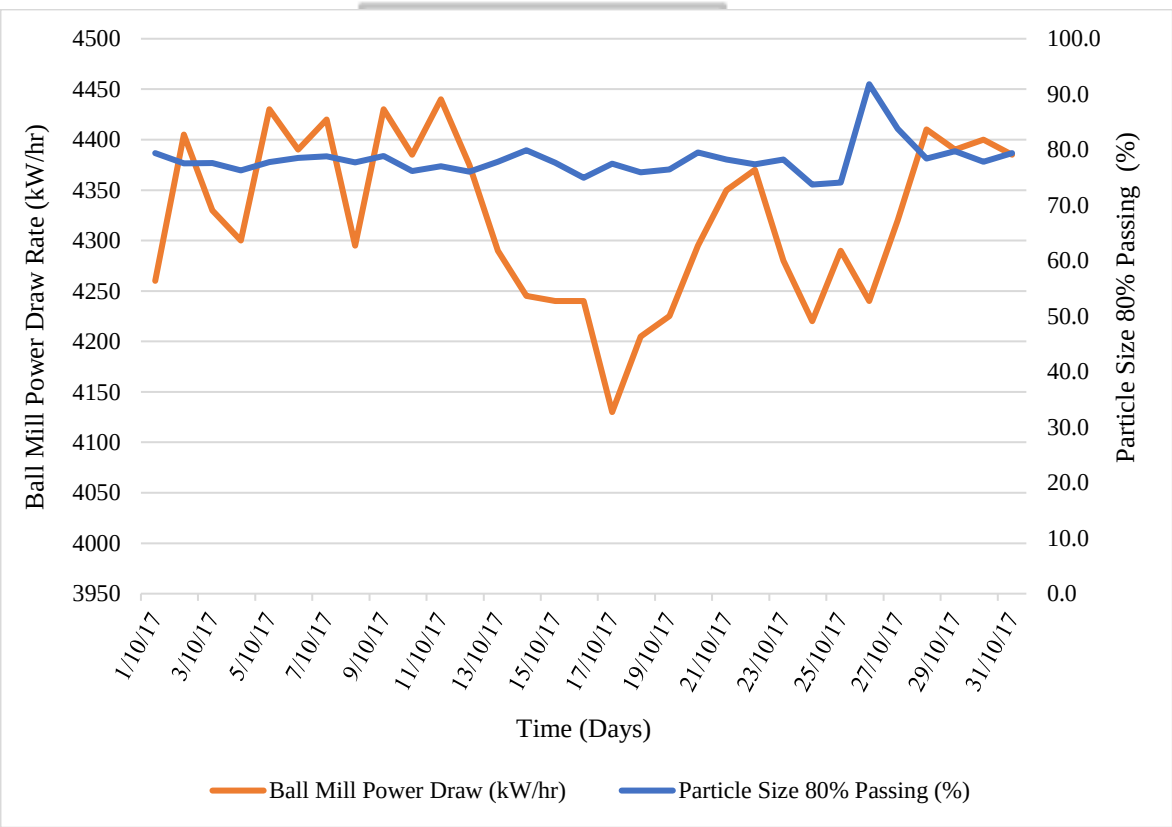

Fig. 3.3 A Graph of Power Draw and Percent Particle Size Passing versus Time for October 2017

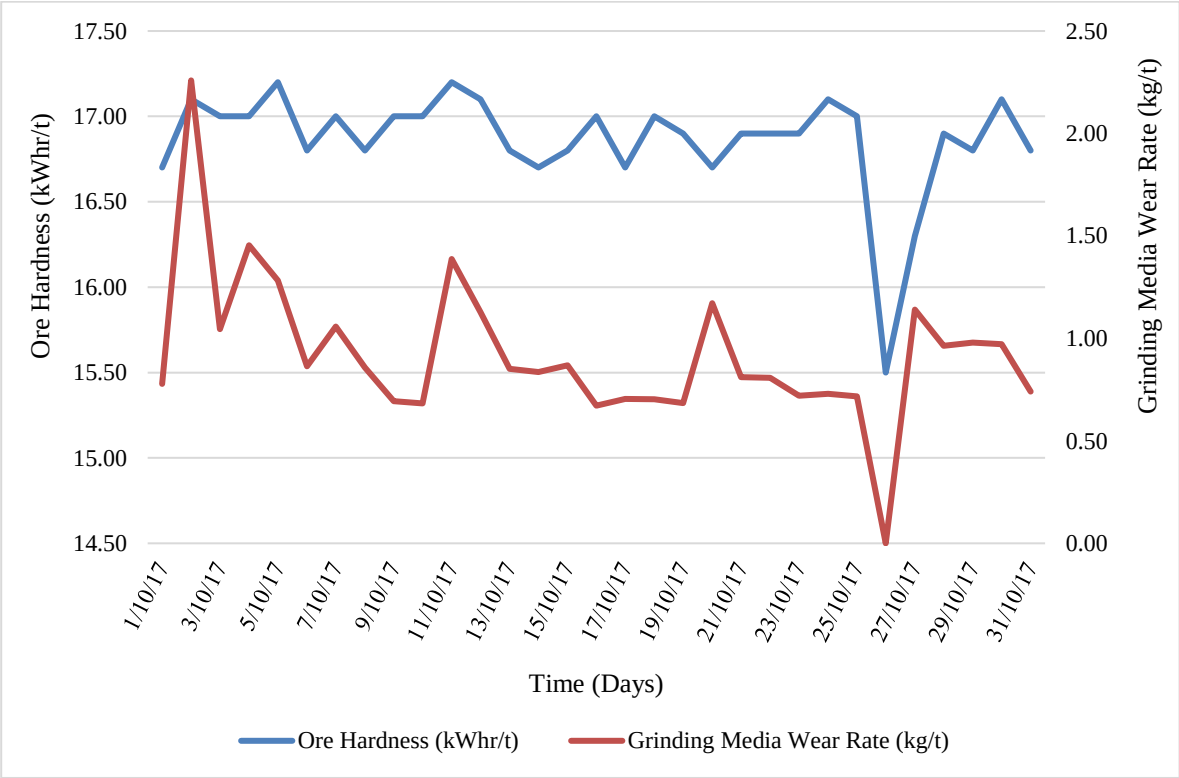

Fig. 3.4 A Graph of Ore Hardness and Grinding Media Wear Rate versus Time for October 2017

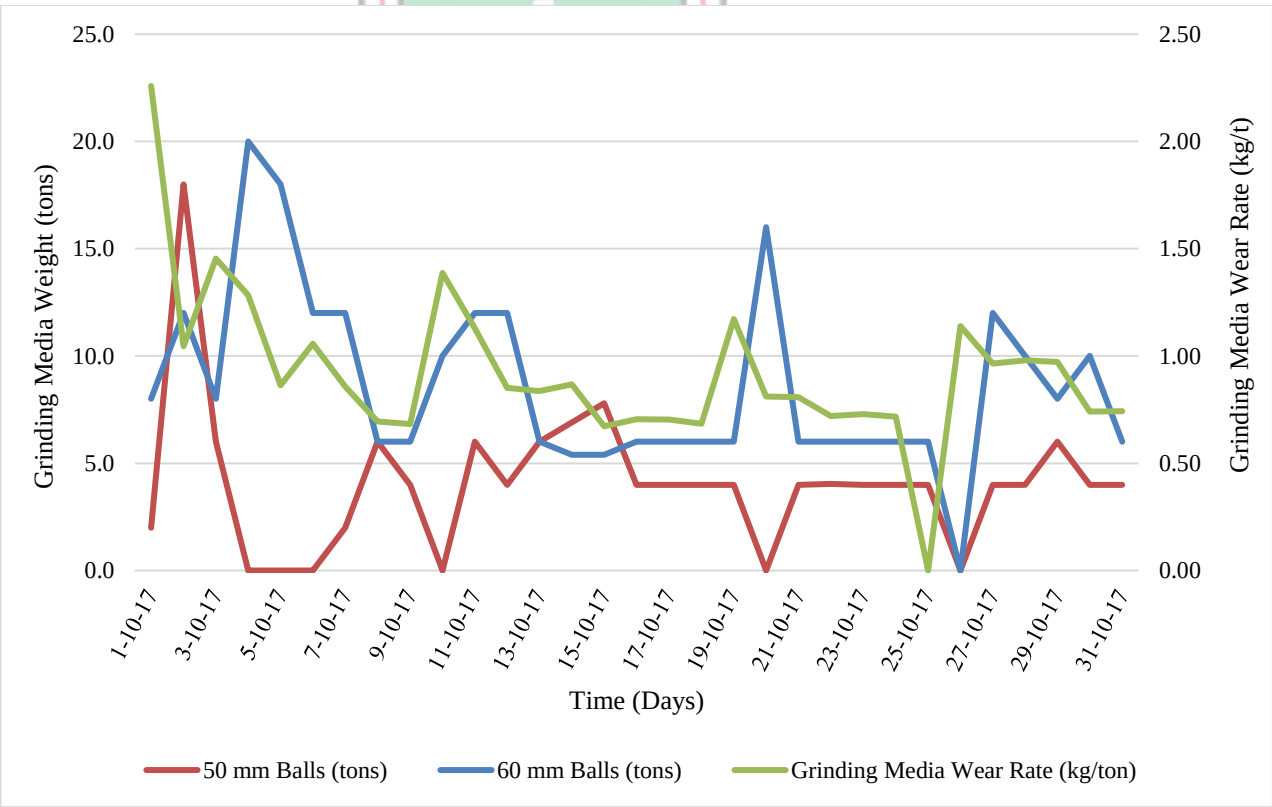

Fig. 3.5 A Graph of Grinding Media Charged and Wear Rate versus Time for October 2017

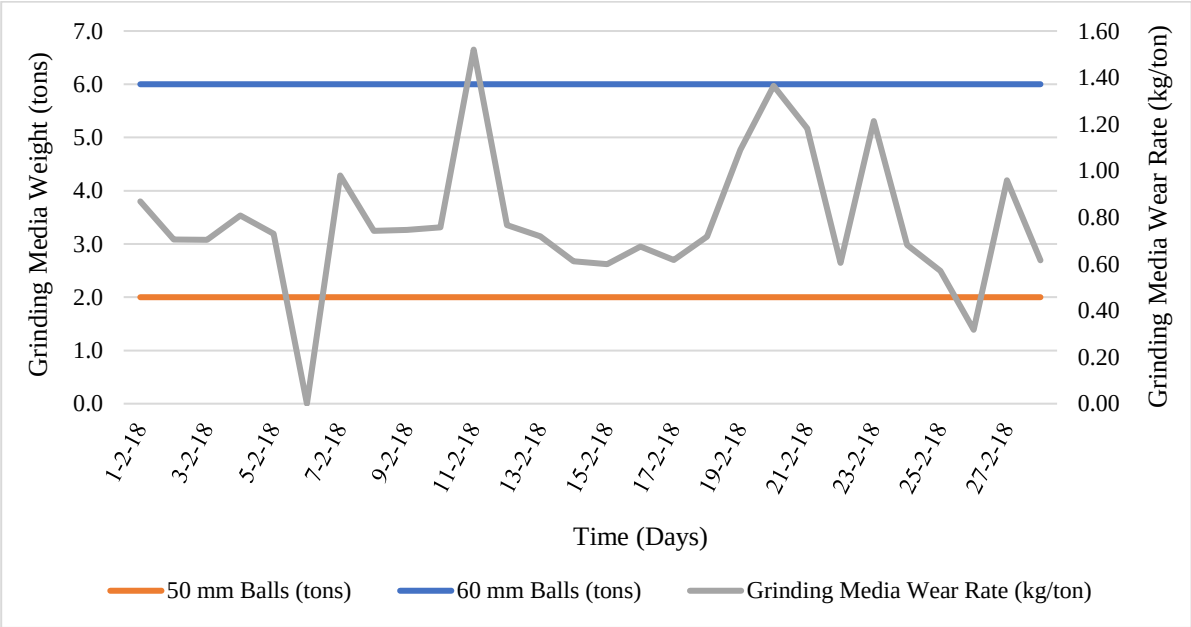

Fig. 3.6 A Graph of Grinding Media Charged and Wear Rate versus Time for February 2018

3.3.3 Data Interpretation

For the purpose of interpretation, data for the month of October 2017 and February 2018 were randomly selected and visualised to better appreciate the major trends existing in the dataset and underlying reasons for those trends.

Power draw as seen by Fig. 3.3 remains a critical parameter that needs to be given due attention just as particle size 80% passing and above remains a non-negotiable parameter since its importance cannot be underestimated. From Fig. 3.3, power draw for the month of October 2017 varied in the range from 4130 kW/hr to 4440 kW/hr. However, power draw variations from the dataset presented in Appendix A for the entire period under consideration varied between 2000 kW/hr and 5000 kW/hr. From empirical studies, it can be deduced that the erratic and wide variation in the power draw as evidenced by the collected data is dependent on a number of dominant parameters such as mill load or charge volume, mill speed, effective diameter and effective length of the grinding chamber. To a greater extent, the latter three parameters outlined are constants, meaning the power draw is proportional to the mill load or charge volume. Cumulatively, mill load is the sum of infeed ore, infeed water and grinding media.

Proportionately, grinding media constitute a greater percentage of the entire mill load. Empirical studies again establishes that 40% load by volume of grinding media results in optimum operation. It can then be inferred that, the current practice of charging grinding media manually at the experience of the mill operator may have the tendency of exceeding the

optimum set limit of 40% load by volume thereby leading to an increased mill load. Unstable mill load as a result of improper charging practices can be attributable to the great variations existing in the presented graph of Fig. 3.3. Though grinding media constitute the greater percentage, the other factors such as mill infeed and mill water can considerably be major contributors to the confirmed power variations.

Finally, the variations of the ore hardness as presented in Fig. 3.4 is another possibility that could contribute to the erratic power variations. Ore hardness can influence greatly the daily power draw. From Fig. 3.4, highest ore hardness of 17.25 kWhr/t occurred on 11/10/2017 and the least hardness was 15.5 kWhr/t of 27/10/2017. The corresponding power draws from Fig. 3.3 were 4445 kW/hr and 4240 kW/hr, respectively. The harder ore drew more electric power compared to the softer ore. However, there were underlying trends that deviated from this normal observation.

The product particle percentage size varied between 70% and 90% for both the cross section of the data that was visualised and the entire data. However, the dataset had a lot of the data points lying between the range of 74% and 83%. Variations of the particle percentage size can be hypothesised as caused by changes in the ore hardness and also either undercharging or overcharging of grinding media. The higher the ore hardness, the more resistant the ore is to grinding and the lower the ore hardness, the less resistant it is to grinding. From Fig. 3.3, there is a peculiar trend worth noting though it is not a dominant trend for most parts of the dataset presented in Appendix A. The particle percentage size recorded on the 26/10/2017 was above 90%. A quick trace onto Fig. 3.4 for the same day gave ore hardness to be around 15.5 kWhr/t which happens to be the lowest value recorded within the dataset. Lower ore hardness resulted in higher product particle percentage size passing the 106 μm.

Fig. 3.4 shows a plot of hardness of ore and grinding media wear rate with time in days for the month of October 2017. It can be deduced from the plots that there was a corresponding trend of the two parameters over the period under review. Ore hardness is a crucial parameter and always considered as a disturbance in most analyses. It can be deduced from the trend shown by Fig. 3.4 that the higher the ore hardness the higher the wear rate. This trend is so because, more collisions are required in reducing size of harder ore. More collisions as a result of harder ores resistance to grinding result in greater wear of the grinding media. Ideally, the charging of grinding media should correspond to the wear rate to augment for the proportions of wear encountered during the abrasion process.

Fig. 3.5 and Fig. 3.6 presented the grinding media charged and the wear rate for the days of the month of October 2017 and February 2018, respectively. It can be realised from the plot of Fig. 3.5 that the wear rate varied so irregularly with the balls that were charged on a daily basis. All things being equal, the amount of grinding media by weight that should be charged should be done in such proportion to compensate for the wear of balls inside the mill as a result of abrasion between the balls and the ore. This is needful to ensure that the stipulated overall mill weight is not exceeded or drastically reduced as these affect the mill efficiency.

Deducing from the trend over the period considered, it can be seen that the grinding media charged varied alongside the wear rate as the days went by, though a significant corresponding trend was not observed. The aforementioned observations leave the tendency to hypothesise the possibility of undercharging or overcharging existing within the plant system. However, an interesting trend in Fig. 3.6 can be seen as an observation which further consolidates the mentioned hypothesis. The charging of the 60 mm and 50 mm balls were replenished at a constant rate of 6 tons of 60 mm and 2 tons of 50 mm daily. However, a critical look at the corresponding grinding media wear rate sees a varying trend. It clearly shows that the grinding media were not replenished in a way that augmented the abrasive wear of balls inside the mill and therefore the tendency to overcharge the mill is very high.

3.4 Methodology of Predictive Model Development

The non-linear model of grinding media charge between the input and output variables is realised in this research by employing ANN-based algorithms in the training and validation of the model. The proposed model is developed with the two major competing output parameters taken into consideration from plant operations: that is, mill power draw and product particle size. Parameters such as infeed ore, water addition rate, grinding media size distribution, wear rate and bond work index are considered as input variables to the model. The Bond work index determines the grindability of the ore which relates to ore hardness. The input parameters are selected based on the fact that they contribute significantly to the overall mill weight which in turn increases the power drawn and affects the grinding efficiency of the mill.

A criterion is developed to determine the actual power required to progressively reduce an ore bearing rock from a particular size to another. The Bond equation gives the ideal power required to reduce an ore of a higher size to a lower size and it is also employed to determine the range of optimality of power drawn during the whole reduction process. The product particle size requirement of 80% passing to be 106 μm is also considered as well in the determination of optimal data sets within the model. A supervised learning approach is then

employed, making use of both the input and the output data points. The model learns and generalises the input – output non-linear relationship to predict the average power draw and product particle size expected. The set of input variables which will satisfy the competing needs of product particle size and mill power draw are considered as Optimal Charging Practice (OPC) and those set of input parameters that fall outside the criteria are considered as Non-optimal Charging Practice (NCP). Fig. 3.7 gives a representation of the proposed predictive models.

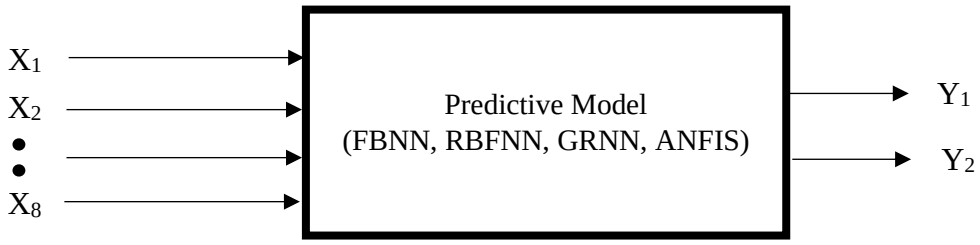

Fig. 3.7 A Representation of the Proposed Predictive Models

Inputs are as follows:

X_1 = Total Tonnes Milled (TTM)

X_2 = Tonnes per Hour Milled (TPH)

X_3 = Mill Infeed Water (MIW)

X_4 = 60 mm Balls (GM_{60})

X_5 = 50 mm Balls (GM_{50})

X_6 = Total Grinding Media (TGM)

X_7 = Grinding Media Wear Rate (GMWR)

X_8 = Bond Work Index

The outputs are:

Y_1 = Power Draw (PD)

Y_2 = Product Particle Size (PPS%)

Machine learning is the art and science of giving machines the ability to learn and make decisions from data without being explicitly programmed. That is to say, they have the ability to learn from a system without having prior knowledge of the system.

The first method looked at in this section is the modelling of the non-linear relationship that exists between the input-output ball mill parameters using the collected data. This requires learning through the multidimensional search space of the training data given to the algorithm. Learning is complete when an approximate best fit is achieved between the input and output variables. Also, tuning of model is conducted to improve the performance of the developed model after it has been tested against test data. The performance of the model is measured by its generalisation ability. After the collection of sufficient data which is the main resource in the development of the proposed model, overcharging and undercharging of the wet ball mill

is investigated. The steps of model development from data collection to the investigation are summarised in Fig. 3.8.

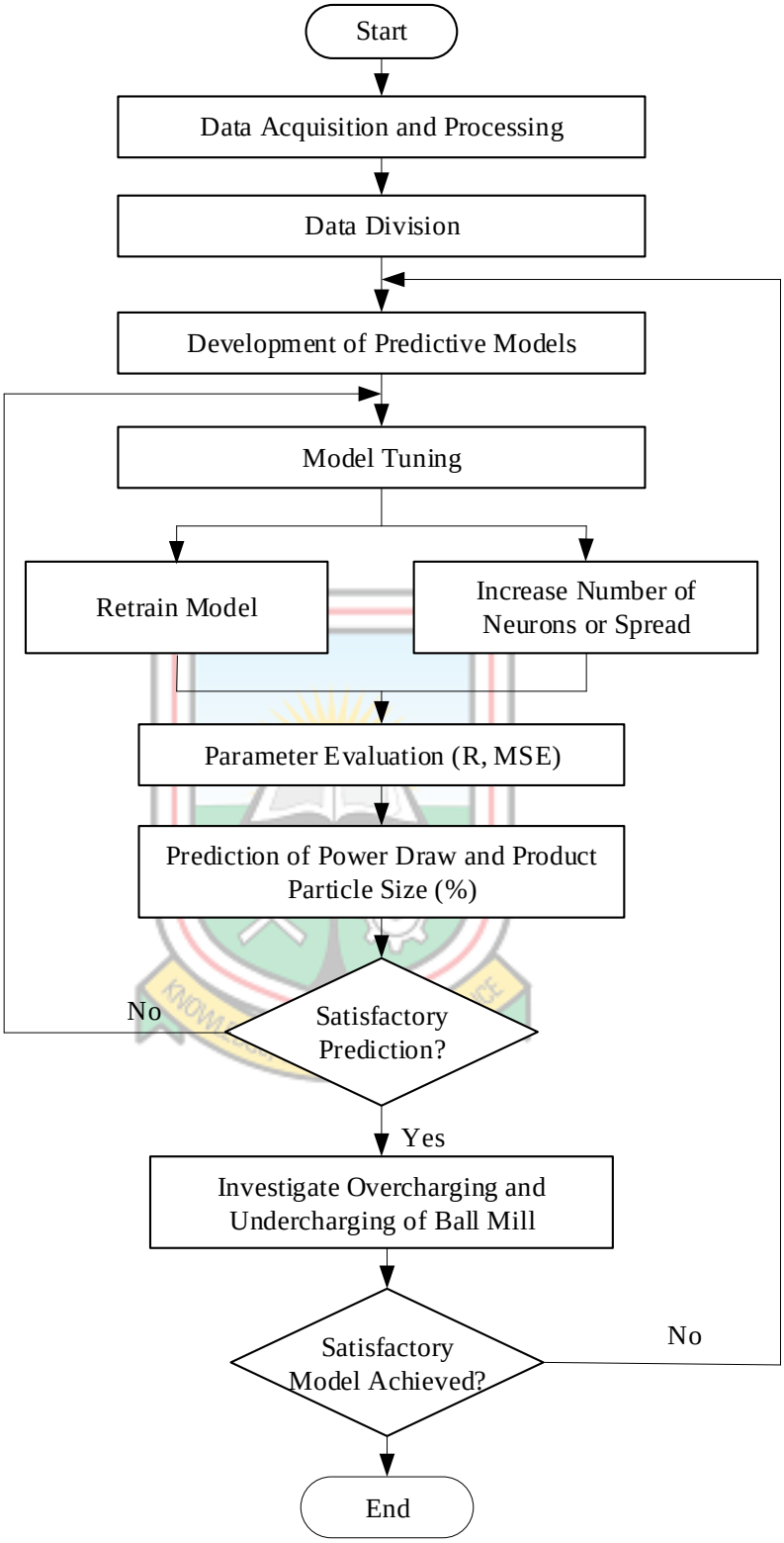

Fig. 3.8 The Design Methodology of Models Development

3.4.1 Data Acquisition and Processing

Data on the input and output variables were acquired and interpreted as presented in Section 3.3. Data pre-processing is an important task, because it affects the degree of accuracy of the learning process. It cannot be underestimated since unprocessed data to a greater degree can hinder the learning ability of the best learning algorithms. Data during the collection stage can usually be utterly noisy and mostly characterised by a lot of missing points in the dataset. Missing data can usually be entirely eliminated or extrapolation is done to fill in for the missing data.

A crucial assumption to ensure that meaningful information is derived from input – output data is that changes in output are solely affected by the input and not some form of noise or disturbances that exist in the data. Cleaning the data to remove underlying trends and major outliers is very crucial to ensure that the data collected represented the process dynamics to a greater extent. Abrupt changes in data points due to downtimes and sudden trips were as well removed to eliminate misleading trends that were likely to be captured during the learning process.

Looping through the collected data, due to the variations of the distinct datasets, normalisation of the data was done to ensure that the dataset was well scaled to be understood by the activation functions. Banadaki *et al*. (2015) affirmed that normalisation of data in the pre-processing stage is very crucial in improving the accuracy of predictive models. Equation (3.1) (Banadaki *et al.*, 2015) shows the mathematical relationship between the normalised data point and the original data point.

$$X_N = \frac{X - X_{min}}{X_{max} - X_{min}} \tag{3.1}$$

where, X_N = normalised data point

X = original data point

X_{min} = minimum value of the data point

X_{max} = maximum value of the data point

3.4.2 Data Division

The pre-processed data were basically divided using default division techniques in MATLAB software environment. The default division techniques divide the data into 70% training data and 30% testing data. The main rationale for this division is to give more room for the models to learn and be able to generalise well. The more the data that is allocated for the training phase, the better the generalising ability of the model.

3.4.3 Development of the Predictive Models

The ball mill grinding circuit is characterised by a lot of non–linear dynamic processes which make it difficult to establish accurate relationships between the variables using conventional means such as statistical methods. ANN from empirical literature has proven to be very robust in the establishment of nearly accurate relationships between input – output parameters which have strong presence of non-linearity. As widely accepted by the intellectual caucus, ANN development is basically in two major phases: Training phase where the model is realised and the prediction phase where the model is tested against a new set of data. Four architectures are employed in the model realisation, namely, Feedforward Back Propagation Neural Network (FBNN), Radial Basis Function Neural Network (RBFNN), General Regression Neural Network (GRNN) and Adaptive Neuro-Fuzzy Inference System (ANFIS). Fig. 3.9 shows the flowchart of the ANN-based model development process.

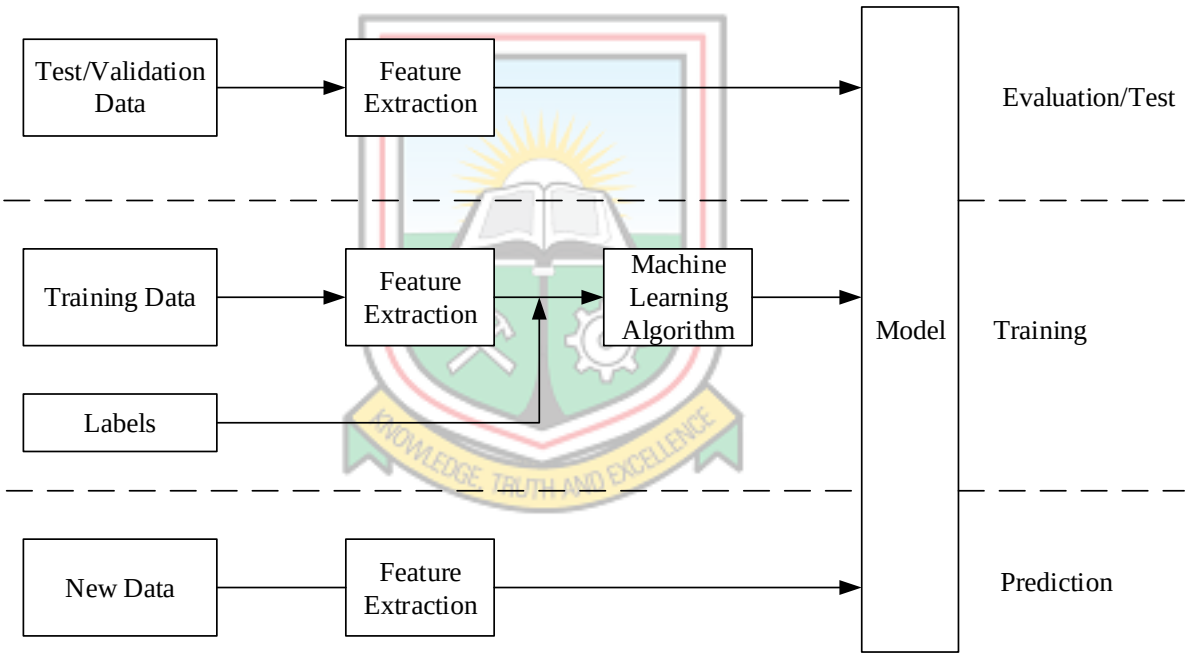

Fig. 3.9 Flowchart of the Model Development Process

Feedforward backpropagation neural network model

The FBNN is a type of ANN that uses the back-propagation algorithm to train its network. It is largely dependent on the error correction rule. The error correction rule primarily consists of forward computing and backwards learning. In forward computing, the feedforward network takes a set of inputs through the input layer and connects them to a set of nodes known as the hidden layer before finally giving an output in the output layer. Equation (3.2) (Gajawada, 2019) gives the mathematical relationship between the input layer and the hidden layer.

Equation (3.3) (Gajawada, 2019) gives the output of the hidden layer after an activation function was applied to it.

$$H_j = \sum_{i=0}^{n} x_{ij} w_j + b_0 \tag{3.2}$$

where, H_j = input to the hidden layer

x_{ij} = inputs from the input layers

w_j = weight indicating the effect of that input variable

b_0 = bias

$$Y_j = \frac{1}{1+e^{-H_j}} \tag{3.3}$$

where, Y_j = transformed hidden layer by the activation function

The backwards learning starts from the output and calculates the error between the output result and the target value and computes the error from each connection back through the various layers to the input layer to adjust both the weights and the biases for another forward computing cycle. Equation (3.4) (Gajawada, 2019) shows the calculation of the error correction during the backwards learning rule of the FBNN algorithm.

$$E_T = \sum_j E_j = \sum_j \frac{1}{2}\left(T_j - Y_j\right)^2 \tag{3.4}$$

where, E_T = total error in the feedforward loop

E_j = error contributed by the jth output neuron

Y_j = output value of the jth output neuron

T_j = desired value of the jth output neuron

The initialised weights and biases are adjusted during each iterative cycle to ensure minimum deviation between the computed output and target values. This key feature of FBNN underscores its learning ability. The learning process according to Al – Masri (2019) is the method of fine-tuning the weights of a neural net based on the error rate obtained in the previous epoch (i.e. iteration). Proper tuning enables reduced error rates and makes the model reliable by increasing its generalisation.

The FBNN was realised using the neural network toolbox in Matlab software version 2019b environment. In employing the FBNN for predicting power draw by the ball mill, the sensitive parameters that contribute significantly to the power drawn are taken into consideration. Input

parameters outlined in the legend of Fig. 3.7 are used as both inputs and outputs for the model realisation stage.

Fig. 3.10 shows the architecture of the FBNN. The total number of neurons were varied between 10 and 100 and a graph of performance of the model against increased neurons was also plotted. The Levenberg-Marquardt algorithm was used in the training process.

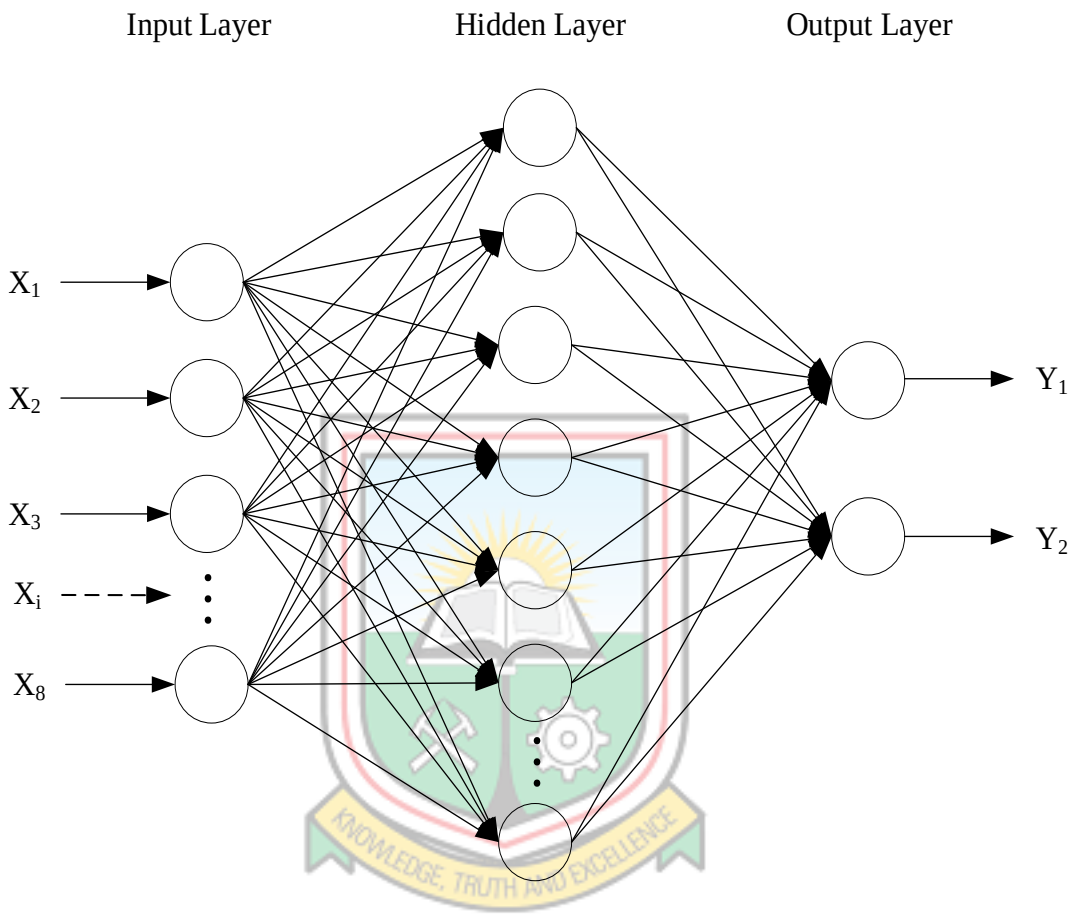

Fig. 3.10 The Architecture of FBNN

Radial basis function neural network model

RBFNN is an ANN that uses radial basis function as the activation function. The distinctive factor of the RBFNN is the network architecture and its activation function. Activation function influences the outputs of processing nodes significantly and usually achieves this by using established mathematical formulae. The formulae have the ability to relate input variables to output variables without compromising on any non-linearity that exists between the input and output relationships.

RBFNNs in their basic form are feedforward networks which have one–way connections commonly employed for prediction and non-linear function fitting. They are always considered

as the preferred choice for the aforementioned functions because of their universal approximation capabilities. Generally, Radial Basis Function (RBF) is represented mathematically as given by Equation (3.5) (Dias *et al*., 2019).

$$G\left(\left\|X-\mu_c\right\|\right) \tag{3.5}$$

where, G = positive nonlinear symmetric radial function

X = input pattern

μ_c = center of the function

In its basic form, it is a three-layered feed forward neural network made up of an input layer, a single hidden layer and an output layer. RBFNN provides a powerful technique for generating multivariate, non-linear mappings. Each RBFNN neuron stores a "prototype", which is just one of the examples from the training data set.

Architecturally, the RBFNN has input vector **X** (X_1, X_2, X_3, …, X_8), radial basis functions φ_i (φ_1, φ_2, φ_3, …, φ_8), weights (w_1, w_2, w_3, …, w_8) and an output (**y**). The input layer transmits inputs from the environment external to the hidden layer without any weight connections. Each hidden layer neuron possesses a radial basis activation function which accounts for the non-linear processing element in the hidden layer. Fig. 3.11 depicts the architectural layout of the RBFNN.

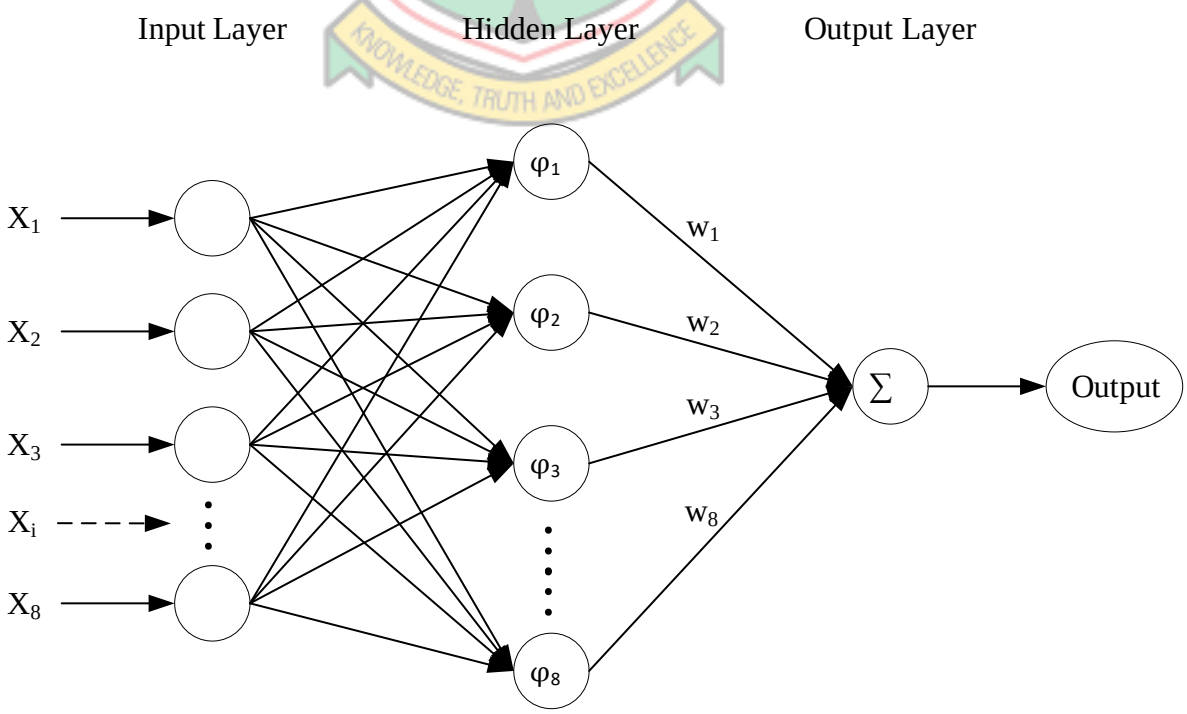

Fig. 3.11 The Architectural Layout of the RBFNN

In the use of the RBFNN for the modelling of the wet ball mill grinding process, the Gaussian function was used in the hidden layer. This is because the Gaussian function has a normal distribution curve or in most instances what is known as the bell curve shape. According to Del Rosario *et al*. (2016), use of the Gaussian function for the modelling of real-world problems is justified by the fact that the function is local in its response and it is more acceptable than most other functions. Equation (3.6) (Chandradeven, 2017) depicts the mathematical representation of the Gaussian function.

$$G(x) = \exp\left(-\frac{(x-\mu_r)^2}{\sigma_r^2}\right) \tag{3.6}$$

where, G(x) = output of the gaussian function with input x

x = input variable

μ_r = center of the radial function

σ_r = radius of the radial function

Each neuron performs the computation expressed by Equation (3.6) that is calculating the Euclidean distance from each input object to the center of the Gaussian function. The choice of the number and centre of the RBF is a very important consideration in RBFNN. The most natural choice was employed to train the dataset, that is, letting each data point in the training set correspond to a basis function centre.

The output of the hidden layer and the output layer are related by way of Equation (3.7) (Chandradeven, 2017). The overall goal of the RBFNN training session is to reduce the error between the predicted output and the actual output. This is achieved by variations of the connection weights and centers of the radial functions.

$$\hat{y}_p = b + \sum_{j=1}^{N} w_{ij} \bullet G(x) \tag{3.7}$$

where, $\hat{y}_p$ = predicted output

w_{ij} = weights applied to the output of the hidden layer

b = bias

N = number of neurons in the hidden layer

G(x) = output of the hidden neuron

Generalised regression neural network model

The GRNN employs a single pass training algorithm in its network development process. It has gained widespread attention over the past years because of its fast learning abilities in

approximating relationships between output and input parameters hence, its suitability for online systems. The basic architecture of a GRNN consists of a four-layer network: The input layer, the pattern layer, summation layer and the output layer. The pattern and summation layers constitute the hidden layer in the case of GRNN.

Entries from the input layer in the form of data points are primarily distributed to the neurons in the first hidden layer (pattern layer). The pattern layer basically contains nodes which help in the processing of the data it received from the input layer. Each node in the pattern layer performs the computation of subtracting the input layer vector, X_i from the vector assigned to the node X_j. The results from the computation are then squared by the node and multiplied to a non-linear kernel which is usually an exponential function (Del Rosario *et al*., 2016).

The second hidden layer known as the summation layer has only two neurons which receive inputs from the pattern layer for a one output architecture. One of the two neurons in the summation layer outputs a summation of the weighted output while the other neuron outputs a summation of the unweighted output of the pattern neurons. Equation (3.8) and Equation (3.9) (Arthur *et al*., 2019) are the parameters employed in the summation of the unweighted and the weighted outputs, respectively.

$$\sum_{i=1}^{n} \exp\left(-\frac{D_i^2}{2\sigma^2}\right) \tag{3.8}$$

$$\sum_{i=1}^{n} Y_i \bullet \exp\left(-\frac{D_i^2}{2\sigma^2}\right) \tag{3.9}$$

Finally, the output layer is a quotient of the two neurons from the summation layer to predict the final value, $\hat{Y}$. Equation (3.10) (Arthur *et al*., 2019) depicts the relationship between the two neurons in the hidden layer to produce the final predicted value.

$$\hat{Y}(X) = \frac{\sum_{i=1}^{n} Y_i \bullet \exp\left(-\frac{D_i^2}{2\sigma_s^2}\right)}{\sum_{i=1}^{n} \exp\left(-\frac{D_i^2}{2\sigma_s^2}\right)} \tag{3.10}$$

where, $\hat{Y}(x)$ = final predicted value

n = total number of neurons in the pattern layer

D = the Euclidean distance between the ith input variable and the ith neuron centre

σ_s = smoothing factor (spread)

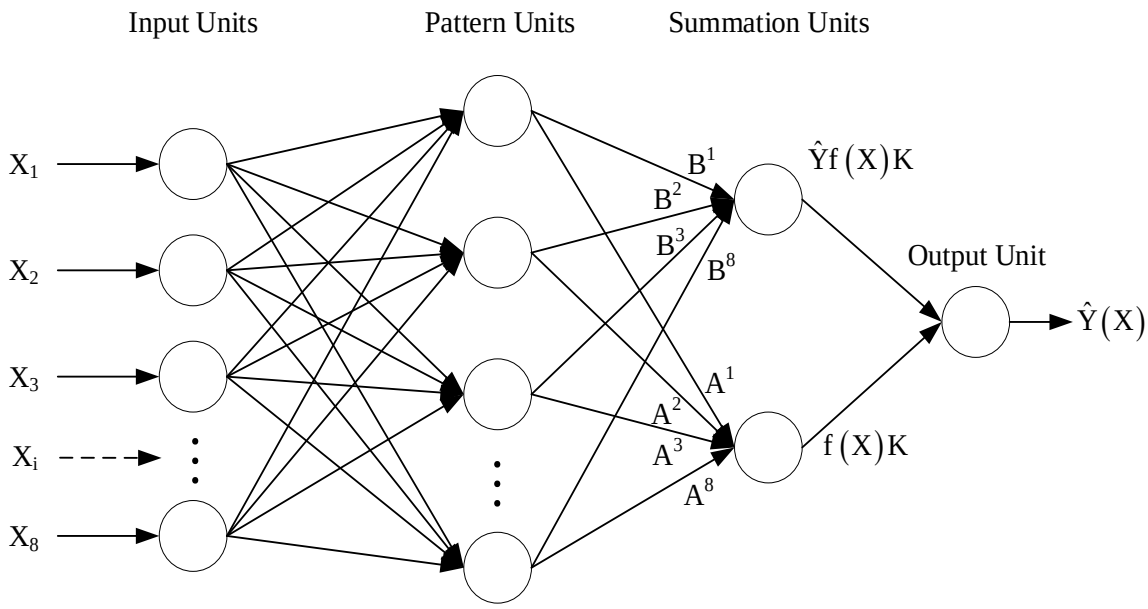

Fig. 3.12 Architectural Layout of the GRNN

In employing GRNN in the development of a model for the grinding media charge, the batch mode method was used. The batch mode method allows the use of observable data collected over a period of time in the training process. In other words, it makes use of data in the offline mode (non-real time data) in the training process which requires a great chunk of datasets to be able to establish accurate relationship between the input and output values. The 520 observable data points which were collected over the period of 18 months were divided into training dataset, and testing data set. Input and output data to the GRNN included parameters outlined in the legend of Fig. 3.7. After the training stage, the trained model was validated using random samples from the validation dataset to ascertain its performance. An average of the validation error was calculated using the k–fold technique. The generalisation ability of the developed model was then tested against the testing data that was employed. A "for" loop function was employed to loop between the 0 and 1 whiles checking the spread that produces a least error between the predicted and the actual values.

Adaptive neuro-fuzzy inference system model

ANFIS is a type of artificial intelligence technique which leverages both the advantages of fuzzy logic system and ANN framework to enhance model performance. ANFIS incorporates the learning ability of the ANN architecture to tune the fuzzy parameters in the fuzzy logic framework. ANFIS empirically eliminates manual enhancement of fuzzy framework parameters and hence, is noted for high accuracy. Apart from the high accuracy, modelling with ANFIS is usually a preferred option because it gives the advantage to know how each input variable influences the final output variable. This is made possible by using the rule

viewer. However, one major drawback of the ANFIS architecture is its inability to handle multiple output parameters (Egrioglu *et al*., 2014).

Generally, the basic structure of a standard ANFIS architecture is presented in Fig. 3.13 (Seesara and Gadit, 2015). Equations (3.11) to (3.16) show the mathematical relationships between the various layers. In Layer 1, the node output is the membership function for the input variables *x* and *y*. The node output of Layer 2 is the product of membership functions for each variable which is called the firing strength. The node output in Layer 3 is a normalised firing strength. The adaptive node is represented by the fourth layer and finally, the summation of all the rules' output is done in Layer 5.

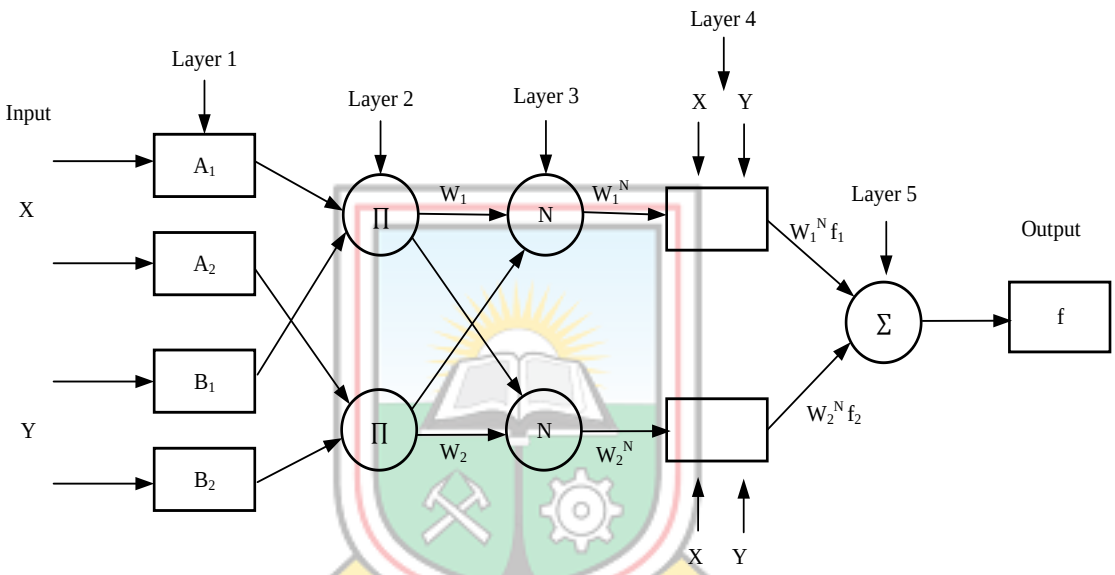

Fig. 3.13 Architectural Layout of ANFIS

The crisp inputs *x* and *y* to the node of the first layer and the output O_{1i} of this node are defined as in Equation (3.11) (Ewees and Elaziz, 2018; Ewees *et al*., 2017).

$$O_{1i} = \mu A_i(x),\ i=1,2,\ O_{1i} = \mu B_{i-2}(y),\ i=3,4, \tag{3.11}$$

where, A_i and B_i = the membership values of the generalised Gaussian membership function

The Gaussian membership function is expressed by Equation (3.12) (Handoyo and Efendi, 2019; Radhakrishna *et al*., 2017).

$$\mu(x) = e^{-}(x - \frac{p_i}{\sigma_i})^2 \tag{3.12}$$

where, p_i and σ_i = the premise parameters

In the second layer, the node's output is the firing strength of a rule given as in Equation (3.13) (Ewees *et al*., 2017; Khalil *et al*., 2018).

$$O_{2i} = \mu A_i(x) \times \mu B_{i-2}(y) \tag{3.13}$$

The node's output in the third layer is the normalised firing strength given by Equation (3.14) (Barman *et al*., 2016; Khalil *et al*., 2018)

$$O_{3i} = \bar{w}_i = \frac{\omega_i}{\sum_{(i-1)}^{2} \omega_i} \tag{3.14}$$

The node in Layer 4 is an adaptive node and its output is computed using Equation (3.15) (Barman *et al*., 2016; Khalil *et al*., 2018)

$$O_{4,i} = \bar{w}_i f_i = \bar{w}_i (p_i x + q_i y + r_i) \tag{3.15}$$

where, p_i, q_i and r_i = the consequent parameters of the node i.

In the last layer, there exists only one node whose output is computed by using Equation (3.16) (Barman *et al*., 2016; Khalil *et al*., 2018).

$$O_5 = \sum_i \bar{w}_i f_i \tag{3.16}$$

In the realisation of the ANFIS model, the ANFIS GUI in Matlab software 2019b software version was employed. Due to the limitation of ANFIS in handling multiple output parameters, both power draw and product particle size were developed separately. Fig. 3.14 and Fig. 3.15 present the development process in both the training and the testing phases. Configuration parameters used in the development process are presented in Table 3.4. Model performance results are presented in Section 3.6.

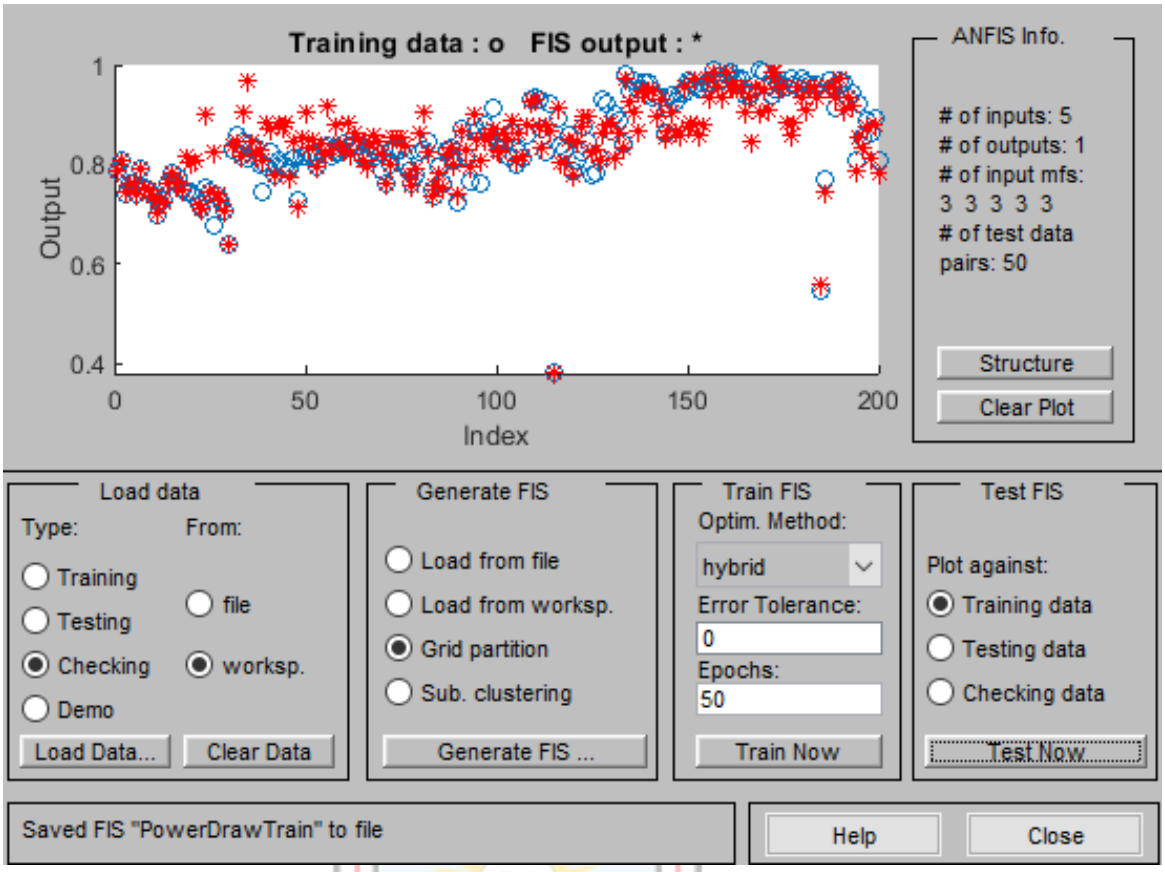

Fig. 3.14 Model Training Interface with Mill Power Draw as Output

Fig. 3.15 Model Training Interface with Product Particle Size as Output

Table 3.4 presents a summarised form of the training configuration parameters used in the development of the predictive models.

Table 3.4 Summarised Configuration Parameters

SN	Parameter	Value /Unit
	FBNN	
1.	Inputs Variables	8
2.	Output Variables	2
3	Training Algorithm	Levenberg – Marquardt
4.	Performance Metric	MSE, R
5	Number of Neurons	10 – 100
	RBFNN	
1	Input Variables	8
2.	Output Variables	2
3.	Sum Squared Error Goal	0.02
4.	Spread Constant	0.1 – 1
5.	Performance Metric	MSE, R
6.	Activation	Gaussian Function
	GRNN	
1.	Input Variables	8
2.	Output Variables	2
3.	Spread Constant	0.1 – 1
4.	Performance Metric	MSE, R
5.	Input Variables	8
	ANFIS	
1.	Error Tolerance	0
2.	Number of Iterations	50
3.	Performance Metric	MSE
4.	Optimisation Method	Hybrid

3.4.4 Prediction of Mill Power Draw and Product Particle Size

After the development of the models, predictions were done using the various models developed to ascertain how well they performed using 151 datasets from the test data presented as in Table B.1 of Appendix B. Graphs of predicted results using the models above were also "Actual Data" presented in section 3.6.1.

3.5 Investigation of Overcharging and Undercharging the Wet Ball Mill

To establish the validity of the hypothesis that undercharging and overcharging of grinding media has direct effect on power draw and product particle size, the best model is used to investigate two major scenarios that affect the power draw and the product particle size of the ball mill considerably. The two major scenarios investigated are outlined.

3.5.1 Overcharging Scenarios

The overcharging scenarios formulated are based on the assumption that, the number of infeed balls to the mill are increased at an incremental order while all other parameters remain constant. At a constant throughput averaged from the collected data, the average ore infeed rate was calculated to be 600 t/h. Considering a constant throughput, the mill filling in percentage will be increased, since greater percentage of the mill volume will be occupied by the grinding media

3.5.1 Undercharging Scenarios

Similarly undercharging scenarios were equally formulated based on the assumption that the infeed balls to the mill are decreased at an incremental order while all other parameters remained fairly constant. Still considering a throughput of 600 t/h, decreasing the grinding media balls fed into the mill reduces considerably the overall mill filling.

Results of the overcharging and undercharging scenarios and their effects on product particle size and mill power draw are presented in Section 3.6.

3.6 Results and Discussions

This section presents the results of the performance of the ANN predictive models based on the evaluation metrics used for the purpose of evaluation. The Mean Square Error (MSE) and Correlation Coefficient (R) were the two major evaluation metrics used to compare the accuracy of the predictive models in matching predicted values to actual values. MSE as an evaluation metric is basically the average squared difference between outputs and targets.

Mathematically, MSE is represented by Equation (3.11) (Dias *et al.*, 2019)

$$\mathrm{MSE} = \frac{1}{N}\sum_{i=1}^{N}\left(\hat{y}_i - y_i\right)^2 \tag{3.11}$$

where, $\hat{y}_i$ = predicted value of ith data

y_i = real value of the ith data

In the evaluation of the predictive models using MSE, the model with the least MSE is always considered as the better predictor since its squared difference between the predicted value and the actual value is very small. The lower the MSE, the better the predictive model. A model which has zero MSE, means it accurately predicted output values given a certain set of inputs without any error.

R on the other hand measures the correlation between the output and the target variables. The model with an R value closer to 1 is always considered as a better model. It is considered a better model because there is a close relationship between the predicted value and the real value.

3.6.1 Results of Model Performance

This section presents the performance graphs of the four developed models based on their MSE and R. It also captured the performances of the models during the iterative stages in search of more accurate models. Finally, graphs of predicted and actual values versus time in days were also plotted to observe the performance of the developed models using test data. The graphs are presented as in Fig. 3.16 to Fig. 3.27.

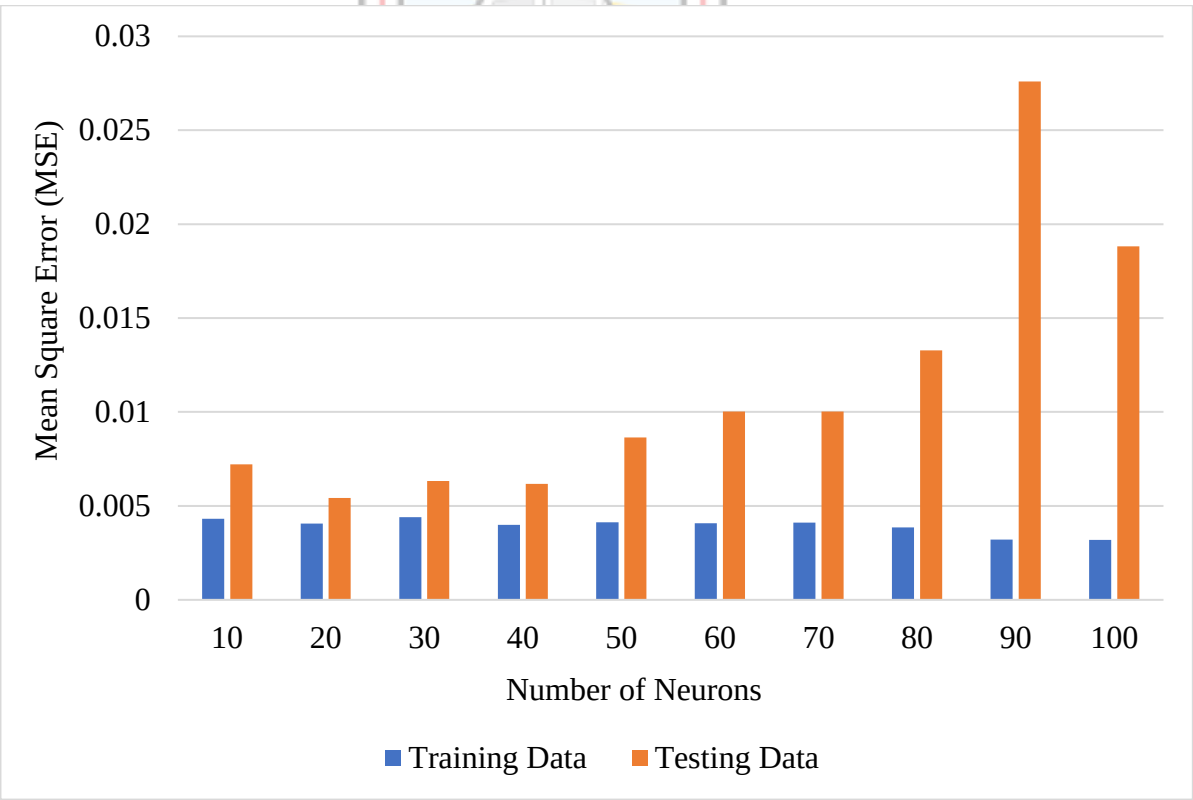

Fig. 3.16 A Graph of Mean Square Error Performance of FBNN against Number of Neurons

Fig. 3.17 A Graph of Correlation Coefficient Performance of FBNN against Number of Neurons

Fig. 3.18 A Graph of Mean Square Error Performance of RBFNN against Spread

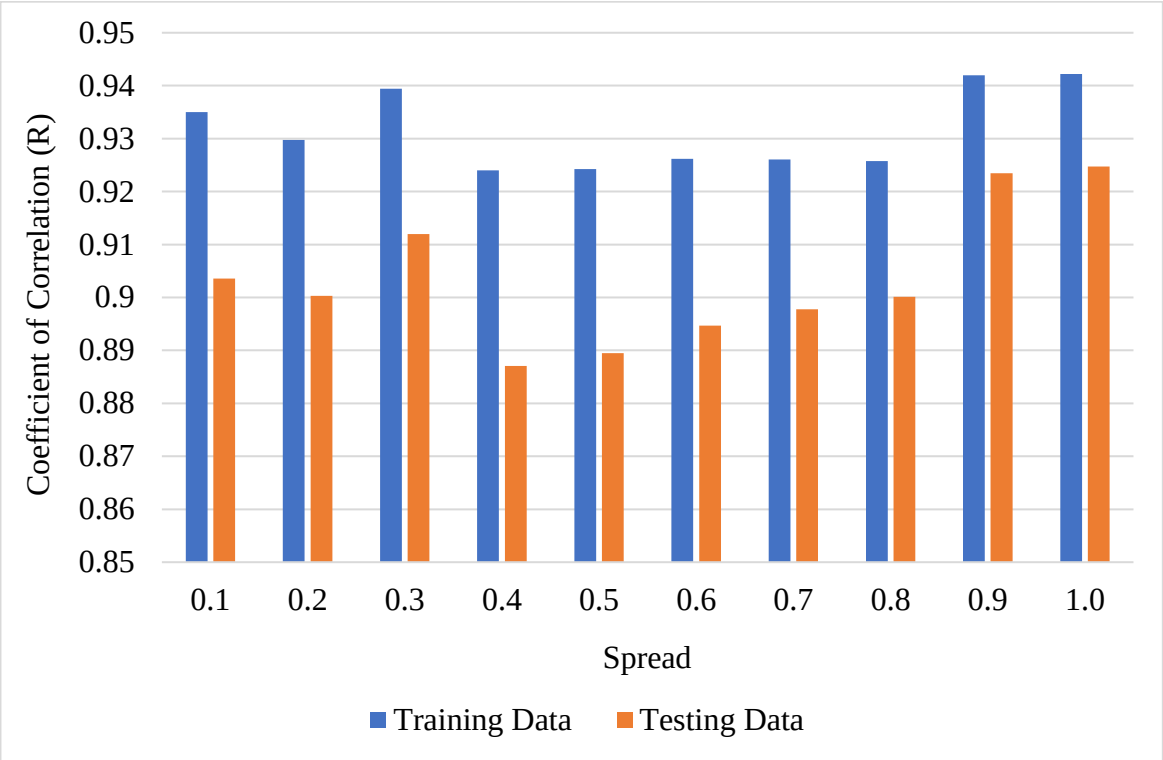

Fig. 3.19 A Graph of Correlation Coefficient Performance of RBFNN against Spread

Fig. 3.20 A Graph of Mean Square Error Performance of GRNN against Spread

Fig. 3.21 A Graph of Correlation Coefficient Performance of GRNN against Spread

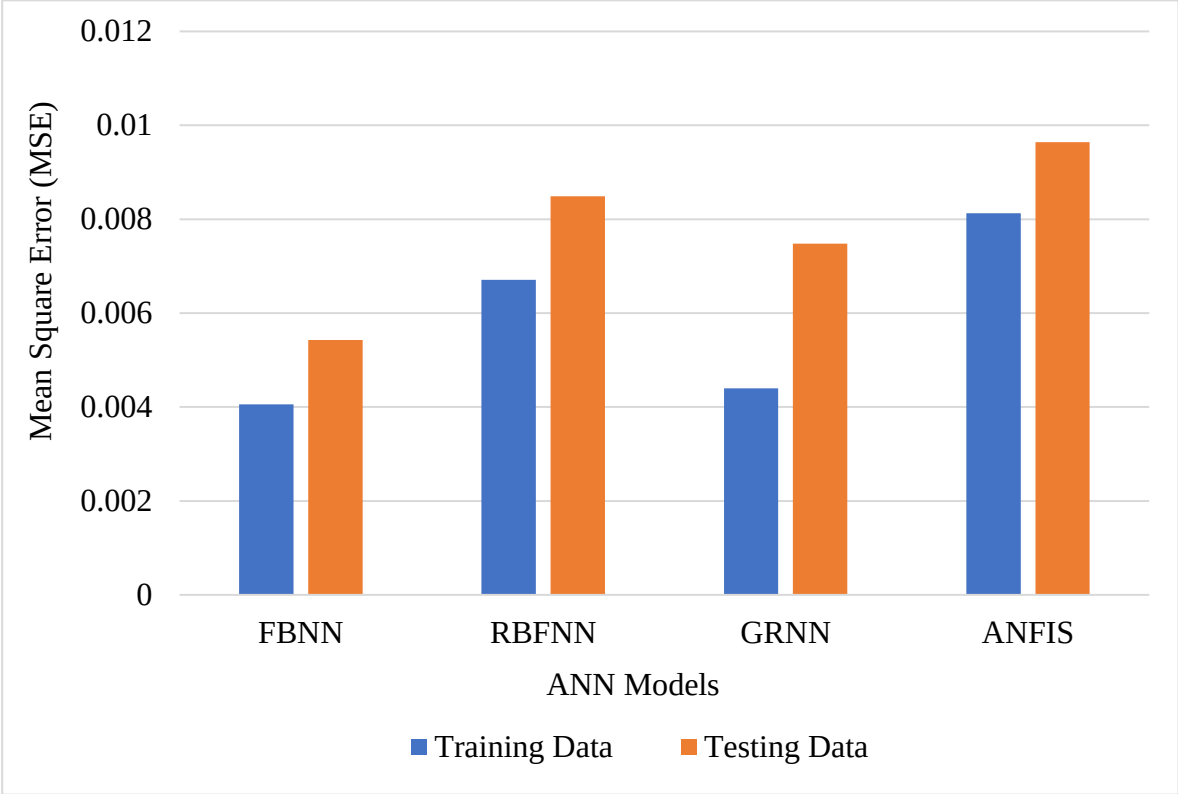

Fig. 3.22 A Graph of Comparison of ANN-based Models Mean Square Error Performances

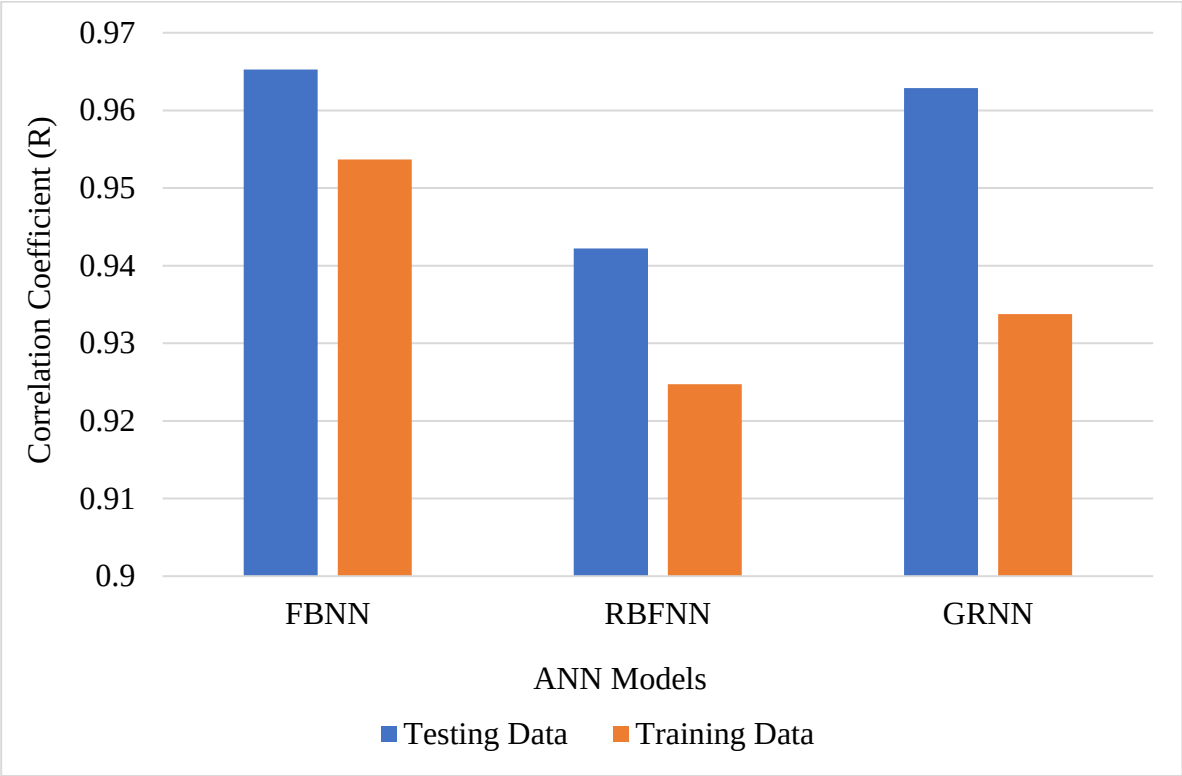

Fig. 3.23 A Graph of Comparison of ANN-based Models Correlation Coefficient Performances

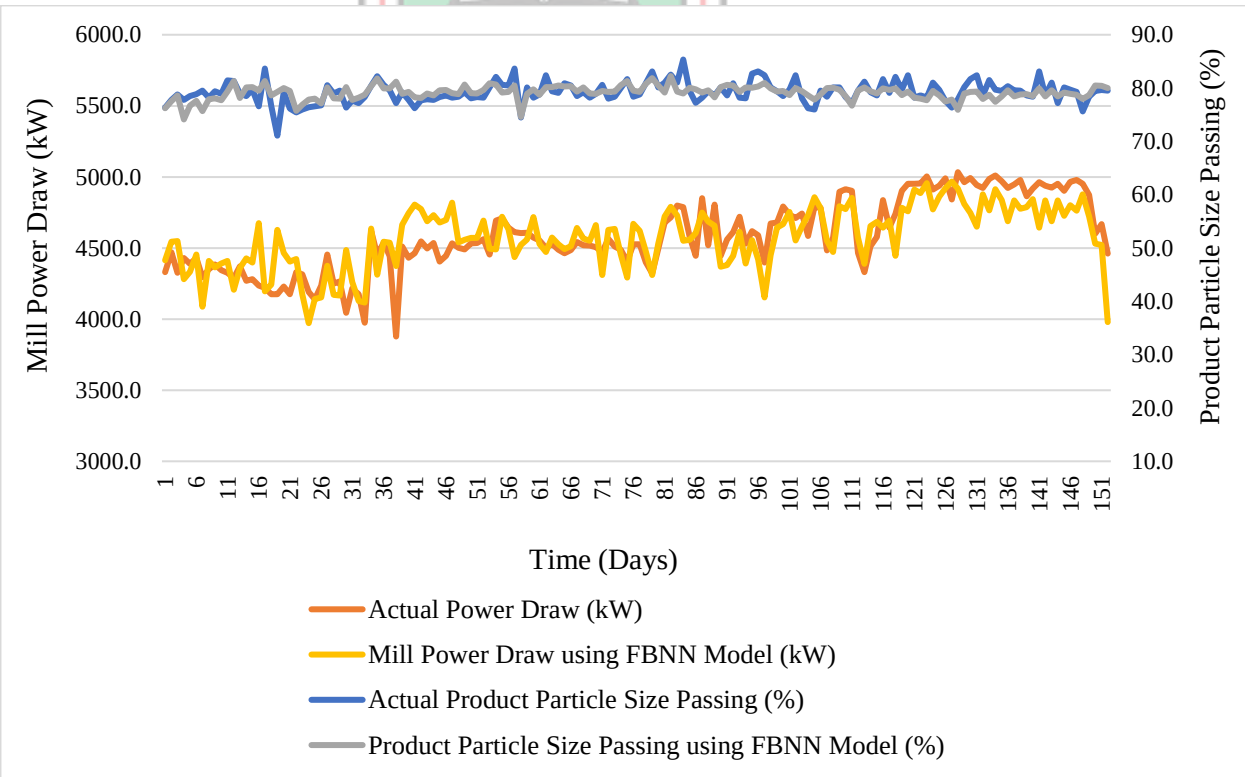

Fig. 3.24 A Graph of FBNN Predicted and Actual Values versus Time

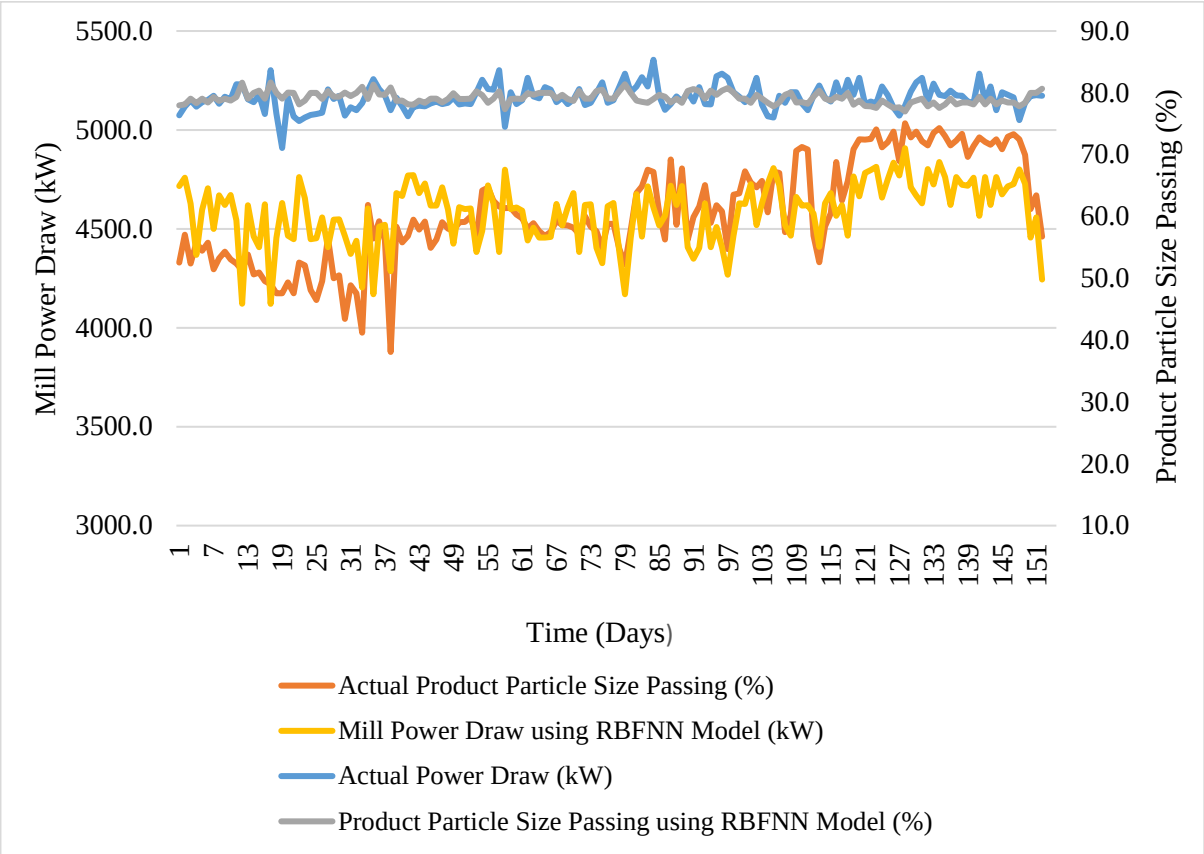

Fig. 3.25 A Graph of RBFNN Predicted and Actual Values versus Time

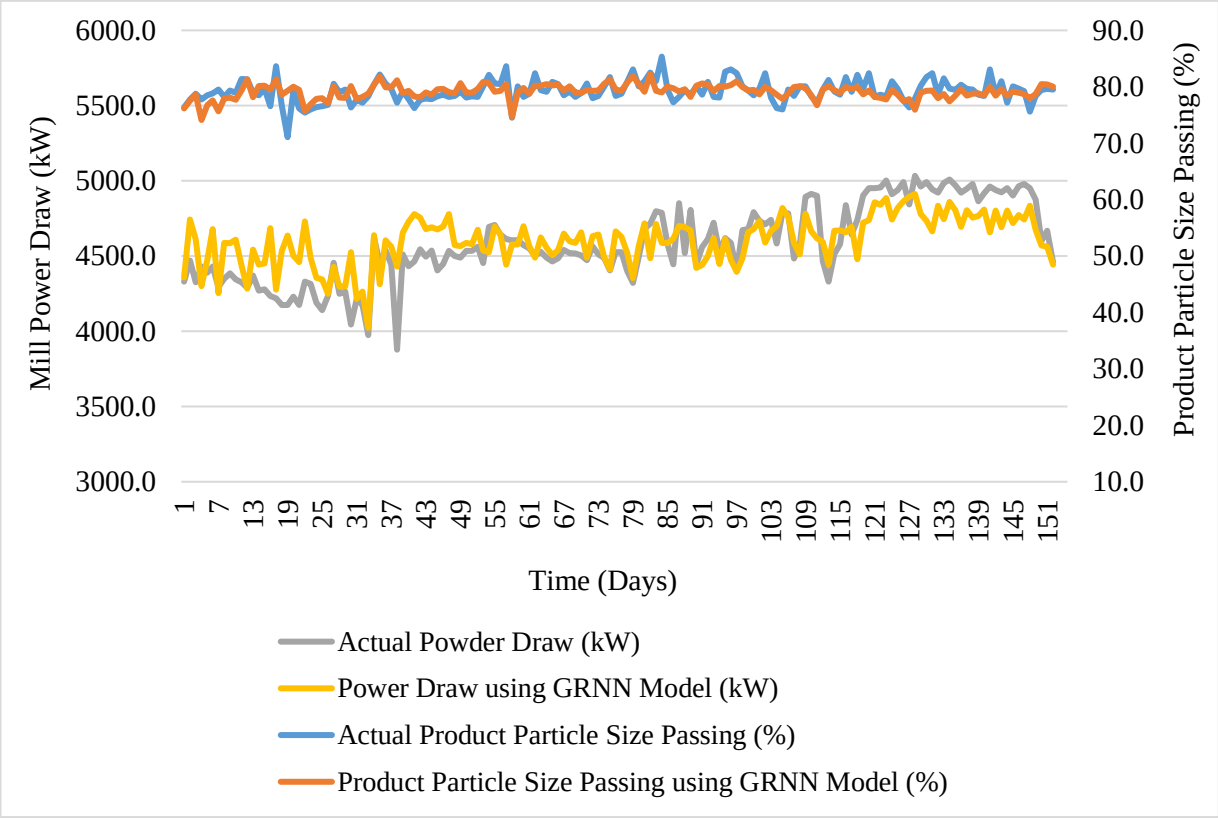

Fig. 3.26 A Graph of GRNN Predicted and Actual Values versus Time

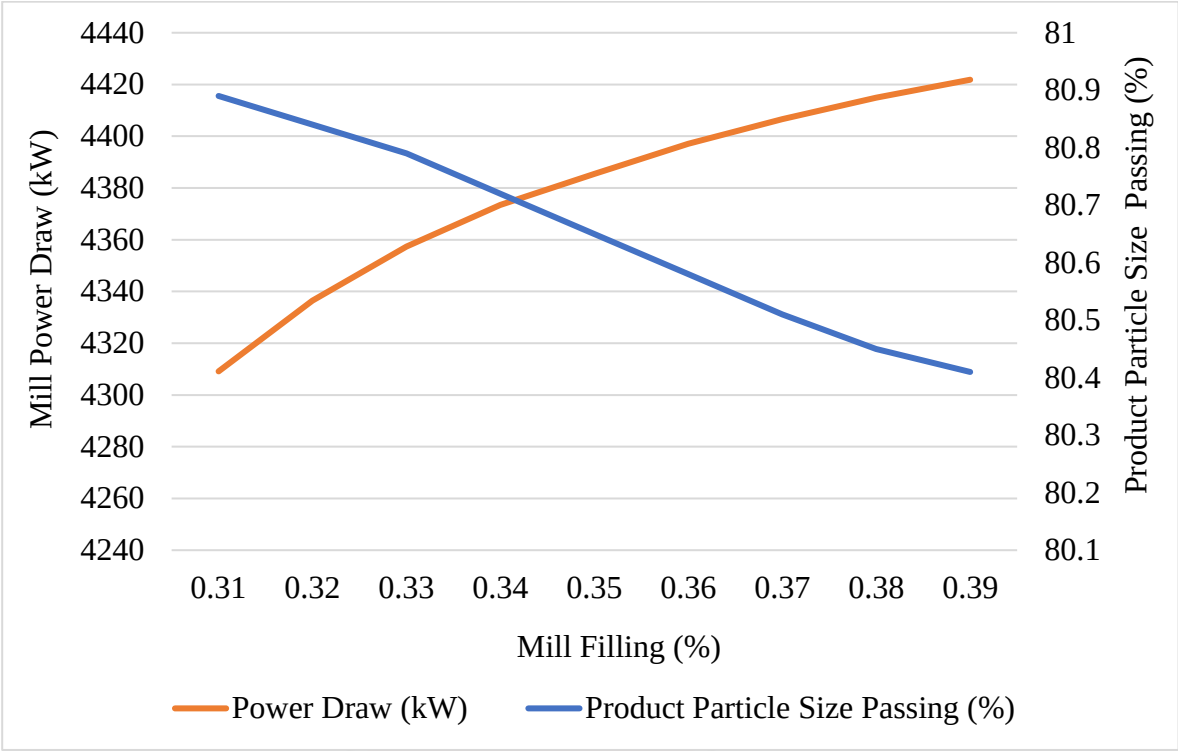

Fig. 3.27 A Graph of Mill Power Draw and Product Particle Size Passing versus Mill Filling

3.6.2 Discussions

To ensure that accurate predictive models are obtained for the purposes of predicting power draw and product particle size, the models were tuned to ensure that the best outcomes were realised. Fig. 3.16 and Fig. 3.17 present the MSE and R performances of the FBNN model, respectively in terms of training and testing data. It can be inferred from the Fig. 3.16 that, the training data recorded lower MSE values across the range of neurons that were varied. This was due to the fact that FBNN model was able to learn the data that it was trained with and so it was able to replicate the trained data with minimum errors. A lower MSE of 0.00320812 was recorded for the FBNN training data when the number of neurons used during the tuning phase was 90. A higher MSE value of 0.00478433 was however recorded when the number of neurons was increased to 100 for the same training data. Testing data which are usually a measure of the generalisation ability of a model recorded an MSE value of 0.0054308 when the number of neurons was 20.

On the other hand, the highest R value for training and testing were 0.971852 and 0.796865 for 90 neurons and 0.965249 and 0.953670 for 20 neurons, respectively. It can be inferred that increasing the number of neurons affected both the MSE value and the R value significantly. An increase in the number of neurons does not necessarily make a model perform better. However, an increase in the number of neurons affects the computational time especially with

other learning algorithms like the Bayesian regularisation. From Fig. 3.16, it can be seen that the MSE for testing data increases steadily after the neurons were increased above 20. Also, variations can be observed in the case of R values as the number of neurons increased.

Fig. 3.18 and Fig. 3.19 show the MSE and R performances of the RBFNN model against the spread. The spread is the parameter that defines the number of Gaussian neurons required to smoothly fit a function. The larger the spread, the smoother will be the function approximation. Too large a spread means more neurons are required to fit a fast changing function. Too small spread means many neurons are required to fit a function smoothly which in most instances may lead to over fitting and affect the generalisation ability of the model. From Fig. 3.18 and Fig. 3.19, the spread was varied over a range of 0.1 to 1 to find the optimal spread that gave the least MSE value and the highest R value. The developed RBFNN model gave the lower MSE and highest R values at a spread of 1 and 6 neurons. The corresponding MSE and R values at the spread of 1 and 6 neurons for both training data and testing data are 0.00671 and 0.94223 and 0.00849 and 0.92474, respectively.

Fig. 3.20 and Fig. 3.21 show the performance evaluation of the GRNN which is a variation of the RBFNN. The major determining factor that affected the performance of the GRNN is the spread or width parameter. Optimal spread constant was found by looping through the data while varying the spread and observing the MSE and R. The lowest MSE values of 0.00440 and 0.00748 and highest R values of 0.96286 and 0.93376 corresponded to an optimal spread of 0.1 for the training data and testing data, respectively. It can also be inferred from the two figures that the performance of the model decreased as the spread increased.

Fig. 3.22 and Fig. 3.23 make a comparative analysis of the MSE and R values of the three optimally tuned ANN models. The optimal MSE values for GRNN, FBNN and RBFNN are 0.00440 and 0.00748, 0.00406 and 0.00543, 0.00671 and 0.00849 for both training data and testing data, respectively. Optimal values of R recorded were 0.96286 and 0.93376, 0.96525 and 0.95367, 0.94223 and 0.92474, respectively for both training and testing data for the respective models being compared. Based on the evaluation criteria established, the FBNN model performed better compared to the other two ANN models since it had the least MSE values and the highest R values for both training and testing data. GRNN comparatively performed better than RBFNN. ANFIS was the worst performer of the MSE.

Fig. 3.24, Fig 3.25 and Fig 3.26 presents graphs of actual power draw and product particle size passing and that of predicted mill power draw and product particle size passing using the developed FBNN, RBFNN and GRNN models respectively. The goal of the prediction was to

determine which of the developed models predicted mill power draw and product particle size passing closest to the actual with minimal errors. It was observed that the predicted values fitted quite well with the actual values for Fig. 3.24, Fig. 3.25 and Fig. 3.26. However, it was noted that the predicted FBNN had the best fit with its turning points following closely on the benchmarked actual data for the 151 observed points.

Fig. 3.27 showed effect of increasing grinding media on mill power draw and product particle size passing at a constant throuphput of 600t/h. At constant throughput, mill filling increases considerably with increased grinding media charge since mill infeed water is a fraction of the throughput and will be constant at constant throughput. It was realised that increasing grinding media charge led to an increase in the overall mill power draw and a decrease in the product particle size passing and vice versa when the grinding media was decrease. This behaviour was partly attributable to the fact that, increasing grinding media charge increases the overall weight of the mill and hence will lead to a corresponding increase in mill power draw. Also increment of grinding media increase the probability of the grinding media collision, which does lead to product size reduction and hence the reduction in the product passing size percentage.

3.7 Summary

In summary, this chapter outlined the steps in the development of ANN models for the prediction of power draw and product particle size of the wet ball mill grinding media circuit. It elaborated on the data acquisition and pre-processing techniques employed, the model development, performance evaluation and the investigation of the model against hypotheses from literature. The performance of the models investigated are to serve as basis for selecting the best model that will be utilised in the next chapter. Based on the performances of all the models, the tuned FBNN model with twenty hidden neurons proved robust when used for the purpose of prediction of product particle size passing and mill power draw. The FBNN model looks promising for further improvement since the error margin between the trained data and the test data is closer and can be easily improved compared to the other error margins. Hence, the FBNN shall be optimised for the purpose of predicting 60 mm grinding media balls and this serves as the focus of Chapter 4.

CHAPTER 4

OPTIMISATION OF GRINDING MEDIA PREDICTION MODEL

4.1 Introduction

This chapter focuses on the development of grinding media prediction model from OCPs obtained from the models of the previous chapter. The criteria used in selecting OCPs, identification of OCPs and development of the model are given attention in this chapter. Fig. 4.1 is a flowchart of the major highlights of the entire chapter.

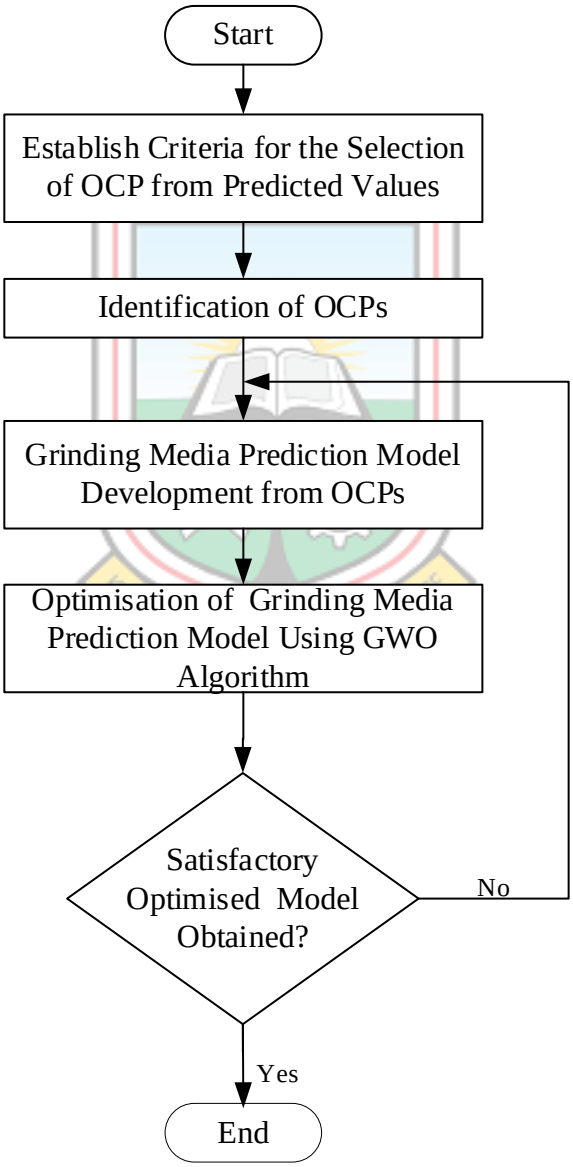

Fig. 4.1 A Flowchart of the Methodology for System Optimisation

4.2 Criteria for Optimal Charging Practice Determination

OCPs are conditions that result in optimum power draw and a greater passing of product particle size. The criteria for the determination of these OCPs are based on theoretical assumptions and key performance indices established by the considered mill under study. A product particle size passing of 80% is required because it leads to higher recovery rates and less leaching time during downstream processing. So to be considered as an OCP, one of the assumptions is that the product particle size passing should be equal or greater than 80%. Also, the theoretical energy required to reduce an ore from 300 μm to 106 μm is calculated using Bond's equation (see Equation 2.4).

In calculating the theoretical energy, the Bond work index of the ore is considered since it determines how resistant the ore is to grinding. The highest Bond work index of the ore in the mine under consideration was 17.5 kWh/t while the lowest index recorded for ore hardness was 15.5 kWh/t. Also, a significant factor is the total tonnes milled per hour. From the 507 datasets in Appendix A, the highest tonnage recorded was 670 t/h and the lowest recorded was 230 t/h. Using both the upper and the lower limits of the Bond work index and the tonnes per hour milled, the average power draw in an hour which is considered optimum based on theoretical assumptions lies between the ranges of 4619 kW for harder ores and 4091 kW for softer ores when running at full capacity. Power draw recorded which is lower than 4091 kW will only be considered optimum if the mill capacity is 70% utilised.

The criteria above form the bedrock for the identification of the OCPs in the next section.

4.3 Identification of Optimal Charging Practices

The OCP conditions are first identified with their corresponding input values in the test data used in the testing phase during development of the predictive models in the previous chapter. The established criteria and assumptions discussed in section 4.2 were employed in the identification of the OCPs. The identification is necessary to ensure that only desired practices are used in the development of the grinding media prediction model. It is also important to eliminate NOCP based on the assumptions to ensure that the developed model only learns from the OCPs. Table 4.1 shows the identified OCPs extracted from the dataset. On Table 4.1, TTM = Total Tonnes Milled; TPH = Tonnes Per Hour; MIW = Mill Infeed Water; GM_{60} = 60 mm Balls; GM_{50} = 50 mm Balls; TGM = Total Grinding Media; GMWR = Grinding Media Wear Rate; BWI = Bond Work Index; PPS = Product Particle Size; PD = Power Draw.

Table 4. 1 Identified Optimal Charging Practices from Dataset

TTM	TPH	MIW	GM_{60}	GM_{50}	TGM	GMWR	BWI	PPS	PD
10922	455	59	6.00	4.00	10.00	0.92	16.70	81.4	4325.0
13406	559	73	8.00	2.00	10.00	0.75	15.90	81.3	4290.0
13078	545	71	6.00	2.00	8.00	0.61	16.40	79.7	4280.0
13425	559	73	6.00	2.00	8.00	0.60	15.90	83.7	4220.0
13239	552	72	6.00	2.00	8.00	0.60	16.50	79.3	4230.0
12541	523	68	6.00	2.00	8.00	0.64	16.40	80.6	4455.0
10907	454	59	6.00	2.00	8.00	0.78	16.80	80.4	4621.3
14432	601	78	4.00	2.00	6.00	1.06	16.00	82.2	4451.7
15848	660	86	6.00	2.00	8.00	0.60	16.50	79.2	4489.5
15348	640	83	6.00	2.00	8.00	0.70	16.40	80.1	4453.8
10487	437	57	4.00	2.00	6.00	0.72	16.60	82.1	4693.5
13449	560	73	6.00	2.00	8.00	0.72	16.80	80.5	4642.6
14313	596	78	6.00	2.00	8.00	1.21	16.50	82.4	4501.5
14391	600	78	8.00	2.00	10.00	0.71	16.50	79.1	4488.8
14026	584	76	6.00	2.00	8.00	0.98	16.50	80.9	4463.3
14124	588	77	6.00	2.00	8.00	0.76	16.50	80.5	4485.7
13922	580	75	6.00	2.00	8.00	0.73	16.40	80.0	4487.5
10572	441	57	2.00	2.00	4.00	0.96	16.30	81.7	4404.5
14715	613	80	6.00	2.00	8.00	0.74	16.00	83.1	4320.6
13926	580	75	6.00	2.00	8.00	0.68	16.60	79.5	4580.1
12332	514	67	6.00	2.00	8.00	0.65	16.40	80.1	4444.6
13467	561	73	4.00	2.00	6.00	0.60	16.40	83.1	4588.6
10268	428	56	6.00	2.00	8.00	0.78	16.20	82.4	4398.0
13361	557	72	6.00	2.00	8.00	0.60	16.50	80.1	4570.6
12916	538	70	6.00	2.00	8.00	0.62	16.40	81.2	4331.0

4.4 Grinding Media Prediction Model Development from Optimal Charging Practices

The prediction of grinding media is supposed to be very imperative in every processing plant as it gives an idea of the quantity of grinding media that should be replenished on a daily basis to ensure that the conditions of the power draw and product particle size passing remain within the expected limits. In the development of the grinding media prediction model from the identified OCPs, FBNN was employed in model realisation because of its superior performance exhibited in Chapter 3. The grinding media prediction model considers the replenishing of only 60 mm balls on a daily basis. This assumption is due to the fact that the 60 mm balls wear as the days go by into the various smaller sizes to fill in-between the mill cavities that exist when the 60 mm balls are used. The weight of the 60 mm balls is then considered as an output during the training of the FBNN. The rest of the variables are considered as inputs in the development

of the model. The whole idea is about finding the weights of FBNN that best fit input variables to the output variable with minimum error.

$$y = \min_{x_1, x_2, x_3 \ldots x_9} \text{fit}\left(x_1, x_2, x_3, x_4, x_5, x_6, x_7, x_8, x_9\right) \tag{4.1}$$

where, y = output variable representing predicted value (t)

x_1 = input variable representing total tonnes milled (t)

x_2 = input variable representing tonnes per hour milled (t/h)

x_3 = input variable representing mill infeed water (m^3/h)

x_4 = input variable representing 50 mm balls (t)

x_5 = input variable representing total grinding media (t)

x_6 = input variable representing grinding media wear rate (kg/t)

x_7 = input variable representing Bond Work Index/ore hardness (kWh/t)

x_8 = input variable representing product particle size passing (%)

x_9 = power draw (kW)

The dataset in Table 4.1 is normalised during the pre-processing stage to ensure that it is well scaled to be understood by the activation functions. The Bayesian Regularisation (BR) algorithm was employed for the training of the model. The reason for the choice of the algorithm was because of its good generalisation capability for difficult, small and noisy datasets. The algorithm stops according to adaptive weight minimisation. Total number of iterations was set to 1000 epochs.

Though the FBNN showed superior performance, optimisation of the developed model is highly recommended to realise an accurate model. Optimisation of the model allows for further reduction of the error between the predicted and the actual grinding media consumed. Grey Wolf Optimisation (GWO) algorithm was proposed to be employed because empirical literature shows that it has a small number of parameters compared to other algorithms when configuring and its performance has been established in several applications, to be good in enhancing the performance of a neural network (Ahmed and Mohamed, 2020). GWO algorithm does the above by exploring different regions of the search space that have many local minima and then reduces the domain of search to the area that contains the global solution. This solves the drawback of the FBNN of having the tendency to get stuck in the local point and therefore impede the performance of the model at arriving at a global solution which is vital at arriving at the best weights that fit input and output variables accurately.

4.5 Grey Wolf Optimisation Algorithm

GWO algorithm is a new nature-inspired, swarm-based meta-heuristic, bionic optimisation algorithm which was introduced by Mirjalili in 2014 (Niu *et al*., 2019). Singh and Singh (2017) developed the GWO algorithm to solve an optimisation problem of nonlinear double-layer grids. The results illustrated that GWO algorithm had better performance than other algorithms in finding the optimal design of non-linear double-layer grids. According to Mirjalili *et al*. (2015), grey wolves live together and hunt in groups. Mirjalili designed the optimisation algorithm imitating the searching and hunting processes of grey wolves. According to Faris *et al*. (2018), GWO algorithm has successfully been applied in the domains of band selection, automatic control, power dispatch, automated offshore crane design, feature selection in neural networks, parameter estimation and shop scheduling. Simplicity, easy implementation, minor parameters, flexibility, derivation-free and local minima avoidance are the merits of GWO algorithm (Emary *et al*., 2016). However, according to Gao and Zhao (2019), the setbacks of GWO algorithm are low solving accuracy, bad local searching ability and slow convergence rate.

GWO algorithm mimics the behaviour of grey wolves to capture prey with a clear division of labour and mutual cooperation. At the top of the food chain, grey wolves mostly prefer to live in a pack. Usually, there are five (5) to twelve (12) wolves in each group. They have a strict hierarchical management system that constitutes a hierarchical pyramid as shown in Fig. 4.2.

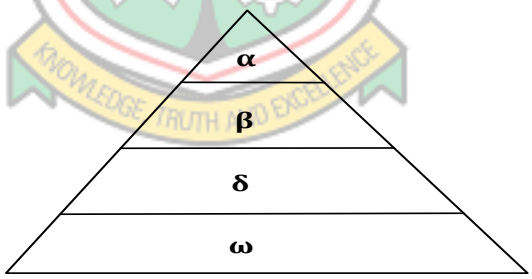

Fig. 4.2 A Social Hierarchy of Grey Wolves

The hierarchy allows the grey wolf pack to efficiently kill the prey. α layer is the head wolf, which is the strongest and most capable individual. It is also the only leader in a wolf pack who directs the team's predation actions, food distribution and other decision-making tasks. β and δ layers are two wolves groupings that are second only to α. Their responsibility is mainly to assist α layer in the behaviour of group organisations. ω layer is at the bottom of the pyramid, which occupies the majority of the total. This ω layer is mainly responsible for balancing the internal relationship of the population and looking after the young wolves (Mirjalili *et al*., 2015). Fig. 4.3 shows the attacking toward prey versus searching for prey.

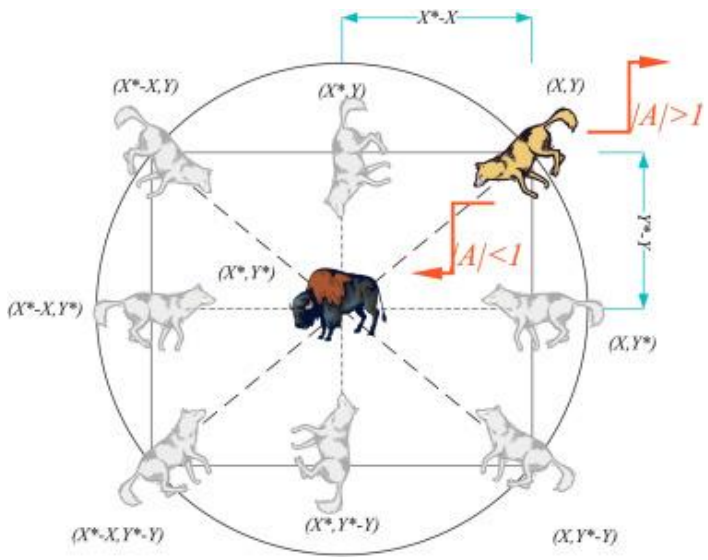

Fig. 4.3 The Position Vectors and their Possible Next Locations

4.6 Mathematical Model of Grey Wolf Optimisation Algorithm

The mathematical models of the encircling, tracking and attacking prey are as follows:

4.6.1 Encircling Prey

The encircling behaviour of the prey is mathematically modelled using the following equations:

$$\vec{D}_p = \left|\vec{C} \times \vec{X}_p(t) - \vec{X}(t)\right| \tag{4.2}$$

$$\vec{X}_p(t+1) = \vec{X}_p(t) - \vec{A} \times \vec{D}_p \tag{4.3}$$

$$\vec{A} = 2\vec{a}\vec{r}_1 - \vec{a} \tag{4.4}$$

$$\vec{C} = 2\vec{r}_2 \tag{4.5}$$

where, $\vec{D}_p$ = distance vector of the prey from a wolf

$\vec{X}(t)$ = position vector of a grey wolf

$\vec{X}_p(t)$ = position vector of the prey

$\vec{A}$ and $\vec{C}$ = coefficient vectors

t = the current iteration i.e the iteration number

$\vec{X}_p(t+1)$ = next position vector that the prey arrives

$\vec{a}$ = convergence vector factor which decreases from 2 to 0 over the iteration

$\vec{r}_1$, $\vec{r}_2$ = random vector numbers in the range [0,1]

4.6.2 Hunting Prey

After encircling the prey under the guidance of α, β, δ grey wolves, they then hunt the prey by moving towards it with the β and δ wolves estimating their own position with reference to the α wolves. Update principle in this hunting action process is represented in Equation (4.6) to Equation (4.12).

$$\vec{D}_{\alpha}(t) = \left|\vec{C}_{\alpha} \times \vec{X}_{\alpha}(t) - \vec{X}(t)\right| \tag{4.6}$$

$$\vec{D}_{\beta}(t) = \left|\vec{C}_{\beta} \times \vec{X}_{\beta}(t) - \vec{X}(t)\right| \tag{4.7}$$

$$\vec{D}_{\delta}(t) = \left|\vec{C}_{\delta} \times \vec{X}_{\delta}(t) - \vec{X}(t)\right| \tag{4.8}$$

$$\vec{X}_1 = \vec{X}_{\alpha}(t) - \vec{A}_{\alpha} \times (\vec{D}_{\alpha}) \tag{4.9}$$

$$\vec{X}_2 = \vec{X}_{\beta}(t) - \vec{A}_{\beta} \times (\vec{D}_{\beta}) \tag{4.10}$$

$$\vec{X}_3 = \vec{X}_{\delta}(t) - \vec{A}_{\delta} \times (\vec{D}_{\delta}) \tag{4.11}$$

$$\vec{X}(t+1) = \frac{\vec{X}_1(t) + \vec{X}_2(t) + \vec{X}_3(t)}{3} \tag{4.12}$$

where, $\vec{D}_{\alpha}$, $\vec{D}_{\beta}$, $\vec{D}_{\delta}$ = distance from α, β, δ to the prey, respectively

$\vec{C}_{\alpha}$, $\vec{C}_{\beta}$, $\vec{C}_{\delta}$ = coefficient vectors of α, β, δ, respectively

$\vec{X}_{\alpha}$, $\vec{X}_{\beta}$, $\vec{X}_{\delta}$ = position vectors of the grey wolf at α, β, δ, respectively

$\vec{X}_1$, $\vec{X}_2$, $\vec{X}_3$ = effects of α, β, δ wolves on the prey, respectively

4.6.3 Attacking Prey

As mentioned, the grey wolves finish the hunt by attacking the prey when it stops moving. In order to mathematically model approaching the prey, α is decreased in terms of its value (convergence and get results) and this can be seen in Equation (4.4). When $|A| < 1$, the wolves pack gather to attack the prey. When $|A| > 1$, the wolves pack diverge and search for the new potential prey. The flowchart of the GWO algorithm is illustrated in Fig. 4.4 (Bozorg-Haddad, 2018) and Fig. 4.5 (Mirjalili *et al*., 2015) shows the pseudocode of GWO algorithm.

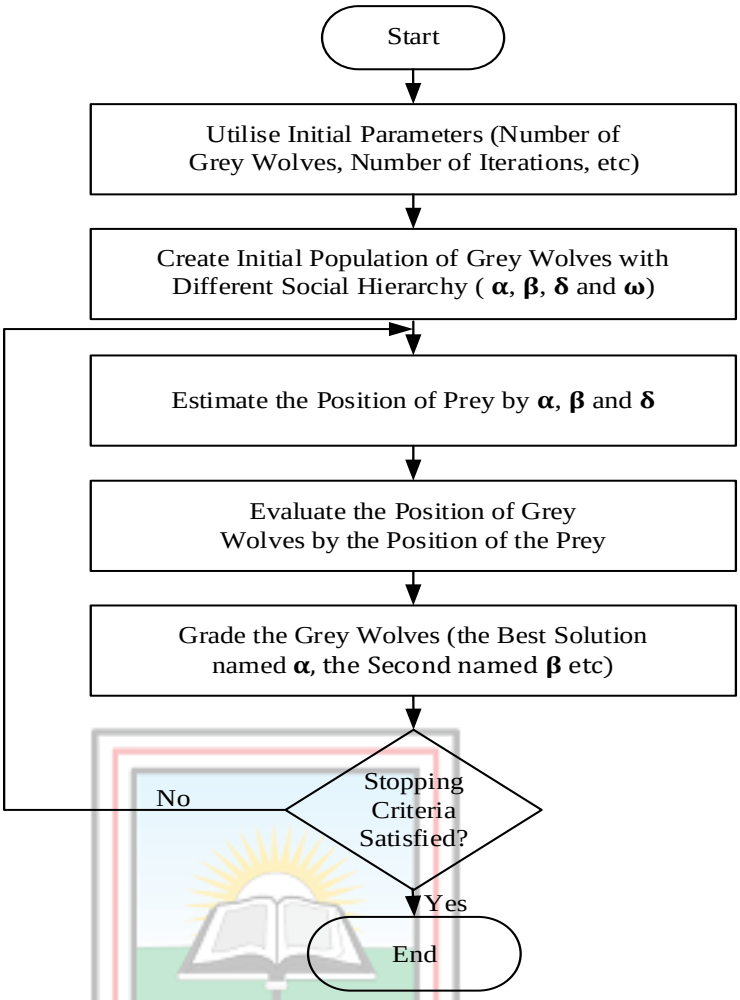

Fig. 4.4 A Flowchart of the Grey Wolf Optimisation Algorithm

Steps of the flowchart

Step 1: Initialise the GWO parameters such as search agents (G_s), design variable size (G_d), vectors a, A, C and maximum number of iterations ($iter_{max}$).

Step 2: Generate wolves randomly based on size of the pack.

Step 3: Estimate the fitness value of each hunt agent.

Step 4: Identify the best hunt agent (G_α), the second best hunt agent (G_β) and the third best hunt agent (G_δ).

Step 5: Renew the location of the current hunt agent.

Step 6: Estimate the fitness value of all hunts.

Step 7: Update the value of G_α, G_β and G_δ.

Step 8: Check for stopping condition i.e., whether the iteration reaches $Iter_{max}$, if yes, print the best value of solutions otherwise go to Step 5.

```
Begin
    Initialise the population of grey wolves Xi (i = 1, 2, ... , n)
    Initialise a, A and C
    Calculate the fitness values of search agents and grade them. (Xα = the best solution in
    the search agent, Xβ = the second best solution in the search agent, and Xδ = the third
    best solution in the search agent)
    t = 0
    While (t < Max number of iterations)
        For each search agent
            Update the position of the current search agent
        End for
    Update a, A and C
    Calculate the fitness values of all search agents and grade them
    Update the positions of Xα, Xβ and Xδ
    t = t +1
    End while
End
```

Fig. 4.5 Pseudocode of the Grey Wolf Optimisation Algorithm

In the use of the GWO algorithm in optimising the FBNN, information on the actual output and predicted output values was obtained and used in updating the weights in the hidden layer of the FBNN. In the training phase, the GWO algorithm started by generating a population X with random positions for each wolf with the size of the population set to size, *N* and dimension, *D* which represented the number of weight parameters in the hidden layer. The values of α, β and δ were updated based on error of the objective function value presented in Equation (4.13) where the best solution was considered as the weights which help generate a minimum objective function value.

$$F_{obj} = \|y - \hat{y}\|^2 \tag{4.13}$$

where, F_{obj} = objective function

y = target value of 60 mm balls

$\hat{y}$ = predicted values of 60 mm balls

The configuration parameter values are presented in Table 4.2 while the full implementation codes used in the optimisation process are presented in Appendix D.

Table 4.2 Configuration Parameters of the GWO – FBNN Algorithm

SN	Configuration Parameter	Value
1.	Population Size (Number of Grey Wolves)	50
2.	Number of Iterations	1000
3.	α, β, δ	Random value 0 to 1

4.7 Results and Discussions

To evaluate performance of FBNN-GWO algorithm in predicting grinding media consumption, it was compared against just the traditional FBNN. The results, presented in the form of graphs are illustrated in Figs. 4.6 to Fig. 4.9 and discussed in Section 4.7.2.

4.7.1 Results

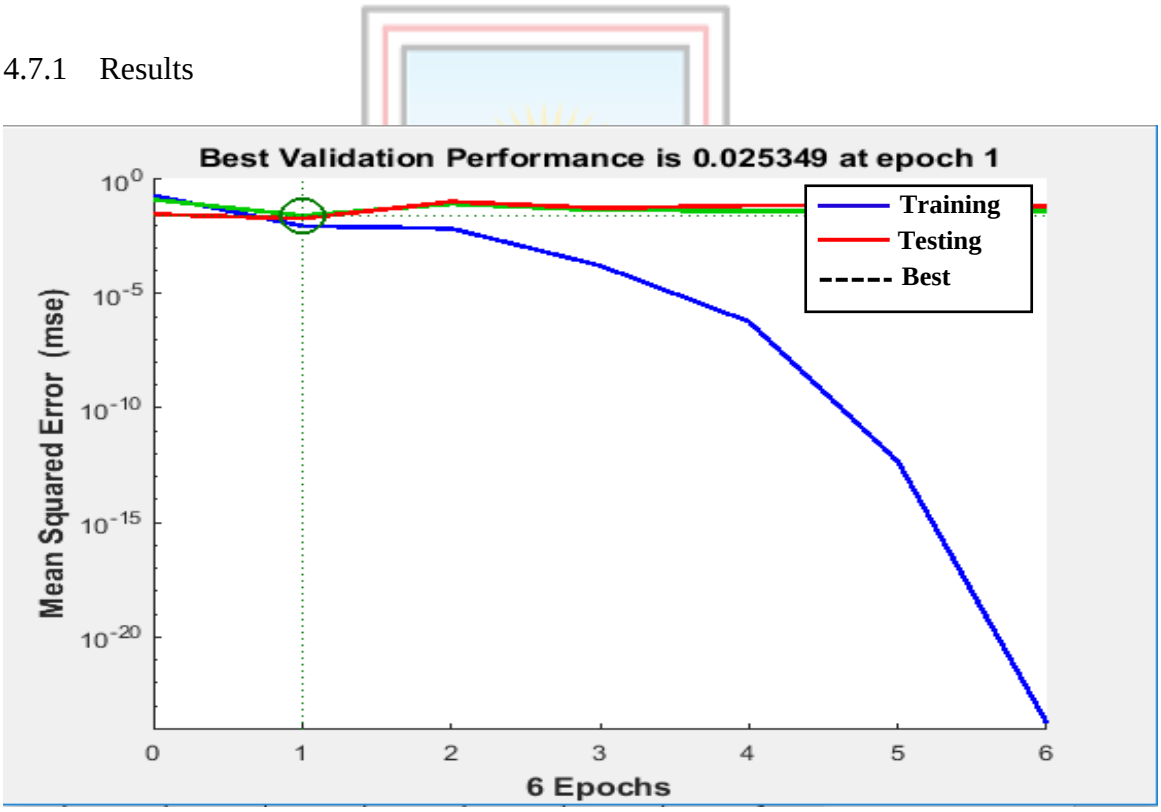

Fig. 4.6 A Graph of Mean Square Error versus Number of Iterations for FBNN Performance

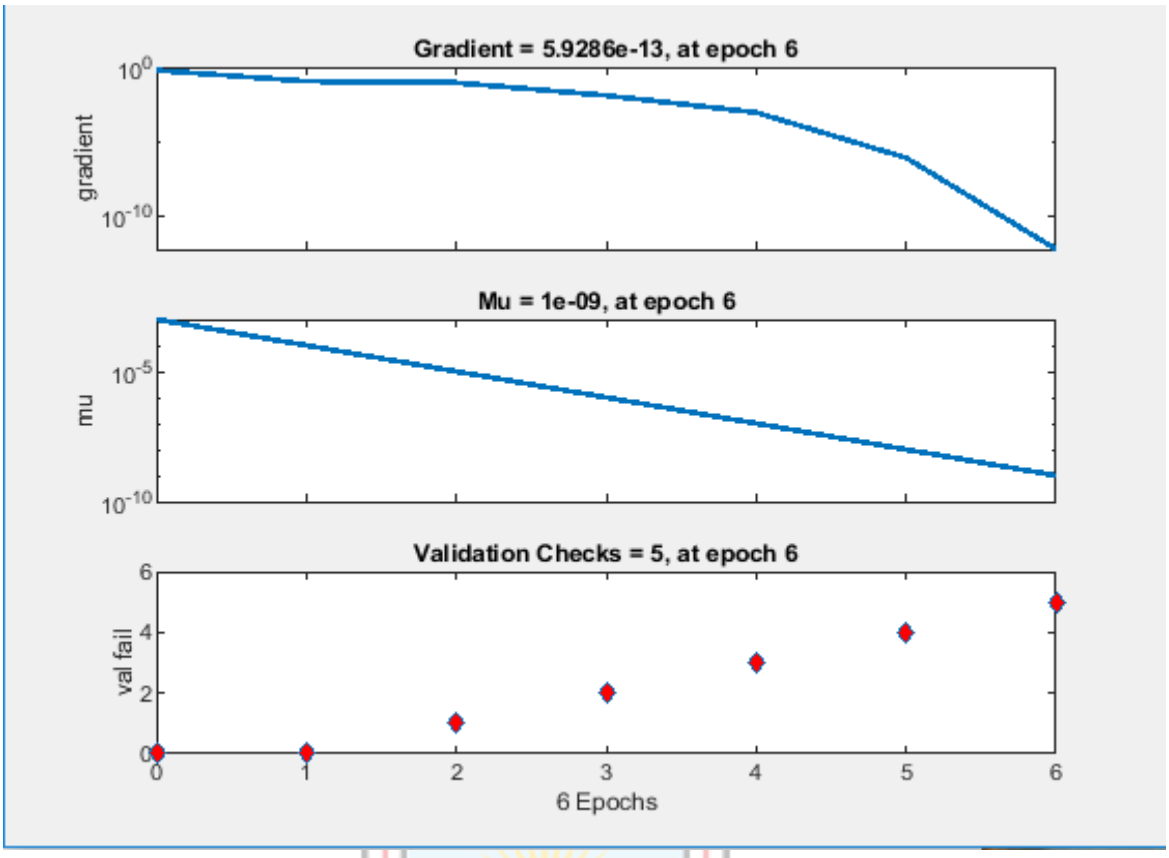

Fig. 4.7 A Graph of Learning Rate versus Number of Iterations for FBNN

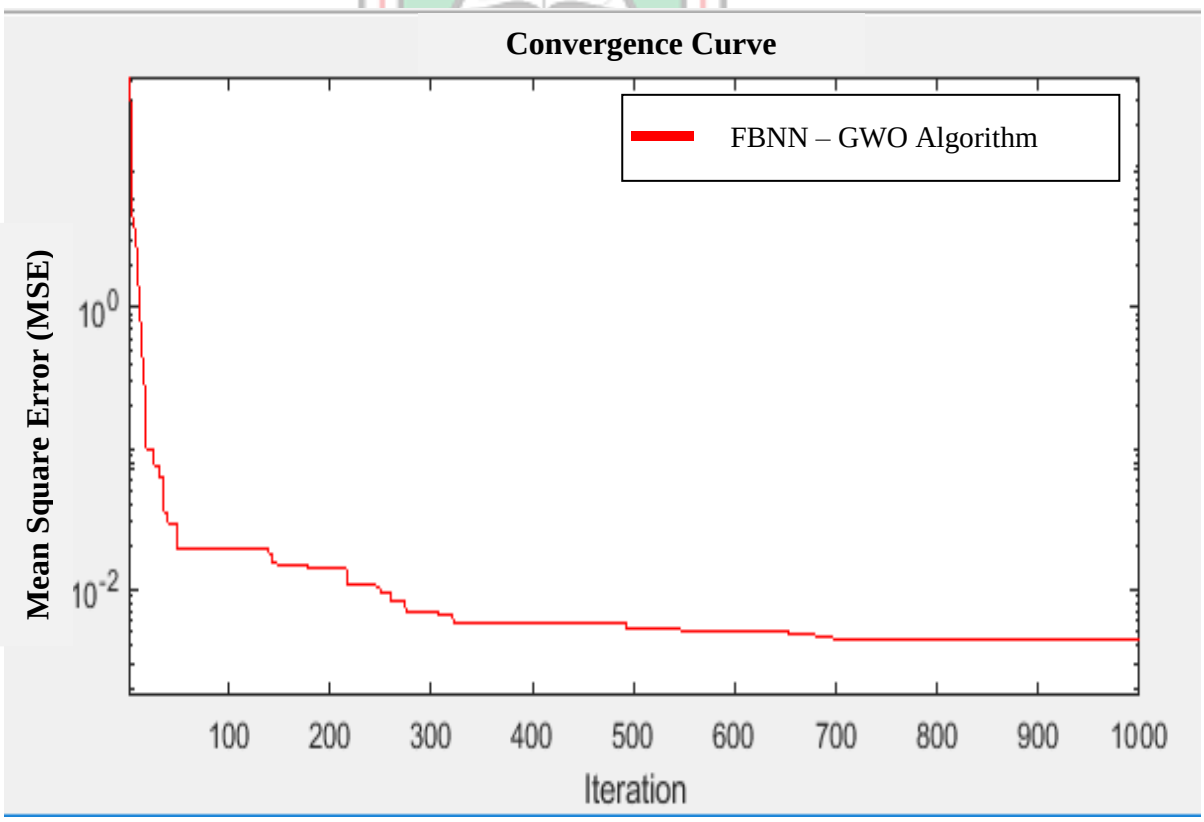

Fig. 4.8 A Graph of Mean Square Error versus Number of Iterations for FBNN – GWO Algorithm Performance during the Training Phase

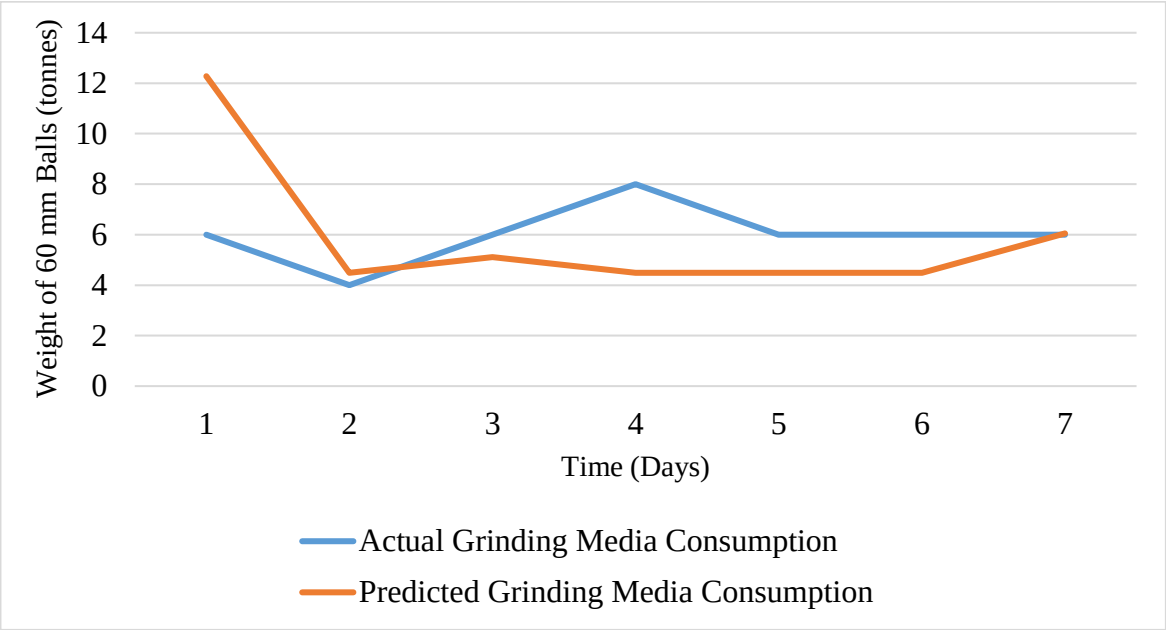

Fig. 4.9 A Graph of Actual and Predicted Grinding Media Weight of 60 mm Balls versus Time

4.7.2 Discussions

The metric used in evaluating performance between the traditional FBNN and the FBNN – GWO algorithm is the MSE. Interpretation of the MSE is guided by the fact that the closer the MSE is to 0, the smaller the error between the predicted value and the actual value of grinding media consumption. Fig. 4.6 and Fig. 4.7 show the performance of the traditional FBNN. The MSE recorded during the training process was 0.008876, 0.0253485 during the validation stage and 0.0187532 during the testing stage. Though the total number of iterations was set to 1000 epochs, the training however ended prematurely after 6 epochs. It was realised after the first epoch that there was great divergence between the trained result and the validation and test results. The training was stopped since the validation results were not improving any further. This is one of the major drawbacks of the traditional FBNN, since the entire search space in search of a global solution was not adequately exploited.

Fig 4.8 presents the performance of the FBNN – GWO algorithm during the training phase. The MSE recorded was 0.0043022 which is far lower than the MSE recorded for the traditional case. Also, the MSE recorded during the testing phase was 0.0084321 which was lower than the value recorded for the traditional FBNN. It is realised that the FBNN – GWO algorithm explored all the search space in search of a global solution which led to its better performance. It however solved the major problem of the traditional FBNN which only stops performing when the generalisation stops and does not go on further in search of a better global solution for better performance.

4.8 Summary

This chapter developed an optimal grinding media prediction model for the purpose of grinding media replenishing of wet ball mills from OCPs identified from the previous chapter. The traditional FBNN and the enhanced FBNN were used in the development process. It was reaslised that the enhanced FBNN – GWO algorithm showed better performance in the prediction of grinding media charging of the wet ball mill. The FBNN – GWO algorithm model is then used for further analysis in the next chapter.

CHAPTER 5

SENSITIVITY ANALYSES

5.1 Introduction

This chapter is dedicated to performance of sensitivity analyses on the best performing optimised model to see the effect of each input variable on power draw and product particle size which is of major concern. The goal of chapter looks at the feasibility of grinding with minimum power draw and minimum grinding media while looking at the possibility of increasing throughput.

5.2 Sensitivity of Grinding Media Charge and Mill Power Draw to Changes in Input Variables

Fig. 5.1 shows FBNN – GWO algorithm based model whilst Fig. 5.2 shows the GWO optimised FBNN.

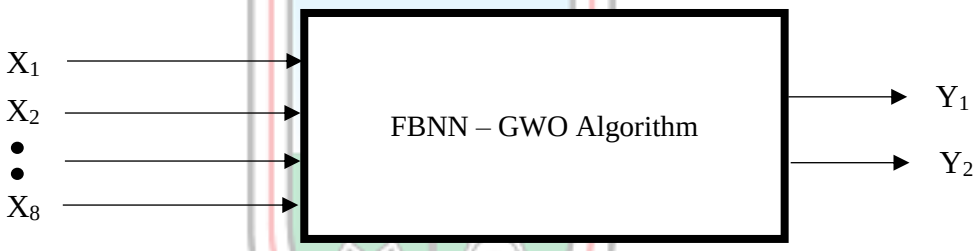

Fig. 5.1 A Representation of FBNN – GWO Algorithm based Model

The input variables are as follows:

X_1 = input variable representing total tonnes of ore milled (t)

X_2 = input variable representing tonnes per hour of ore milled (t/h)

X_3 = input variable representing mill infeed water (m^3/h)

X_4 = input variable representing 50 mm balls (t)

X_5 = input variable representing total grinding media (t)

X_6 = input variable representing grinding media wear rate (kg/t)

X_7 = input variable representing Bond Work Index/ore hardness (kWh/t)

X_8 = input variable representing product particle size passing (%)

The outputs are:

Y_1 = output variable representing grinding media charge (t)

Y_2 = output variable representing power draw (kW)

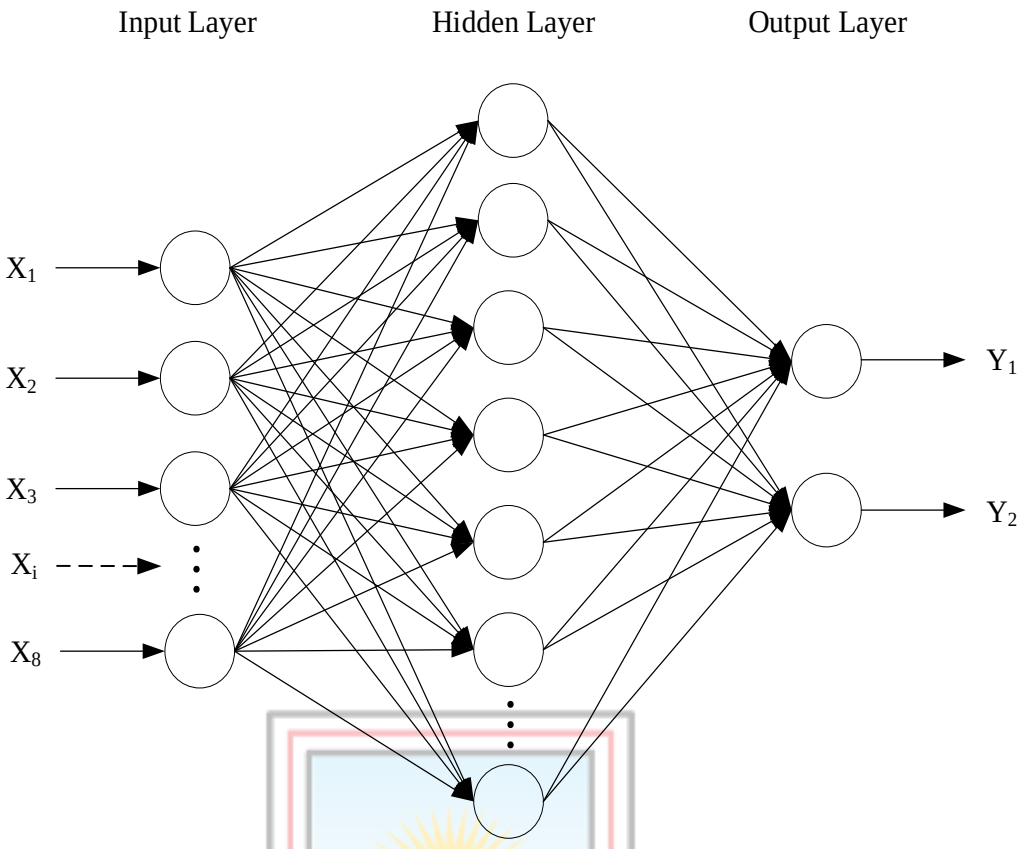

Fig. 5.2 The Network of FBNN – GWO based Algorithm

The sensitive analyses were performed using the FBNN-GWO algorithm based model shown in Fig. 5.1. Codes for the development of the model are presented in Appendix D. The architecture of the model considered grinding media charge and mill power draw as the critical output parameters since the goal remains investigating the feasibility of grinding with minimum power draw and minimum grinding media charge with the possibility of maximising throughput. The choice of the FBNN-GWO algorithm was due to its superior prediction capability with minimum error exhibited in previous chapters. In the investigation of the sensitivity of grinding media charge and mill power draw to changes in input variables, throughput (tonnes per hour milled), grinding media wear rate and ore hardness were varied to see the effect on the aforementioned output variables under observation. The rationale for the choice in varying the above input variables was to mirror the practice of mill operators at most mineral processing plants.

The varying of throughput has a direct effect on input parameters such as mill load (total tonnes milled) and mill infeed water since the mill load is a function of the throughput. Mill water on the other hand is always a percentage of the mill throughput. It therefore implies that an increase or decrease in throughput will have similar reflections in both mill load and mill infeed

water. The minimum and maximum values of the selected inputs for the purposes of the sensitivity analyses are presented in Table 5.1.

Table 5.1 Minimum and Maximum Values of the Varying Input Variables

SN	Input Parameter	Minimum	Maximum
1.	Throughput (t/h)	400	700
2.	Ore hardness (kWhr/t)	15.0	17.5
3.	Grinding Media Wear Rate (kg/t)	0.4	1.0

The minimum and maximum values help to determine the range in which the variation can be made. The minimum and maximum values are mainly extracted from the dataset which is a depiction of the usual practice in the mill under consideration. The reason for the determination of the range is to establish a benchmark to contrast between the current practice and the possibility of improving the practice that is currently being used.

5.2.1 Sensitivity Regarding Changes in One Input Variable

In this section, the interest lies in investigating how sensitive grinding media consumption and power draw are to changes in one single variable. As mentioned earlier, all the selected input variables that are to be varied are usual practices in the plant under consideration. For instance, in an attempt to increase productivity, there is always the likelihood of increasing the tonnes milled per hour in an attempt to maximise throughput. Also, ore hardness to a larger extent is dependent on the pit from which the ore was sourced. The hardness varies from one pit to another and from one depth to another. Varying the ore hardness attempts to investigate how ore hardness affects the two outputs under consideration in this section. Grinding media wear rate always is a function of the type of grinding media used and in most instances accelerated by the type of ore that is being milled.

Variations were carried out with the product particle size percentage passing 106 μm which is one of the input variables held constant at 80% passing. Alternate possibility of achieving more than the required 80% passing is always desirable at every processing plant since it leads to higher recovery rates and so considered as a scenario. Finally, the situation where the percentage passing of the product particle size falls below the required 80% remains a likely event hence, it was also investigated. For the three scenarios of product particle size passing of 80.0%, 82.4% and 79.10%, under one input variable variation, the throughput, ore hardness and grinding media wear rate were treated to the incremental steps of 20 t/h, 0.2 kWhr/t and 0.1 kg/t, respectively. The initial values of all variables for the three scenarios are summarised in Table 5.2.

Table 5.2 Initial Values of Variables Under Consideration

SN	PPS Passing 106 μm (%)	Throughput (t/h)	TPH (t/h)	MIW (m^3/hr)	GM_{50} (t)	TGM (t)	GMWR (kg/t)	BWI (kWhr/t)
1.	80.0	13921	580	75.0	2	8	0.730	16.4
2.	82.4	10267	428	55.0	2	8	0.779	16.2
3.	79.1	14391	599	78.0	2	8	0.705	16.5

5.2.2 Sensitivity Relative to Changes in Multiple Input Variables

Multiple variations of the selected input parameters are an attempt to exploit the limitation of varying only one parameter and find the possibility of grinding with minimum power draw and minimum grinding media. Variation of two or three of the selected input variables are possible cases that encompass real circumstances in the plant under consideration. There is the possibility of wanting to increase throughput while encountering changes in ore hardness. There is also the possibility of encountering changes in ore hardness while grinding media wear rate increases or decreases due to changes in the internal grinding action. Finally, changes in the three selected input variables were investigated since there is the possibility of having to increase throughput under varying conditions of ore hardness and grinding media wear rate. For the changes in the multiple input variables, once again, throughput, ore hardness and grinding media wear rate were incremented at the steps of 20 t/h, 0.2 kWhr/t and 0.1 kg/t, respectively. The initial values for the variations of all the scenarios aforementioned are summarised into the Table 5.2 earlier presented. Also, for the changes in multiple input variables for the three scenarios, ten cases of combination of the variations in the three variables were actualised and these are summarised in Table 5.3, Table 5.4 and Table 5.5 for 80.0%, 82.4% and 79.1% passing 106 μm .

Table 5.3 The Ten Cases of Variation of Inputs for 80.0% Passing 106 μm

SN	Input	Cases									
		1	2	3	4	5	6	7	8	9	10
1.	TPH	500	520	540	560	580	600	620	640	660	680
2.	BWI	15.6	15.8	16.0	16.2	16.4	16.6	16.8	17.0	17.2	17.4
3.	GMWR	0.329	0.429	0.529	0.629	0.729	0.829	0.929	1.029	1.129	1.229

Table 5.4 The Ten Cases of Variation of Inputs for 82.4% Passing 106 μm

SN	Input	Cases									
		1	2	3	4	5	6	7	8	9	10
1.	TPH	368	388	408	428	448	468	488	508	528	548
2.	BWI	15.6	15.8	16.0	16.2	16.4	16.6	16.8	17.0	17.2	17.4
3.	GMWR	0.479	0.579	0.679	0.779	0.879	0.979	1.079	1.179	1.279	1.379

Table 5.5 The Ten Cases of Variation of Inputs for 79.1% Passing 106 μm

SN	Input	Cases									
		1	**2**	**3**	**4**	**5**	**6**	**7**	**8**	**9**	**10**
1.	TPH	520	540	560	580	600	620	640	660	680	700
2.	BWI	15.7	15.9	16.1	16.3	16.5	16.7	16.9	17.1	17.3	17.5
3.	GMWR	0.305	0.405	0.505	0.605	0.705	0.805	0.905	1.005	1.105	1.205

5.3 Results and Discussions

5.3.1 Simulation Results for Changes in One Input Variable

The simulation results are presented in Fig. 5.3 to Fig. 5.11 for the changes in one input variable for the three scenarios of product particle size passing.

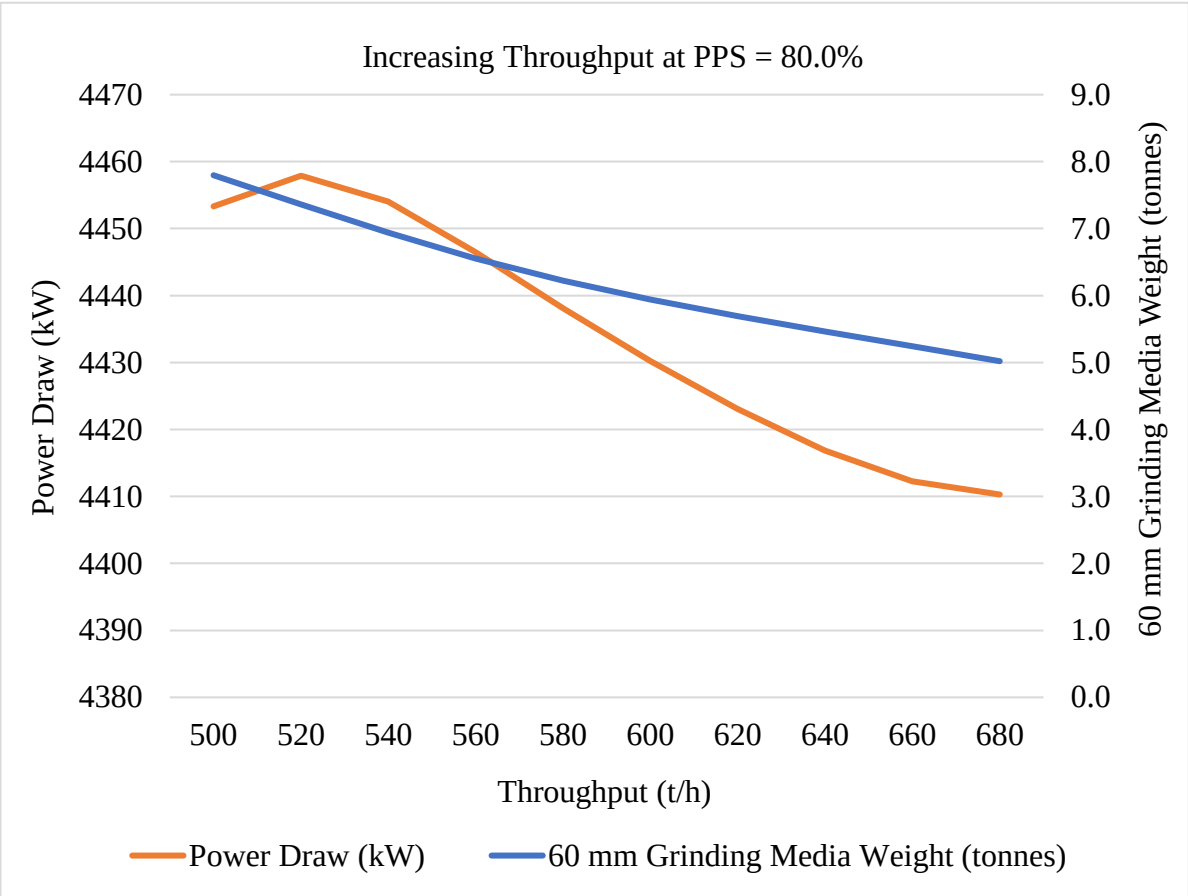

Fig. 5.3 A Graph of Power Draw and 60 mm Grinding Media Weight versus Throughput at 80.0% Product Particle Size Passing 106 μm

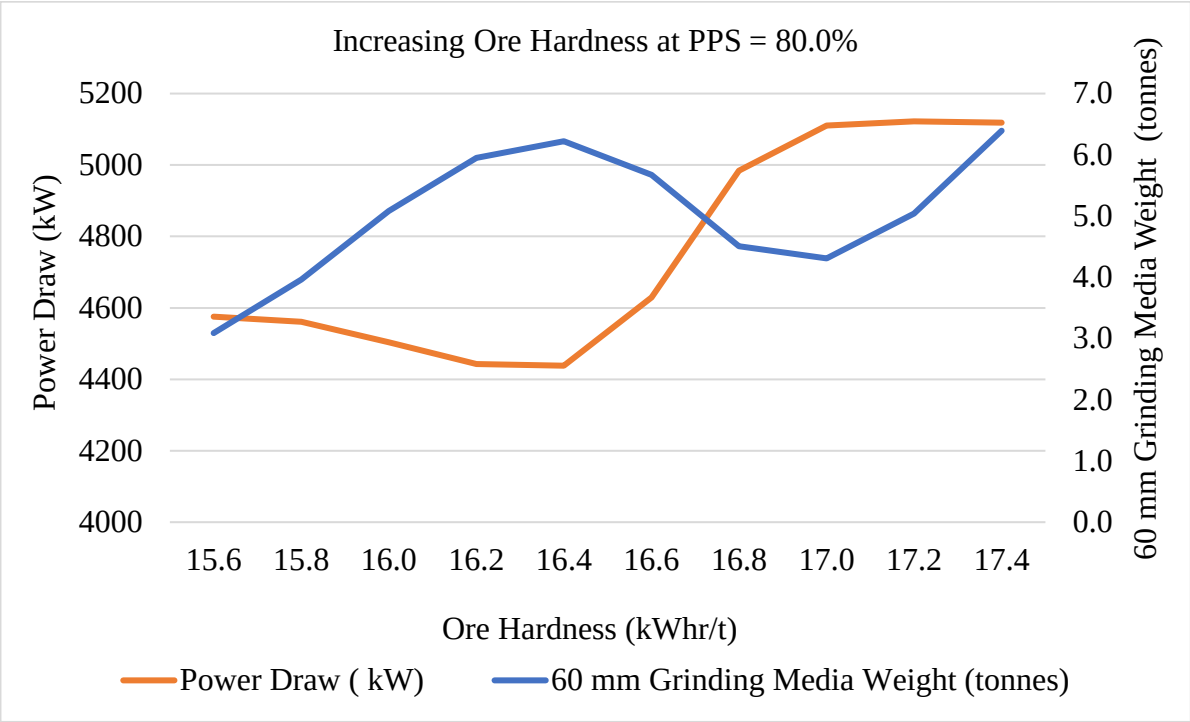

Fig. 5.4 A Graph of Power Draw and 60 mm Grinding Media Weight versus Ore Hardness at 80.0% Product Particle Size Passing 106 μm

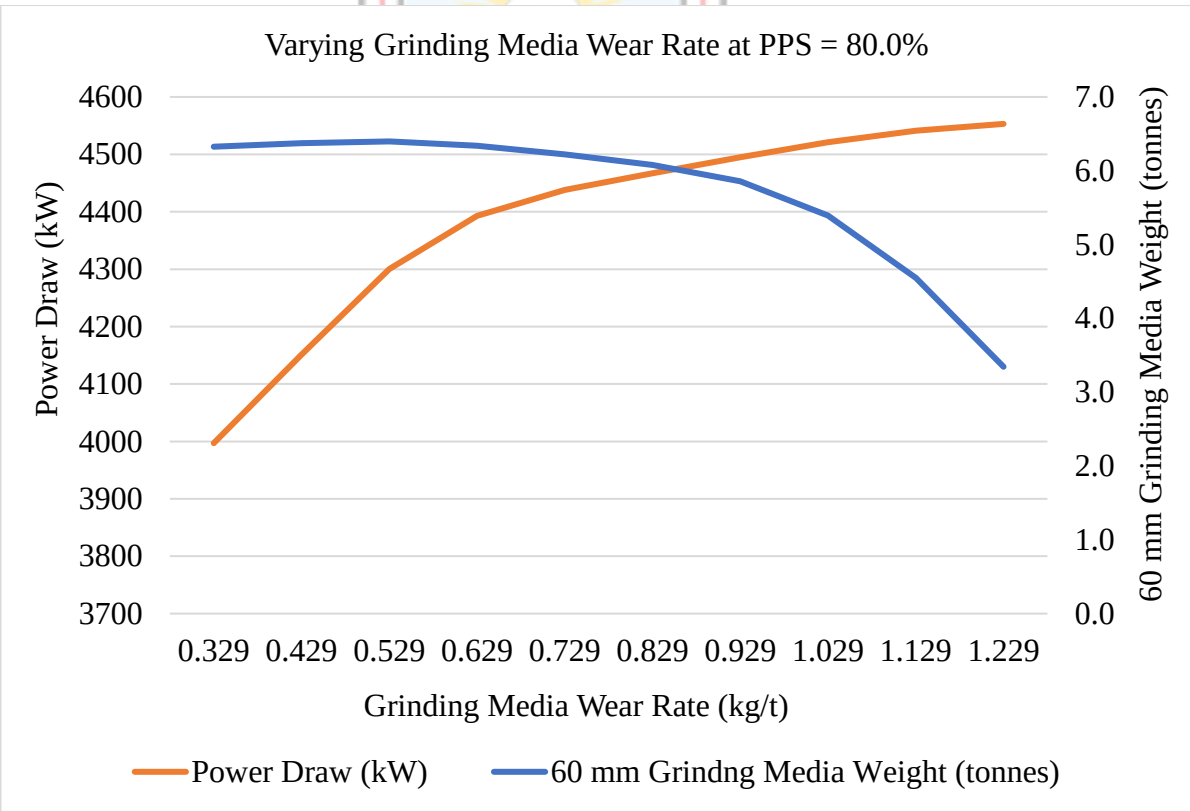

Fig. 5.5 A Graph of Power Draw and 60 mm Grinding Media Weight versus Grinding Media Wear Rate at 80.0% Product Particle Size Passing 106 μm

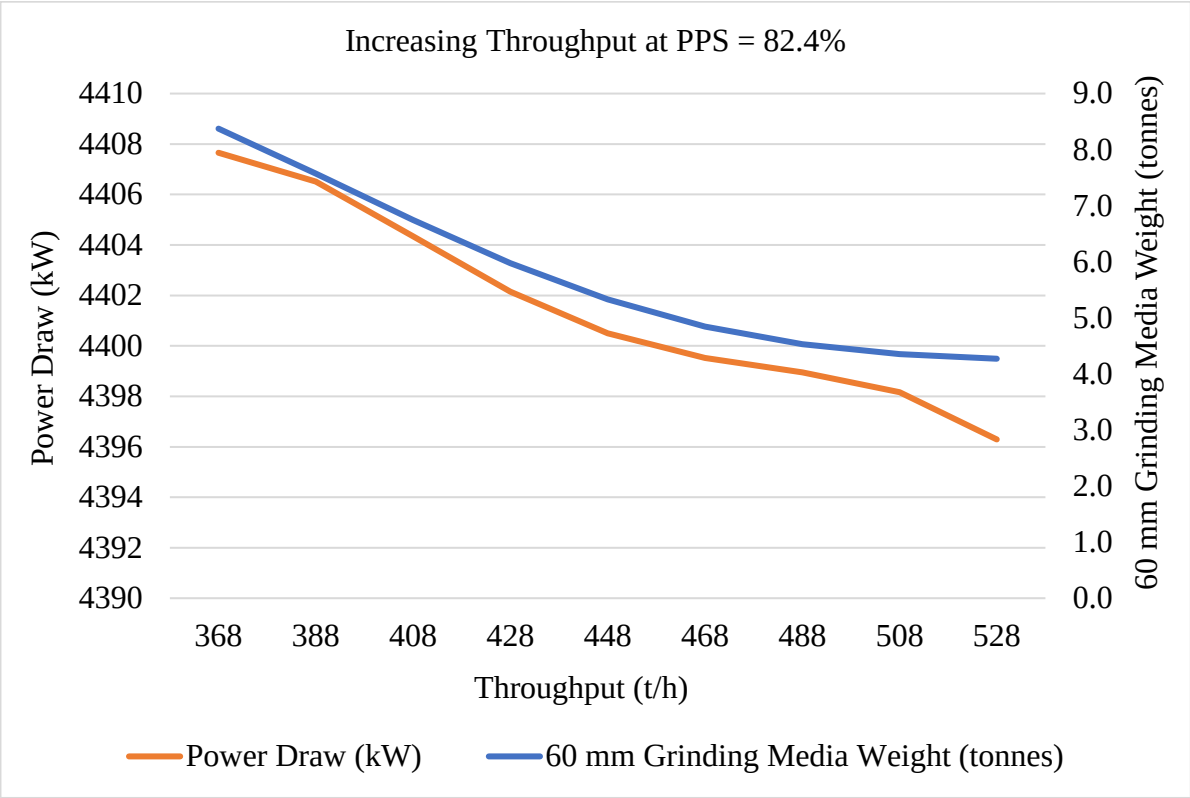

Fig. 5.6 A Graph of Power Draw and 60 mm Grinding Media Weight versus Throughput at 82.4% Product Particle Size Passing 106 μm

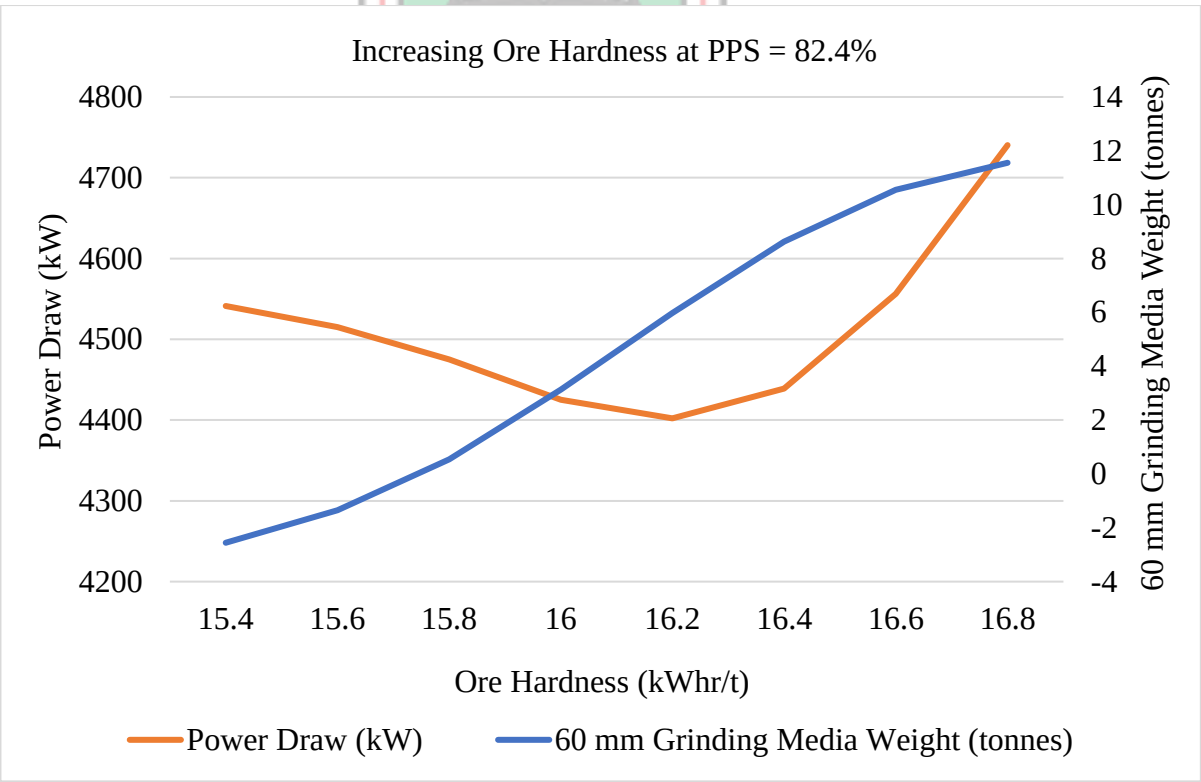

Fig. 5.7 A Graph of Power Draw and 60 mm Grinding Media Weight versus Ore Hardness at 82.4% Product Particle Size Passing 106 μm

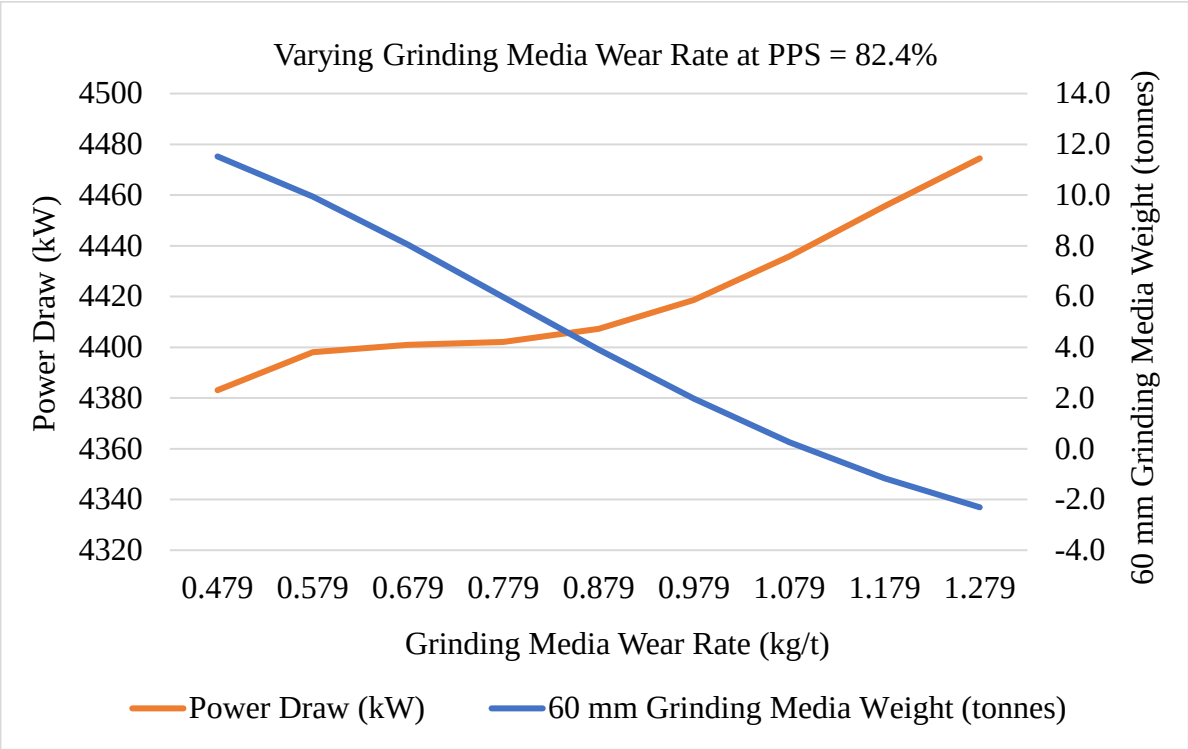

Fig. 5.8 A Graph of Power Draw and 60 mm Grinding Media Weight versus Grinding Media Wear Rate at 82.4% Product Particle Size Passing 106 μm

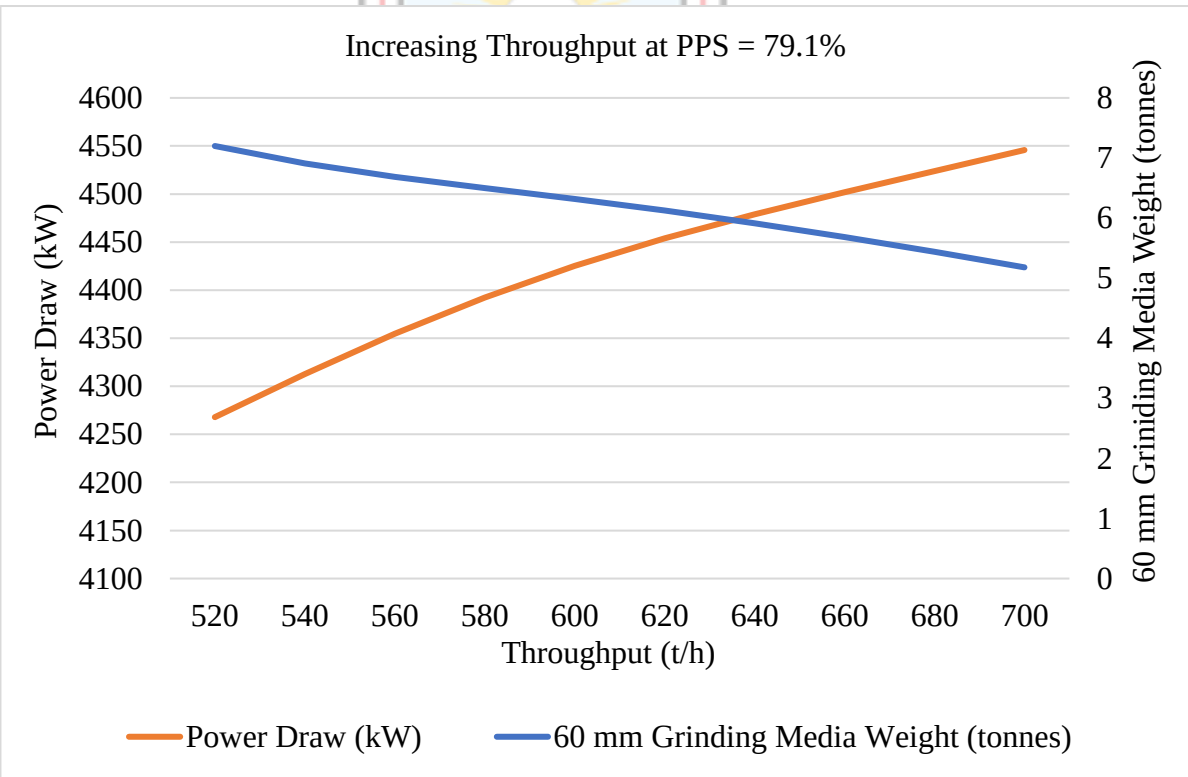

Fig. 5.9 A Graph of Power Draw and 60 mm Grinding Media Weight versus Throughput at 79.1% Product Particle Size Passing 106 μm

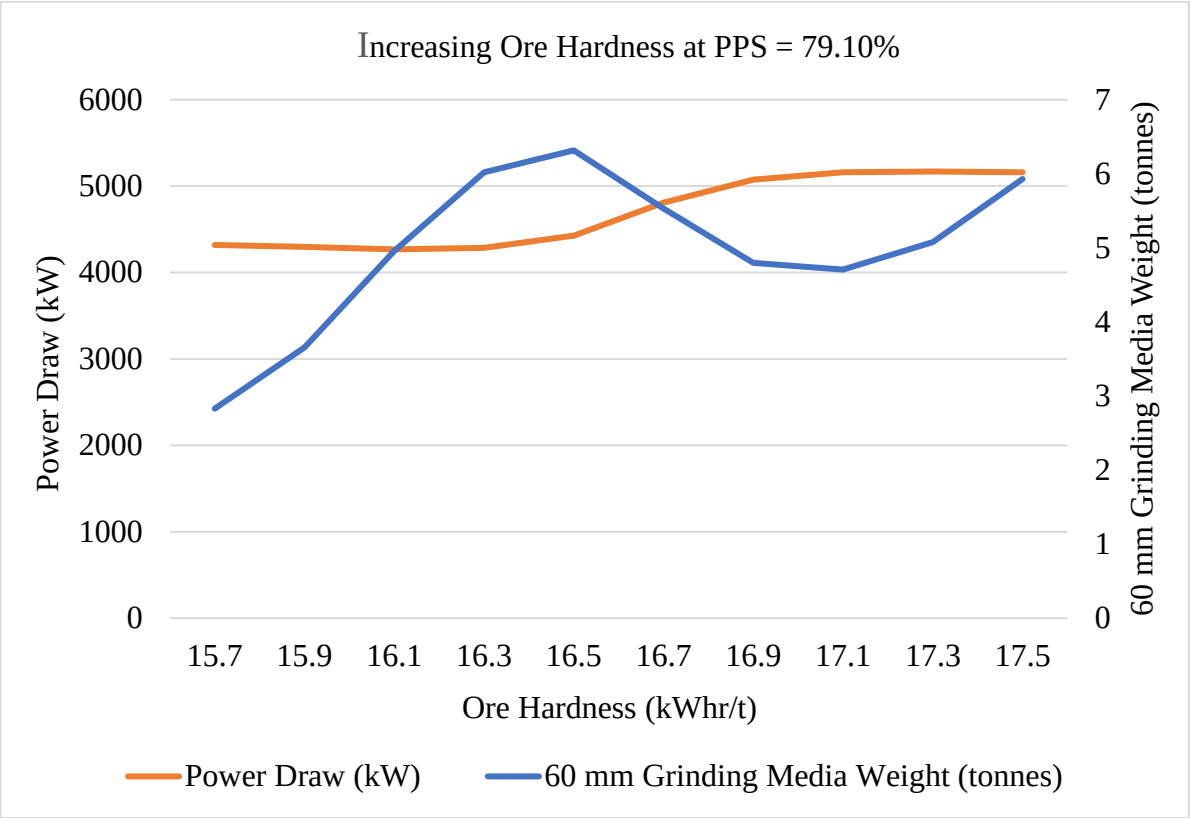

Fig. 5.10 A Graph of Power Draw and 60 mm Grinding Media Weight versus Ore Hardness at 79.1% Product Particle Size Passing 106 μm

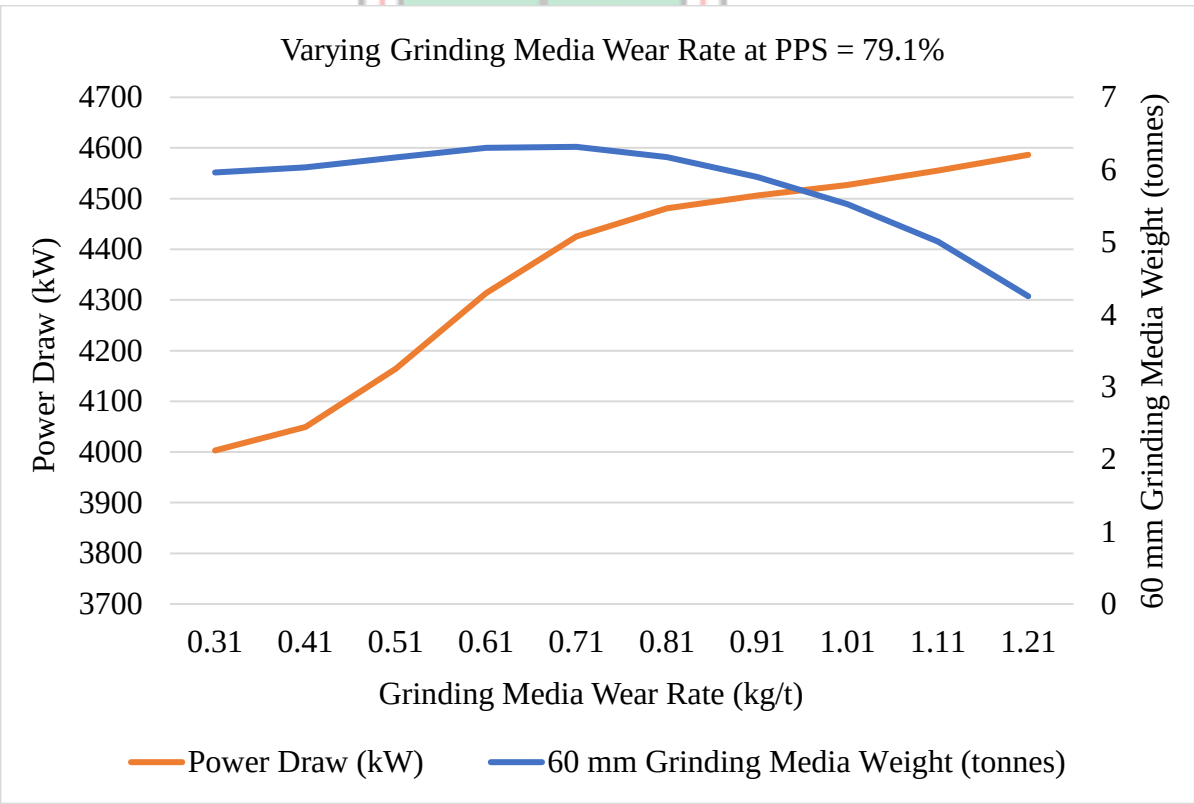

Fig. 5.11 A Graph of Power Draw and 60 mm Grinding Media Weight versus Grinding Media Wear Rate at 79.1% Product Particle Size Passing 106 μm

5.3.2 Simulation Results for Changes in Multiple Input Variables

Due to simultaneous variations of multiple parameters in the x – axis, numbers were used to represent the combinations of two or three changing variables. Corresponding values of the changing variables were presented in Table 5.3, Table 5.4 and Table 5.5 on pages 86 and 87. The results for the changes in multiple input variables are as shown in Fig. 5.12 to Fig. 5.23.

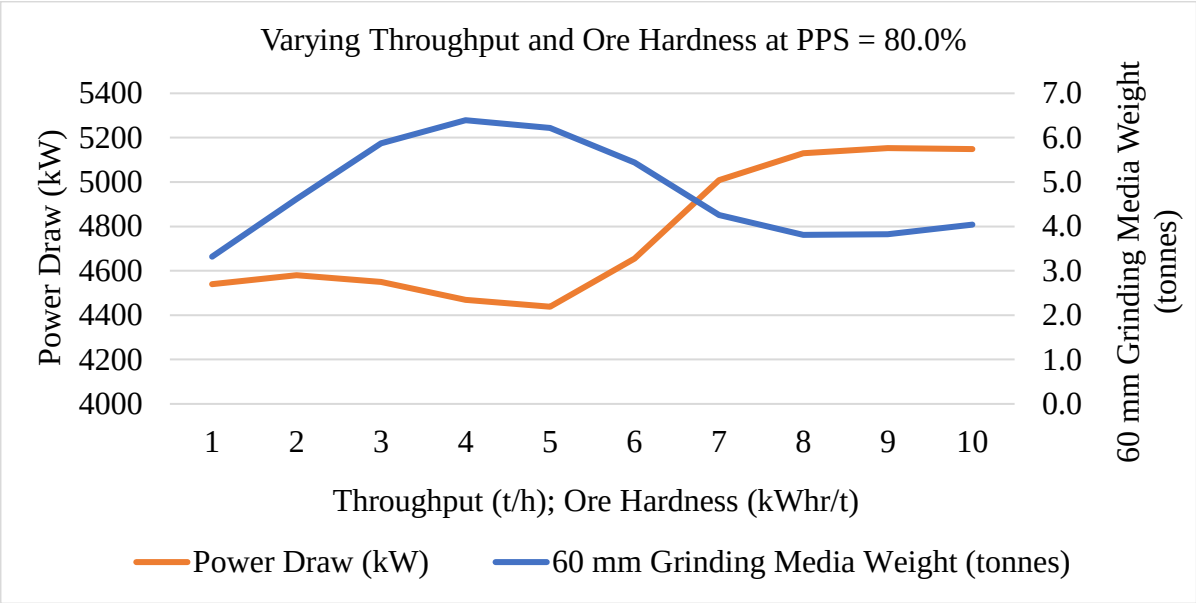

Fig. 5.12 A Graph of Power Draw and 60 mm Grinding Media Weight versus Variations in Throughput and Ore Hardness at 80.0% Product Particle Size Passing 106 μm

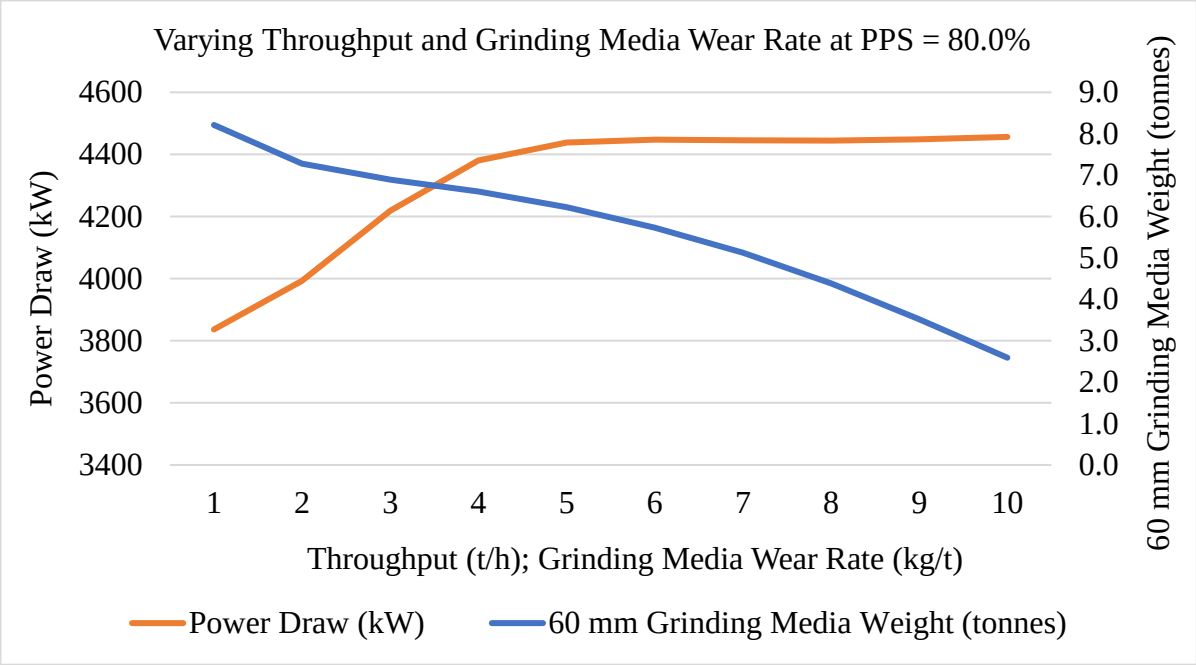

Fig. 5.13 A Graph of Power Draw and 60 mm Grinding Media Weight versus Variations in Throughput and Grinding Media Wear Rate at 80.0% Product Particle Size Passing 106 μm

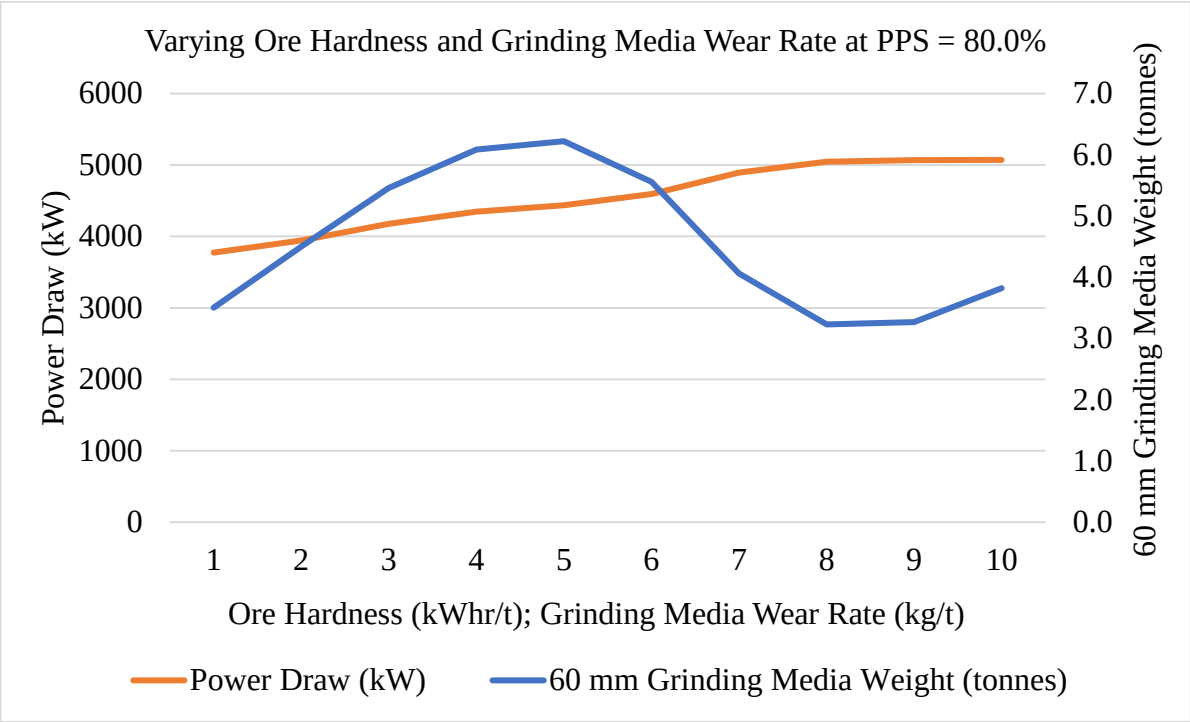

Fig. 5.14 A Graph of Power Draw and 60 mm Grinding Media Weight versus Variations in Ore Hardness and Grinding Media Wear Rate at 80.0% Product Particle Size Passing 106 μm

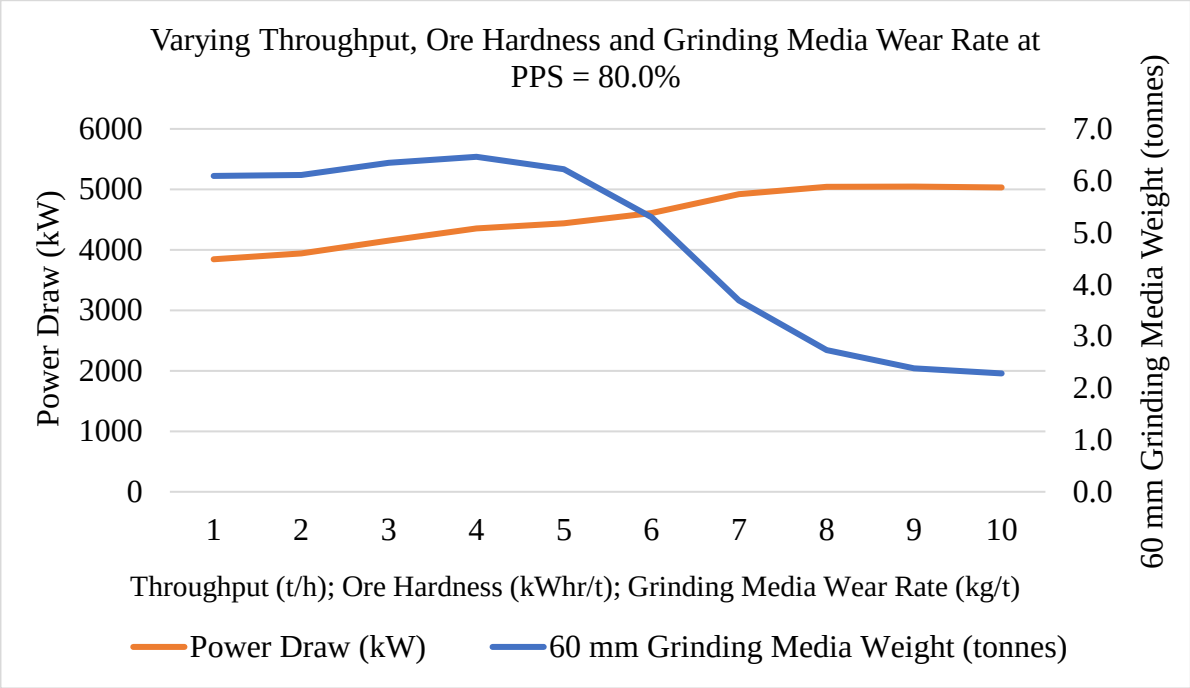

Fig. 5.15 A Graph of Power Draw and 60 mm Grinding Media Weight versus Variations in Throughput, Ore Hardness and Grinding Media Wear Rate at 80.0% Product Particle Size Passing 106 μm

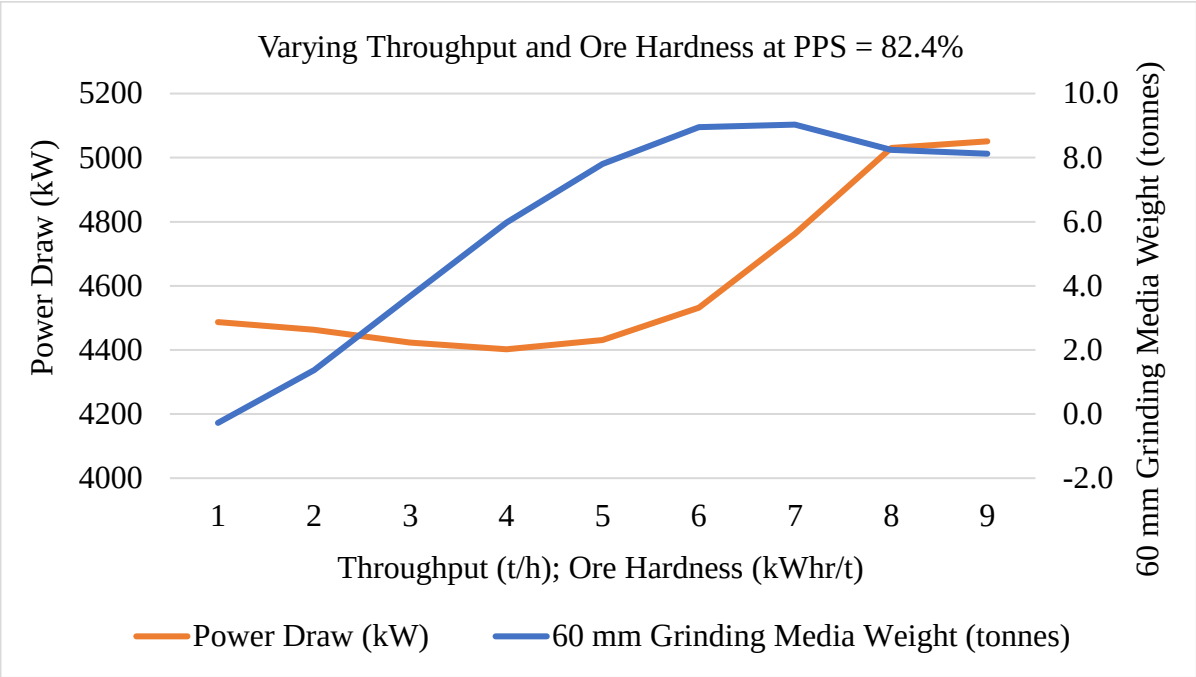

Fig. 5.16 A Graph of Power Draw and 60 mm Grinding Media Weight versus Variations in Throughput and Ore Hardness at 82.4% Product Particle Size Passing 106 μm

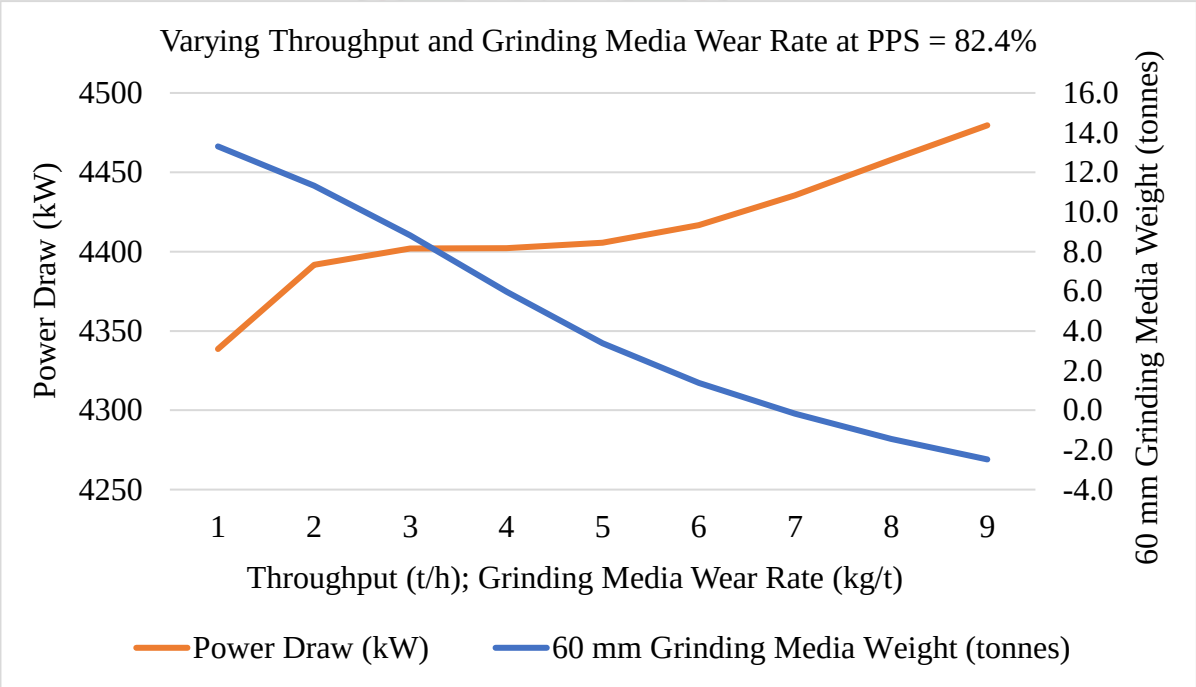

Fig. 5.17 A Graph of Power Draw and 60 mm Grinding Media Weight versus Variations in Throughput and Grinding Media Wear Rate at 82.4% Product Particle Size Passing 106 μm

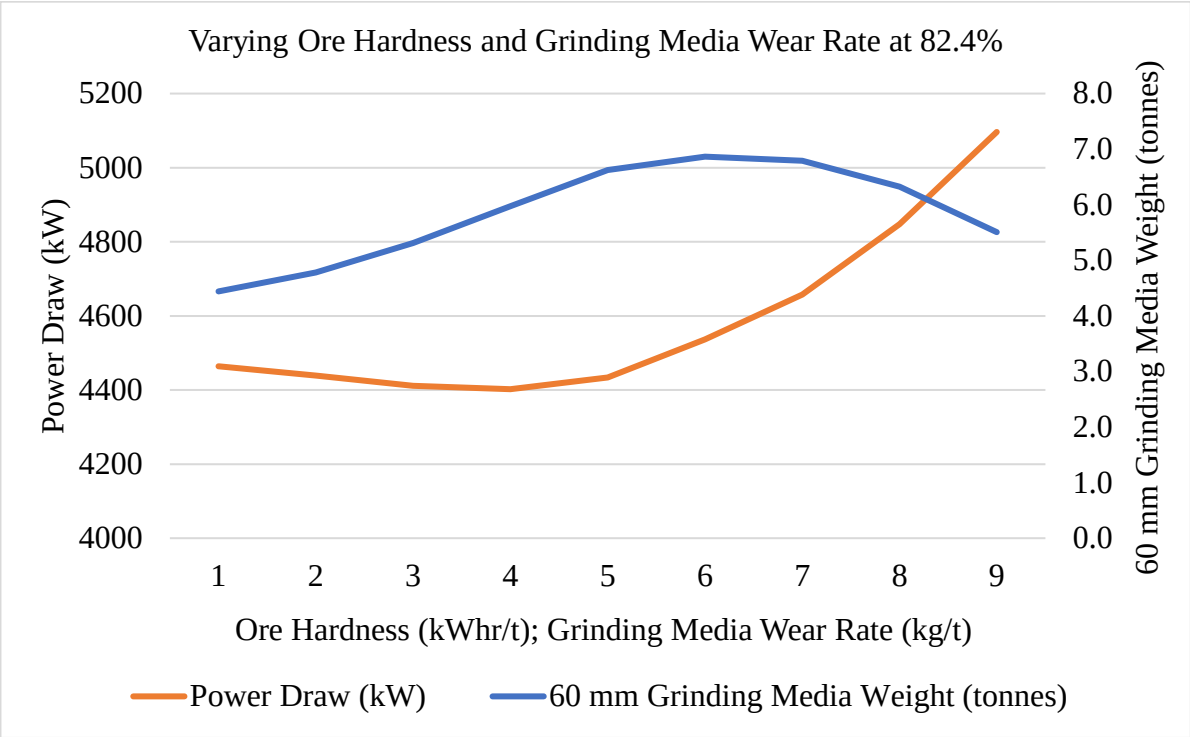

Fig. 5.18 A Graph of Power Draw and 60 mm Grinding Media Weight versus Variations in Ore Hardness and Grinding Media Wear Rate at 82.4% Product Particle Size Passing 106 μm

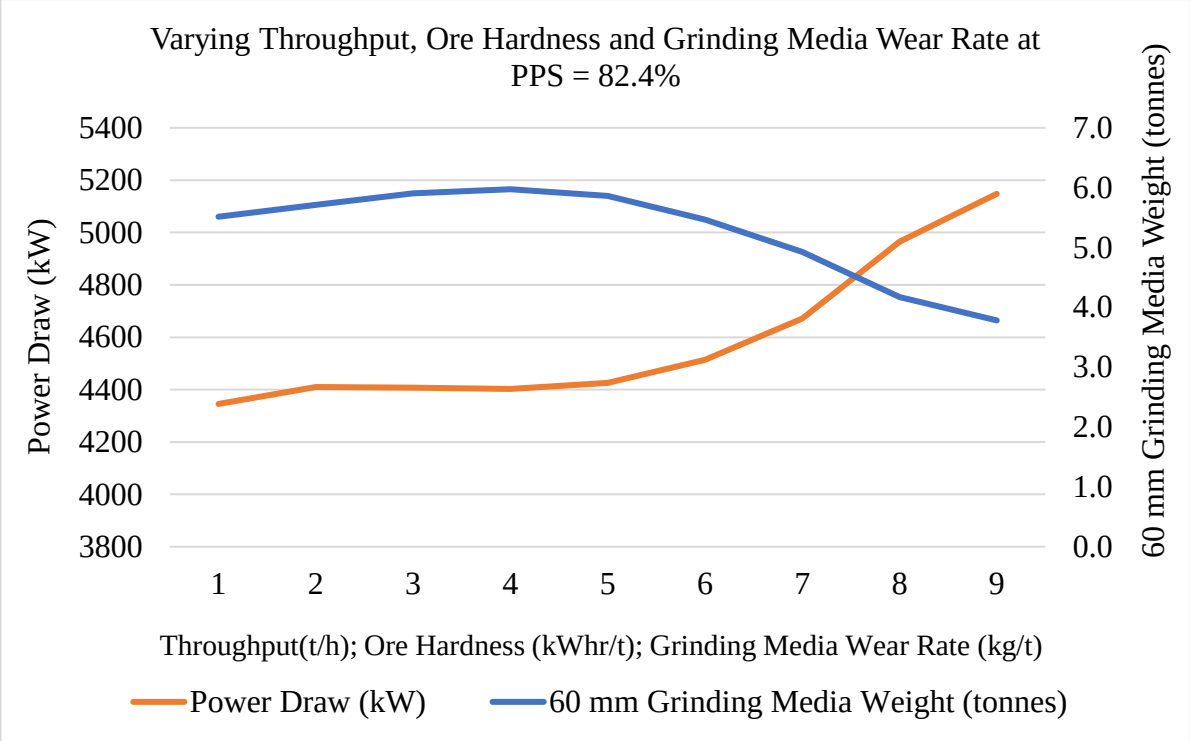

Fig. 5.19 A Graph of Power Draw and 60 mm Grinding Media Weight versus Variations in Throughput, Ore Hardness and Grinding Media Wear Rate at 82.4% Product Particle Size Passing 106 μm

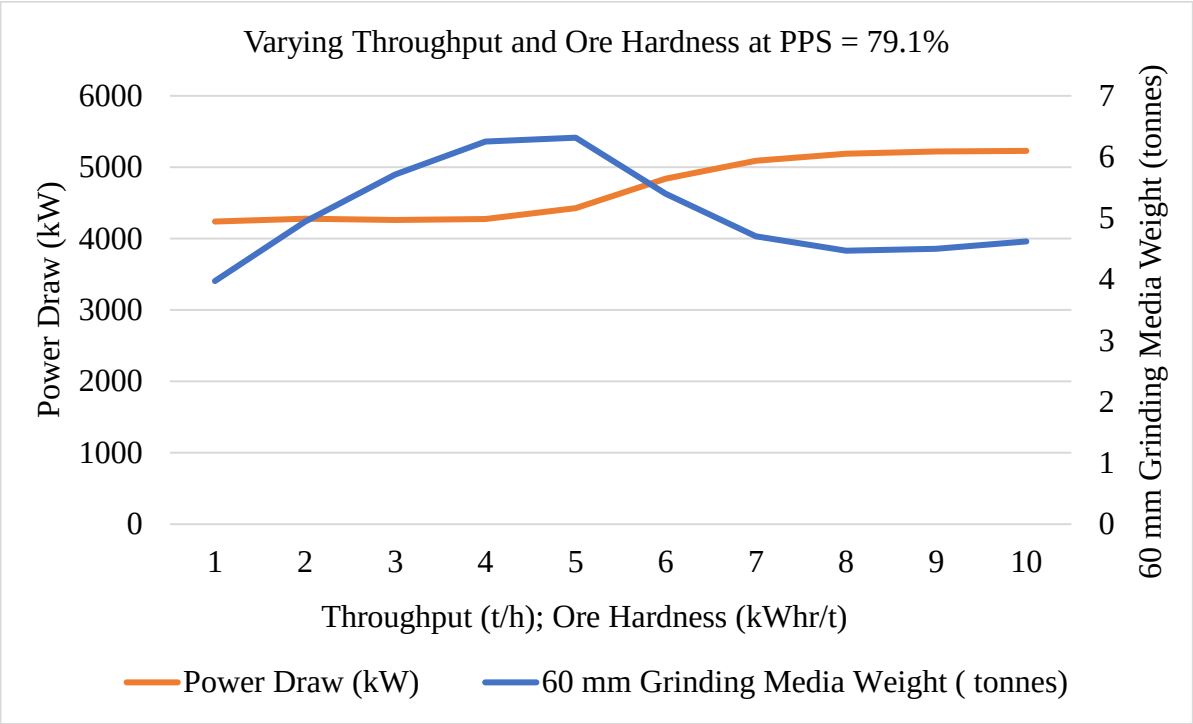

Fig. 5.20 A Graph of Power Draw and 60 mm Grinding Media Weight versus Variations in Throughput and Ore Hardness at 79.1% Product Particle Size Passing 106 μm

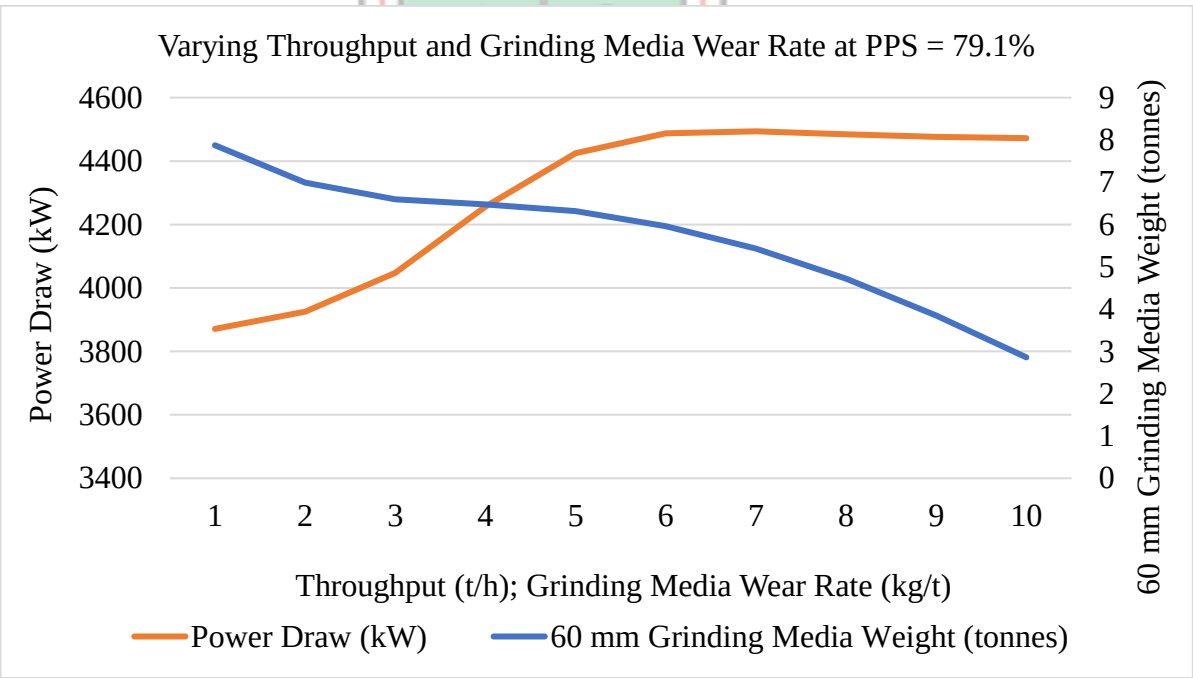

Fig. 5.21 A Graph of Power Draw and 60 mm Grinding Media Weight versus Variations in Throughput and Grinding Media Wear Rate at 79.1% Product Particles Size Passing 106 μm

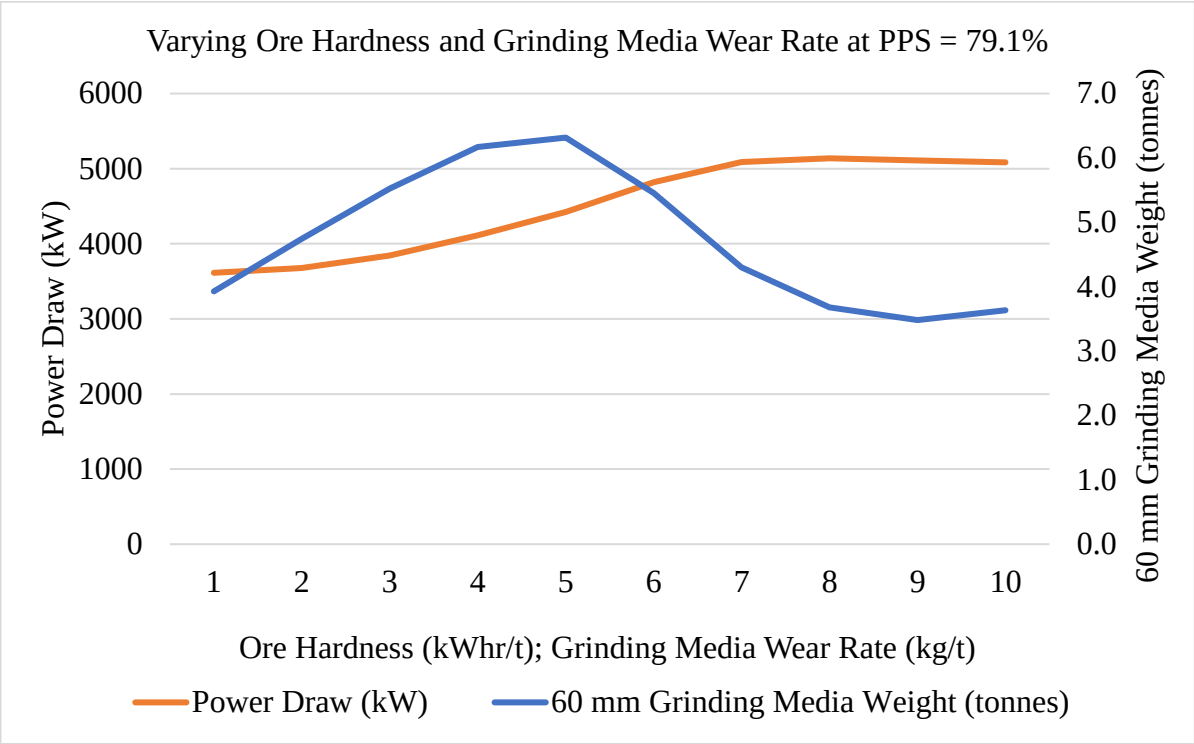

Fig. 5. 22 A Graph of Power Draw and 60 mm Grinding Media Weight versus Variations in Ore Hardness and Grinding Media Wear Rate at 79.1% Product Particle Size Passing 106 μm

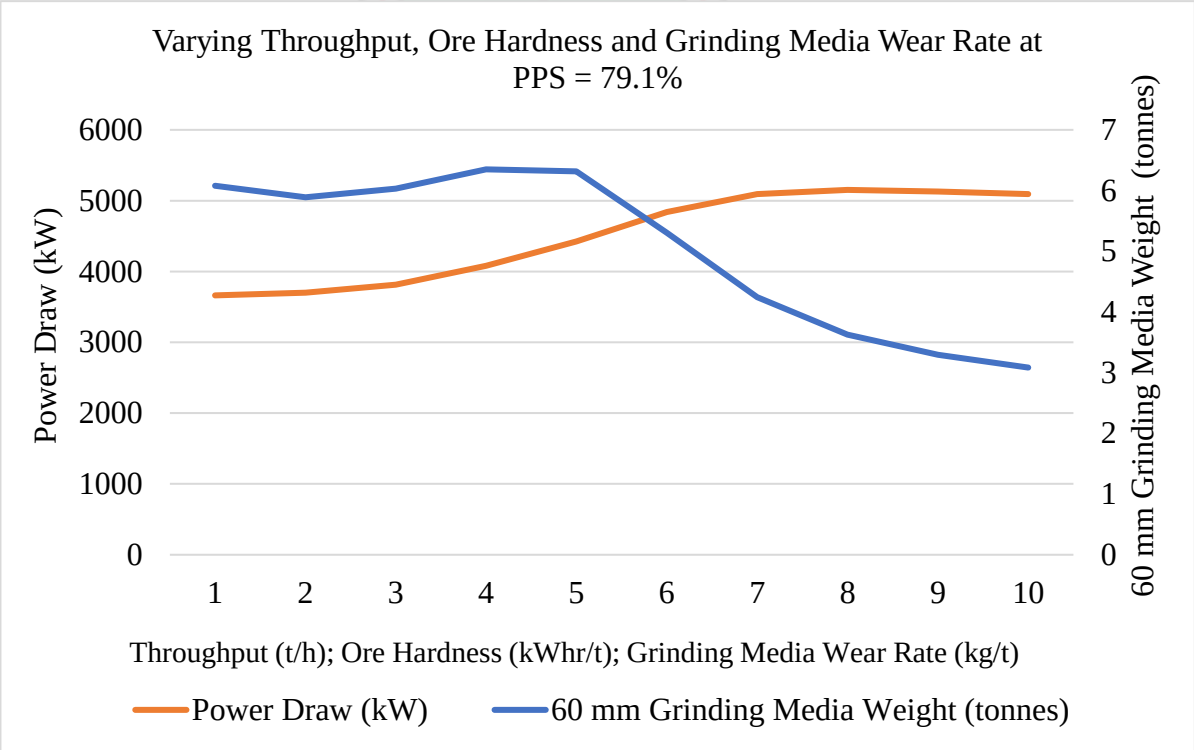

Fig. 5.23 A Graph of Power Draw and 60 mm Grinding Media Weight versus Variations in Throughput, Ore Hardness and Grinding Media Wear Rate at 79.1% Product Particle Size Passing 106 μm

5.3.3 Discussion of Simulation Results

This section is dedicated to the discussion of the simulation results presented in the previous section. The graphs presented in Section 5.3 are discussed accordingly.

Discussions of results of changes in one input variable

With regards to throughput, results presented in Fig. 5.3 and Fig. 5.6 suggest that a decrease in grinding media consumption and power draw are achievable at 80.0% product particle size and above. This occurred at increasing the throughput from 520 t/h for the 80.0% passing (Fig. 5.3) and 388 t/h for 82.4% passing (Fig. 5.6). At 79.1% passing from Fig. 5.9, grinding media consumption decreased whilst power draw increased for throughputs of 630 t/h and above and vice versa for throughputs below 630 t/h. This striking difference at 79.1% passing could be explained by the relatively higher throughputs that consequently require more power draw for effective mill load dynamics. It is to be noted that any addition of grinding media would have caused more mill load and hence, further increase in the power draw. Clearly, from the perspective of throughputs only, it is preferable to operate the mill not below 80.0% passing in the throughput range of 400 t/h to 680 t/h.

Simulation outcomes on variation of ore hardness presented in Fig. 5.4, Fig. 5.7 and Fig. 5.10 suggest noticeable increases in grinding media consumption and mill power draw for ore hardness of 17.0 kWhr/t and above at 80.0% passing, 16.2 kWhr/t and above at 82.4% passing and 17.1 kWhr/t and above for 79.1% passing 106 µm. At the respective indicated ore hardness, 4.25 tonnes and 5100 kW, 2 tonnes and 4540 kW and 4.8 tonnes and 5150 kW, respectively were consumed for the respective grindings at 80.0%, 82.4% and 79.1% passing 106 µm. Clearly, the lower the ore hardness the less consumption of grinding media and the less power drawn by mill. Operational plant practice beholds high ore hardness especially from deeper pits and the need for mixing of ores from a number of pits in order to reduce the effective hardness of ore. Judging from Fig. 5.4, it is preferable to grind at an ore hardness in the range of 16.4 kWhr/t to 17.2 kWhr/t giving 60 mm grinding media consumption in the range of 5 tonnes to 6.3 tonnes and power draw in the range of 4420 kW to 5140 kW at 80.0% passing 106 µm.

From Fig. 5.5, Fig. 5.8 and Fig. 5.11, a grinding media wear rate of 0.63 t/h and beyond led to a rise in power draw and a decrease in demand of 60 mm grinding media balls for the three scenarios. The reverse case is true for wear rates below 0.63 kg/t. Ideally, higher grinding media wear rates should result in higher levels of replenishment of grinding media balls to result in additional power draw. This anomaly of decrement in 60 mm balls demanded for increased wear rates could be due to the possibility of exceeding the filling limit of the wet ball mill due

to the cumulative filling effect of grinding media. Increment of the grinding media wear rate from 0.63 t/h to 0.93 t/h resulted in a decrease of 0.5 tonnes (from 6.5 tonnes to 6.0 tonnes) in grinding media ball demand and increase of 100 kW (from 4400 kW to 4500 kW) in mill power draw at 80.0% passing 106 µm. Similarly, at 82.4% passing, grinding balls demand reduced by 6 tonnes (from 9 tonnes to 3 tonnes) and power draw increased by 1100 kW (from 4400 kW to 5500 kW). At 79.1% passing 106 µm, grinding media demanded reduced by 0.5 tonnes (from 6.3 tonnes to 5.8 tonnes) and power draw increased by 150 kW (from 4350 kW to 4500 kW). It stands to reason that it is beneficial to operate at 80.0% passing in the grinding media wear rate range of 0.63 t/h to 0.93 t/h as this offers minimal changes in grinding media consumption and power draw.

Discussion of results of changes in multiple input variables

From Fig. 5.12, Fig. 5.16 and 5.20, throughput and ore hardness significantly influenced power draw and required 60 mm grinding media weight. At 80.0% passing from Fig. 5.12, increasing throughput and ore hardness above Case 5 (throughput of 580 t/h and ore hardness of 16.4 kWhr/t from Table 5.3) resulted in an increase in power draw and a decrease of grinding media charge and vice versa for cases below 5. Fig. 5.12 however suggested that decrease in power draw of nearly 200 kW is achievable from Case 2 to Case 5 but at a trade-off of additional grinding media charge of about 1 tonne. Fig. 5.16, however, revealed no hope of achieving close to insignificant changes in the output variables to result in their minimum values. Achieving minimum power draw from Case 1 to Case 5 gave a change of 500 kW that is from 4500 kW to 5000 kW. Also, beyond Case 5, both output variables increased to high unacceptable values for the 82.4% passing 106 μm. Fig. 5.20 showed a general increase in power draw and a decrease in grinding media charge for Case 5 (which from Table 5.5 corresponded to 600 t/h and 16.5 kWhr/t) and vice versa for the predicted variables below Case 5. From the three scenarios as presented in Fig. 5.12, Fig. 5.16 and Fig. 5.20, it can be seen that, the better option is to grind not beyond Case 5 at 80.0% passing 106 μm and this corresponds to throughputs up to 580 t/h and ore hardness up to 16.4 kWhr/t.

From Fig. 5.13, 5.17 and Fig 5.21, similar patterns of influence of variations in throughput and grinding media wear rate are observable. Quite gradual decreases in 60 mm grinding media weight charge result in gradual increases in mill power draw from Case 1 to Case 10. There is a conflicting desire to grind more at less grinding media wear rate. The minimum and maximum grinding media wear rates are 0.4 kg/t and 1 kg/t, respectively. Maximum throughput stands at 700 t/h. These translate into focus on Cases 2 to 7 on Fig. 5.15, Cases 1 to 6 on Fig. 5.17 and Cases 2 to 7 on Fig. 5.21. The corresponding throughputs are 520 t/h to 620 t/h, 368 t/h to 468

t/h and 540 t/h to 640 t/h, respectively. A standard minimum throughput of 400 t/h could not be achieved by Fig. 5.17 for 82.4% passing. More so, its corresponding throughput range was low compared to the other two scenarios of 80.0 % and 79.1% passing. To grind at less than the stipulated 6 tonnes of 60 mm grinding media weight strongly suggested operating at Cases 6 and 7 for the two scenarios resulting in a grinding media weight not below 5 tonnes. For this, the power draw stood at a constant 4450 kW at the 80.0 % passing (Fig. 5.13) and 4500 kW, respectively giving a savings of 50 kW at the scenario of 80.0% passing. Further reduction in grinding media weight on Fig. 5.13 hardly affected the power drawn, though assuring of increased throughput, it also led to higher wear rate of balls beyond the maximum value.

Variation of ore hardness and grinding media wear rate reflected a steady increase of power draw whilst grinding media increased to a point and decreased to lower values as depicted in Fig. 5.14, Fig. 5.18 and Fig. 5.22. From Fig. 5.18, the increase in both predicted variables from Case 3 to Case 7 was untenable and this rules out grinding at 82.4% passing. From Fig. 5.14 and Fig. 5.22, increasing ore hardness and grinding media wear rate from Case 6 to Case 8 resulted in less 60 mm grinding media weight demand below 6 tonnes to as low as 3 tonnes for 80.0% passing and 3.6 tonnes for 79.1% passing both for power draw increment of 350 kW. The 0.6 tonnes of weight reduction achievable at 80.0% passing instead of 79.1% passing is highly desirable. Grinding at the 80.0% passing offered ore hardness in the range 16.6 kWhr/t to 17.0 kWhr/t and grinding media wear rate range of 0.829 kg/t to 1.029 kg/t offering a throughput range of 600 t/h to 640 t/h (see Table 5.3). So, a wear rate beyond the standard 1 kg/t could be risked to achieve some reduced weight of balls, grind harder ore and achieve throughput of 640 t/h.

Variations in three variables, simply, throughput, ore hardness and grinding media wear rate are an attempt to exploit the possible improvements in power draw and grinding media charge minimisations. A closer look at Fig. 5.15, 5.19 and 5.23, reveal much similarity with results regarding variations in ore hardness and grinding media wear rate (see Fig. 5.14, Fig. 5.18 and Fig. 5.22). The exception has to do with the increment in 60 mm grinding media weight at the lower cases due to the inclusion of throughput. The need for more throughput and grinding of harder ores change significantly the internal grinding dynamics of the mill and hence, the need for more grinding media at the lower cases and comparative need for less grinding media at the higher cases of 7 to 10 whilst the power draw remained quite unchanged with regard to the corresponding scenarios in the variation of ore hardness and grinding media wear rate. In the midst of increasing throughput, there is the possibility of reducing the 60 mm grinding media charge for an increment in power draw of about 350 kW for a grind at 80.0% passing 106 μm.

Further increase in the three input variables based on Fig. 5.15, gave the possibility of only achieving minimum grinding media charge at a trade-off of mill power draw.

5.4 Summary

This section investigated how sensitive power draw and grinding media charge were to changes in selected input variables namely, throughput, ore hardness and grinding media wear rate. Both single and multiple variables analyses were performed in an attempt to find out the possibility of grinding with minimal power draw and minimal grinding media charge while maximising throughput. The analysed scenarios and cases revealed that, it is desirable to grind at 80.0% passing 106 μm and that minimisation of 60 mm grinding media charge is achievable at the expense of the mill power draw.

CHAPTER 6

CONCLUSIONS AND RECOMMENDATIONS

6.1 Conclusions

This research sought to predict grinding media charge for optimum power draw using developed ANN-based models. The ANN-based models were developed making use of tumbling wet ball mill operational data collected over a period of time at the plant under consideration. The goal was to achieve an accurate model for the purpose of predicting power draw and grinding media charge. Four types of ANN models namely, FBNN, RBFNN, GRNN and ANFIS were utilised in predicting accurately, power draw and product particle size percentage passing 106 μm from operational data. All the four models showed promising results however, results from the FBNN were however outstanding compared to the other three though its accuracy was not entirely 100%.

A criterion for determining OCPs from the predicted data was formulated and used to identify OCPs from the predicted dataset. The accuracy of the model was further optimised using GWO algorithm to better predict grinding media charge and power draw. Finally, sensitivity analyses were performed to determine how sensitive power draw and grinding media charge were to changes in three input variables namely, throughput, ore hardness and grinding media wear rate. Conclusively, reductions in grinding media charge are achievable at the expense of mill power draw. Also, throughputs up to 640 t/h with regard to the studied wet ball mill stand to be implemented.

6.2 Recommendations

It is recommended that online data logging methods should be improved in order to improve the accuracy of predictive models for the purposes of grinding media charge and power draw predictions. Also, possible deployment schemes should be investigated on a pilot basis before full deployment.

6.3 Research Contributions

The contributions of this research are as follows:

i. A developed ANN – based optimised model for the purpose of predicting grinding media charge and power draw; and
ii. Informed knowledge on how sensitive grinding media charge and power draw are to changes in some varying input variables.

6.4 Future Research Directions

The following research directions can be considered as future work:

i. With improved data logging schemes, dynamic mode training should be investigated to explore the possibilities of capturing intermittent trends; and

ii. Other bionic metaheuristic optimisation algorithms such as Flower Pollination Algorithm and Whale Optimisation Algorithm can be looked at as an alternative to better enhance the accuracy of the developed predictive models.

REFERENCES

Abazarpoor, A. and Halali, M. (2017), "Investigation of the Particle Size and Shape of Iron Ore Pellet Feed Using Ball and HPGR Grinding Methods", *Physicochemical Problems of Mineral Processing*, Vol. 53, No. 2, pp. 908 – 919.

Abbey, C. E., Bansah, K. J., Galecki, G. and Boateng, K. A. (2015), "Rock Characteristics and Ball Mill Energy Requirements at Goldfields Ghana Limited, Tarkwa Gold Mine", *Ghana Mining Journal*, Vol.15, No. 1, pp. 50 – 57.

Abdelhaffez, G. S. (2018), "Estimation of the Wear Rate Associated with Ball Mill of Mahd Ad Dahab Gold Mine, Saudi Arabia (KSA)", *Mining of Mineral Deposits*, Vol. 12, Issue 3, pp. 36 - 44.

Aguila-Camacho, N., Le Roux, J. D., Duarte-Mermoud, M. A. and Orchard, M. E. (2017), "Control of a Grinding Mill Circuit Using Fractional Order Controllers", *Journal of Process Control*, Vol. 53, No. 1, pp. 80 – 94.

Ahmed, A. E. and Mohamed, A. E. (2020), "Improved Adaptive Neuro–Fuzzy Inference System Using Gray Wolf Optimisation: A Case Study in Predicting Biochar Yield", Journal of Intelligent Systems, Vol. 29, No. 1, pp. 924 – 940.

Al-Masri (2019), "How Does Back-Propagation in Artificial Neural Networks Work", *https://towardsdatascience.com/how-does-back-propagation-in-artificial-neuralnetworks-work-c7cad873ea.* Accessed: June 18, 2020.

Arthur, C.K., Temeng, V. A. and Ziggah, Y. Y. (2019), "Soft Computing-Based Technique as A Predictive Tool to Estimate Blast-Induced Ground Vibration", *Journal of Sustainable Mining*, Vol. 3, No. 1, pp. 1 – 10.

Azizi, A., Shafael, S. Z. and Rooki, R. (2016), "Wear Rate Prediction of Grinding Media Using BPNN and MLR Models in Grinding of Sulphide Ores", *International Journal of Materials Science and Engineering*, Vol. 13, No. 2, pp. 1 – 12.

Avalos, S., Kracht, W. and Ortiz, J. M. (2020), "Machine Learning and Deep Learning Methods in Mining Operations: A Data-Driven SAG Mill Energy Consumption Prediction Application", *Mining, Metallurgy and Exploration*, Vol. 37, pp. 1 - 16.

Banadaki, H. D., Nozari, H. A. and Shoorehdeli, M. A. (2015), "Short-Term and Long-Term Thermal Prediction of a Walking Beam Furnace Using Neuro-Fuzzy Techniques", *Journal of Thermal Science*, Vol. 19, No. 2, pp. 703 – 721.

Barman, B., Kanjilal, R. and Mukhopadhyay, A. (2016), "Neuro-Fuzzy Controller Design to Navigate Unmanned Vehicle with Construction of Traffic Rules to avoid

Obstacles", *International Journal of Uncertainty, Fuzziness and Knowledge-Based Systems*, Vol. 24, No.03, pp. 433 - 449.

Bazin, C. and Lavoie, G. (2016), "Ball Mill Rotation Speed and Rate of Particle Breakage: Results for a Full-scale Unit", *Mineral Processing and Extractive Metallurgy*, Vol. 109, No. 3, 161 – 164.

Bian, X., Wang, G., Wang, H., Wang, S. and Lv, W. (2017), "Effect of Lifters and Mill Speed on Particle Behaviour, Torque and Power Consumption of a Tumbling Ball Mill: Experimental Study and DEM Simulation" *Journal of Minerals Engineering*, Vol. 105, No. 1, pp. 22 – 35.

Botha, S., Craig, I. K. and Le Roux, J. D. (2015), "Switching Cyclones to Increase Product Particle Size Range for Ore Milling Circuits", *International Federation of Automatic Control*, Vol. 48, No. 17, pp. 92 – 97.

Bozorg-Haddad, O. (2018), *Advanced Optimisation by Nature-inspired Algorithms*, Springer, Singapore, 1st edition, 159 pp.

Breitung-Faes, S. (2016), "Estimation of Product Relating Energy of Wet Operated Stirred Media Mills in Terms of Process Transfer to other Mill Geometries and Sizes", *Minerals Engineering*, Vol. 103, pp. 33 - 42.

Bunker, R. P. and Thabtah, F. (2019), "A Machine Learning Framework for Sport Result Prediction", *Applied Computing and Informatics*, Vol. 15, Issue 1, pp. 27 - 33.

Cai, G., Liu, X., Dai, C., Zong, L. and Luo, X. (2020), "Load State Identification Method for Wet Ball Mills based on the MEEMD Singular Value Entropy and PNN Classification", *Mining, Metallurgy and Exploration*, Vol. 37, Issue 1, pp. 1 - 11.

Calistus, O. (2016), "Ball Mill", *https://www.pharmapproach.com/ball-mill*. Accessed: June 9, 2018.

Chandradeven, R. (2017), "Radial Basis Functions Neural Networks", *https://towardsdatascience.com/radial-basis-functions-neural-networks-all-we-need-to-know-9a88cc053448*. Accessed: June 12, 2020.

Chimwani, N. and Hildebrandt, D. (2019), "Modelling of an Open Mill with Scalped Feed for the Maximum Production of a Desired Particle Size Range", *Particulate Science and Technology*, Vol. 37, No. 3, pp. 314 - 324.

Chimwani, N., Mulenga, F. K. and Hildebrandt, D. (2015), "Ball Size Distribution for the Maximum Production of a Narrowly-sized Mill Product", *Journal of Powder Technology*, Vol. 284, No. 1, pp. 12 – 18.

Cleary, P. W. and Owen, P. (2018), "Development of Models Relating Charge Shape and Power Draw to SAG Mill Operating Parameters and their Use in Devising Mill Operating Strategies to Account for Liner Wear", *Minerals Engineering*, Vol. 117, pp. 42 - 62.

Collins, A. R. (2016), "Classification of Multi-component Feeds in a Hydrocyclone", *Unpublished BSc Thesis*, University of Queensland, Brisbane, 179 pp.

Costea, C. R., Gergely, E., Husi, G., Coroiu, L., Silaghi, H. and Bara, A. (2017), "A Control Design Technique for Grinding Systems with Feedforward Under-compensation and Feedback Control", *Journal for Feedback Control*, Vol. 1, No. 1, pp. 1 – 6.

Davey, G. (2017), "Prediction of the Performance of Regrind/Floatation Circuits Using Laboratory Tests and Quantitative Mineralogical Information", *Unpublished Master's Thesis Report*, University of Exeter, Exeter, United Kingdom, 101 pp.

Del Rosario Martinez-Blanco, M., Castañeda-Miranda, V. H., Ornelas-Vargas, G., Guerrero-Osuna, H. A., Solis-Sanchez, L. O., Castañeda-Miranda, R., Celaya-Padilla, J. M., Galvan-Tejada, C. E., Galvan-Tejada, J. I., Vega-Carrillo, H. R. and Martínez-Fierro, M. (2016), *Generalised Regression Neural Networks with Application in Neutron Spectrometry*, InTech Open Publishers, Rijeka, Croatia, 412 pp.

Deniz, V. (2016), "An Investigation on the Effects of the Ball Filling on the Breakage Parameters of Natural Amorphous Silica", *Advanced Powder Technology*, Vol. 27, No. 4, pp. 1272 – 1279.

Dias, L., Bhosekar, A. and Lerapetritou, M. (2019), "Adaptive Sampling Approaches for Surrogate-Based Optimisation", *Journal Computer Aided Chemical Engineering*, Vol. 47, No. 1, pp. 377 – 384.

Díaz, E., Voisin, L., Kracht, W. and Montenegro, V. (2018), "Using Advanced Mineral Characterisation Techniques to Estimate Grinding Media Consumption at Laboratory Scale", *Minerals Engineering*, Vol. 121, pp. 180 - 188.

Ebadnejad, A. (2016), "Investigating of the Effect of Ore Work Index and Particle Size on the Grinding Modeling of Some Copper Sulphide Ores" *Journal of Materials Research and Technology*, Vol. 5, No. 2, pp.101 – 110.

Egrioglu, E., Aladag, C. H., Yolcu, U. and Bas, E. (2014), "A New Adaptive Network based Fuzzy Inference System for Time Series Forecasting", *Aloy Journal of Soft Computing and Applications*, Vol. 2, Issue 1, pp. 25 - 32.

Emary, E., Zawbaa, H. M. and Hassanien, A. E. (2016), "Binary Grey Wolf Optimisation Approaches for Feature Selection', *Neurocomputing*, Vol. 172, pp. 371 - 381.

Esteves, P. M., Stopa, M. M., Filho, B. J. C. and Galery, R. (2015), "Charge Behaviour Analysis in Ball Mill by Using Estimated Torque", *IEEE Transactions on Industry Applications*, Vol. 51, No. 3, pp. 2600 – 2606.

Ewees, A. A. and Elaziz, M. A. (2018), "Improved Adaptive Neuro-Fuzzy Inference System using Gray Wolf Optimization", *Journal of Intelligent Systems*, Vol. 29, No. 1, pp. 924 - 940.

Ewees, A. A., El Aziz, M. A. and Elhoseny, M. (2017), "Social-Spider Optimisation Algorithm for Improving ANFIS to Predict Biochar Yield", *8th International Conference on Computing, Communication and Networking Technologies*, Delhi, India, pp. 1 - 6.

Faria, P., Rajamani, R. K. and Tavares, L. M. (2019), "Optimization of Solids Concentration in Iron Ore Ball Milling through Modeling and Simulation", *Minerals*, Vol. 9, No. 6, pp. 1 – 17.

Faris, H., Aljarah, I., Al-Betar, M. A. and Mirjalili, S. (2018), "Grey Wolf Optimiser: A Review of Recent Variants and Applications", *Neural Computing and Applications*, Vol. 30, No. 2, pp. 413 - 435.

Flach, F., Konnerth, C., Peppersack, C., Schmidt, J., Damm, C., Breitung-Faes, S., Peukert, W. and Kwade, A. (2016), "Impact of Formulation and Operating Parameters on Particle Size and Grinding Media Wear in Wet Media Milling of Organic Compounds: A Case Study for Pyrene", *Advanced Powder Technology*, Vol. 27, No. 6, pp. 2507 - 2519.

Foucher, R. J., Lazenby, C. S., Popp, B. M. and Knight, R. C. (2014), "Automatic Ball Charging System for a Ball Mill Assembly", *Patent Application Publication*, Publication No. US2014/0197257A1, 14 pp.

Fragnière, G., Beinert, S., Overbeck, A., Kampen, I., Schilde, C. and Kwade, A. (2018), "Predicting Effects of Operating Condition Variations on Breakage Rates in Stirred Media Mills", *Chemical Engineering Research and Design*, Vol. 138, pp. 433 - 443.

Francioli, D. M. (2015), "Effect of Operational Variables on Ball Milling", *Unpublished BSc Thesis*, UFRJ Escola Politecnica, Rio de Janeiro, Brazil, 90 pp.

Gajawada, S. K. (2019), "The Math behind Artificial Neural Networks", *https://towardsdatascience.com/the-heart-of-artificial-neural-networks-26627e8c03ba*. Accessed: June 23, 2020.

Gao, Z. M. and Zhao, J. (2019), "An Improved Grey Wolf Optimisation Algorithm with Variable Weights", *Computational Intelligence and Neuroscience*, Vol 1, No. 1, pp. 1 – 14.

Ghanei, J. (2020), "Evaluation of the Relation between Ore Texture and Grindability", *Unpublished Master's Thesis Report*, Luleå University of Technology, Luleå, Sweden, 106 pp.

Gharehgheshlagh, H. H., Ergun, L. and Chehreghani, S. (2017), "Investigation of Laboratory Conditions Effect on Prediction Accuracy of Size Distribution of Industrial Ball Mill Discharge by using a Perfect Mixing Model. A Case Study: Ozdogu Copper-Molybdenum Plant", *Physicochemical Problems of Mineral Processing*, Vol. 53, No. 2, pp. 1 – 13.

Ghasemi, E., Kalhori, H. and Bagherpour, R. (2016), "A New Hybrid ANFIS–PSO Model for Prediction of Peak Particle Velocity due to Bench Blasting", *Engineering with Computers*, Vol. 32, No. 4, pp. 607 - 614.

Ghassa, S., Gharabaghi, M., Azadmehr, A. R. and Nasrabadi, M. (2016), "Effects of Flow Rate, Slurry Solid Content and Feed Size Distribution on Rod Mill Efficiency", *International Journal of Particulate Science and Technology*, Vol. 34, No. 5, pp. 533 – 539.

Griffin, P. W., Hammond, G. P. and Norman, J. B. (2016), "Industrial Energy Use and Carbon Emissions Reduction", *Wiley Interdisciplinary Reviews: Energy and Environment*, Vol. 5, No. 6, pp. 684 - 714.

Gupta, A. and Yan, D. S. (2016), *Mineral Processing Design and Operations: An Introduction*, Elsevier Publishers, The Boulevard, Langford Lane, Kidlington, Oxford, UK, 2th edition, 856 pp.

Handoyo, S. and Efendi, A. (2019), "Generating of Fuzzy Rule Bases with Gaussian Parameters Optimized via Fuzzy C-Mean and Ordinary Least Square", *International Journal of Recent Technology and Engineering*, Vol. 8, No. 4, pp. 5787 - 5794.

Hassanzadeh, A. (2015), "Increasing Primary Grinding Circuit Efficiency Considering Grinding Capacity Enhancement", *Proceedings of the 16th Balkan Mineral Processing Congress*, Belgrade, Serbia, pp. 171 – 177.

Hassanzadeh, A. (2017a) "Measurement and Modeling of Residence Time Distribution of Overflow Ball Mill in Continuous Closed Circuit", *Geosystem Engineering*, Vol. 20, No. 5, pp. 251 - 260.

Hassanzadeh, A. (2017b), "The Effect of Make-Up Ball Size Regime on Grinding Efficiency of Full-Scale Ball Mill", *Proceedings of the 17th Balkan Minerals Processing Congress*, Antalya, Turkey, pp. 117 – 123.

Hassanzadeh, A. (2018a), "A New Statistical View to Modelling of Particle Residence Time Distribution in Full-Scale Overflow Ball Mill Operating in Closed-Circuit", *Geosystem Engineering*, Vol. 21, No. 4, pp. 199 - 209.

Hassanzadeh, A. (2018b), "A Survey on Troubleshooting of Closed-circuit Grinding System" *Canadian Metallurgical Quarterly*, Vol. 57, No.3, pp. 328 – 340.

Helmi, M., Hall, M. R., Stevens, L. A. and Rigby, S. P. (2016), "Effects of High-Pressure/Temperature Curing on Reactive Powder Concrete Microstructure Formation", *Construction and Building Materials*, Vol. 105, pp. 554 - 562.

Hlabangana, N., Danha, G. and Muzenda, E. (2018), "Effect of Ball and Feed Particle Size Distribution on the Milling Efficiency of a Ball Mill: An Attainable Region Approach", *South African Journal of Chemical Engineering*, Vol. 25, No. 1, pp. 79 – 84.

Hoseinian, F. S., Abdollahzadeh, A. and Rezai, B. (2018), "Semi-Autogenous Mill Power Prediction by a Hybrid Neural Genetic Algorithm", *Journal of Central South University*, Vol. 25, No. 1, pp. 151 - 158.

Hoseinian, F. S., Faradonbeh, R. S., Abdollahzadeh, A., Rezai, B. and Soltani-Mohammadi, S. (2017), "Semi-Autogenous Mill Power Model Development Using Gene Expression Programming", *Powder Technology*, Vol. 308, pp. 61 - 69.

Iwata, N. and Mori, T. (2020), "Determination of Optimum Slurry Evaluation Method for the Prediction of BaTiO3 Green Sheet Density", *Journal of Asian Ceramic Societies*, Vol. 8, No. 1, pp. 183 - 192.

Jankovic, A., Wills, T. and Dikmen, S. (2016), "A Comparison of Wear Rates of Ball Mill Grinding Media", *Journal of Mining and Metallurgy*, Vol. 52, No. 1 pp. 1 – 10.

Jeswiet, J. and Szekeres, A. (2016), "Energy Consumption in Mining Comminution", *23rd CIRP Conference on Life Cycle Engineering*, Ontario, Canada, pp. 140 – 145.

Kabezya, K. M. and Motjotji, H. (2015), "The Effect of Ball Size Diameter on Milling Performance", *Journal of Material Science and Engineering*, Vol. 4, No. 1, pp. 1 – 4.

Khalil, A. S., Starovoytov, S. V. and Serpokrylov, N. S. (2018), "The Adaptive Neuro-fuzzy Inference System Application for the Ammonium Removal from Aqueous Solution Predicting by Biochar", *Materials Science Forum*, Vol. 931, pp. 985 - 990.

Khodadadi, H. and Ghadiri, H. (2019), "Fuzzy Logic Self – Tuning PID Controller Design for Mill Grinding Circuits Using an Improved Disturbance Observer", *Journal of Mining, Metallurgy and Exploration*, Vol. 36, No. 6, pp. 1075 – 1090.

Kim, H. J., Jo, N. O. and Shin, K. S. (2016), "Optimisation of Cluster-based Evolutionary Undersampling for the Artificial Neural Networks in Corporate Bankruptcy Prediction", *Expert Systems with Applications*, Vol. 59, pp. 226 - 234.

King, R. P. (2012), *Modelling and Simulation of Mineral Processing Systems*, Society for Mining, Metallurgy and Exploration, Colorado, USA, 2nd edition, 457 pp.

Larsson, S., Pålsson, B. I., Parian, M. and Jonsén, P. (2020), "A Novel Approach for Modelling of Physical Interactions between Slurry, Grinding Media and Mill Structure in Wet Stirred Media Mills", *Minerals Engineering*, Vol. 148, pp. 1 - 11.

Lee, H., Kim, K. and Lee, H. (2019), "Analysis of Grinding Kinetics in a Laboratory Ball Mill Using Population-Balance-Model and Discrete-Element-Method", *Advanced Powder Technology*, Vol. 30, No. 11, pp. 1 - 10.

Le Roux, J. D., Olivier, L. E., Naidoo, M. A., Padhi, R. and Craig, I. K. (2016), "Throughput and Product Quality Control for a Grinding Mill Circuit Using Non – Linear MPC", *Journal of Process Control*, Vol. 42, No. 1, pp. 35 – 45.

Le Roux, J. D., Steinboeck, A., Kugi, A. and Craig, I. K. (2020), "Steady-state and Dynamic Simulation of a Grinding Mill using Grind Curves" Journal of Minerals Engineering, Vol. 152, No. 1, pp. 1 – 11.

Li, C., Chen, X., Tang, Y. and Li, L. (2017), "Selection of Optimum Parameters in Multi Pass Face Milling for Maximum Energy Efficiency and Minimum Production Cost", *Journal of Cleaner Production*, Vol. 140, pp. 1805 - 1818.

Lv, W., Wang, G. and Tian, H. (2018), "Electromechanical Dynamic Behaviour and Start-Up Evaluation of Tumbling Ball Mills", *Mathematical Problems in Engineering*, Vol. 20, pp. 1 - 13.

Machalek, D., Young, A., Blackburn, L., Rogers, P. and Powell, K. M. (2020), "Mine Operations as a Smart Grid Resource: Leveraging Excess Process Storage Capacity to Better Enable Renewable Energy Sources" *Journal of Minerals Engineering*, Vol. 145, No.1 pp.106 – 103.

Makokha, A. B. and Letting, L. K. (2019), "Dynamic Modelling of Temperature in a Wet Ball Mill Based on Integrated Energy-Mass-Size Balance Approach", *International Journal of Control Science and Engineering*, Vol. 9, No. 1, pp. 1 – 8.

Makokha, A. B., Madara, D. S., Namago, S. S. and Ataro, E. (2014), "Effect of Slurry Solids Concentration and Ball Loading on Mill Residence Time Distribution", *International Journal of Mining Engineering and Mineral Processing*, Vol. 3, No. 2, pp. 21 – 27.

Melero, M. G., Cano, J. M., Norniella, J., Pedrayes, F., Cabanas, M. F., Rojas, C. H., Alonso, G., Aguado, J. M. and Ardural, P. (2014), "Electric Motors Monitoring: An Alternative to Increase the Efficiency of Ball Mills", *Proceedings of the International Conference on Renewable Energies and Power Quality*, Cordoba, Spain, pp. 1 – 6.

Metayer, M., Breyer, C. and Fell, H. J. (2015), "The Projections for the Future and Quality in the Past of the World Energy Outlook for Solar PV and other Renewable Energy Technologies", *Proceedings of the 31st European Photovoltaic Solar Energy Conference and Exhibition*, Hamburg, Germany, 27 pp.

Mirjalili, S., Mirjalili, S. M. and Lewis, A. (2015), "Grey Wolf Optimiser", *Advances in Engineering Software*, Vol. 69, pp. 46 – 61.

Monov, V., Sokolov, B. and Stoenchev, S. (2012), "Grinding in Ball Mills: Modelling and Process Control", *Bulletin of the Bulgarian Academy of Sciences, Cybernetics and Information Technologies*, Vol. 12, No. 2, pp. 51 – 68.

Mor, R.S., Bhardwaj, A., Singh, S. and Sachdeva, A. (2019), "Productivity Gains Through Standardisation-of-Work in a Manufacturing Company", *Journal of Manufacturing Technology Management*, Vol. 2, No. 1, pp. 899 – 919.

Morrell, S. (2016), "Modelling the Influence on Power Draw of the Slurry Phase in Autogenous (AG), Semi-Autogenous (SAG) and Ball Mills", *Minerals Engineering*, Vol. 89, pp. 148 - 156.

Mulenga, F. K. (2017a), "Effects of Slurry Hold-up on the Pool Volume of a Batch Mill", *Minerals Engineering*, Vol. 111, pp. 124 - 130.

Mulenga, F. K. and Bwalya, M. M. (2019), "Determination of the Formal Powder Filling of a Wet Ball Mill in Open Circuit Configuration", *Minerals Engineering*, Vol. 130, pp. 1 - 4.

Napier–Munn, T. (2015), "Is Progress in Energy-Efficient Comminution Doomed?", *Minerals Engineering Journal*, Vol. 73, No. 1, pp. 1 – 6.

Nath, L. (2017), "Synthesis of Nanostructured Al_2O_3-Ni Particles Using High-Energy Mechanical Alloying Process for High Velocity Oxy-fuel Coatings Development", *Unpublished Master's Thesis Report*, University of New Brunswick, Fredericton, Canada, 139 pp.

Niu, D., Chen, X., Yang, J. and Zhou, X. (2017), "Disturbance Rejection Control for Raymond Mill Grinding System based on Disturbance Observer", *Journal of Central South University*, Vol. 24, No. 1, 2019 – 2027.

Niu, P., Niu, S. and Chang, L. (2019), "The Defect of the Grey Wolf Optimisation Algorithm and its Verification Method", *Knowledge-based Systems*, Vol. 171, pp. 37 - 43.

Nunan, T. O and Delboni Junior, H. (2017), "Simulation of the Mineração Serra Grande Industrial Grinding Circuit", *International Engineering Journal*, Vol. 70, No. 3, pp. 347 – 355.

Panjipour, R. and Barani, K. (2018), "The Effect of Ball Size Distribution on Power Draw, Charge Motion and Breakage Mechanism of Tumbling Ball Mill by Discrete Element Method Simulation", *Physicochemical Problems of Mineral Processing*, Vol. 53, No. 1, pp. 1 – 15.

Pedrayes, F., Norniella, J. G., Melero, M. G., Menendez-Aguado, J. M. and del Coz-Diaz, J. J. (2018), "Frequency Domain Characterisation of Torque in Tumbling Ball Mills using DEM Modelling: Application to Filling Level Monitoring", *Powder Technology*, Vol. 323, pp. 433 - 444.

Peng, Y. X., Ni, X., Zhu, Z. C., Yu, Z. F., Yin, Z. X., Li, T. Q., Liu, S. Y. and Xu, J. (2017), "Friction and Wear of Liner and Grinding Ball in Iron Ore Ball Mill", *Tribology International*, Vol. 115, pp. 506 - 517.

Petrakis, E., Stamboliadis, E. and Komnitsas, K. (2017a), "Evaluation of the Relationship between Energy Input and Particle Size Distribution in Comminution with the Use of Piecewise Regression Analysis", *International Journal of Particulate Science and Technology*, Vol. 35, No. 4, pp. 479 – 489.

Petrakis, E., Stamboliadis, E. and Komnitsas, K. (2017b), "Identification of Optimal Mill Operating Parameters during Grinding of Quartz with the use of Population Balance Modelling", *KONA Powder and Particle Journal*, Vol. 34, pp. 213 – 223.

Petrakis, E. and Komnitsas, K. (2017), "Improved Modelling of the Grinding Process through the Combined Use of Matrix and Population Balance Models", *Minerals*, Vol. 7, No. 5, pp. 1 – 17.

Piras, C. C., Fernández-Prieto, S. and De Borggraeve, W. M. (2019), "Ball Milling: A Green Technology for the Preparation and Functionalisation of Nanocellulose Derivatives", *Journal of Nanoscale Advances*, Vol. 1, No. 3, pp. 937 – 947.

Radhakrishna, V., Kumar, P. V., Aljawarneh, S. A. and Janaki, V. (2017), "Design and Analysis of a Novel Temporal Dissimilarity Measure using Gaussian Membership Function", *International Conference on Engineering*, Monastir, Tunisia, pp. 1 - 5.

Rashidi, S., Rajamani, R. K. and Fuerstenau, D. W. (2017), "A Review of the Modelling of High Pressure Grinding Rolls", *KONA Powder and Particle Journal*, Vol. 34, pp. 125 - 140.

Resabal, V. (2017), "Investigation of the Breakage Mechanism in High Speed Disk-Type Impeller Stirred Mills and its Influence on the Mineral Liberation", *Unpublished Master's Thesis Report*, University of Queensland, St Lucia QLD 4072, Australia, 139 pp.

Rocha, D., Spiller, E., Taylor, P. and Miller, H. (2018), "Predicting the Product Particle Size Distribution from a Laboratory Vertical Stirred Mill", *Minerals Engineering*, Vol. 129, pp. 85 - 92.

Rosales-Marín, G., Andrade, J., Alvarado, G., Delgadillo, J. A. and Tuzcu, E. T. (2019), "Study of Lifter Wear and Breakage Rates for Different Lifter Geometries in Tumbling Mill: Experimental and Simulation Analysis using Population Balance Model", *Minerals Engineering*, Vol. 141, pp. 1 – 11.

Rupare, W. F., Nyanga, L., Van der Merwe, A. F., Matope, S. and Mhlanga, S. (2013), "Design of an Automated Grinding Media Charging System for Ball Mills", *Proceedings of SAIIE25 Conference*, Stellenbosch, South Africa, pp. 619 – 630.

Seesara, S. and Gadit, J. (2015), "Smart Traffic Control Using Adaptive Neuro Fuzzy Inference System", *International Journal of Advanced Engineering and Research Development*, Vol. 2, Issue 5, pp. 295 – 302.

Shahbazi, B., Jafari, M., Parian, M., Rosenkranz, J. and Chelgani, S. C. (2020), "Study on the Impacts of Media Shapes on the Performance of Tumbling Mills: A Review", *Minerals Engineering*, Vol. 157, pp. 1 – 10.

Shi, F. (2016), "An Overfilling Indicator for Wet Overflow Ball Mills", *Minerals Engineering*, Vol. 95, pp. 146 - 154.

Simba, K. P. and Moys, M. H. (2014), "Effects of Mixtures of Grinding Media of Different Shapes on Milling Kinetics", *Materials Engineering Journal*, Vol. 61, No. 1, pp. 101 – 106.

Singh, N. and Singh, S. B. (2017), "Hybrid Algorithm of Particle Swarm Optimisation and Grey Wolf Optimiser for Improving Convergence Performance", *Journal of Applied Mathematics*, Vol. 2017, pp. 1 - 15.

Singh, V., Banerjee, P. K., Tripathy, S. K., Saxena, V. K. and Venugopal, R. (2013), "Artificial Neural Networks Modelling of Ball Mill Grinding Process", *Journal of Powder Metallurgy and Minerals*, Vol. 2, Issue 2, pp. 1 – 4.

Sinnott, M. D., Cleary, P. W. and Morrison, R. D. (2017). "Combined DEM and SPH Simulation of Overflow Ball Mill Discharge and Trommel Flow", *Minerals Engineering*, Vol. 108, pp. 93 - 108.

Siwella, M. (2017), "Process Monitoring with Economic Performance Functions: Feasibility Assessment for Milling Circuits", *Unpublished MEng Thesis*, Stellenbosch University, Stellenbosch, South Africa, 185 pp.

Soleymani, M. M., Fooladi, M. and Rezaeizadeh, M. (2015), "Experimental Investigation of the Power Draw of Tumbling Mills in Wet Grinding", *Proceedings of the Institution of*

Mechanical Engineers, Journal of Mechanical Engineering Science, Vol. 230, No. 15, pp. 2709 – 2719.

Sorgenfrei, M. (2016), "Analysis of IGCC-based Plants with Carbon Capture for an Efficient and Flexible Electric Power Generation", *Unpublished Master's Thesis Report*, Technische Universität Berlin, Berlin, Germany, 141 pp.

Tang, J., Qiao, J. F., Liu, Z., Chai, T. Y. and Yu, W. (2017), "Modelling Mill Load Parameter based on LASSO using Multi-scale High Dimensional Frequency Spectra Data", *IEEE International Conference on Information and Automation*, Macau SAR, China, pp. 909 - 914.

Tang, J., Qiao, J., Liu, Z., Zhou, X., Yu, G. and Zhao, J. (2018), "Mechanism Characteristic Analysis and Soft Measuring Method Review for Ball Mill Load based on Mechanical Vibration and Acoustic Signals in the Grinding Process", *Minerals Engineering*, Vol. 128, pp. 294 - 311.

Tavares, L. M. (2017), "A Review of Advanced Ball Mill Modelling", *KONA Powder and Particle Journal*, Vol. 34, pp. 106 - 124.

Taylor, L., Skuse, D., Blackburn, S. and Greenwood, R. (2020), "Stirred Media Mills in the Mining Industry: Material Grindability, Energy-Size Relationships and Operating Conditions", *Powder Technology*, Vol. 369, pp. 1 – 16.

Tripathy, S. K., Murthy, Y. R., Singh, V., Srinivasulu, A., Ranjan, A. and Satija, P. (2017), "Performance Optimisation of an Industrial Ball Mill for Chromite Processing", *The Journal of the Southern African Institute of Mining and Metallurgy*, Vol. 117, No. 1, pp. 75 – 81.

Tohry, A., Chelgani, S. C., Matin, S. S. and Noormohammadi, M. (2020), "Power-draw Prediction by Random Forest based on Operating Parameters for an Industrial Ball Mill", *Advanced Powder Technology*, Vol. 31, No. 3, pp. 967 - 972.

Usman, H. (2015), "Measuring the Efficiency of the Tumbling Mill as a Function of Lifter Configurations and Operating Parameters", *Unpublished PhD Thesis*, Colorado School of Mines, Colorado, USA, 191 pp.

Vijayakumar, N. (2016), "Development of an AG/SAG Mill Batch Test Methodology", *Unpublished Master's Thesis Report*, University of Queensland, St Lucia QLD 4072, Australia, 117 pp.

Vos, C. F. (2017), The Effect of Mineral Grain Textures at Particle Surfaces on Flotation Response", *Unpublished Master's Thesis Report*, University of Queensland, St Lucia QLD 4072, Australia, 389 pp.

Wang, M. (2012), "Modelling of Particle Breakage in Tumbling Ball Mills", *Unpublished MSc Thesis*, University of New South Wales, Sydney, Australia, 118 pp.

Wang, L., Fu, P., Yang, Z., Lin, T. E., Yang, Y. and Tsatsaronis, G. (2020), "Advanced Exergoeconomic Evaluation of Large-scale Coal-fired Power Plant", *Journal of Energy Engineering*, Vol. 146, Issue 1, pp. 1 – 32.

Wang, Z. and Srinivasan, R. S. (2017), "A Review of Artificial Intelligence based Building Energy Use Prediction: Contrasting the Capabilities of Single and Ensemble Prediction Models", *Renewable and Sustainable Energy Reviews*, Vol. 75, pp. 796 - 808.

Wentao, Z., Yuexin, H., Yanjun, L., Jinlin, Y., Shaojian, M. and Yongsheng, S. (2019), "Research on Prediction Model of Ore Grinding Particle Size Distribution", *Journal of Dispersion Science and Technology*, Vol. 41, No. 4, pp. 537 – 546.

Wills, B. A. and Finch, J. (2016), *Will's Mineral Processing Technology: An Introduction to the Practical Aspects of Ore Treatment and Mineral Recovery*, Butterworth-Heinemann Publishers, Oxford, UK, 8th edition, 496 pp.

Xiao, Q., Li, B. and Kang, H. (2014), "The Effect of Fine Grinding Medium Feature on Grinding Results", *American Applied Science Research Institute Conference on Power and Energy Systems*, Kumming, China, pp. 120 – 125.

Yang, Y., Rowson, N. A., Tamblyn, R. and Ingram, A. (2017), "Effect of Operating Parameters on Fine Particle Grinding in a Vertically Stirred Media Mill", *Separation Science and Technology*, Vol. 52, No. 6, pp. 1143 - 1152.

Yu, P. (2017), "A Generic Dynamic Model Structure for Tumbling Mills", *Unpublished PhD Thesis*, University of Queensland, Brisbane, Australia, 233 pp.

Zuo, W., Shi, F. and Manlapig, E. (2015), "Modelling of High Voltage Pulse Breakages of Ores", *Minerals Engineering*, Vol. 83, No. 1, pp. 168 – 174.

APPENDICES

APPENDIX A

BALL MILL OPERATIONAL DATA

Table A.1 Ball Mill Operational Data from September 2017 to February 2019

Date	TTM	TPH	MIW	GM_{60}	GM_{50}	TGM	GWR	BWI	PPS%	PD
24-09-17	13932	580	75	0	0	0	0	17.2	76.4	4330
25-09-17	13935	581	75	16	4	20	1.44	17.3	76.8	4405
26-09-17	13819	576	75	4	4	8	0.58	17.1	77.8	4470
27-09-17	9158	382	50	0	0	0	0	17.3	76.5	4400
28-09-17	13900	579	75	8	2	10	0.72	16.8	77.9	4265
29-09-17	9223	384	50	8	2	10	1.08	16.8	79.8	4320
30-09-17	13303	554	72	8	2	10	0.75	16.8	78.8	4325
01-10-17	12842	535	70	8	2	10	0.78	16.7	79.4	4260
02-10-17	13281	553	72	12	18	30	2.26	17.1	77.6	4405
03-10-17	13394	558	73	8	6	14	1.05	17	77.6	4330
04-10-17	13747	573	74	20	0	20	1.45	17	76.3	4300
05-10-17	14037	585	76	18	0	18	1.28	17.2	77.8	4430
06-10-17	13896	579	75	12	0	12	0.86	16.8	78.5	4390
07-10-17	13239	552	72	12	2	14	1.06	17	78.8	4420
08-10-17	13992	583	76	6	6	12	0.86	16.8	77.7	4295
09-10-17	14407	600	78	6	4	10	0.69	17	78.9	4430
10-10-17	14642	610	79	10	0	10	0.68	17	76.2	4385
11-10-17	12980	541	70	12	6	18	1.39	17.2	77	4440
12-10-17	14177	591	77	12	4	16	1.13	17.1	76	4375
13-10-17	14098	587	76	6	6	12	0.85	16.8	77.8	4290
14-10-17	14704	613	80	5.4	6.9	12.3	0.84	16.7	79.9	4245
15-10-17	15209	634	82	5.4	7.8	13.2	0.87	16.8	77.6	4240
16-10-17	14873	620	81	6	4	10	0.67	17	75	4240
17-10-17	14184	591	77	6	4	10	0.71	16.7	77.5	4130
18-10-17	14218	592	77	6	4	10	0.7	17	75.9	4205
19-10-17	14608	609	79	6	4	10	0.68	16.9	76.5	4225
20-10-17	13650	569	74	16	0	16	1.17	16.7	79.5	4295
21-10-17	12330	514	67	6	4	10	0.81	16.9	78.2	4350
22-10-17	12440	518	67	6	4	10	0.81	16.9	77.4	4370
23-10-17	13893	579	75	6	4	10	0.72	16.9	78.2	4280
24-10-17	13710	571	74	6	4	10	0.73	17.1	73.7	4220
25-10-17	13935	581	75	6	4	10	0.72	17	74.1	4290
26-10-17	1276	53	7	0	0	0	0	15.5	91.8	4240
27-10-17	14038	585	76	12	4	16	1.14	16.3	83.8	4320
28-10-17	14513	605	79	10	4	14	0.96	16.9	78.4	4410

Table A.1 Cont'd

Date	TTM	TPH	MIW	GM_{60}	GM_{50}	TGM	GWR	BWI	PPS%	PD
29-10-17	14285	595	77	8	6	14	0.98	16.8	79.8	4390
30-10-17	14397	600	78	10	4	14	0.97	17.1	77.8	4400
31-10-17	13493	562	73	6	4	10	0.74	16.8	79.4	4385
01-11-17	13466	561	73	6	4	10	0.74	16.9	78.9	4345
02-11-17	10922	455	59	6	4	10	0.92	16.7	81.4	4325
03-11-17	13395	558	73	8	2	10	0.75	16.9	77.3	4345
04-11-17	14190	591	77	6	4	10	0.7	16.7	81	4305
05-11-17	13741	573	74	6	4	10	0.73	16.9	78.2	4360
06-11-17	13197	550	71	6	4	10	0.76	17.1	78.3	4425
07-11-17	13945	581	76	6	4	10	0.72	16.8	79.7	4355
08-11-17	13406	559	73	8	2	10	0.75	15.9	81.3	4290
09-11-17	13156	548	71	12	8	20	1.52	16.8	79.9	4315
10-11-17	13243	552	72	6	4	10	0.76	16.6	82.5	4430
11-11-17	13039	543	71	6	4	10	0.77	17	79.7	4455
12-11-17	12340	514	67	6	4	10	0.81	16.8	79	4370
13-11-17	12835	535	70	6	4	10	0.78	16.8	81.7	4425
14-11-17	13181	549	71	6	4	10	0.76	15.9	81	4280
15-11-17	13910	580	75	6	4	10	0.72	16	80.4	4285
16-11-17	13506	563	73	6	4	10	0.74	16.9	77.2	4305
17-11-17	12046	502	65	6	2	8	0.66	16.5	78.5	4270
18-11-17	13078	545	71	6	2	8	0.61	16.4	79.7	4280
19-11-17	13920	580	75	6	2	8	0.57	16.8	76.6	4235
20-11-17	13575	566	74	6	2	8	0.59	16.4	79.2	4255
21-11-17	13345	556	72	6	2	8	0.6	16	82.4	4290
22-11-17	13425	559	73	6	2	8	0.6	15.9	83.7	4220
23-11-17	13610	567	74	6	2	8	0.59	15.7	84.5	4140
24-11-17	11855	494	64	6	2	8	0.67	15.7	85.4	4245
25-11-17	13067	544	71	10	2	12	0.92	16.3	79.5	4200
26-11-17	12972	540	70	6	2	8	0.62	16.1	79.4	4175
27-11-17	13471	561	73	6	2	8	0.59	15.8	80.8	4100
29-11-17	4929	205	27	0	0	0	0	16.6	76.6	4230
30-11-17	11156	465	60	6	2	8	0.72	16.6	77.3	4205
01-12-17	13732	572	74	6	2	8	0.58	16.4	78.1	4180
02-12-17	13502	563	73	14	2	16	1.18	16.8	74.9	4115
03-12-17	12851	535	70	10	4	14	1.09	16.5	77.1	4145
04-12-17	13937	581	75	12	4	16	1.15	16.4	73.5	4060
05-12-17	13194	550	71	12	6	18	1.36	16.5	77	4140
06-12-17	13994	583	76	8	0	8	0.57	16.5	76.6	4175

Table A.1 Cont'd

Date	TTM	TPH	MIW	GM_{60}	GM_{50}	TGM	GWR	BWI	PPS%	PD
07-12-17	13040	543	71	6	2	8	0.61	16.8	71.1	4175
08-12-17	13239	552	72	6	2	8	0.6	16.5	79.3	4230
09-12-17	13539	564	73	12	4	16	1.18	16.8	77.7	4200
10-12-17	14188	591	77	10	2	12	0.85	16.5	76.2	4175
11-12-17	13224	551	72	6	2	8	0.6	16.9	76.2	4305
12-12-17	13432	560	73	12	4	16	1.19	17	74.8	4275
13-12-17	12894	537	70	6	2	8	0.62	16.6	76.9	4070
14-12-17	13190	550	71	16	0	16	1.21	16.9	75.5	4255
15-12-17	13659	569	74	8	0	8	0.59	17	76	4225
16-12-17	12715	530	69	14	0	14	1.1	16.5	76.3	4160
17-12-17	11749	490	64	8	0	8	0.68	17	76.2	4230
18-12-17	13481	562	73	8	0	8	0.59	17.1	75.4	4330
19-12-17	14044	585	76	6	2	8	0.57	16.9	76	4360
20-12-17	12872	536	70	4	0	4	0.31	16.8	78.8	4355
21-12-17	12298	512	67	4	0	4	0.33	16.9	76	4315
22-12-17	12617	526	68	4	0	4	0.32	16.5	76.4	4190
23-12-17	12768	532	69	8	4	12	0.94	16.5	76.6	4140
24-12-17	12513	521	68	8	4	12	0.96	16.8	76.8	4255
25-12-17	12473	520	68	6	2	8	0.64	17	75.3	4220
26-12-17	12655	527	69	6	2	8	0.63	16.4	79.7	4170
27-12-17	13595	566	74	6	2	8	0.67	16.8	76.6	4215
28-12-17	13621	568	74	6	2	8	0.59	17	75.2	4200
29-12-17	12999	542	70	6	2	8	0.62	17.1	74.5	4190
30-12-17	13396	558	73	10	6	16	1.19	16.8	76.8	4235
31-12-17	12542	523	68	6	8	14	1.12	17	75.3	4400
01-01-18	12541	523	68	6	2	8	0.64	16.4	80.6	4455
02-01-18	12271	511	66	2	6	8	0.65	16.7	79	4250
03-01-18	12321	513	67	2	6	8	0.65	16.7	79.5	4265
05-01-18	8170	340	44	0	0	0	0	16.8	80.4	4360
06-01-18	13939	581	76	2	6	8	0.57	16.7	78.6	4210
07-01-18	12829	535	69	2	6	8	0.62	16.6	77.2	4245
08-01-18	12673	528	69	2	6	8	0.63	16.5	76	4090
09-01-18	13343	556	72	2	6	8	0.6	16.4	77.6	4135
10-01-18	13595	566	74	6	2	8	0.59	16.5	76.3	4045
11-01-18	13464	561	73	6	2	8	0.59	16.5	77.8	4185
12-01-18	9895	412	54	2	6	8	0.81	16.5	77.3	4190
13-01-18	13547	564	73	4	12	16	1.18	16.6	77.7	4215
14-01-18	13808	575	75	2	6	8	0.58	16.6	77.2	4230
15-01-18	13645	569	74	2	6	8	0.59	16.5	77.2	4175

Table A.1 Cont'd

Date	TTM	TPH	MIW	GM_{60}	GM_{50}	TGM	GWR	BWI	PPS%	PD
16-01-18	13582	566	74	0	0	0	0	16.4	77.5	4060
17-01-18	13648	569	74	12	4	16	1.17	16.4	77.7	4040
18-01-18	13225	551	72	0	16	16	1.21	16.4	77.8	4070
19-01-18	11566	482	63	0	8	8	0.69	15.9	79.2	3965
20-01-18	13427	559	73	0	8	8	0.6	16.6	75.9	4055
21-01-18	13392	558	73	0	8	8	0.6	16.1	78.3	3975
22-01-18	11581	483	63	0	16	16	1.38	16.3	79.8	4310
23-01-18	12772	532	69	0	10	10	0.78	16.2	78.4	3955
24-01-18	13976	582	76	6	2	8	0.58	16.6	80.1	4532
25-01-18	13596	566	74	6	2	8	0.72	16.9	79.2	4527
26-01-18	10907	454	59	6	2	8	0.78	16.8	80.4	4621
27-01-18	14978	624	81	6	2	8	2.62	16.8	78.2	4485
28-01-18	14432	601	78	6	2	8	1.06	16	82.2	4452
29-01-18	14010	584	76	6	2	8	0.68	17	78.2	4577
30-01-18	14735	614	80	6	2	8	0	16.9	77.9	4475
31-01-18	13815	576	75	6	2	8	0.32	16.6	80.6	4538
01-02-18	13662	569	74	6	2	8	0.87	16.6	80.1	4547
02-02-18	13528	564	73	6	2	8	0.71	16.6	79.6	4443
03-02-18	13501	563	73	6	2	8	0.7	16.4	78.3	4278
04-02-18	14267	594	77	6	2	8	0.81	16.2	77.2	3878
05-02-18	12431	518	67	6	2	8	0.73	16.8	78.2	4447
06-02-18	13580	566	74	6	2	8	0	16.7	79.5	4428
07-02-18	13443	560	73	6	2	8	0.98	16.2	81.2	4426
08-02-18	13109	546	71	6	2	8	0.74	16.9	79.2	4511
09-02-18	13906	579	75	6	2	8	0.75	15.8	80.1	4179
10-02-18	14695	612	80	6	2	8	0.76	16.2	79.4	4185
11-02-18	13742	573	74	6	2	8	1.52	16.5	79.2	4370
12-02-18	14053	586	76	6	2	8	0.77	17	78.2	4470
13-02-18	14456	602	78	6	2	8	0.72	16.9	77.8	4434
14-02-18	14460	603	78	6	2	8	0.61	16.9	77.8	4432
15-02-18	13694	571	74	6	2	8	0.6	17.1	76.2	4463
16-02-18	13460	561	73	6	2	8	0.67	17.1	77.7	4546
17-02-18	13206	550	72	6	2	8	0.62	16.9	77.9	4496
18-02-18	13997	583	76	6	2	8	0.72	16.6	79	4463
19-02-18	13742	573	74	6	2	8	1.09	16.8	78.1	4467
20-02-18	13607	567	74	6	2	8	1.36	17	78.6	4519
21-02-18	14328	597	78	6	2	8	1.18	16.4	79.6	4207
22-02-18	12853	536	70	6	2	8	0.6	17	77.8	4536
23-02-18	14358	598	78	6	2	8	1.21	17.3	75.6	4437
24-02-18	14375	599	78	6	2	8	0.68	16.8	78.3	4404

Table A.1 Cont'd

Date	TTM	TPH	MIW	GM_{60}	GM_{50}	TGM	GWR	BWI	PPS%	PD
25-02-18	14351	598	78	6	2	8	0.57	16.8	78.6	4446
26-02-18	14085	587	76	6	2	8	0.32	17	78.2	4534
27-02-18	15226	634	82	6	2	8	0.96	16.6	79.2	4434
28-02-18	15601	650	85	6	2	8	0.62	16.8	78.7	4431
01-03-18	15388	641	83	6	2	8	1.12	16.4	80.2	4420
02-03-18	15601	650	85	6	2	8	0.65	16.6	79.9	4480
03-03-18	15492	645	84	6	2	8	0.57	16.8	78.1	4513
04-03-18	15735	656	85	6	2	8	0.6	15.9	81.7	4224
05-03-18	15051	627	82	6	2	8	0.59	16.6	78.6	4489
06-03-18	14400	600	78	6	2	8	0.58	16.9	77.6	4490
07-03-18	14529	605	79	6	2	8	1.17	16.8	78.4	4500
08-03-18	14825	618	80	6	2	8	1.21	16.8	78.6	4534
09-03-18	15848	660	86	6	2	8	0.6	16.5	79.2	4490
10-03-18	16123	672	87	6	2	8	1.38	16.5	79.8	4427
11-03-18	14204	592	77	6	2	8	1.08	16.8	78.1	4533
12-03-18	14783	616	80	6	2	8	1.06	16.8	78.3	4535
13-03-18	15033	626	81	6	2	8	0.68	16.8	78.2	4562
14-03-18	14561	607	79	6	2	8	0.32	16.8	78.4	4555
15-03-18	15305	638	83	6	2	8	0.68	16.5	79.1	4493
16-03-18	14868	619	81	6	2	8	0.81	17	77.9	4515
17-03-18	14745	614	80	6	2	8	1.14	16.8	78.6	4559
18-03-18	14792	616	80	6	2	8	0.97	16.7	79.1	4538
19-03-18	15369	640	83	6	2	8	0.74	16.5	79.8	4487
20-03-18	15348	640	83	6	2	8	0.7	16.4	80.1	4454
21-03-18	10487	437	57	6	2	8	0.72	16.6	82.1	4693
22-03-18	11805	492	64	6	2	8	0.76	17	80.6	4708
23-03-18	10393	433	56	6	2	8	0.81	17.2	79.9	4711
24-03-18	13449	560	73	6	2	8	0.72	16.8	80.5	4643
25-03-18	14956	623	81	6	2	8	0.66	17	77.2	4584
26-03-18	15273	636	83	6	2	8	0.59	17.1	78.5	4604
27-03-18	13494	562	73	6	2	8	0.6	17	79.7	4643
28-03-18	13792	575	75	6	2	8	0.67	17.2	76.6	4650
29-03-18	15015	626	81	6	2	8	0.62	16.9	79.2	4583
30-03-18	14887	620	81	6	2	8	0.72	16.4	82.4	4581
31-03-18	14672	611	79	6	2	8	1.18	16.4	83.7	4613
01-04-18	13188	550	71	6	2	8	1.36	16.3	84.5	4674
02-04-18	11147	464	60	6	2	8	0.61	17	79.7	4692
03-04-18	15540	648	84	6	2	8	1.18	17.4	74.5	4604
04-04-18	15191	633	82	6	2	8	0.6	16.6	80.4	4585
05-04-18	14553	606	79	6	2	8	0.62	17.2	76.3	4628

Table A.1 Cont'd

Date	TTM	TPH	MIW	GM_{60}	GM_{50}	TGM	GWR	BWI	PPS%	PD
06-04-18	14941	623	81	6	2	8	1.21	17	77.2	4631
07-04-18	14620	609	79	6	2	8	1.1	16.8	80.1	4607
08-04-18	14854	619	80	6	2	8	0.57	16.8	78.2	4573
09-04-18	15079	628	82	6	2	8	0.33	16.8	78.1	4555
10-04-18	16086	670	87	6	2	8	0.96	16.9	77.8	4532
11-04-18	15608	650	85	6	2	8	0.62	16.8	78.6	4558
12-04-18	15155	631	82	6	2	8	1.12	16.6	80.9	4559
13-04-18	14907	621	81	6	2	8	0.65	16.8	78.9	4547
14-04-18	14914	621	81	6	2	8	0.57	16.5	81.7	4510
15-04-18	14365	599	78	6	2	8	0.6	16.5	81.2	4562
16-04-18	14932	622	81	6	2	8	0.59	16.8	78.4	4546
17-04-18	14771	615	80	6	2	8	1.18	16.8	78.8	4552
18-04-18	14602	608	79	6	2	8	0	16.6	80.9	4523
19-04-18	14313	596	78	6	2	8	1.21	16.5	82.4	4502
20-04-18	14301	596	77	6	2	8	0.69	16.8	78.3	4569
21-04-18	15019	626	81	6	2	8	0.6	16.6	80.1	4553
22-04-18	14919	622	81	6	2	8	0.58	16.5	82.1	4509
23-04-18	14443	602	78	6	2	8	0.78	16.4	82.4	4469
24-04-18	13247	552	72	6	2	8	1.06	16.5	80.1	4470
25-04-18	14207	592	77	6	2	8	0.32	16.6	79.4	4528
26-04-18	14391	600	78	6	2	8	0.71	16.5	79.1	4489
27-04-18	14354	598	78	6	2	8	0.81	16.4	81.1	4414
28-04-18	14026	584	76	6	2	8	0.98	16.5	80.9	4463
29-04-18	14124	588	77	6	2	8	0.76	16.5	80.5	4486
30-04-18	13836	576	75	6	2	8	0.77	16.8	78.5	4542
01-05-18	13984	583	76	6	2	8	0.6	16.6	79.2	4520
02-05-18	14086	587	76	6	2	8	0.62	16.4	80.2	4497
03-05-18	13907	579	75	6	2	8	1.09	16.5	79.9	4486
04-05-18	13246	552	72	6	2	8	0.6	16.5	79.5	4491
05-05-18	13343	556	72	6	2	8	0.68	16.8	78.2	4556
06-05-18	14224	593	77	6	2	8	0.32	16.8	78.6	4528
07-05-18	13931	580	75	6	2	8	0.62	16.5	80.1	4473
08-05-18	13922	580	75	6	2	8	0.65	16.4	82.4	4438
09-05-18	12546	523	68	6	2	8	0.6	16.8	78.6	4518
10-05-18	13874	578	75	6	2	8	1.17	16.8	78.2	4518
11-05-18	13967	582	76	6	2	8	0.6	16.5	80.1	4486
12-05-18	13661	569	74	6	2	8	0.58	16.5	80.9	4461
13-05-18	13889	579	75	6	2	8	1.08	16.4	81.1	4434
14-05-18	13292	554	72	6	2	8	0.78	16.9	78.9	4506
15-05-18	13426	559	73	6	2	8	0	16.8	78.2	4510

Table A.1 Cont'd

Date	TTM	TPH	MIW	GM_{60}	GM_{50}	TGM	GWR	BWI	PPS%	PD
16-05-18	13933	581	75	6	2	8	0.86	16.5	79.9	4487
17-05-18	13832	576	75	6	2	8	0.69	16.4	80.1	4485
18-05-18	13221	551	72	6	2	8	0	16.4	80.6	4473
19-05-18	14084	587	76	6	2	8	0.87	16.8	78	4565
20-05-18	14066	586	76	6	2	8	0.7	16.8	78.1	4526
21-05-18	13920	580	75	6	2	8	0.81	16.8	78.4	4512
22-05-18	13922	580	75	6	2	8	0.73	16.4	80	4487
23-05-18	10572	441	57	6	2	8	0.96	16.3	81.7	4405
29-05-18	14265	594	77	6	2	8	0.97	16.1	82.7	4323
30-05-18	15023	626	81	6	2	8	0.74	16.3	81.2	4437
31-05-18	14577	607	79	6	2	8	0.75	16.8	78.4	4526
01-06-18	14278	595	77	6	2	8	0.76	16.8	78.9	4535
02-06-18	13217	551	72	6	2	8	0.75	16.8	78.8	4526
03-06-18	14716	613	80	6	2	8	0.76	16.7	78.9	4439
04-06-18	15063	628	82	6	2	8	0.81	16.4	80.9	4400
05-06-18	14040	585	76	6	2	8	0.76	16.1	82.4	4399
06-06-18	14715	613	80	6	2	8	0.74	16	83.1	4321
07-06-18	11338	472	61	6	2	8	0.61	16.1	82.4	4382
08-06-18	14614	609	79	6	2	8	0.59	16.3	81.5	4456
09-06-18	14311	596	78	6	2	8	0.6	16.1	82.4	4379
10-06-18	13511	563	73	6	2	8	0.67	16.8	78.3	4511
11-06-18	13798	575	75	6	2	8	0.59	16.8	78.6	4503
12-06-18	13614	567	74	6	2	8	0.58	16.9	77.9	4527
13-06-18	13360	557	72	6	2	8	1.09	16.6	80.1	4579
14-06-18	14066	586	76	6	2	8	0.57	16.1	83.4	4368
15-06-18	14276	595	77	6	2	8	1.18	16	81.9	4285
16-06-18	14471	603	78	6	2	8	0.6	15.9	82.1	4249
17-06-18	12758	532	69	6	2	8	1.21	16.4	80.9	4426
18-06-18	13883	578	75	6	2	8	1.1	16.1	82.4	4321
19-06-18	13921	580	75	6	2	8	0.31	16.4	83.1	4524
20-06-18	13912	580	75	6	2	8	0.32	16.5	82.4	4541
21-06-18	12755	531	69	6	2	8	0.96	16.3	81.5	4463
22-06-18	14373	599	78	6	2	8	1.19	16	82.4	4212
23-06-18	14038	585	76	6	2	8	1.12	16.1	82.4	4339
24-06-18	13535	564	73	6	2	8	0.65	16.8	78.6	4655
25-06-18	14373	599	78	6	2	8	0.62	16.5	80.1	4494
26-06-18	13647	569	74	6	2	8	0.59	16.2	82.1	4391
27-06-18	13040	543	71	6	2	8	1.18	16.3	82.4	4470
28-06-18	13484	562	73	6	2	8	1.17	16.3	81.5	4438
29-06-18	13922	580	75	6	2	8	0.69	16.2	81.4	4335

Table A.1 Cont'd

Date	TTM	TPH	MIW	GM_{60}	GM_{50}	TGM	GWR	BWI	PPS%	PD
30-06-18	13903	579	75	6	2	8	0.6	16.9	81	4680
01-07-18	13570	565	74	6	2	8	0.78	16.8	78.2	4645
02-07-18	13218	551	72	6	2	8	0.72	16.4	79.7	4320
03-07-18	12031	501	65	6	2	8	2.62	17	82.5	4715
04-07-18	11590	483	63	6	2	8	0.76	17	81	4798
05-07-18	13908	580	75	6	2	8	0.77	16.8	78.5	4681
06-07-18	14384	599	78	6	2	8	0.6	16.7	79.7	4635
07-07-18	13812	575	75	6	2	8	0.72	16.9	83.7	4738
08-07-18	13814	576	75	6	2	8	1.18	16.8	85.4	4788
09-07-18	13926	580	75	6	2	8	0.68	16.6	79.5	4580
10-07-18	15010	625	81	6	2	8	0.96	16.5	80.8	4571
11-07-18	14637	610	79	6	2	8	1.12	16.8	77.3	4531
12-07-18	14417	601	78	6	2	8	0.57	16.7	78.1	4561
13-07-18	14095	587	76	6	2	8	0.59	16.9	76.6	4452
14-07-18	13545	564	73	6	2	8	1.17	16.7	77.7	4493
15-07-18	13852	577	75	6	2	8	1.38	16.7	79.7	4626
16-07-18	13779	574	75	6	2	8	0.68	16.4	80.4	4437
17-07-18	14312	596	78	6	2	8	0.68	16.8	77.8	4515
18-07-18	14264	594	77	6	2	8	0.81	16.7	77.3	4446
19-07-18	14551	606	79	6	2	8	0.97	16.7	77.2	4481
20-07-18	14457	602	78	6	2	8	0.72	16.9	75.9	4617
21-07-18	9629	401	52	6	2	8	0.6	16.9	79.8	4832
22-07-18	11741	489	64	6	2	8	0.62	17	78.2	4851
23-07-18	13724	572	74	6	2	8	1.18	16.8	80.6	4831
24-07-18	14590	608	79	6	2	8	0.6	16.5	79.6	4661
25-07-18	14514	605	79	6	2	8	1.21	16.4	78.2	4456
26-07-18	14123	588	76	6	2	8	0.57	16.8	79.4	4520
27-07-18	13902	579	75	6	2	8	0.96	17	78.6	4806
28-07-18	12332	514	67	6	2	8	0.65	16.4	80.1	4445
29-07-18	9742	406	53	6	2	8	0.6	15.4	78.5	3174
30-07-18	13674	570	74	6	2	8	1.18	16.9	79.9	4725
31-07-18	13575	566	74	6	2	8	1.21	16.4	79.5	4599
01-08-18	13561	565	73	6	2	8	0.69	16.3	78.6	4560
02-08-18	13858	577	75	6	2	8	0.58	16.4	80.9	4612
03-08-18	13893	579	75	6	2	8	1.06	16.6	78.9	4688
04-08-18	13276	553	72	6	2	8	0.81	16.8	78.2	4721
05-08-18	14195	591	77	6	2	8	0.76	16.4	79.9	4544
06-08-18	12992	541	70	6	2	8	0.6	16.4	78.1	4530
07-08-18	11905	496	64	6	2	8	1.09	16.8	78.4	4724
08-08-18	13972	582	76	6	2	8	0.32	16.6	82.7	4619

Table A.1 Cont'd

Date	TTM	TPH	MIW	GM_{60}	GM_{50}	TGM	GWR	BWI	PPS%	PD
09-08-18	13467	561	73	6	2	8	0.6	16.4	83.1	4589
10-08-18	11944	498	65	6	2	8	0.6	16.8	82.4	4747
11-08-18	10268	428	56	6	2	8	0.78	16.2	82.4	4398
12-08-18	12952	540	70	6	2	8	0.62	16.5	80.1	4673
13-08-18	14914	621	81	6	2	8	0.54	16.4	82.1	4558
14-08-18	13385	558	73	6	2	8	0.6	16.8	79.4	4679
15-08-18	13583	566	74	6	2	8	0.59	16.8	81.4	4782
16-08-18	12399	517	67	6	2	8	0.65	16.6	81	4683
17-08-18	13743	573	74	6	2	8	0.58	16.5	81.3	4524
18-08-18	13909	580	75	6	2	8	0.58	17	79.9	4566
19-08-18	13938	581	75	6	2	8	0.57	16.4	79.7	4473
20-08-18	14782	616	80	6	2	8	0.54	16.7	81	4582
21-08-18	7945	331	43	6	2	8	1.01	15.6	80.4	3367
22-08-18	13805	575	75	6	2	8	0.58	16.8	78.5	4791
23-08-18	13498	562	73	6	2	8	0.59	17	79.7	4735
24-08-18	13757	573	75	6	2	8	0.58	16.6	82.4	4710
25-08-18	14269	595	77	6	2	8	0.56	16.4	84.5	4713
26-08-18	13545	564	73	6	2	8	0.59	16.8	78.1	4742
27-08-18	12984	541	70	6	2	8	0.62	17	76.2	4584
28-08-18	13392	558	73	6	2	8	0.6	17.1	76	4679
29-08-18	13817	576	75	6	2	8	0.58	17.2	76	4790
30-08-18	13181	549	71	6	2	8	0.61	17.3	76.8	4868
31-08-18	13444	560	73	6	2	8	0.6	16.8	79.7	4849
01-09-18	14536	606	79	6	2	8	0.55	17.1	75.2	4585
02-09-18	14525	605	79	6	2	8	0.55	16.5	80.6	4524
03-09-18	13706	571	74	6	2	8	0.58	16.3	79	4344
04-09-18	13983	583	76	6	2	8	0.57	17	79.5	4782
05-09-18	13424	559	73	6	2	8	0.6	16.8	80.4	4761
06-09-18	13870	578	75	6	2	8	0.58	16.8	78.6	4552
07-09-18	13720	572	74	6	2	8	0.58	17	79.2	4746
08-09-18	11556	482	63	6	2	8	0.69	17	78.3	4786
09-09-18	13257	552	72	6	2	8	0.6	16.9	79.8	4743
10-09-18	13720	572	74	6	2	8	0.58	16.6	78.4	4483
11-09-18	13361	557	72	6	2	8	0.6	16.5	80.1	4571
12-09-18	12037	502	65	6	2	8	0.66	17.1	78.2	4792
13-09-18	9923	413	54	6	2	8	0.81	17	80.1	4895
14-09-18	9005	375	49	6	2	8	0.89	17	78.3	4914
15-09-18	8407	350	46	6	2	8	0.95	17.1	77.2	4901
16-09-18	13033	543	71	6	2	8	0.61	16.7	79.5	4466
17-09-18	12916	538	70	6	2	8	0.62	16.4	81.2	4331

Table A.1 Cont'd

Date	TTM	TPH	MIW	GM_{60}	GM_{50}	TGM	GWR	BWI	PPS%	PD
18-09-18	13577	566	74	6	2	8	0.59	16.8	79.2	4512
19-09-18	11588	483	63	6	2	8	0.69	17	78.2	4667
20-09-18	13064	544	71	6	2	8	0.61	16.9	78.6	4579
21-09-18	14371	599	78	6	2	8	0.56	16.4	79.6	4378
22-09-18	13428	559	73	6	2	8	0.6	16.6	78.2	4394
23-09-18	13433	560	73	6	2	8	0.6	16.4	80.2	4482
25-09-18	14014	584	76	6	2	8	0.57	17.2	78.1	4881
26-09-18	14307	596	77	6	2	8	0.56	16.7	81.7	4838
27-09-18	14114	588	76	6	2	8	0.57	16.9	78.4	4819
28-09-18	14046	585	76	6	2	8	0.57	16.8	79.8	4805
29-09-18	13797	575	75	6	2	8	0.58	16.9	78.4	4846
30-09-18	14230	593	77	6	2	8	0.56	16.8	79.1	4644
01-10-18	12834	535	70	6	2	8	0.62	16.5	82.1	4741
02-10-18	12262	511	66	6	2	8	0.65	16.8	80.6	4710
03-10-18	13767	574	75	6	2	8	0.58	16.6	80.5	4567
04-10-18	11077	462	60	6	2	8	0.72	17.3	77.2	4914
05-10-18	11886	495	64	6	2	8	0.67	17.1	79.7	4902
06-10-18	10060	419	54	6	2	8	0.8	17.3	76.6	4899
11-10-18	5545	231	30	6	2	8	1.44	15.5	79.2	2030
12-10-18	14485	604	78	6	2	8	0.55	16.9	82.4	4952
13-10-18	14529	605	79	6	2	8	0.55	16.8	83.7	4936
14-10-18	14649	610	79	6	2	8	0.55	16.5	84.5	4875
15-10-18	14700	612	80	6	2	8	0.54	16.9	80.4	4818
16-10-18	13313	555	72	6	2	8	0.6	17	80.1	4939
17-10-18	14864	619	81	6	2	8	0.54	17.2	78.2	4952
18-10-18	13929	580	75	6	2	8	0.57	17.2	78.1	4967
19-10-18	14320	597	78	6	2	8	0.56	17.2	78.6	4955
20-10-18	13871	578	75	6	2	8	0.58	16.9	81	4939
21-10-18	15028	626	81	6	2	8	0.53	17.3	78.3	5003
22-10-18	14887	620	81	6	2	8	0.54	17.1	79.7	4978
23-10-18	15108	630	82	6	2	8	0.53	17.1	79.9	4990
24-10-18	14767	615	80	6	2	8	0.54	17.1	79	4930
25-10-18	14772	616	80	6	2	8	0.54	16.9	81	4912
26-10-18	13534	564	73	6	2	8	0.59	17.2	78.5	4982
27-10-18	15823	659	86	6	2	8	0.51	17	79.7	4884
28-10-18	16452	686	89	6	2	8	0.49	16.8	83.7	4951
29-10-18	16341	681	89	6	2	8	0.49	17.1	79.5	4939
30-10-18	14759	615	80	6	2	8	0.54	17.1	79.4	4961
31-10-18	14642	610	79	6	2	8	0.55	16.7	80.8	4896
01-11-18	13508	563	73	6	2	8	0.59	17.1	78.1	5001

Table A.1 Cont'd

Date	TTM	TPH	MIW	GM_{60}	GM_{50}	TGM	GWR	BWI	PPS%	PD
02-11-18	16261	678	88	6	2	8	0.49	17.4	76.6	4893
03-11-18	15389	641	83	6	2	8	0.52	17.1	79.3	4940
04-11-18	14672	611	79	6	2	8	0.55	17.1	79.7	4938
05-11-18	15565	649	84	6	2	8	0.51	16.7	80.6	4833
06-11-18	14266	594	77	6	2	8	0.56	17.3	77.6	4991
07-11-18	16068	669	87	6	2	8	0.5	17.3	76.3	4842
08-11-18	15245	635	83	6	2	8	0.52	16.8	79.2	4855
09-11-18	13084	545	71	6	2	8	0.61	17	78.4	4941
10-11-18	12652	527	69	6	2	8	0.63	17.5	77.9	5033
11-11-18	10920	455	59	6	2	8	0.73	17	80.1	5045
12-11-18	14090	587	76	6	2	8	0.57	17.2	78.2	4993
13-11-18	15447	644	84	6	2	8	0.52	17.4	75.6	4911
14-11-18	14843	618	80	6	2	8	0.54	17.2	78.2	4959
15-11-18	14555	606	79	6	2	8	0.55	17	80.2	4963
16-11-18	14290	595	77	6	2	8	0.56	16.9	81.7	4992
17-11-18	15022	626	81	6	2	8	0.53	17.3	77.9	4904
18-11-18	14446	602	78	6	2	8	0.55	17	80.1	4942
19-11-18	14756	615	80	6	2	8	0.54	16.9	79.9	4849
20-11-18	14716	613	80	6	2	8	0.54	16.9	79.2	4884
21-11-18	14892	621	81	6	2	8	0.54	17.1	79.7	4937
22-11-18	14861	619	80	6	2	8	0.54	16.8	80.4	4878
23-11-18	15467	644	84	6	2	8	0.52	16.8	79.1	4785
24-11-18	14911	621	81	6	2	8	0.54	16.8	80.9	4813
25-11-18	14731	614	80	6	2	8	0.54	16.8	80.2	4887
26-11-18	15173	632	82	6	2	8	0.53	17	79.5	4845
27-11-18	15126	630	82	6	2	8	0.53	16.5	78.6	4626
28-11-18	14553	606	79	6	2	8	0.55	16.7	81.1	4782
29-11-18	14009	584	76	6	2	8	0.57	16.9	78.2	4865
30-11-18	14573	607	79	6	2	8	0.55	16.7	80.1	4819
01-12-18	14110	588	76	6	2	8	0.57	16.7	81.2	4870
02-12-18	14163	590	77	6	2	8	0.56	17.1	78.4	4875
03-12-18	14148	590	77	6	2	8	0.57	16.8	80.9	4855
04-12-18	13509	563	73	6	2	8	0.59	16.8	82.4	4943
05-12-18	14163	590	77	6	2	8	0.56	16.8	82.4	4935
06-12-18	14156	590	77	6	2	8	0.57	17.2	78.6	4922
07-12-18	14155	590	77	6	2	8	0.57	16.7	83.4	4900
08-12-18	13877	578	75	6	2	8	0.58	16.8	82.1	4900
09-12-18	13700	571	74	6	2	8	0.58	17	81.5	4985
10-12-18	14147	589	77	6	2	8	0.57	17.2	78.6	4933
11-12-18	14078	587	76	6	2	8	0.57	16.8	82.4	4948

Table A.1 Cont'd

Date	TTM	TPH	MIW	GM_{60}	GM_{50}	TGM	GWR	BWI	PPS%	PD
12-12-18	14192	591	77	6	2	8	0.56	17.1	79.7	4929
13-12-18	14164	590	77	6	2	8	0.56	17	81	4936
14-12-18	14156	590	77	6	2	8	0.57	17.3	79.7	5010
15-12-18	14136	589	77	6	2	8	0.57	17	85.4	5006
16-12-18	14186	591	77	6	2	8	0.56	17.1	79.5	4970
17-12-18	14162	590	77	6	2	8	0.56	17	79.7	4951
18-12-18	14160	590	77	6	2	8	0.56	16.8	80.4	4922
19-12-18	14161	590	77	6	2	8	0.56	17.3	77.8	4986
20-12-18	14090	587	76	6	2	8	0.57	17.1	79.8	4995
21-12-18	14167	590	77	6	2	8	0.56	17.1	79.6	4947
22-12-18	14192	591	77	6	2	8	0.56	17.1	79.4	4967
23-12-18	14156	590	77	6	2	8	0.57	17.1	78.6	4967
24-12-18	13996	583	76	6	2	8	0.57	16.9	79.9	4864
25-12-18	13907	579	75	6	2	8	0.58	17	79.5	4980
26-12-18	14124	589	77	6	2	8	0.57	17	78.6	4864
27-12-18	13024	543	71	6	2	8	0.61	16.7	80.9	4868
28-12-18	14297	596	77	6	2	8	0.56	17.1	78.4	4918
29-12-18	14322	597	78	6	2	8	0.56	16.7	83.1	4962
30-12-18	13772	574	75	6	2	8	0.58	16.8	82.4	4922
31-12-18	8173	341	44	6	2	8	0.98	15.7	79.4	2922
01-01-19	12570	524	68	6	2	8	0.64	16.8	81	4812
02-01-19	13362	557	72	6	2	8	0.6	17	79.7	4957
03-01-19	13916	580	75	6	2	8	0.57	16.9	80.4	5016
04-01-19	13280	553	72	6	2	8	0.6	17.1	82.4	5001
05-01-19	14266	594	77	6	2	8	0.56	16.9	84.5	4927
06-01-19	13976	582	76	6	2	8	0.57	17.3	76.2	4863
07-01-19	13374	557	72	6	2	8	0.6	17.3	76	4896
08-01-19	14149	590	77	6	2	8	0.57	17.1	78.3	4963
09-01-19	14143	589	77	6	2	8	0.57	17.1	78.6	4939
10-01-19	14262	594	77	6	2	8	0.56	17.1	77.9	4918
11-01-19	14162	590	77	6	2	8	0.56	16.8	82.4	4908
12-01-19	14161	590	77	6	2	8	0.56	17.1	78.6	4963
13-01-19	14083	587	76	6	2	8	0.57	16.7	82.1	4961
14-01-19	14146	589	77	6	2	8	0.57	16.8	81.5	4952
15-01-19	14147	589	77	6	2	8	0.57	16.8	81	4924
16-01-19	14159	590	77	6	2	8	0.57	17.1	78.2	4905
17-01-19	14157	590	77	6	2	8	0.57	17.1	77.2	4952
18-01-19	14122	588	76	6	2	8	0.57	17	79.2	4957
19-01-19	14146	589	77	6	2	8	0.57	16.9	80.2	4940
20-01-19	14158	590	77	6	2	8	0.57	17.1	78.4	4923

Table A.1 Cont'd

Date	TTM	TPH	MIW	GM_{60}	GM_{50}	TGM	GWR	BWI	PPS%	PD
21-01-19	13860	577	75	6	2	8	0.58	17.1	78.4	4904
22-01-19	12157	507	66	6	2	8	0.66	17	80.6	5023
23-01-19	10404	434	56	6	2	8	0.77	17.5	76.6	5034
24-01-19	12568	524	68	6	2	8	0.64	17	82.4	5003
25-01-19	14387	599	78	6	2	8	0.56	16.5	84.5	4898
26-01-19	13908	580	75	6	2	8	0.58	16.9	80.1	4903
27-01-19	14130	589	77	6	2	8	0.57	17.1	78.2	4966
28-01-19	13529	564	73	6	2	8	0.59	17.1	78.6	4979
29-01-19	14360	598	78	6	2	8	0.56	17	79.7	4965
30-01-19	14039	585	76	6	2	8	0.57	17	79	4920
31-01-19	13661	569	74	6	2	8	0.59	17	79.3	4979
01-02-19	10945	456	59	6	2	8	0.73	15.8	79.7	3670
02-02-19	11987	499	65	6	2	8	0.67	15.9	80.6	4357
03-02-19	14130	589	77	6	2	8	0.57	17.1	76.3	4946
04-02-19	14023	584	76	6	2	8	0.57	17.1	78.4	4908
05-02-19	14130	589	77	6	2	8	0.57	17	77.9	4789
06-02-19	14166	590	77	6	2	8	0.56	17.2	75.6	4952
07-02-19	14355	598	78	6	2	8	0.56	16.5	80.2	4610
08-02-19	14151	590	77	6	2	8	0.57	16.9	80.1	4837
09-02-19	14138	589	77	6	2	8	0.57	16.8	80.4	4844
10-02-19	14143	589	77	6	2	8	0.57	17	80.9	4903
11-02-19	14227	593	77	6	2	8	0.56	16.9	81.1	4935
12-02-19	14177	591	77	6	2	8	0.56	17	78.2	4849
13-02-19	12524	522	68	6	2	8	0.64	17	78.4	4874
14-02-19	11421	476	62	6	2	8	0.7	17	80.9	4917
15-02-19	13857	577	75	6	2	8	0.58	16.2	83.4	4642
16-02-19	14109	588	76	6	2	8	0.57	16	81.5	4470
17-02-19	13842	577	75	6	2	8	0.58	16.7	82.4	4809
18-02-19	14308	596	78	6	2	8	0.56	16.5	79.5	4600
19-02-19	14171	590	77	6	2	8	0.56	16.5	79.7	4669
20-02-19	13636	568	74	6	2	8	0.59	16.8	79.8	4708
21-02-19	13016	542	71	6	2	8	0.61	16.5	79.6	4636
22-02-19	13761	573	75	6	2	8	0.58	16.8	79.4	4734
23-02-19	13877	578	75	6	2	8	0.58	16.8	79.9	4724
24-02-19	9105	379	49	6	2	8	0.88	16.2	79.5	4461

APPENDIX B

PREDICTED RESULTS OF DEVELOPED MODELS

Table B.1 Comparison of Predicted Results from Developed Models

Actual Data		FBNN Prediction		RBFNN Prediction		GRNN Prediction	
PPS	PD	PPS	PD	PPS	PD	PPS	PD
76.4	4330.0	76.2	4412.9	77.9	4715.5	76.8	4357.1
77.8	4470.0	77.5	4544.9	78.1	4758.0	78.4	4743.9
78.8	4325.0	78.6	4548.2	79.0	4626.9	79.1	4612.0
77.8	4430.0	74.1	4280.4	78.3	4368.9	76.3	4300.2
78.5	4390.0	76.7	4333.0	79.0	4597.2	78.5	4472.8
78.9	4430.0	77.6	4454.1	78.4	4705.3	78.5	4679.0
79.5	4295.0	75.6	4088.2	79.3	4498.8	77.7	4252.9
78.2	4350.0	77.9	4408.3	78.7	4669.3	78.7	4587.1
79.4	4385.0	78.1	4364.5	79.0	4621.3	79.0	4585.2
78.9	4345.0	77.7	4391.1	78.7	4671.4	78.7	4609.1
81.4	4325.0	79.4	4409.2	79.3	4542.9	80.6	4438.8
81.3	4290.0	81.3	4206.2	81.7	4121.4	81.5	4284.1
79.0	4370.0	78.1	4358.6	79.0	4619.7	79.0	4543.3
78.5	4270.0	80.1	4427.5	80.0	4462.0	79.4	4443.7
79.7	4280.0	80.2	4397.7	80.3	4408.0	79.7	4450.8
76.6	4235.0	79.5	4674.6	79.1	4624.5	79.5	4684.7
83.7	4220.0	81.3	4196.1	81.7	4121.4	81.6	4277.6
76.6	4175.0	78.6	4242.3	80.0	4453.9	79.9	4534.2
71.1	4175.0	79.3	4628.5	79.0	4630.9	79.2	4635.6
79.3	4230.0	80.0	4464.5	80.0	4465.3	79.7	4502.7
76.2	4175.0	79.5	4403.7	80.0	4447.8	79.4	4460.1
75.4	4330.0	75.7	4421.9	78.1	4761.8	78.4	4730.5
76.0	4315.0	76.9	4173.8	78.7	4655.0	77.5	4487.1
76.4	4190.0	77.9	3971.8	80.0	4447.2	78.2	4356.2
76.6	4140.0	78.0	4141.7	80.0	4451.9	78.9	4346.0
76.8	4235.0	77.1	4153.0	79.0	4558.1	77.2	4250.0
80.6	4455.0	80.1	4374.9	80.3	4407.5	79.6	4427.9
79.0	4250.0	78.1	4171.1	79.4	4547.2	79.2	4296.7
79.5	4265.0	78.0	4166.3	79.4	4547.5	79.1	4297.4
76.3	4045.0	80.2	4485.6	80.0	4463.5	79.9	4526.4
77.7	4215.0	77.8	4260.6	79.5	4372.7	77.7	4215.1
77.2	4175.0	78.2	4127.4	80.0	4439.7	78.5	4265.1
78.3	3975.0	78.8	4115.8	81.0	4203.0	78.1	4023.3
80.4	4621.3	80.3	4637.5	79.0	4603.4	79.6	4638.0
82.2	4451.7	81.8	4312.6	81.3	4170.0	82.1	4312.4
80.6	4538.5	79.9	4545.0	79.7	4510.5	80.1	4605.6
79.6	4443.3	79.9	4536.8	79.7	4521.0	79.6	4562.6
77.2	3877.8	81.2	4374.2	80.9	4285.6	80.9	4429.6
79.2	4511.3	78.9	4663.1	78.7	4681.3	78.9	4655.3
77.8	4432.3	79.3	4744.9	78.7	4665.9	79.2	4728.5

Table B.1 Cont'd

Actual Data		FBNN Prediction		RBFNN Prediction		GRNN Prediction	
PPS	**PD**	**PPS**	**PD**	**PPS**	**PD**	**PPS**	**PD**
76.2	4463.2	78.3	4805.2	78.1	4769.0	78.6	4778.6
77.7	4545.9	78.1	4774.3	78.1	4771.6	78.6	4755.0
77.9	4496.5	79.0	4687.7	78.7	4681.2	79.0	4678.6
77.8	4536.4	78.6	4731.5	78.4	4729.0	78.7	4692.2
78.3	4404.5	79.6	4679.2	79.0	4618.2	79.4	4677.7
78.6	4446.3	79.7	4697.7	79.1	4617.8	79.5	4696.1
78.2	4533.9	79.0	4819.3	78.4	4710.1	79.1	4779.3
78.4	4500.5	78.8	4539.5	79.0	4597.6	79.0	4572.5
79.2	4489.5	80.7	4558.9	80.0	4424.6	80.2	4566.2
78.1	4533.4	79.0	4571.2	79.0	4609.0	79.1	4586.8
78.3	4535.5	79.0	4570.6	79.0	4599.3	79.0	4579.7
78.2	4562.0	79.6	4693.8	79.0	4603.5	79.4	4675.9
80.1	4453.8	80.9	4494.4	80.3	4382.8	80.5	4537.1
82.1	4693.5	80.7	4491.4	79.6	4489.9	80.3	4526.0
80.6	4707.7	79.1	4718.8	78.4	4718.9	78.7	4696.2
80.5	4642.6	79.3	4632.7	79.0	4629.5	79.2	4642.7
83.7	4612.7	80.5	4436.1	80.2	4383.6	80.2	4443.5
74.5	4604.3	74.6	4521.1	77.4	4799.2	76.5	4576.8
80.1	4606.6	78.9	4559.9	79.0	4600.3	79.0	4576.4
78.2	4573.0	79.8	4717.4	79.1	4607.2	79.5	4698.3
78.8	4552.3	78.8	4528.2	79.0	4591.8	79.0	4565.6
82.4	4501.5	80.2	4471.8	79.9	4442.1	79.8	4489.7
79.4	4528.4	80.2	4574.3	79.7	4506.0	80.2	4623.0
79.1	4488.8	80.5	4526.9	80.0	4455.7	80.1	4555.6
80.9	4463.3	80.3	4492.8	80.0	4455.7	79.8	4506.7
80.5	4485.7	80.4	4512.0	80.0	4459.0	80.0	4538.1
78.5	4541.6	79.3	4640.8	79.0	4625.6	79.3	4649.0
79.2	4519.6	80.1	4566.4	79.7	4516.5	79.9	4598.1
78.2	4517.6	79.0	4552.0	79.0	4607.8	79.2	4586.7
78.9	4505.5	78.9	4661.2	78.7	4680.1	79.0	4658.2
80.6	4473.3	79.4	4309.7	80.3	4383.7	80.6	4490.5
78.0	4564.5	79.3	4627.0	79.0	4620.2	79.2	4631.6
78.4	4511.5	79.3	4635.1	79.0	4623.8	79.2	4641.9
80.0	4487.5	80.6	4453.1	80.3	4404.1	80.1	4491.9
81.7	4404.5	81.3	4292.1	80.5	4325.6	81.5	4410.2
78.4	4525.6	79.5	4669.8	79.0	4613.8	79.3	4664.5
78.8	4525.6	79.3	4620.0	79.0	4630.4	79.2	4627.3
80.9	4400.4	80.8	4477.8	80.3	4387.8	80.4	4520.9
83.1	4320.6	81.9	4310.4	81.4	4170.0	81.9	4353.8
80.1	4494.0	80.5	4531.8	80.0	4455.7	80.2	4565.5
81.0	4680.2	79.1	4722.3	78.7	4675.2	79.2	4716.4
82.5	4715.5	82.2	4790.3	78.5	4461.0	78.2	4484.8
81.0	4798.1	79.3	4729.3	78.4	4714.8	78.8	4713.9

Table B.1 Cont'd

Actual Data		FBNN Prediction		RBFNN Prediction		GRNN Prediction	
PPS	**PD**	**PPS**	**PD**	**PPS**	**PD**	**PPS**	**PD**
79.5	4580.1	80.0	4558.7	79.7	4517.6	79.8	4585.3
77.3	4445.9	79.7	4604.4	79.4	4566.6	79.5	4614.2
78.2	4851.1	79.2	4748.7	78.4	4718.2	78.6	4701.4
79.4	4520.0	79.6	4686.2	79.1	4621.6	79.5	4691.5
78.6	4806.1	78.2	4657.8	78.4	4715.7	78.7	4671.1
80.1	4444.6	80.2	4369.3	80.3	4406.6	79.5	4420.7
78.6	4559.7	80.6	4379.8	80.6	4348.7	80.1	4440.7
80.9	4612.4	80.5	4446.0	80.3	4403.9	80.1	4500.8
78.2	4720.6	79.3	4613.3	79.0	4629.3	79.1	4620.4
78.1	4530.1	80.1	4391.7	80.3	4407.9	79.7	4447.1
82.7	4619.3	80.0	4556.4	79.7	4508.8	80.2	4613.2
83.1	4588.6	80.3	4420.8	80.3	4406.7	79.9	4473.5
82.4	4398.0	81.0	4151.5	80.8	4268.0	81.6	4395.5
80.1	4673.0	80.0	4450.2	80.0	4465.9	79.6	4485.4
79.4	4678.7	79.3	4644.4	79.0	4629.6	79.3	4657.2
78.5	4791.3	79.5	4667.9	79.1	4625.9	79.4	4679.7
79.7	4734.8	78.7	4753.3	78.4	4726.8	78.9	4732.9
82.4	4710.3	80.0	4553.2	79.7	4518.6	79.8	4588.8
78.1	4741.6	79.4	4653.0	79.1	4628.5	79.4	4666.5
76.2	4584.0	78.6	4731.7	78.4	4729.2	78.7	4698.4
76.0	4789.6	77.9	4857.7	77.8	4807.3	78.4	4820.0
79.5	4782.4	78.8	4779.8	78.4	4720.9	79.0	4759.5
78.4	4483.1	80.0	4550.9	79.7	4519.0	79.8	4586.6
80.1	4570.6	80.1	4471.4	80.0	4464.8	79.8	4510.6
80.1	4894.7	79.7	4794.4	78.4	4662.0	79.4	4780.3
78.3	4913.7	78.5	4774.3	78.5	4617.2	79.5	4663.1
77.2	4901.3	76.7	4853.7	78.2	4619.1	79.1	4617.8
79.5	4465.9	79.5	4571.5	79.4	4577.8	79.4	4593.6
81.2	4331.0	80.1	4389.6	80.3	4408.1	79.6	4442.9
79.2	4512.4	79.4	4654.8	79.1	4628.2	79.4	4668.3
78.6	4578.7	79.0	4683.6	78.7	4681.5	79.0	4670.8
81.7	4838.1	80.0	4642.7	79.4	4566.1	79.8	4658.2
79.1	4643.8	79.6	4692.7	79.1	4619.8	79.5	4695.0
82.1	4740.8	80.0	4445.1	80.0	4465.9	79.6	4479.0
79.7	4901.8	78.7	4783.1	78.1	4764.5	78.5	4722.7
82.4	4952.1	79.4	4758.2	78.7	4664.6	79.3	4737.9
78.2	4951.6	78.2	4911.8	77.8	4783.4	78.5	4857.3
78.6	4954.9	78.0	4885.6	77.8	4797.9	78.4	4841.1
78.3	5003.0	77.7	4956.7	77.6	4812.8	78.2	4884.8
81.0	4911.8	79.4	4771.4	78.7	4657.8	79.3	4742.0
79.7	4937.7	78.6	4861.6	78.1	4749.7	78.8	4820.2
77.6	4991.0	77.5	4920.0	77.5	4834.7	78.2	4864.1
76.3	4842.2	77.8	4967.2	77.6	4769.0	77.7	4893.0

Table B.1 Cont'd

Actual Data		FBNN Prediction		RBFNN Prediction		GRNN Prediction	
PPS	**PD**	**PPS**	**PD**	**PPS**	**PD**	**PPS**	**PD**
80.2	4962.5	79.0	4810.5	78.4	4709.6	79.0	4778.9
81.7	4992.0	79.3	4748.0	78.7	4668.6	79.3	4733.4
82.4	4943.1	79.4	4651.0	79.1	4628.8	79.4	4664.5
78.6	4921.9	78.0	4876.5	77.8	4801.4	78.4	4835.0
81.5	4985.0	78.7	4764.0	78.4	4724.8	78.9	4745.0
79.7	5009.8	77.4	4913.9	77.5	4837.1	78.2	4860.5
79.5	4969.6	78.5	4836.7	78.1	4761.0	78.7	4804.4
80.4	4922.5	79.6	4688.7	79.1	4620.9	79.5	4693.0
79.6	4946.5	78.4	4835.6	78.1	4761.4	78.7	4803.6
79.5	4979.6	78.8	4775.5	78.4	4722.1	78.9	4755.9
78.6	4863.9	78.9	4787.8	78.4	4718.6	79.0	4765.5
78.4	4917.9	78.5	4842.8	78.1	4758.7	78.7	4808.6
83.1	4962.0	80.0	4643.5	79.4	4565.8	79.8	4658.6
78.6	4939.2	78.4	4834.3	78.1	4761.9	78.7	4802.7
81.0	4924.4	79.6	4688.0	79.1	4621.1	79.5	4692.7
77.2	4951.8	78.4	4835.1	78.1	4761.6	78.7	4803.2
80.1	4903.2	79.2	4726.4	78.7	4674.8	79.2	4719.8
79.7	4965.1	78.9	4800.7	78.4	4714.0	79.0	4773.7
79.3	4978.8	78.7	4761.8	78.4	4725.2	78.9	4742.8
75.6	4952.2	78.0	4877.1	77.8	4801.2	78.4	4835.4
78.4	4873.9	78.7	4723.0	78.4	4727.9	78.6	4675.9
79.5	4600.0	80.5	4530.7	80.0	4455.9	80.2	4570.1
79.7	4668.8	80.4	4522.3	80.0	4557.7	80.2	4563.1
79.5	4460.7	80.0	3979.5	80.6	4243.3	80.3	4443.9

APPENDIX C

SIMULATION RESULTS

Table C.1 Sensitivity Results for Varying Throughput at PPS = 80.0%

SN	TTM	TPH	MIW	GM	TGM	GMWR	BWI	PPS	GM	PD
1.	13830	500	65	2	8	0.729	16.4	80.0	**7.8**	**4453**
2.	13853	520	68	2	8	0.729	16.4	80.0	**7.4**	**4458**
3.	13876	540	70	2	8	0.729	16.4	80.0	**6.9**	**4454**
4.	13899	560	73	2	8	0.729	16.4	80.0	**6.6**	**4446**
5.	13922	580	75	2	8	0.729	16.4	80.0	**6.2**	**4438**
6.	13945	600	78	2	8	0.729	16.4	80.0	**5.9**	**4430**
7.	13968	620	81	2	8	0.729	16.4	80.0	**5.7**	**4423**
8.	13991	640	83	2	8	0.729	16.4	80.0	**5.5**	**4417**
9.	14014	660	86	2	8	0.729	16.4	80.0	**5.2**	**4412**
10.	14037	680	88	2	8	0.729	16.4	80.0	**5.0**	**4410**

Table C.2 Sensitivity Results for Varying Ore Hardness at PPS = 80.0%

SN	TTM	TPH	MIW	GM	TGM	GMWR	BWI	PPS	GM	PD
1.	13922	580	75	2	8	0.729	15.6	80.0	**3.1**	**4576**
2.	13922	580	75	2	8	0.729	15.8	80.0	**4.0**	**4561**
3.	13922	580	75	2	8	0.729	16.0	80.0	**5.1**	**4504**
4.	13922	580	75	2	8	0.729	16.2	80.0	**6.0**	**4442**
5.	13922	580	75	2	8	0.729	16.4	80.0	**6.2**	**4438**
6.	13922	580	75	2	8	0.729	16.6	80.0	**5.7**	**4629**
7.	13922	580	75	2	8	0.729	16.8	80.0	**4.5**	**4984**
8.	13922	580	75	2	8	0.729	17.0	80.0	**4.3**	**5110**
9.	13922	580	75	2	8	0.729	17.2	80.0	**5.0**	**5122**
10.	13922	580	75	2	8	0.729	17.4	80.0	**6.4**	**5119**

Table C.3 Sensitivity Results for Varying Grinding Media Wear Rate at PPS = 80%

SN	TTM	TPH	MIW	GM	TGM	GMWR	BWI	PPS	GM	PD
1.	13922	580	75	2	8	0.329	16.4	80.0	**6.3**	**3997**
2.	13922	580	75	2	8	0.429	16.4	80.0	**6.4**	**4151**
3.	13922	580	75	2	8	0.529	16.4	80.0	**6.4**	**4301**
4.	13922	580	75	2	8	0.629	16.4	80.0	**6.3**	**4393**
5.	13922	580	75	2	8	0.729	16.4	80.0	**6.2**	**4438**
6.	13922	580	75	2	8	0.829	16.4	80.0	**6.1**	**4467**
7.	13922	580	75	2	8	0.929	16.4	80.0	**5.9**	**4495**
8.	13922	580	75	2	8	1.029	16.4	80.0	**5.4**	**4521**
9.	13922	580	75	2	8	1.129	16.4	80.0	**4.5**	**4541**
10.	13922	580	75	2	8	1.229	16.4	80.0	**3.3**	**4553**

Table C.4 Sensitivity Results for Varying Throughput at PPS = 82.4%

SN	TTM	TPH	MIW	GM	TGM	GMWR	BWI	PPS	GM	PD
1.	10199	368	48	2	8	0.779	16.2	82.4	**8.4**	**4408**
2.	10222	388	50	2	8	0.779	16.2	82.4	**7.6**	**4407**
3.	10245	408	53	2	8	0.779	16.2	82.4	**6.7**	**4404**
4.	10268	428	56	2	8	0.779	16.2	82.4	**6.0**	**4402**
5.	10291	448	58	2	8	0.779	16.2	82.4	**5.3**	**4401**
6.	10314	468	61	2	8	0.779	16.2	82.4	**4.8**	**4400**
7.	10337	488	63	2	8	0.779	16.2	82.4	**4.5**	**4399**
8.	10360	508	66	2	8	0.779	16.2	82.4	**4.4**	**4398**
9.	10383	528	69	2	8	0.779	16.2	82.4	**4.3**	**4396**

Table C.5 Sensitivity Results for Varying Ore Hardness at PPS = 82.4%

SN	TTM	TPH	MIW	GM	TGM	GMWR	BWI	PPS	GM	PD
1.	10268	428	56	2	8	0.479	15.6	82.4	**11.5**	**4383**
2.	10268	428	56	2	8	0.579	15.8	82.4	**9.9**	**4398**
3.	10268	428	56	2	8	0.679	16.0	82.4	**8.0**	**4401**
4.	10268	428	56	2	8	0.779	16.2	82.4	**6.0**	**4402**
5.	10268	428	56	2	8	0.879	16.4	82.4	**3.9**	**4407**
6.	10268	428	56	2	8	0.979	16.6	82.4	**2.0**	**4419**
7.	10268	428	56	2	8	1.079	16.8	82.4	**0.3**	**4436**
8.	10268	428	56	2	8	1.179	17.0	82.4	**-1.2**	**4456**
9.	10268	428	56	2	8	1.279	17.2	82.4	**-2.3**	**4474**

Table C.6 Sensitivity Results for Varying Grinding Media Wear Rate at PPS = 82.4%

SN	TTM	TPH	MIW	GM	TGM	GMWR	BWI	PPS	GM	PD
1.	10268	428	56	2	8	0.479	16.2	82.4	**11.5**	**4383**
2.	10268	428	56	2	8	0.579	16.2	82.4	**9.9**	**4398**
3.	10268	428	56	2	8	0.679	16.2	82.4	**8.0**	**4401**
4.	10268	428	56	2	8	0.779	16.2	82.4	**6.0**	**4402**
5.	10268	428	56	2	8	0.879	16.2	82.4	**3.9**	**4407**
6.	10268	428	56	2	8	0.979	16.2	82.4	**2.0**	**4419**
7.	10268	428	56	2	8	1.079	16.2	82.4	**0.3**	**4436**
8.	10268	428	56	2	8	1.179	16.2	82.4	**-1.2**	**4456**
9.	10268	428	56	2	8	1.279	16.2	82.4	**-2.3**	**4474**

Table C.7 Sensitivity Results for Varying Throughput at PPS = 79.1%

SN	TTM	TPH	MIW	GM	TGM	GMWR	BWI	PPS	GM	PD
1.	14299	520	68	2	8	0.705	16.5	79.10	**7.2**	**4268**
2.	14322	540	70	2	8	0.705	16.5	79.10	**6.9**	**4313**
3.	14345	560	73	2	8	0.705	16.5	79.10	**6.7**	**4355**
4.	14368	580	75	2	8	0.705	16.5	79.10	**6.5**	**4392**
5.	14391	600	78	2	8	0.705	16.5	79.10	**6.3**	**4425**
6.	14414	620	81	2	8	0.705	16.5	79.10	**6.1**	**4454**
7.	14437	640	83	2	8	0.705	16.5	79.10	**5.9**	**4479**
8.	14460	660	86	2	8	0.705	16.5	79.10	**5.7**	**4502**
9.	14483	680	88	2	8	0.705	16.5	79.10	**5.4**	**4524**
10.	14506	700	91	2	8	0.705	16.5	79.10	**5.2**	**4546**

Table C.8 Sensitivity Results for Varying Ore Hardness at PPS = 79.1%

SN	TTM	TPH	MIW	GM	TGM	GMWR	BWI	PPS	GM	PD
1.	14391	600	78	2	8	0.705	15.7	79.1	**2.8**	**4321**
2.	14391	600	78	2	8	0.705	15.9	79.1	**3.7**	**4296**
3.	14391	600	78	2	8	0.705	16.1	79.1	**5.0**	**4268**
4.	14391	600	78	2	8	0.705	16.3	79.1	**6.0**	**4284**
5.	14391	600	78	2	8	0.705	16.5	79.1	**6.3**	**4425**
6.	14391	600	78	2	8	0.705	16.7	79.1	**5.5**	**4806**
7.	14391	600	78	2	8	0.705	16.9	79.1	**4.8**	**5076**
8.	14391	600	78	2	8	0.705	17.1	79.1	**4.7**	**5159**
9.	14391	600	78	2	8	0.705	17.3	79.1	**5.1**	**5169**
10.	14391	600	78	2	8	0.705	17.5	79.1	**5.9**	**5159**

Table C.9 Sensitivity Results for Varying Grinding Media Wear Rate at PPS = 79.1%

SN	TTM	TPH	MIW	GM	TGM	GMWR	BWI	PPS	GM	PD
1.	14391	600	78	2	8	0.305	16.5	79.10	**6.0**	**4003**
2.	14391	600	78	2	8	0.405	16.5	79.10	**6.0**	**4050**
3.	14391	600	78	2	8	0.505	16.5	79.10	**6.2**	**4164**
4.	14391	600	78	2	8	0.605	16.5	79.10	**6.3**	**4313**
5.	14391	600	78	2	8	0.705	16.5	79.10	**6.3**	**4425**
6.	14391	600	78	2	8	0.805	16.5	79.10	**6.2**	**4481**
7.	14391	600	78	2	8	0.905	16.5	79.10	**5.9**	**4506**
8.	14391	600	78	2	8	1.005	16.5	79.10	**5.5**	**4527**
9.	14391	600	78	2	8	1.105	16.5	79.10	**5.0**	**4556**
10.	14391	600	78	2	8	1.205	16.5	79.10	**4.3**	**4587**

Table C.10 Sensitivity Results for Varying Throughput and Ore Hardness at PPS = 80.0%

Case	TTM	TPH	MIW	GM	TGM	GMWR	BWI	PPS	GM	PD
1.	13830	500	65	2	8	0.729	15.6	80.0	**7.8**	**4453**
2.	13853	520	68	2	8	0.729	15.8	80.0	**7.4**	**4458**
3.	13876	540	70	2	8	0.729	16.0	80.0	**6.9**	**4454**
4.	13899	560	73	2	8	0.729	16.2	80.0	**6.6**	**4446**
5.	13922	580	75	2	8	0.729	16.4	80.0	**6.2**	**4438**
6.	13945	600	78	2	8	0.729	16.6	80.0	**5.9**	**4430**
7.	13968	620	81	2	8	0.729	16.8	80.0	**5.7**	**4423**
8.	13991	640	83	2	8	0.729	17.0	80.0	**5.5**	**4417**
9.	14014	660	86	2	8	0.729	17.2	80.0	**5.2**	**4412**
10.	14037	680	88	2	8	0.729	17.4	80.0	**5.0**	**4410**

Table C.11 Sensitivity Results for Varying Throughput and Grinding Media Wear Rate at PPS = 80.0%

Case	TTM	TPH	MIW	GM	TGM	GMWR	BWI	PPS	GM	PD
1.	13830	**500**	65	2	8	0.329	16.4	80.0	**8.2**	**3836**
2.	13853	520	68	2	8	0.429	16.4	80.0	**7.3**	**3993**
3.	13876	540	70	2	8	0.529	16.4	80.0	**6.9**	**4219**
4.	13899	560	73	2	8	0.629	16.4	80.0	**6.6**	**4380**
5.	13922	580	75	2	8	0.729	16.4	80.0	**6.2**	**4438**
6.	13945	600	78	2	8	0.829	16.4	80.0	**5.7**	**4447**
7.	13968	620	81	2	8	0.929	16.4	80.0	**5.1**	**4445**
8.	13991	640	83	2	8	1.029	16.4	80.0	**4.4**	**4445**
9.	14014	660	86	2	8	1.129	16.4	80.0	**3.5**	**4449**
10.	14037	680	88	2	8	1.229	16.4	80.0	**2.6**	**4456**

Table C.12 Sensitivity Results for Varying Ore Hardness and Grinding Media Wear Rate at PPS = 80.0%

Case	TTM	TPH	MIW	GM	TGM	GMWR	BWI	PPS	GM	PD
1.	13922	580	75	2	8	0.329	15.6	80.0	**3.5**	**3774**
2.	13922	580	75	2	8	0.429	15.8	80.0	**4.5**	**3945**
3.	13922	580	75	2	8	0.529	16.0	80.0	**5.5**	**4177**
4.	13922	580	75	2	8	0.629	16.2	80.0	**6.1**	**4346**
5.	13922	580	75	2	8	0.729	16.4	80.0	**6.2**	**4438**
6.	13922	580	75	2	8	0.829	16.6	80.0	**5.6**	**4592**
7.	13922	580	75	2	8	0.929	16.8	80.0	**4.1**	**4895**
8.	13922	580	75	2	8	1.029	17.0	80.0	**3.2**	**5047**
9.	13922	580	75	2	8	1.129	17.2	80.0	**3.3**	**5069**
10.	13922	580	75	2	8	1.229	17.4	80.0	**3.8**	**5071**

Table C.13 Sensitivity Results for Varying Throughput, Ore Hardness and Grinding Media Wear Rate at PPS = 80.0%

Case	TTM	TPH	MIW	GM	TGM	GMWR	BWI	PPS	GM	PD
1.	13830	500	65	2	8	0.329	15.6	80.0	**6.1**	**3844**
2.	13853	520	68	2	8	0.429	15.8	80.0	**6.1**	**3941**
3.	13876	540	70	2	8	0.529	16.0	80.0	**6.3**	**4156**
4.	13899	560	73	2	8	0.629	16.2	80.0	**6.5**	**4352**
5.	13922	580	75	2	8	0.729	16.4	80.0	**6.2**	**4438**
6.	13945	600	78	2	8	0.829	16.6	80.0	**5.3**	**4608**
7.	13968	620	81	2	8	0.929	16.8	80.0	**3.7**	**4919**
8.	13991	640	83	2	8	1.029	17.0	80.0	**2.7**	**5040**
9.	14014	660	86	2	8	1.129	17.2	80.0	**2.4**	**5046**
10.	14037	680	88	2	8	1.229	17.4	80.0	**2.3**	**5034**

Table C.14 Sensitivity Results for Varying Throughput and Ore Hardness at PPS = 82.4%

Case	TTM	TPH	MIW	GM	TGM	GMWR	BWI	PPS	GM	PD
1.	10199	368	48	2	8	0.779	15.6	82.4	**8.4**	**4408**
2.	10222	388	50	2	8	0.779	15.8	82.4	**7.6**	**4407**
3.	10245	408	53	2	8	0.779	16.0	82.4	**6.7**	**4404**
4.	10268	428	56	2	8	0.779	16.2	82.4	**6.0**	**4402**
5.	10291	448	58	2	8	0.779	16.4	82.4	**5.3**	**4401**
6.	10314	468	61	2	8	0.779	16.6	82.4	**4.8**	**4400**
7.	10337	488	63	2	8	0.779	16.8	82.4	**4.5**	**4399**
8.	10360	508	66	2	8	0.779	17.0	82.4	**4.4**	**4398**
9.	10383	528	69	2	8	0.779	17.2	82.4	**4.3**	**4396**

Table C.15 Sensitivity Results for Varying Throughput and Grinding Media Wear Rate at PPS = 82.4%

Case	TTM	TPH	MIW	GM	TGM	GMWR	BWI	PPS	GM	PD
1.	10199	368	48	2	8	0.479	16.2	82.4	**13.3**	**4339**
2.	10222	388	50	2	8	0.579	16.2	82.4	**11.3**	**4392**
3.	10245	408	53	2	8	0.679	16.2	82.4	**8.8**	**4402**
4.	10268	428	56	2	8	0.779	16.2	82.4	**6.0**	**4402**
5.	10291	448	58	2	8	0.879	16.2	82.4	**3.4**	**4406**
6.	10314	468	61	2	8	0.979	16.2	82.4	**1.4**	**4417**
7.	10337	488	63	2	8	1.079	16.2	82.4	**-0.2**	**4435**
8.	10360	508	66	2	8	1.179	16.2	82.4	**-1.4**	**4458**
9.	10383	528	69	2	8	1.279	16.2	82.4	**-2.5**	**4480**

Table C.16 Sensitivity Results for Varying Ore Hardness and Grinding Media Wear Rate at PPS = 82.4%

Case	TTM	TPH	MIW	GM	TGM	GMWR	BWI	PPS	GM	PD
1.	10268	428	56	2	8	0.479	15.6	82.4	**4.4**	**4464**
2.	10268	428	56	2	8	0.579	15.8	82.4	**4.8**	**4439**
3.	10268	428	56	2	8	0.679	16.0	82.4	**5.3**	**4412**
4.	10268	428	56	2	8	0.779	16.2	82.4	**6.0**	**4402**
5.	10268	428	56	2	8	0.879	16.4	82.4	**6.6**	**4434**
6.	10268	428	56	2	8	0.979	16.6	82.4	**6.9**	**4536**
7.	10268	428	56	2	8	1.079	16.8	82.4	**6.8**	**4657**
8.	10268	428	56	2	8	1.179	17.0	82.4	**6.3**	**4847**
9.	10268	428	56	2	8	1.279	17.2	82.4	**5.5**	**5096**

Table C.17 Sensitivity Results for Varying Throughput, Ore Hardness, Grinding Media Wear Rate at PPS = 82.4%

Case	TTM	TPH	MIW	GM	TGM	GMWR	BWI	PPS	GM	PD
1.	10199	368	48	2	8	0.479	15.6	82.4	**5.5**	**4345**
2.	10222	388	50	2	8	0.579	15.8	82.4	**5.7**	**4410**
3.	10245	408	53	2	8	0.679	16.0	82.4	**5.9**	**4408**
4.	10268	428	56	2	8	0.779	16.2	82.4	**6.0**	**4402**
5.	10291	448	58	2	8	0.879	16.4	82.4	**5.9**	**4426**
6.	10314	468	61	2	8	0.979	16.6	82.4	**5.5**	**4514**
7.	10337	488	63	2	8	1.079	16.8	82.4	**4.9**	**4672**
8.	10360	508	66	2	8	1.179	17.0	82.4	**4.2**	**4965**
9.	10383	528	69	2	8	1.279	17.2	82.4	**3.8**	**5148**

Table C.18 Sensitivity Results for Varying Throughput and Ore Hardness at PPS = 79.1%

Case	TTM	TPH	MIW	GM	TGM	GMWR	BWI	PPS	GM	PD
1.	14299	520	68	2	8	0.705	15.7	79.10	**4.0**	**4239**
2.	14322	540	70	2	8	0.705	15.9	79.10	**4.9**	**4278**
3.	14345	560	73	2	8	0.705	16.1	79.10	**5.7**	**4261**
4.	14368	580	75	2	8	0.705	16.3	79.10	**6.3**	**4273**
5.	14391	600	78	2	8	0.705	16.5	79.10	**6.3**	**4425**
6.	14414	620	81	2	8	0.705	16.7	79.10	**5.4**	**4837**
7.	14437	640	83	2	8	0.705	16.9	79.10	**4.7**	**5091**
8.	14460	660	86	2	8	0.705	17.1	79.10	**4.5**	**5190**
9.	14483	680	88	2	8	0.705	17.3	79.10	**4.5**	**5222**
10.	14506	700	91	2	8	0.705	17.5	79.10	**4.6**	**5229**

Table C.19 Sensitivity Results for Varying Throughput and Grinding Media Wear Rate at PPS = 79.1%

Case	TTM	TPH	MIW	GM	TGM	GMWR	BWI	PPS	GM	PD
1.	14299	520	68	2	8	0.305	16.5	79.10	**7.9**	**3871**
2.	14322	540	70	2	8	0.405	16.5	79.10	**7.0**	**3925**
3.	14345	560	73	2	8	0.505	16.5	79.10	**6.6**	**4047**
4.	14368	580	75	2	8	0.605	16.5	79.10	**6.5**	**4256**
5.	14391	600	78	2	8	0.705	16.5	79.10	**6.3**	**4425**
6.	14414	620	81	2	8	0.805	16.5	79.10	**6.0**	**4488**
7.	14437	640	83	2	8	0.905	16.5	79.10	**5.4**	**4494**
8.	14460	660	86	2	8	1.005	16.5	79.10	**4.7**	**4485**
9.	14483	680	88	2	8	1.105	16.5	79.10	**3.9**	**4477**
10.	14506	700	91	2	8	1.205	16.5	79.10	**2.9**	**4473**

Table C.20 Sensitivity Results for Varying Ore Hardness and Grinding Media Wear Rate at PPS = 79.1%

Case	TTM	TPH	MIW	GM	TGM	GMWR	BWI	PPS	GM	PD
1.	14391	600	78	2	8	0.305	15.7	79.1	**3.9**	**3613**
2.	14391	600	78	2	8	0.405	15.9	79.1	**4.7**	**3676**
3.	14391	600	78	2	8	0.505	16.1	79.1	**5.5**	**3844**
4.	14391	600	78	2	8	0.605	16.3	79.1	**6.2**	**4114**
5.	14391	600	78	2	8	0.705	16.5	79.1	**6.3**	**4425**
6.	14391	600	78	2	8	0.805	16.7	79.1	**5.5**	**4818**
7.	14391	600	78	2	8	0.905	16.9	79.1	**4.3**	**5090**
8.	14391	600	78	2	8	1.005	17.1	79.1	**3.7**	**5138**
9.	14391	600	78	2	8	1.105	17.3	79.1	**3.5**	**5108**
10.	14391	600	78	2	8	1.205	17.5	79.1	**3.6**	**5082**

Table C.21 Sensitivity Results for Varying Throughput, Ore Hardness and Grinding Media Wear Rate at PPS = 79.1%

Case	TTM	TPH	MIW	GM	TGM	GMWR	BWI	PPS	GM	PD
1.	14299	520	68	2	8	0.305	15.7	79.10	**6.1**	**3662**
2.	14322	540	70	2	8	0.405	15.9	79.10	**5.9**	**3699**
3.	14345	560	73	2	8	0.505	16.1	79.10	**6.0**	**3813**
4.	14368	580	75	2	8	0.605	16.3	79.10	**6.3**	**4081**
5.	14391	600	78	2	8	0.705	16.5	79.10	**6.3**	**4425**
6.	14414	620	81	2	8	0.805	16.7	79.10	**5.3**	**4842**
7.	14437	640	83	2	8	0.905	16.9	79.10	**4.2**	**5093**
8.	14460	660	86	2	8	1.005	17.1	79.10	**3.6**	**5152**
9.	14483	680	88	2	8	1.105	17.3	79.10	**3.3**	**5131**
10.	14506	700	91	2	8	1.205	17.5	79.10	**3.1**	**5094**

APPENDIX D

DEVELOPMENT CODES OF MODELS

General Regression Neural Network

```
clc;
% Load datasets
load('targetTrain.mat'); % Training input target dataset
load('dataTrain.mat'); % Input training dataset
load('targetTest.mat'); % Training testing target dataset
load('dataTest.mat'); % Input testing dataset
% Loop for spread between 0.1 and 1 with step size of 0.1
for r = 0.1:0.1:1
        net1 = newgrnn(dataTrain', targetTrain', r); % net is the trained model.
        save('net1.mat','net1');
        % Simulate Network with training dataset
        hb = sim(net1,dataTrain');
        % Calculate MSE of training dataset
        mb = mse(net1,targetTrain,hb');
        % Simulate Network with testing dataset
        nb = sim(net1,dataTest');
        % Calculate MSE of testing dataset
        db = mse(net1,targetTest,nb');
        % Print out results
        formatSpec = 'MSE for training data %1.5f and test data %1.5f\n';
        fprintf(formatSpec,mb,db)
end
```

Radial Basis Function Neural Network

```
clc;
% Load datasets
load('targetTrain.mat'); % Training input target dataset
load('dataTrain.mat'); % Input training dataset
load('targetTest.mat'); % Training testing target dataset
load('dataTest.mat'); % Input testing dataset
% Loop for spread between 0.1 and 1 with step size of 0.1
for r = 0.1:0.1:1
        net = newrb(dataTrain', targetTrain', 0.02, r); % net is the trained model.
        save('net.mat','net');
        % Simulate Network with training dataset
        yb = sim(net,dataTrain');
        % Calculate MSE of training dataset
        pb = mse(net,targetTrain,yb');
        % Simulate Network with testing dataset
        kb = sim(net3,dataTest');
        % Calculate MSE of testing dataset
        ib = mse(net3,targetTest,kb');
        % Print out results
        formatSpec = 'MSE for training data %1.5f and test data %1.5f\n';
        fprintf(formatSpec,pb,ib)
end
```

Grey Wolf Optimisation: Main File

```
clc;
SearchAgents_no=200; % Number of search agents
Max_iteration=1000; % Maximum number of iterations
% Load details of the selected benchmark function
fobj=@MLP_Grinding; % Minimization function
lb=-100; %lower bounds
ub=5; %upper bounds
dim=156; % specify number of penalty agents

% Start training using GWO
[Best_MSE,Best_NN,cg_curve]=GWO(SearchAgents_no,Max_iteration,lb,ub,dim,fobj);
% Draw the convergence curve
figure('Position',[500 500 660 290])
semilogy(cg_curve,'Color','r')
hold on
title('Convergence curve')
xlabel('Iteration');
ylabel('MSE');
axis tight
grid off
box on
legend('GWO')
```

Grey Wolf Optimisation

```
% Grey Wolf Optimizer
function
[Alpha_score,Alpha_pos,Convergence_curve]=GWO(SearchAgents_no,Max_iter,lb,ub,dim,f
ob)

% initialize alpha, beta, and delta_pos
Alpha_pos=zeros(1,dim);
Alpha_score=inf;  %change this to -inf for maximization problems

Beta_pos=zeros(1,dim);
Beta_score=inf; %change this to -inf for maximization problems

Delta_pos=zeros(1,dim);
Delta_score=inf; %change this to -inf for maximization problems

%Initialize the positions of search agents
Positions=initialization(SearchAgents_no,dim,ub,lb);
Convergence_curve=zeros(1,Max_iter);
l=0; % Loop counter

% Main loop
while l<Max_iter
   for i=1:size(Positions,1)
      % Calculate objective function for each search agent
      fitness=fobj(Positions(i,:));
      % Update Alpha, Beta, and Delta
      if fitness<Alpha_score
         Alpha_score=fitness; % Update alpha
         Alpha_pos=Positions(i,:);
      end
      if fitness>Alpha_score && fitness<Beta_score
         Beta_score=fitness; % Update beta
         Beta_pos=Positions(i,:);
      end
```

```
    if fitness>Alpha_score && fitness>Beta_score && fitness<Delta_score
        Delta_score=fitness; % Update delta
        Delta_pos=Positions(i,:);
    end
end
a=2-l*((2)/Max_iter); % a decreases linearly from 2 to 0

% Update the Position of search agents including omegas
for i=1:size(Positions,1)
    for j=1:size(Positions,2)
        r1=rand(); % r1 is a random number in [0,1]
        r2=rand(); % r2 is a random number in [0,1]
        A1=2*a*r1-a; % Equation (3.3)
        C1=2*r2; % Equation (3.4)
        D_alpha=abs(C1*Alpha_pos(j)-Positions(i,j)); % Equation (3.5)-part 1
        X1=Alpha_pos(j)-A1*D_alpha; % Equation (3.6)-part 1
        r1=rand();
        r2=rand();
        A2=2*a*r1-a; % Equation (3.3)
        C2=2*r2; % Equation (3.4)
        D_beta=abs(C2*Beta_pos(j)-Positions(i,j)); % Equation (3.5)-part 2
        X2=Beta_pos(j)-A2*D_beta; % Equation (3.6)-part 2
        r1=rand();
        r2=rand();
        A3=2*a*r1-a; % Equation (3.3)
        C3=2*r2; % Equation (3.4)
        D_delta=abs(C3*Delta_pos(j)-Positions(i,j)); % Equation (3.5)-part 3
        X3=Delta_pos(j)-A3*D_delta; % Equation (3.5)-part 3
        Positions(i,j)=(X1+X2+X3)/3;    % Equation (3.7)
    end
    % Return back the search agents that go beyond the boundaries of the search space
    Flag4ub=Positions(i,:)>ub;
    Flag4lb=Positions(i,:)<lb;
    Positions(i,:)=(Positions(i,:).*(~(Flag4ub+Flag4lb)))+ub.*Flag4ub+lb.*Flag4lb;
end
```

```
    l=l+1;
    Convergence_curve(l)=Alpha_score;

    if mod(l,50)==0
        display(['At iteration ', num2str(l), ' the MSE is ', num2str(Alpha_score)]);
    end
end
```

Grey Wolf Optimisation: MLP_Grinding

```
function o=MLP_Grinding(solution) % Minimizing function
        load('targetTrain.mat'); % Training input target dataset
        load('dataTrain.mat'); % Input training dataset

        % Organizing Penalty Agents for Layer Weights and Biases
        for ww=1:160
           W1(ww)=solution(1,ww);
        end
        for bb=161:200
           W2(bb-160)=solution(1,bb);
        end
        for cc=201:220
           B1(cc-200)=solution(1,cc);
        end
        for dd=221:222
           B2(dd-220)=solution(1,dd);
        End

        % Predict Values using Neural Network and GWO Penalty Agents
        actualvalue = myNeuralNetworkFunctionb(dataTrain, W1, W2, B1, B2);
        % Error between Predicted values and Target values
        e = targetTrain-actualvalue;
        fitness=mean(e(:).^2);  % calculating MSE
        o=fitness;
end
```

Grey Wolf Optimisation: myNeuralNetworkFunctionb

```
function [Y, Xf, Af] = myNeuralNetworkFunctionb (X, W1,W2, B1,B2,~,~)
% ===== NEURAL NETWORK CONSTANTS =====

% Input 1
x1_step1.xoffset = [0;0;0;0;0;0;0.111111111111111;0];
x1_step1.gain = [2;2;2;2;2;2;2.25;2.285];
x1_step1.ymin = -1;

% Layer 1
b1_1 = [-1.8835376404642052428;-1.5982856271486525213;-0.9988010649813621189;-
1.2172028960407785814;0.76323811209739900185;1.1053073655276306475;-
0.21586737588303747 67;0.19304914566990677427;-
0.32915823848525355144;0.42301747668088474086;0.81079674048937888653;-
1.1621157581285357363;-1.5462685198619612326;2.2530323984224218 67];
IW1_1_1 = [0.70932565488281817956 -0.73725472122962187882 -
0.86668374177447815576 0.70428562876941203097 0.69208368701313793814 -
0.62211087280381516251 -0.03693483813252365 6329 -
0.75579377715128048809;0.43616366419387814224 -0.33137264007990757664 -
0.99401421357373864751 0.50540716213352199215 -0.29817403771853534522 -
0.32234013636851066575 1.0392052636351853945
1.2831451726698834825;1.1376696238840044995 0.98783961633198036356 -
0.55399655304066885986 -1.2892350620646086945 -0.66860770796513790959 -
0.63580957475872545981 0.28170413551008505193 0.614743333239366474;-
0.00359904518189829020 21 0.44498252001044968917 0.06861469156365621 0471
0.64148068956985582201 -0.81414470743636291328 0.70043648642286082673 -
0.96514230945675616447 -0.03669599397243702 9873;0.07871357045869840918 2
0.35128324320210191356 1.1707234606705319013 0.97558715295075604246
0.51636451992827803181 -1.1994836377775766056 0.89897455578694629441 -
0.63206035698041862503;-0.36722505293747809141 0.27632237273688331491
0.61782692270213168673 -0.63325966090492391558 -1.4538075165489756646
1.52412178307930124 0.20163991165149044993
1.7154601140990182184;1.0266667531791011658 0.98433967139055478235 -
0.13325957311935979 21 0.12758216436780256409 1.0479546764208051979 -
0.20980594285831988266 -0.52216249608007880845 -0.11390462431194131598;-
```

0.29081690120635633745 0.37991078351971863114 0.07398114301287367355 9 -
0.87754675477779942039 -0.12958110974372824553 0.00702381648838130284 72 -
1.729769650861296526 -0.43411740067301313184;-0.55971278327184725843 -
0.09285664129572893110 7 -0.53715839015838540149 -1.0955819131285844392
0.04532036845865755614 3 0.64406114437495898262 0.53482818601690718108
1.16114270092591520 54;0.64824850764200381281 0.22404888773597550489
0.47055743583315101652 1.1443207481606711973 1.3162223595295288181 -
0.55267011613897454314 2.2988069732753992902
0.24674567917567480357;1.2631662088769406438 -0.30037906642433109816 -
0.16556069813494597 72 1.1017881282348833683 0.38660702450287054432 -
0.26375291735744715 86 0.29257342462360819146 -0.44305105430288688195;-
0.16364294744466995057 0.39241487535269459208 -0.46456774555490748524 -
0.59767022319622897797 0.54552719835305363283 0.91670858107893982147 -
1.3732007786703559482 -0.51004183132951352864;-1.3329393647181639881 -
0.20234149810497156774 -0.97216455895551634 47 0.76674957900080487061
0.39234081575447399 27 -0.87426961149713822152 0.48689782231620143405 -
0.04399120748921526991;0.33845437999792638006 0.42083182170467359207
0.35263721735977876515 0.68667726781432669725 -1.2197650941295459237
0.16408570641237577026 -0.20141306986245990918 0.80547237263939941432];

% Layer 2

b2_1 = [0.47807069611306596268;-0.50044963622964833139];

LW2_1_1 = [0.65546977986319154841 0.88477152713734785738 1.385449619760525497
-0.23621996193881517057 -0.50040597750766790952 0.15345487039587307754 -
0.18201422395101476 97 0.25159077470769336538 -0.24720413513866146271 -
0.27892507312418562959 0.51411640187143814451 -0.48105325507821450337
0.89393144056918139029 -0.04097695219955518192 2;-0.78593362049306059181
0.12396748221861751682 0.19874832459059382783 0.14783510780138472973 -
0.58385317932002434027 1.9441699443451285756 -0.77657702631630998 18 -
0.65462745593509774622 -0.79375898301787350952 1.438010773029072098
0.22098692923616028438 0.37787261381678949324 0.01333209069238201760 5 -
0.19077382104835477472];

% GWO weights and biases

w1 = reshape(W1,14,8);

```
w2 = reshape(W2,2,14);
B1 = B1';
B2 = B2';

% New weights and biases
IW1_1 = w1.*IW1_1_1;
LW2_1 = w2.*LW2_1_1;
b1 = B1.*b1_1;
b2 = B2.*b2_1;

% Output 1
y1_step1.ymin = -1;
y1_step1.gain = [2;2.42033430455451];
y1_step1.xoffset = [0;0.0211197702169];

% ===== SIMULATION ========
% Format Input Arguments
isCellX = iscell(X);
if ~isCellX
   X = {X};
end

% Dimensions
TS = size(X,2); % timesteps
if ~isempty (X)
   Q = size (X {1},1); % samples/series
else
   Q = 0;
end

% Allocate Outputs
Y = cell(1,TS);

% Time loop
for ts=1:TS
```

```
    % Input 1
    X{1, ts} = X{1,ts}';
    Xp1 = mapminmax_apply(X{1,ts},x1_step1);

    % Layer 1
    a1 = tansig_apply(repmat(b1,1,Q) + IW1_1*Xp1);

    % Layer 2
    a2 = repmat(b2,1,Q) + LW2_1*a1;

    % Output 1
    Y{1,ts} = mapminmax_reverse(a2,y1_step1);
    Y{1,ts} = Y{1,ts}';
end

% Final Delay States
Xf = cell(1,0);
Af = cell(2,0);

% Format Output Arguments
if ~isCellX
    Y = cell2mat(Y);
end
end

% ===== MODULE FUNCTIONS ========
% Map Minimum and Maximum Input Processing Function
function y = mapminmax_apply(x,settings)
y = bsxfun(@minus,x,settings.xoffset);
y = bsxfun(@times,y,settings.gain);
y = bsxfun(@plus,y,settings.ymin);
end

% Sigmoid Symmetric Transfer Function
```

```
function a = tansig_apply(n,~)
a = 2 ./ (1 + exp(-2*n)) - 1;
end

% Map Minimum and Maximum Output Reverse-Processing Function
function x = mapminmax_reverse(y,settings)
x = bsxfun(@minus,y,settings.ymin);
x = bsxfun(@rdivide,x,settings.gain);
x = bsxfun(@plus,x,settings.xoffset);
end
```